Swansea University
Prifysgol Abertawe

Modelling of Beach State Variability

By

Blessing Chinasa Nwanosike

Submitted to Swansea University in fulfilment of the requirements for the Degree of

Ph.D.

2023

Declarations

This work has not previously been accepted in substance for any degree and is not being concurrently submitted in candidature for any degree.

Signed.....  .....

Date.....25/05/2023.....

This thesis is the result of my own investigations, except where otherwise stated. Other sources are acknowledged by footnotes giving explicit references. A bibliography is appended.

Signed.....  .....

Date.....25/05/2023.....

I hereby give my consent for my work, if relevant and accepted, to be available for photocopying and for inter-library loans **after expiry of a bar on access approved by the University.**

Signed.....  .....

Date.....25/05/2023.....

The University's ethical procedures have been followed and, where appropriate, that ethical approval has been granted.

Signed.....  .....

Date.....25/05/2023.....

Dedicated to God Almighty

And

My beloved mother, who sacrificed her life for me to live.

Acknowledgements

Completing my PhD thesis has been a long and challenging journey, and I would like to extend my sincere gratitude to everyone who assisted me in the completion of my research. To everyone who has inspired me and given me the confidence to succeed in this journey, thank you.

Firstly, I would like to express my deepest gratitude to my supervisor, Professor Harshinie Karunarathna for her unwavering support, encouragement, and invaluable guidance throughout my research. Her expertise, insight, and constructive feedback were crucial in shaping my work and helping me stay on track. I am truly fortunate to have had such an outstanding mentor. I would also like to thank Professor Dominic E. Reeve for his critical reviews and recommendations throughout my studies.

I am grateful to Energy and Environmental research group, where I was blessed enough to work with a talented and supportive community of researchers. I would like to thank my colleagues, especially for their support, friendship, and guidance during these research periods. Further thanks are due to all my friends across Swansea University who have supported me and often provided much needed escape from my studies, to help me regain focus.

I am also deeply indebted to Petroleum Technology Development Fund (PTDF) for providing financial support for my PhD studies. This support enabled me to conduct my research and attend conferences, which helped me broaden my knowledge and skills. Award Ref Number: PTDF/ED/PHD/NBC/1317/17,

Lastly, I would like to express my heartfelt gratitude to my family and friends for their unconditional love, support, and encouragement throughout my PhD journey. Their unwavering support and belief in me have been my driving force and source of motivation. Thank you all for being part of this journey and for making it a meaningful and fulfilling experience.

Abstract

Beaches change their shape in response to the incoming wave conditions. They may exhibit changes both in their longshore configuration and their cross-section. Beach cross-sections have been classified into different categories, broadly corresponding to different states that represent different balances between the physical forces arising between the waves, currents, and sediments. In this approach, beach evolution over time can be considered as a sequence of changes between different beach states. It is important to forecast impending morphodynamic states of a given beach. The main goal of this thesis focuses on deriving an empirical relationship between different beach states and incident wave conditions, using synthetic beach state simulations from a numerical coastal model, which would provide coastal managers with a simple and effective means of predicting how beaches will evolve over different timescales and therefore assist with the management of the beach. To create a database from which an empirical beach state variability model was developed, a process-based morphodynamic numerical model (XBeach :1D) was employed to generate different beach profiles based on over 300 wave simulations. The XBeach model was validated against a set of large-scale experimental data in order to develop a practical empirical model for evaluating different beach states. This numerical model was able to simulate morphodynamic changes of beaches with widely varying sediment characteristics and slopes from a large number of incident wave conditions. Different parameters were examined, but particular focus was put on describing the response of the nearshore berm formation and shoreline change with respect to the beach states. Hence, the Dean parameter, was used to represent the beach state.

Berm crest, berm height, berm length and shoreline change were extracted from the numerical simulations. An empirical formulation was derived to predict each of these parameters, thus determining the beach state variability for incident wave conditions. The formulation takes into account several factors, such as water depth, wave steepness, the slope of the beach, and a derived parameter from the data, which can all contribute to determining beach state variability.

The empirical formulation was also validated against beach profile change at a number of field sites with a wide range of characteristics (Narrabeen Beach, NSW, Australia, Hasaki Beach, Japan, Duck Beach, NC, United States, and an experimental data by Andrea Polidoro). The validation was based on selected storm profile on each field analysed.

In most cases, the empirical model captured underwater berm development satisfactorily, but shoreline change was not adequately captured. As a result of these findings, the results demonstrate that the shape of the antecedent beach profile is crucial, as all parameters are calculated based on the profile. Thus, the empirical model functions better for intermediate to dissipative beaches, whereas it underestimates all quantities for

highly dissipative beaches. The model's performance is particularly notable in accurately predicting various parameters for these types of beaches, enhancing our understanding of the complex interplay between beach states and wave conditions. Despite limitations, the model's practical implications are noteworthy for coastal management. It offers a valuable tool for informing strategies such as infrastructure planning. Additionally, its applicability to different coastal systems holds promise for broader insights into coastal morphodynamics, benefiting coastal communities globally. The empirical model will enhance understanding of the relationship between beach state and wave conditions, facilitating more effective coastal management and decision-making processes.

Table of Contents

List of Figures

List of Tables

List of Abbreviations

BSS	Brier Skill Score
CIEM	Canal d'Investigacio i Experimentacio Maritima (wave f lume)
DOC	Depth Of Closure
FRF	Field Research Facility
GLM	Generalised Lagrangean Mean
HORS	Hasaki Oceanographic Research Station
HPC	High Performance Computer
NLSWE	Non-linear Shallow Water Equations
NSW	New South Wales
SWL	Still Level
RESIST	Influence of StormSequencing and BeachRecovery onSediment Transport andBeachResilience
RMSE	Root Mean Square Error
UN	United Nations
UPC	Barcelona's Universitat Politècnica

List of symbols

A Wave action

A_{sb} Bed load coefficient.

A_{sb} Suspended load coefficient

B_c Berm crest

B_h Berm height

B_L Berm length

C Depth-averaged sediment concentration

c Wave speed

c_θ Propagation speed in directional space

C_d Drag coefficient.

Ceq Equilibrium sediment concentration

cg Wave group speed

cx Wave speed in x direction

cy Wave speed in y direction

Dh Sediment diffusion coefficient

Dw Wave dissipation

Er Total roller energy

Ew Total wave energy

f Coriolis coefficient

$fmor$ Morphological acceleration factor

g Acceleration due to gravity

h Water depth

H_b Breaking wave height

H_0 Deep water wave height

H_s Significant wave height

Hs/Lo Wave steepness

$Hrms$ Root mean square wave height

k Wave number

Lo Deep water wavelength

m Bed slope.

m_{cr} Critical bed slope

p	Porosity
Ps	Sediment density
Ps	Water density
Qb	Fraction of breaking waves
qx	Sediment transport rate in x direction
qx	Sediment transport rate in y direction
shc	Shoreline change
Sr	Roller energy
t	Time
Tp	Peak wave period
u^e	Eulerian velocity in x direction
u^L	Cross-shore depth-averaged Lagrangian velocity
u_{rms}	Near bed short-wave orbital velocity
v	Kinetic viscosity
v^e	Eulerian velocity in y direction
v^L	Alongshore depth averaged Lagrangian velocity
d	Sphere diameter.
ws	Sediment fall velocity.
zb	Bed level.
σ	Intrinsic wave frequency
$\tau_{sx}\tau_{sy}$	Wind shear stresses in the x-and y-direction, respectively.
$\tau_{bx}\tau_{by}$	Bed shear stresses in the x-and y-direction, respectively.
ξ	Surf similarity parameter.
Ω	Dimensionless sediment settling velocity.

Chapter 1: Introduction

1.1 Background

The coastline is the boundary between land and ocean which forms different morphologies. It has been reported that the coastline is one of the 21 most important surface features of the earth (Liu et al.,2019; Chen et al., 2019; Chen et al., 2022). Through history, coastal areas were preferred for settlement due to their distinctiveness in ecosystem diversity (Ercanlı et al., 2021), their potentials for offering rich and diverse activities like fishing and transport (Sardain et al., 2019; Elsayed et al., 2022), as well as for being rich trade and extensive tourism centres. These benefits along the coastline have led to an increasing rate of coastal habitation in time. In the 1990s, around 23% of the worldwide population lived within 100 km of the shoreline (Small and Nicholls, 2003; Valiela, 2006). This increased to 41% in 2003 (Martinez et al., 2007). Furthermore, the United Nations (UN) Atlas of the Oceans (2010) specified that the world's population of about 44% lives within 150 km of the coastline and the supporting infrastructure is concentrated in these regions. The coastal zone has progressively evolved because of the exploitation of the ecosystem services and the evolution of socio-economic activities.

Despite the benefits provided by the coastal areas, 24% of sandy/gravel beaches are eroding at a rate exceeding 0.5 m per year (Luijendijk et al., 2018). The increase in population and development of coastal cities has led to coastal squeeze and potential to influence transport pathways. As a result, these cities are subjected to various hazards including storm-induced flooding and sea level rise and other climate -related erosion and degradation (Figure 1) which has threatened the safety of coastal regions (Nguyen et al. 2020).

Coastal erosion from changing storms and global climatic conditions is bound to increase beach state variability. In the coastal zone, ocean waves are very dynamic and irregular by randomly shoaling, breaking, and dissipation of the energy. In doing so they interact with the seabed and influence the beach morphology or shape (Short and Jackson, 2013). Most beaches such as sand, gravel and mix beaches undergo non-linear evolution that is governed by hydrodynamic conditions, near-shore bathymetry, and geological setting as they exhibit rapid responses to high impact storm events (Stive et al., 2002; Caastelle et al., 2015; Masselink et al., 2015; Poelhekke et al., 2016)

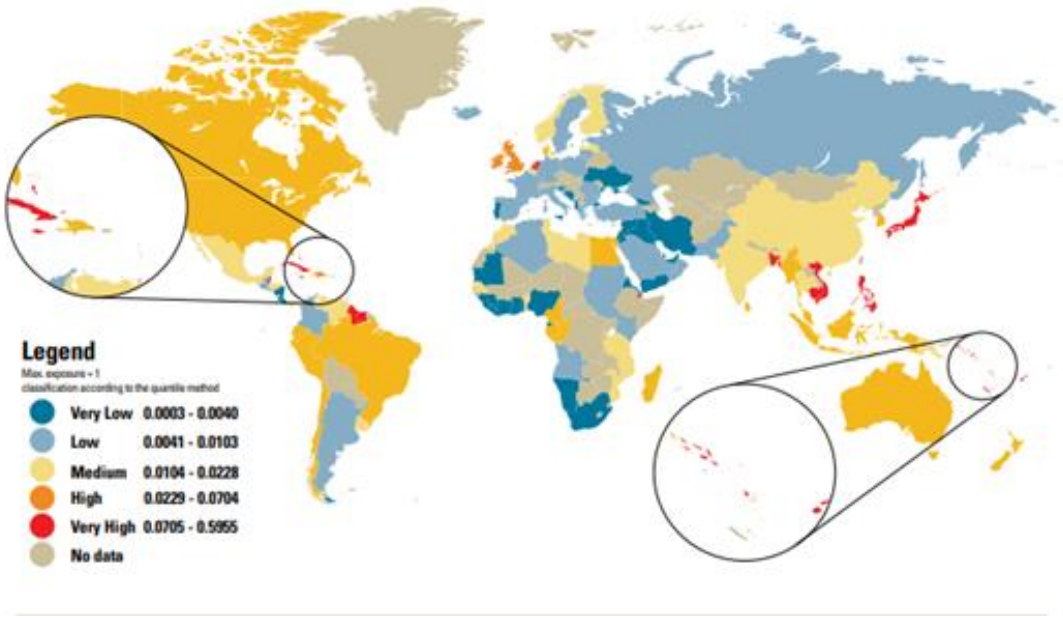

Figure 1.1 Exposure of Global nations to hazards (Becks,2014)

Beaches are highly dynamic and continually adjust to waves and tides. These changes cover a wide range of time scales, from hours to decades and longer, through large seasonal and interannual variability (Reeve et al., 2018; Stive 2004). This time variability is reflected in the evolution of the shoreline position for most existing proxies e.g., "high water line (HWL) or mean high water (MHW) (Boak & Turner, 2005) and in detailed evolution of the beach-dune profile. It is believed that beaches erode, and sediment is transported offshore during energetic/storm conditions, and they undergo natural post-storm recovery because of onshore sediment transport during calmer weather conditions (Wright and short,1984; Stive et al., 2002; Senechal et al., 2015; Karunarathna et al., 2016; Angnuureng et al., 2017). Storm-driven beach erosion typically occurs over hours to days (e.g., Harley et al., 2017; Lerma et al., 2022). After a beach is rapidly eroded during a storm, the post-storm recovery is a slow process (Eichentopf et al., 2019), typically taking days to months, (Angnuureng et al., 2017; Phillips et al., 2019; Castelle & Harley, 2020) while foredune recovery can take years to decades (Lee et al., 1998; Morton et al., 1994).

Erosion on beaches depends on several features. Sand beaches have gentler cross-shore slopes, and sediment size decreases from the backshore to the foreshore as swash intensity decreases. When the energy dissipation is at its greatest, the largest variation in sediment sizes occurs, whereas gravel beaches have a tendency for net onshore transport due to more energetic wave uprush followed by less energetic backwash (Komar, 1998; Pedrozo-Acuna et al., 2007; Karunarathna et al., 2012). Smaller sediment will be eroded rapidly than larger sediment. Provided that the morphology is in equilibrium with hydrodynamics, Wright and short 1984 indicate

that beaches could be dissipative, intermediate, and reflective based on the values of the dimensionless fall velocity which is calculated as:

$$\Omega = H_s/w_s T_p \quad (1.1)$$

Where:

H_s (m): Wave height

T_p (s): Wave period

W_s (m/s): Sediment settling velocity.

Beach states can be distinguished by morphological beach features where bar and berm are two of the most striking features of the two-dimensional plane of a cross-shore beach profile (Eichentopf et al., 2019). Beach state variability reflects either erosional or accretional sequences Figure 1.1. An increase of **Ω** values indicates a shift from reflective state (steeper profiles with greater amount of sand volume) to dissipative state (gentle slopes) with a pronounced bar/berm. On the other hand, decrease of **Ω** values indicates a shift from dissipative stage to either intermediate or reflective state. Several findings (Ranasinghe et al., 2012; Le Cozannet et al., 2019) suggest that global varying wave climates could be important for wave-dominated coastlines and subsequently in beach state variability.

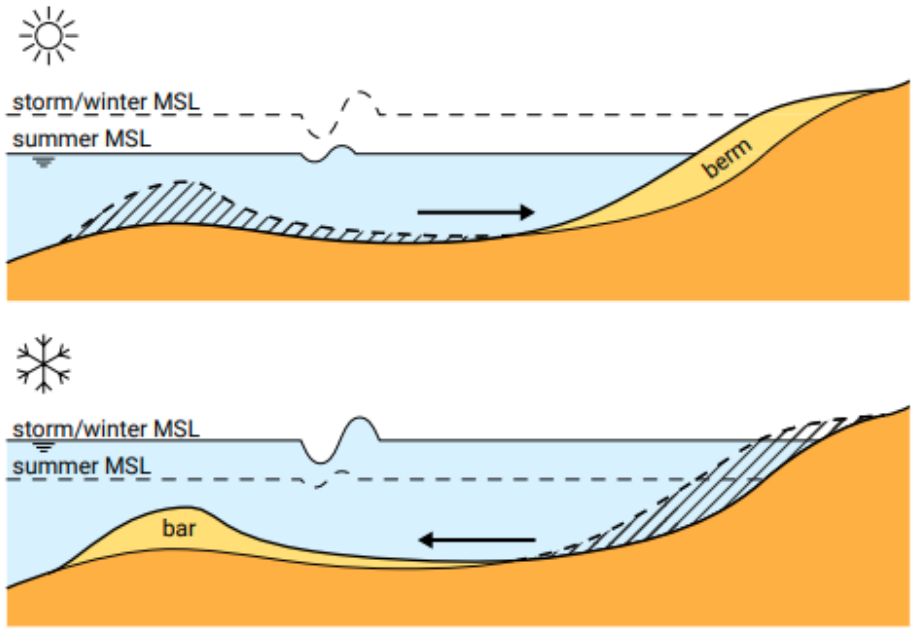

Figure 1.2 Seasonal transformation from a summer beach to a winter beach (Bosboom and Stive 2021)

Beaches that experience a wide range in wave breaker conditions through time will change state in an ordered sequence as energy levels increase or decrease (Sonu 1973; Short 1979). This ordered behaviour means that

by studying a set of beaches that represent a range of beach-states, insight can be gained into how morphodynamic processes evolve with cycles of incident wave energy (Wright et al., 1979; Wright 1982; Aagaard et al., 2013). A similar approach was adopted in this study to assess the morphology of beach states over different physical parameters that drive the beach change processes. Several approaches have been used to predict morphological changes or beach variability. For instance, physics-based numerical model's examples of these models are XBeach, Delft3D, and MIKE21are commonly used by coastal planners and engineers for shoreline management (Larson and Kraus, 1989; Steetzel 1993; Kobayashi 2016). The applications of such numerical models include simulating waves and sediment transport, illustrating changes in nearshore beach morphology and hence showing beach change. These models provide a detailed and accurate account of beach changes. Numerous conceptual and empirical models have also been developed (Kriebel and Dean, 1993; Larson et al., 2004; Palmsten and Holman, 2012; Simmons and Splinter 2022). They are seen as a comparable alternative to highly computationally intensive numerical methods. In addition, data driven models (Horrillo-Caraballo and Reeve 2010; Karunarathna et al., 2012a; Karunarathna et al., 2012b; van Veerserveld et al., 2015; Beuzen et al., 2019; Sanuy and Jimenez, 2021) that predict the morphological of the beach state variability have also been developed.

Currently, understanding beach variability remains a global challenge. Using numerical models is widely known to be laborious and computationally expensive (Murray 2007, Ranasinghe R. 2013, French et al.,2016). Also, they require extensive calibration and validation before applying to a specific site, which thus demands field measurements. Even data-driven models applied in beach studies which are largely site-specific require large number of historic measurements which mostly are not widely available, predicting beach morphology is difficult and this has been an underlying argument for employing data-driven methods (Reeve et al.,2016; Horrillo-Caraballo et al., 2016; Goldstein et al., 2019; Itzkin et al., 2022 Peach et al., 2023). To overcome these complexities some researchers have resulted in reduced physics or empirical approaches which include some aspects of physical processes, but these models still require either laboratory or field measurements. Following these literatures, it becomes challenging to conduct beach state variability study along coastal environment where data is limited particularly in the global south where this problem is compounded by limited resources. Nonetheless most literatures have no alternative because there is no simplified empirical formulation that can give strong predictive capabilities for beach state variabilities. For instance, to evaluate beach state variability using a numerical model such as XBeach over 20 validated parameters are required but in a simplified empirical formulation beach state variability can be understood with just a few parameters. Thus, there is the need to develop a simplified computationally less expensive model or formulation which is more generalised that could take in fewer parameters and come out with the desired result as other models. The empirical formulation can be utilised by coastal engineers and environmental agencies to enhance beach management strategies or mitigate the impacts of changing beach states. Efficient models address the need for timely, cost-effective, and accessible predictions of beach state variability in the nearshore zone, making them

practical for broad usage in coastal management. This study therefore focuses on the development of an Empirical model to predict beach state variability which surpasses the limitations of current approaches. This seems to be the first time that an empirical formulation is being developed for assessing morphodynamic response of beaches to incoming waves and beach state variability. For this purpose, the following aims and objectives are developed.

1.2 Aims and Objectives

The overall aim of this research is to develop a practical approach for assessing morphodynamic response of beaches to incoming waves and beach state variability. Here, we use a well calibrated process-based numerical model to develop a new empirical formulation that can recognize beach state variability based on varying wave climates without having the need to use computationally expensive process-based numerical models to have extensive beach measurements.

1.2.1 Specific Objectives

The following specific objectives will be considered in this thesis:

1. To develop a numerical model of cross-shore beach profiles based on process-based XBeach.

2. To calibrate and validate the numerical beach profile model using life-scale laboratory beach profile change measurements.

3. To simulate beach profile change of profiles with different slopes and sediment characteristics from different storm scenarios and determine the response of different beach states to a large number of storms conditions.

4. To assess the morphology of beach states over different physical parameters that drives the beach change processes.

5. To develop and validate an empirical formula using the synthetic beach profile change data in (3).

6. To validate the empirical model against beach state change at field sites with inherently different characteristics.

1.3 Thesis Outline

This thesis comprises of six chapters. A brief description of the contents of these chapters below:

- Chapter 2 presents literature on terminologies used in this thesis, types of beaches, model techniques, the hydrodynamic and morphological characteristics of beaches with particular emphasis on the well-known concept of beach states (Wright and Short, 1984).
- Chapter 3 describes the beach morphodynamic modelling and validation in XBeach model.
- In chapter 4 an analysis of the beach states is given. The analysis provides a basis for developing the empirical formulation and influence of water level on empirical formulation.
- Chapter 5 describes the field data sets and the methodology used to obtain the data and the verification of the empirical formulation against filed data.
- Chapter 6 gives a summary and perspective of this thesis. The chapter discussed the key contribution to research and presented some directions into future work.

Chapter 2: Morphodynamics of Beaches and Coastal Zones

2.1 Introduction

Coastal zones are among the most critical areas in the world and remain under pressure. Coastal zones are dynamic regions where the transformation of waves and energy dissipation drive various physical processes and restore the ecosystem (Masselink and Kroon, 2009; Reeve et al., 2012; Samaras et al., 2016). The physical processes that control the morphodynamics of the coastal zone are significant to scientists, policymakers, numerical coastal modellers and for forecasting the response of the coastal zones to variable ecological conditions (Dyke 2007; Omstedt 2011; Spalding et al., 2014).

In the nearshore region, there seems to be a strong nonlinear relationship between the hydro- and morphodynamic conditions. In the occurrence of waves propagating between the shore and the offshore, sediment from the coast could be eroded and deposited back offshore as an offshore inner bar or outer bar (Dean and Dalrymple,2004). Subsequently, a recovery process controlled by onshore transport of the eroded sediment from the offshore zone during low wave conditions could happen. The physical processes relating to the movement of sediment are responsible for erosion and accretion and the sediment process themselves in reverse influence the intensity of waves arriving at the coast (Bird 1976; Masselink et al., 2014; Angnuureng et al., 2017; Kamphuis 2020). The interplay between accretion and erosion due to the various forces at the shore has been happening since the last glacial age. These dynamics have become complex to predict (e.g., Wright and Short 1984, 1985) a consequence of inadequate comprehensive information such as beach states, hydrodynamic forces, and some form of morphology.

This Chapter provides a review on the physical processes, beach morphologies, beach characteristics, beach states and beach hydro- and morphodynamic processes that are relevant for the modelling of beach state variabilities. This study focuses on the nearshore region, and more specifically on the processes that are responsible for sub-tidal beach state variability related to underwater sandbars (hereafter berms) and shoreline changes.

2.2 The coastal zone presentation

The coastal zone has been defined in several ways depending on the thematic area. It is an area of social, economic, and ecological significance, all of which depend upon its physical characteristics, appealing landscape, cultural heritage, natural resources, and terrestrial biodiversity (Nicholls et al., 2007; Barbier et al., 2011, Reeve et al., 2018). The coastal zone can be made up of bays, beaches, and headlands. It is important to

understand how the coastal zone functions on a wider scale both in time and space (Viles and Spencer 2014; Reeve, 2018). Sediment of coastal zones are usually either sandy, rocky, gravel or mixed beaches that occur at uplifted lowland coasts and may be categorized into subzones, as shown in Figure 2.1. Each zone exhibits specific hydrodynamics and morphological features.

One of the important parts of the coastal zones is the nearshore, defined as the region between the beach and the edge of the offshore (usually measured from depths larger than 20 m as shown in Figure 2.1) The nearshore region is the region in which sediment is brought into motion by waves, currents, and tide (Dean and Dalrymple, 2002). The nearshore characterizes shorelines, sandbars, and beach cusps, that are highly dynamic and can be changed by changing hydrodynamic conditions on both short and long term (Wang and Davis, 1998; Dunkin 2010) scales. Figure 2.2 gives a pictorial view of the nearshore zone divided into zones of wave shoaling, the surf/breaking and swash. Most nearshore changes relate significantly to the type of sediment, the strength of the wave climate (Chowdhury and Behera, 2017; Dissanayake et al., 2021), and the influence of anthropogenic activities. For instance, sandy beaches erode rapidly compared to rocky beaches. The physical processes relating the fluid motions (hydrodynamics) to the movement of the sediments responsible for erosion and accretion are site-specific. In the lower latitudes or tropics, wave climate is stable compared to the higher latitudes. Thus, the understanding of the nearshore changes in those areas would also respond to the site-specific conditions.

The nearshore zone is widely known as the zone where sediment motion can be detected, beach sediment losses, erosion and accretion sources, and profile changes. Apart from the deep areas, i.e., the Depth of Closure (DOC), to the seaward limit of the breaking wave where it is assumed there is no sediment transport, the entire nearshore region experiences sediment movement as waves propagate to the shoreline. The shoaling zone on the other hand is where wave heights increase with dominance of infragravity-/skewed waves and onshore transport of sediment. The surf zone also known as the breaker zone is where waves become unstable due to speedier crest with depth decrease and breaking. Wave breaking is the most important process in the nearshore region. These phenomena control sandbar/berm formation in and out of the subtidal zone.

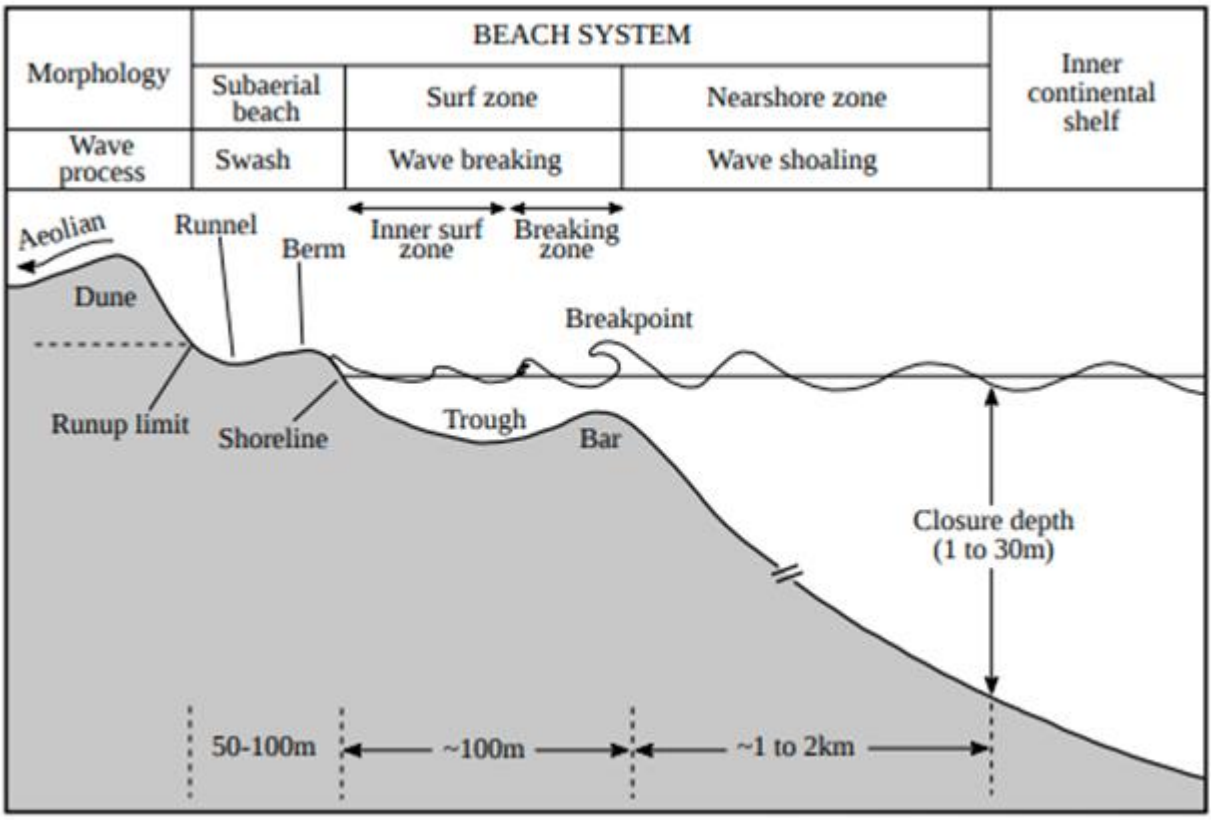

Figure 2.1 Coastal zone classification (Short 1999)

The surf zone also has control over subtidal morphology like the sandbar height, length, crest and subsequently the shoreline changes (Kroon and Masselink 2002; Leonardo and Ruggiero 2015; Cohn et al., 2017). Apart from the surf zone, the swash zone where the beach face is alternately covered by the run up and run down of waves also contributes sediments to morphodynamic processes. Horn and Mason (1994) found that as sediment moves through the swash zone, there is a big effect on the shape of the beach face.

Because the flow conditions change quickly and are not linear, moving sediment is a very complicated process in the nearshore (Kaczmarek et al., 2005; Aagaard et al., 2013; Angnuureng et al, 2017). It is believed that the correlation between waves and morphology is weak in the nearshore because there is a non-linear relation between them. Several studies on sediment transport in swash zones have been conducted over the years (Fredsøe and Deigaard, 1992; Turner and Masselink, 1998; Butt and Russell, 1999; Larson et al., 2004; Pritchard and Hogg, 2005) on swash zone sediment movement but most of these studies are not conclusive. Up to date information is limited on many other beaches.

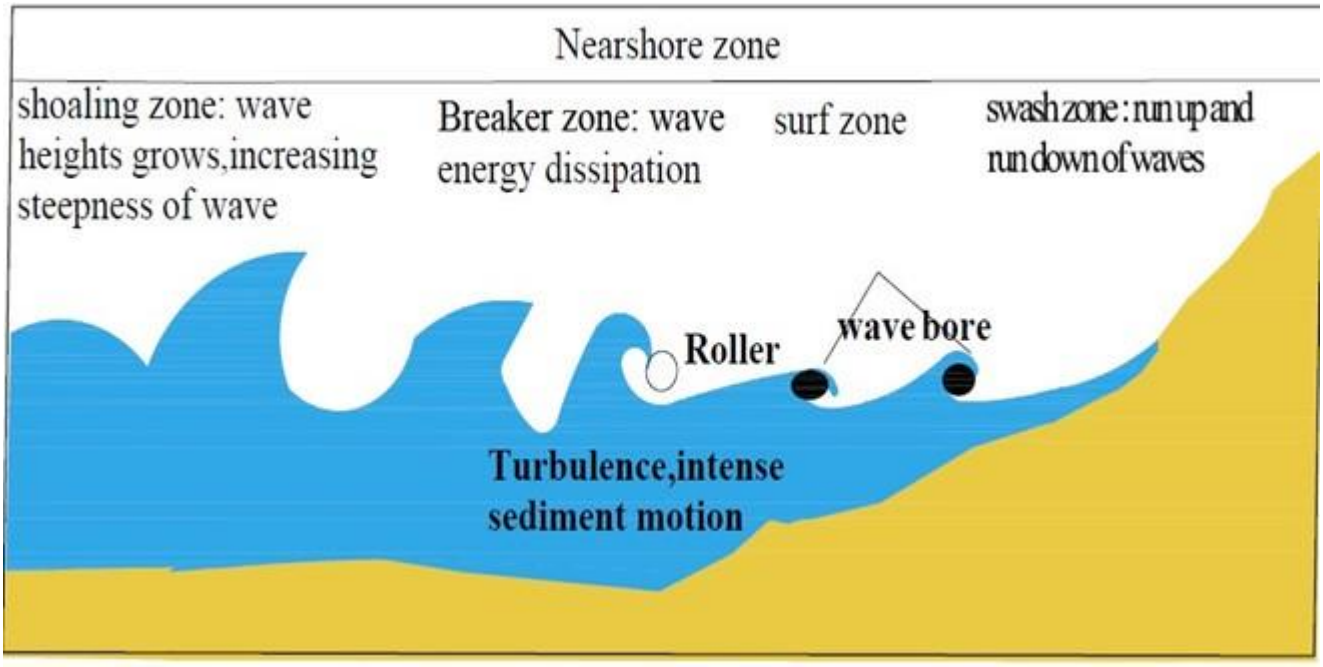

Figure 2.2 Schematic characterisation of near shore zone

2.3 Coastal Hydrodynamics

Predominantly coastal zones are subject to dynamic hydrological processes that drive beach morphology. Hydrodynamics could be defined as the interaction between waves, currents, sediment, and shoreline in coastal environments. It involves the complex dynamics of nearshore waves, tides, and currents, as a function of sediment transport and morphological evolution of the nearshore zone (Larson and Karus 1989; Komar, 1998; Fredsoe and Deigaard, 1992; Masselink and Hughes 2003; Ashton and Murray, 2006; Dean and Dalrymple 2004).

2.3.1 Wave generation and transformation

Most waves are generated by the effects of wind and local pressure. Both introduce energy to the oceanic water in the form of short waves. Globally, there are more severe forms of wave generation including earthquakes and volcanic eruptions. Tsunamis are caused by large-scale underwater disturbances, such as earthquakes, volcanic eruptions, and landslides. These events can displace a large amount of water, creating a series of large waves that can travel long distances and cause severe damage along coastlines. As waves propagate from deep into intermediate shores, the waves transform in wave height, length, and direction until they finally break and dissipate energy. Wave transformation takes place through various processes such as diffraction, refraction, shoaling, bottom friction, and wave breaking.

2.3.2 Wave refraction

When waves approach the underwater bottom contours at an angle, there is a variance in wave velocity along the wave crest due to variations in water depth along the wave crest (Pierson 1955; Nielsen 2009). This causes the wave crests to bend and align with the local bottom contours. This bending effect is called refraction. However, with different bottom shapes, refraction can cause both a convergence and divergence of wave energy in shallow and intermediate water depths. This change in direction can be determined using Snell's law:

$$\frac{sin\ (\varphi_2\ )}{c_2} = \frac{sin(\varphi_1)}{c_1} \tag{2.1}$$

With:

φ = angle between the local wave direction relative to the local bathymetry contours [degrees]

c = wave phase speed [m/s].

There are areas of erosion and accretion observed along many coastal areas that depend primarily on the direction of wave approach, the wave period, and the wave refraction pattern. In the nearshore zone, the movement of sand alongshore is due to the action of waves and currents. Wave refraction is an important process responsible for effecting changes in coastal configuration. As noted from several studies (Dalrymple, 1998; Siegle and Asp, 2007; Falques et al., 2021), the wave convergent and divergent zones are associated to wave refraction and the wave refraction can have greater transport rates. For example, longshore sediment transport was found to be higher in the northerly direction than in the southerly direction on SE Tamilnadu coast, India (Saravanan and Chandrasekar, 2015).

2.3.3 Effects of wave shoaling on bed slope

The process of shoaling is the increase of wave height and steepness as a result of declining water depth and reduced propagation velocity (Battjes and Jansseen, 1978; Holthuijsen 2010; Dongeren et al., 2007). Wave shoaling is the growth in wave height (H). Generally, waves slow down as they enter shallow water depths. The wavelength (L) reduces followed by a large decrease in celerity (c), while group celerity (cg) and wave period (T) remain constant. Shoaling is one of the processes that ensures the wave energy is conserved from deep water to shallow regions.

The effect of shoaling comes with the skewness of waves. The potential relevance of skewed wave and sloping beds on morphodynamic predictions is important for modelling nearshore bar dynamics (Walstra et al., 2007) as it influences the suspended wave related transports (magnitude and direction). Velocity skewness results in a phase shift between the orbital motion and the instantaneous bed shear stress increasing onshore bed load transport. Though the influence may be small, it affects bar migration and helps predict the observed

asymmetric bar shape. Skewed waves initiate sediment motion that could affect the suspended transports on steeper slopes. The modifications of bed-load direction and magnitude significantly affect the horizontal and vertical scour (Walstra et al., 2007).

2.3.4 Wave breaking

According to Babanin (2011), wave breaking is the process in which the surface of a wave folds or rolls over and intersects itself, causing large amounts of wave energy to be dissipated. This occurring form depends mostly on its bathymetry and wave conditions which results in various locations of breaking and differences in wave dissipation (The Open University, 1999a). Two factors influence the breaking of a wave; the wave's steepness (H/L), measured as the first factor, and the breaking index (γ) or the ratio of H to water depth (H/d). The limiting values for each criterion are 1/7 and 0.78, respectively, although γ may vary between 0.4-1.2 in practice (Reeve et al., 2004 Svendsen, 2005; Davidson-Arnott, 2010).

The analysis of the wave breaking phenomenon has been ongoing for almost 150 years (Robertson et al., 2013), and many research papers have been published approximating both the local geographic and geometric characteristics of breaking waves (Altomare et al., 2020). Review of original empirical work and the regions of applicability as provided by Bryson et al. (2013), give a historical perspective of wave breaking research which also illustrates advances in recent years. These published validity investigations by various authors show the variability and limitations and how the understanding in wave breaking parameters has progressed considerably. The understanding of wave breaking though has progressed annually, predicting the location, depth, and shape of the wave at breaking is still not universally defined and the impact the wave breaking could have on the general beach state changes or morphology is still not clear. This is in part due to the inherent variability in nature of breaking waves; however, it is compounded by a lack of a collective measurement and definition system for wave breaking parameters. Longuet Higgins (1970) analyses how longshore currents develop due to radiation stresses caused by oblique wave breaking.

Depending on the wave steepness and beach slope, four types of waves breaking; spilling, plunging, collapsing and a surging breaker have been categorized (Wiegel 1964; Galvin, 1968; Battjes, 1974; Wang et al., 2002). These breaker types can be estimated based on the surf similarity parameter (Battjes, 1974) given in Equation 2.2, which relates the bed slope to the wave steepness.

$$\xi = \frac{tan\beta}{\frac{\sqrt{H_0}}{L_0}} \qquad (2.2)$$

$$\xi_b = \frac{tan\beta}{\sqrt{H_b}/L_0}$$

where:

ξ = surf similarity parameter

$tan\beta$ = ratio of beach slope

H_b = breaking wave height

H_0= deep water wave height

L_0= deep water wavelength

The different breaker types are provided in the Figure 2.3, along with the associate ξ range.

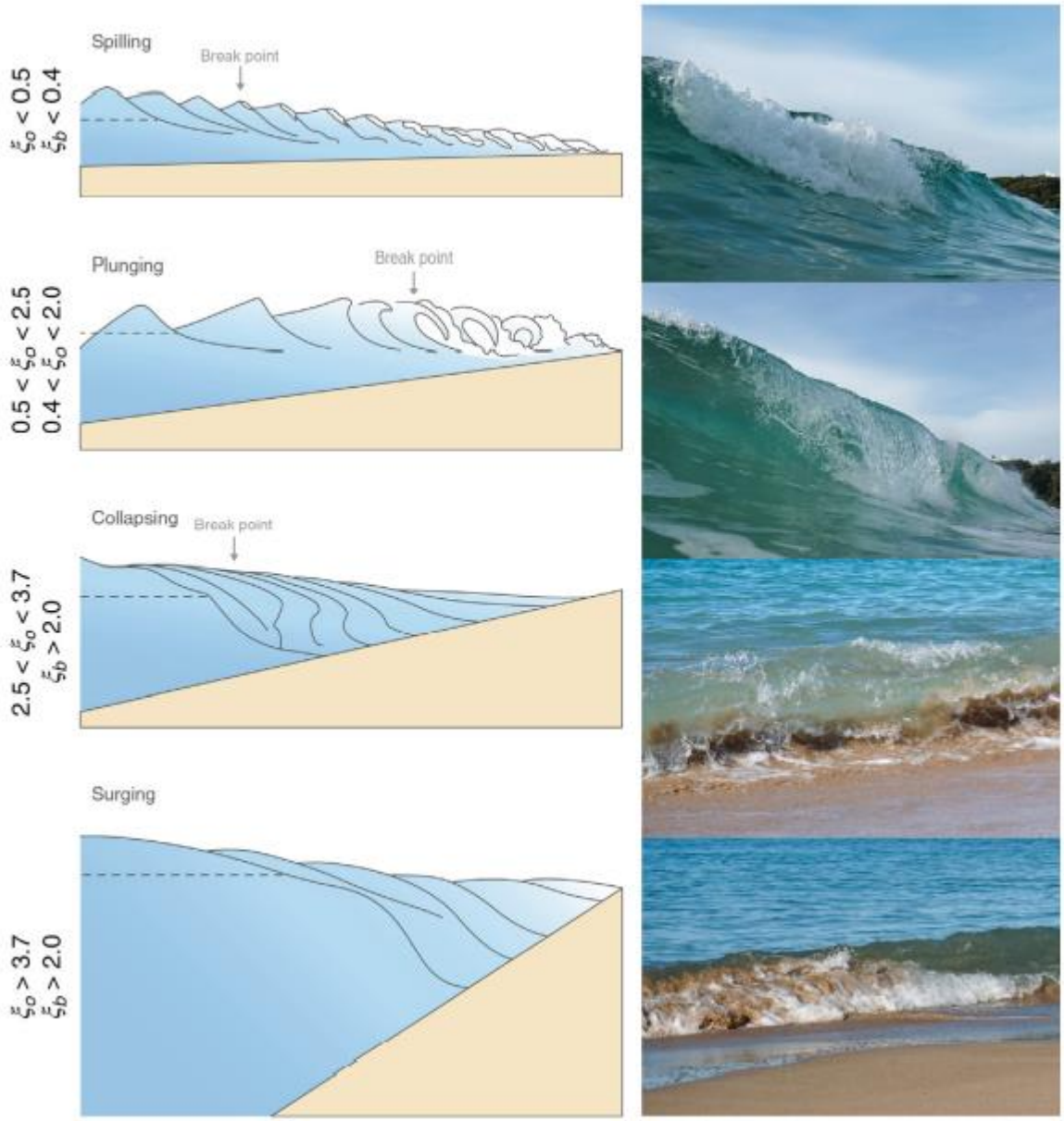

Figure 2.3 Different breaker types and its Iribarren number (Jackson and Short,2010)

Collapsing breaker results from a transformation between spilling, plunging and surging breakers depending on the value of ξ. The transition from plunging to surging is referred to as collapsing. Galvin (1968) defined collapsing breaker another type of breaker between a plunging and a surging breaker and thus in between breaking and non-breaking.

Spilling breaker are usually found along flat gentle beaches and are characterised by white water at the wave crest, and breaking begins at a relatively great distance from shore and gradually to the shore. Gradual reflection of wave energy back towards the sea occurs and all wave energy is dissipated in the breaking process.

Plunging breaker occur on steep beach slopes. Characteristic of this breaker type is the curling top. This wave causes typical curling top where most of the wave energy is dissipated into turbulence and only a small amount reflected.

Surging breaker occur along rather steep shores for relatively long swell waves and low steepness waves. In surging breaker, when the water becomes very shallow, it's the base of the wave front that becomes unstable, preventing overturning of the wave crest.

Wave diffraction

Diffraction occurs when propagation of a regular wave train has been obstructed by structures such as barriers, channels, breakwaters, or islands. These structures cause sudden transfer of energy along the wave crest, as the wave propagates into the sheltered region around the structure which results in a circular shaped wave pattern (Dalrymple and Kirby 1988). Reeve et al., (2018) stated that though these structures can take quite a few different shapes, their geometry is such that, as with the offshore break water, wave diffraction is used to assist in holding the beach in the lee of the structure. Diffracted waves are of less energy compared to the incident waves.

2.3.5 Wave-induced setup and runup

Much is dissipated when waves approach the coast by means of wave breaking in the surf zone in the form of a bore (Brocchini and Baldock, 2008), translating into runup on the beach. Wave set up can be defined as the set of discrete water level elevation maxima, which are measured on the foreshore with respect to the still water level (Goulay 1992; Stockdon et al., 2006).

Both waves and water level combine to influence beach evolution. Water level is governed by the tide, being either diurnal or semidiurnal, one and two tides a day, respectively. These water level variations control the area of the beach face that is being impacted by the wave action, for example under a constant water level, beach change is located around mean water level (Trim et al., 2002). Ground water flows are also strongly linked to the water level, as the water table responds to the pressure of tidal fluctuations (Kim et al., 2005). Infiltration and exfiltration are intricately linked to the water table, impacting the near bed velocities, and play a large part on coarse-grained beaches.

However, wave runup determines the potential for coastal erosion and flooding under energetic conditions following the transition between morphodynamic response e.g., beach erosion to dune erosion (Sallenger,2000) and over wash of coastal dunes (Matias et al., 2016). Stockdon et al., (2006) developed a parameterization scheme for runup on sandy coast using different beaches and wave conditions based on peak deep-water wavelength (L_O)deep water significant wave height (H_0)and foreshore beach slope (β). To accurately estimate shoreline location, quantifying the magnitude of runup or wave induced setup is crucial.

Plant et al., (2007) stated from empirical correction model that, to reduce shoreline elevation errors by 50%, setup and swash amplitudes are estimated.

2.3.6 Coastal Currents for sediment transport

As waves approach shore, they become asymmetric or skew and break nearshore to generate currents. Wave breaking generates longshore currents, undertow, rip currents and so on that shape the beach uniformly or non-uniformly depending on the beach state energy.

Undertow is a significant offshore directed current that is induced by a shoreward water mass flux under wave breaking and Eulerian drift in non-wave-breaking conditions (Borribunnangkun and Suzuki 2019). When wave breaking occurs, there is an onshore-directed mass flux of water that is balanced, in the nearshore, by an offshore-directed undertow. The undertow generates offshore sediment transport and affects swimming safety. The backwash created by breaking waves creates the undertow, with it being pulled underneath the next breaker, producing an undertow current. These currents extend seawards as far as the next breaker, with the magnitude of the breakers controlling its strength. (Clark et al., 2010; Dubarbier et al., 2017).

When the wave energy flux level is high, the undertow becomes larger (Borribunnangkun and Suzuki 2019). Undertow can be greater for low-tide than those for high-tide and the full data at a low wave energy level. Using a morphodynamic model (Kuroiwa et al., 2002), which considers the vertical distribution of undertow and suspended load concentration in the surf zone, undertow profiles were determined by using quasi three-dimensional model proposed by Kuroiwa et al. (2001). The sediment transport rate was considered the effect of the suspended. The presence of reflective structures or seawalls has an effect on wave breaking processes and mean flow distribution throughout the surf zone (Hoque et al., 2012). The presence of reflective structures therefore results in a meaningful change of wave breaking characteristics and turbulence structure in the surf zone. The organized large vortexes, which cause shoreward mass transport, will also be changed thus changing the undertow considerably. Storms cause significant undertows and offshore sandbar migration due to intense wave breaking, which also causes beach erosion (e.g., Sallenger et al., 1985; Roelvink and Stive, 1989; Gallagher et al., 1998). Undertow is associated with uniform 2-Dimensional beaches as this current does not result in changes on the Z-axis.

Rip currents on the other hand can develop when a barred shoreline has a strong undertow current because of morphological flaws in the bars. These are essential components of the bar region for the offshore transport of water as rip currents. Longshore feeder currents transport water into a fast-flowing rip-neck that extends from the confluence of two opposing feeder currents and transports water seaward to the rip head, which is a region of lower velocities seaward of the surf zone (Masselink and Hughes, 2003). Rip currents have substantially higher velocities than undertow currents, which can result in the offshore transfer of significant

amounts of sediment and make them extremely dangerous for leisure activities (Haller et al., 2014; Castelle et al., 2016). Because of the intensity of rips, they can change the beach state into a non-uniform 3-D beach.

2.4 Beach Morphologies and Sediment Transport

Morphodynamics could be defined as the study of dynamic interactions between hydrodynamic processes and the morphology of the seabed over a range of time space scales (Short and Jackson, 2013). The beach morphodynamics comprises the study of beach morphology, beach profile variability, beach profile and sedimentology including beach stability. The link between the hydrodynamic processes and the morphological changes is the sediment transport. Sediment transport in nearshore environments is driven by short waves (seas and swell), infragravity motions, and wave-induced currents. The short timescales of seas and swell are computationally challenging for models that must integrate their effects over storm-event timescales, thus most morphodynamic models consider time-averaged waves and resolve more slowly varying currents. Beach changes originate from in ambient and antecedent conditions, and a dynamic equilibrium exists between the two, with the nature of morphological change controlled by both the ambient and antecedent beach morphology (Wright and Short ,1984; Masselink and Short, 1993; Jackson et al., 2022). Sediment diameter plays a significant role in the changes of the beach slope (β) due to the natural angle of repose of the sediment and the effect the sediment has on the ground water flow within the beach. The distribution of sediment on a beach also affects their transport. While the sediment distribution is usually described by the median size D_{50} the uniformity, grading, and sorting on composite beaches other factors such as wave characteristics, breaker type, tidal range, long shore currents and the swash of sediments play a very crucial roles in changing the beach profile.

Typically, sediment transport consists of two different processes, bed load transport, where the sediment is moved along the bed or close to it, and suspended load transport, where sediment particles are carried in suspension within a turbulent water column (Reeve et al., 2012). Whether bed load or suspended load, the controlling factor remains to be the grain sizes. The first theoretical description of sediment transport was proposed by Einstein (1950). He based it on the number of particles deposited in a unit area being dependent on the number of particles in motion and the probability that the dynamical forces permit deposition. The number of particles eroded from that same area is dependent on the number of particles within the area and on the probability that the hydrodynamic forces on these grains are sufficiently strong to move them. Thus, for equilibrium conditions, the number of grains deposited must equal the number of particles eroded. This theory has since been further revised to consider several initial assumptions (Bagnold, 1954; Luque, 1974; Fernandez Luque and Van Beek, 1976). Most current formulations for bed load transport combine several concepts related to the bed shear stress and the critical threshold for the initiation of motion (Fredsøe and Deigaard, 1992). When the effects of waves are considered alongside the current, sediment transport is more

difficult to predict as the bed shear stress, sediment mobility, and near-bed currents are altered (Soulsby, 1997; Roelvink and Reniers, 2012).

Whereas the bed load transport reacts quickly to changes in flow and wave conditions, suspended transport is indirectly related, as the sediment concentration field adjusts. When the flow accelerates due to wave action and currents, the concentration will be lower than for uniform conditions, as the sediment must be transported upwards through turbulence. When the conditions are calmer the sediment settles out as it can no longer be supported in suspension (Roelvink and Reniers, 2012).

Whether it is bedload or suspended load, sediment is either transported cross-shore or alongshore. The direction of transport depends on the strength and direction of currents and waves. On many beaches cross-shore transport is limited to undertow and rib currents which subsequently generate underwater berms. Cross-shore sediment transport may however result in permanent loss of sediment in trenches and no recovery at eroded parts. Longshore transport contributes more to the provision of sediment to adjacent beaches.

2.4.1 Beach gradients

Beach gradient refers to the slope of the beach, the angle between the horizontal plane and the beach surface. The gradient of a beach can be steep or gentle, depending on several factors including the type of sediment, wave energy, tidal range, and coastal erosion. (Doornkamp and King 1971; King 1972).

In general, beaches with finer sediments (such as sand) tend to have gentler gradient, while those with coarser sediment (such as pebbles or boulders) tend to have a steeper gradient. Wave energy plays a role, as beaches that are exposed to high energy waves tend to have gentle gradients due to constant reshaping and erosion of the beach (Bascom 1951; Short 1996).

Tidal range can also affect the beach gradient, as beaches in areas with large tidal ranges may have a more gradual slope as sediment is constantly redistributed by tides. Finally, coastal erosion can also impact beach gradient, as erosion can cause the beach to become steeper as sediment is removed from the shoreline (Passeri et al., 2015). Beach gradient is therefore an important consideration for coastal engineering projects, as it can impact the stability of coastal structures and affect the behaviour of waves and currents in the nearshore environment.

2.4.2 Bar-berm beach dynamics

Beaches exhibit seasonal onshore/offshore sand transport (Shepard, 1950; Shepard and Inman, 1951). This follows summer-winter (or bar-berm) behaviour (e.g., Shepard, 1950) as a straightforward yet well-known example of parameterization. It is based on such observations that the shape of many beaches is believed to progress from non-barred to barred profiles. All beaches are in one-dimensional structure of erosion or accretion. The two most common beach profiles are the swell profile, which is created when the waves are low in steepness, and the barred profile, also known as the storm profile, which is created when the waves are

high in steepness. Variations in the driving conditions cause uniform sediment migration onshore and offshore (Bird, 1983; Mentaschi et al., 2018). It is anticipated that no material will be lost offshore during the exchange of material between the bar and the berm. The volume that has been eroded due to berm erosion is thought to be contained in a single offshore bar (or, representative morphological volume), which will eventually attain a specific equilibrium bar volume assuming the wave conditions are stable, and the grain size does not change. The sandbar volume will increase and vice versa if the bar volume is currently less than the equilibrium volume. Figure 2.4 illustrates how high bar elevation or volume results in a decrease in berm volume (and shoreline retreat) and decay in bar volume causes an increase in berm volume (and shoreline advance). Hence, alongshore averaged (or two-dimensional 2D) cross-shore sandbar dynamics can be seen as a morphological adjustment to the hydrodynamic forcing (Aagaard et al., 1998), and more specifically, as the convergence of sediment transport at the breakpoint.

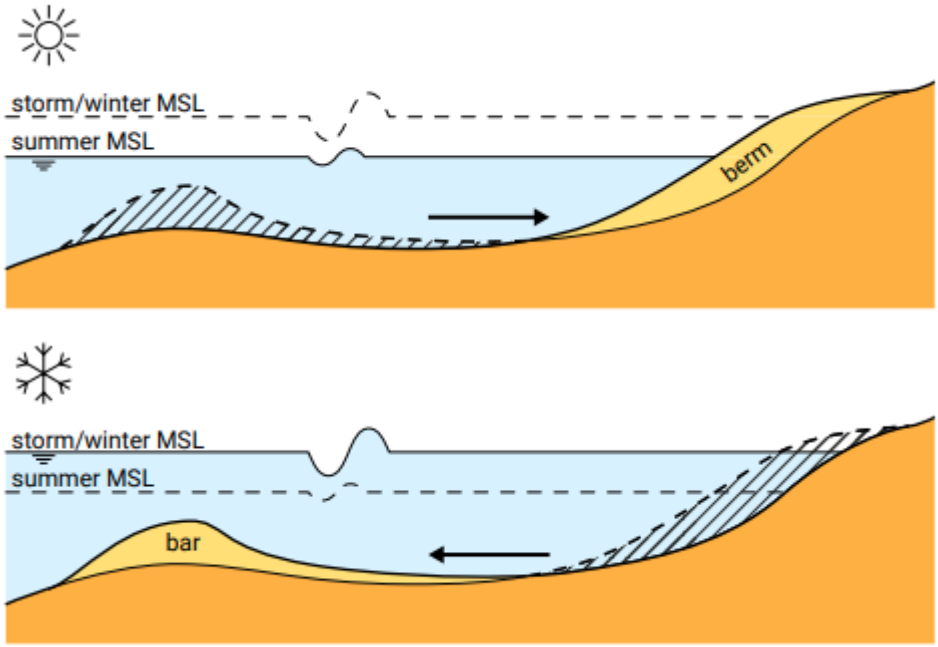

Figure 2.4 Seasonal transformation from a summer beach to a winter beach (adapted from Bosboom and Stive, 2021)

Longshore bars are in regular view on wave-exposed beaches and have an impact on the foreshores (Takeda and Sunamura, 1992; Larson and Kraus, 1992; Schwartz, 2012). They make up the predominant form of bed variability in the submerged nearshore region. While most coastlines exhibit annual cycles, with offshore migration during the active winter months, major shifts also happen on a much shorter time limit, notably in reaction to storms. It has long been understood that during storms or energetic conditions, sandbars move seaward (via the undertow current) and move landward under low energetic conditions (Birkemeier, 1984; Gallagher et al., 1998; Hoefel and Elgar, 2003). A sandbar is typically placed further out to sea after the high-wave months of autumn and winter than after the low-wave seasons of spring and summer. Long-standing research has shown that sandbars strongly influence where waves break (Lippmann and Holman, 1989; Plant

and Holman, 1998; Ruessink et al., 2007) and, consequently, the patterns of cross-shore sediment transport. This control over wave breaking location and subsequent cross-shore sediment transport patterns may reinforce further bathymetric modifications like slope of the beach profile (Plant et al., 2001) through feedback on hydro-morphodynamics. A wave breaking across an outer bar, for instance, has an impact on the hydrodynamics and, consequently, the development of an inner bar. The frequency of obliquely breaking waves will affect sediment movement because they cause longshore transport (Bodge, 1989; Miller, 1999). They will also have an impact on the type of sandbars that form. The most common sandbar morphologies, according to Lippmann and Holman [1990], are longshore-periodic (rhythmic) bars, which are unstable linear bars that appear under high wave conditions (mean residence time = 2 days). Shore-attached rhythmic bars, which typically form 5–16 days after peak wave events, were determined to be the most stable (a mean residence period of 11 days). The beach modifications are more complex than the typical 2D structure due to the non-rhythmic, three-dimensional bars, which have a short average resident time of just three days. This suggests that up-state, erosional transitions (based on offshore bar migration) are better described by an equilibrium model where response is better correlated with incident wave energy than with the preceding morphological state. Transitions to higher states occur under increasing wave energy among the possible higher beach states.

2.4.3 Shoreline dynamics

For coastal scientists, engineers, and those involved in coastal management and engineering design, shoreline change is a crucial factor. The position of the shoreline (Boak and Turner, 2005) and its historical rate of change can offer crucial information for the design of coastal protection, plans for coastal development, the calibration and testing of numerical models (Hanson et al., 1988).

The shoreline has been extensively studied for example, Crowell et al., (1991) Moore et al., (2000) Stockdon et al., (2002) Boak and Turner, (2005). Indicators (proxies) based on geographic, morphological, or hydrodynamical considerations are frequently used to identify shoreline (e.g., List and Farris, 1999; Zhang et al., 2002; Stockdon et al., 2002; Boak and Turner, 2005). To study shoreline variability and trends, the temporal and spatial variations of a coastline must be researched based on a functional definition of the term "shoreline" (Boak and Turner, 2005).

A shoreline is best described as the physical interface of land and water (DOLAN et al., 1980; Horikawa, 1988; Boak and Turner 2005). Although it seems simple, it might be challenging to put this definition into practice. In reality, the position of the shoreline shifts throughout time as a result of cross-shore and alongshore sediment movement in the littoral zone and, in particular, as a result of the dynamic nature of water levels at the coastal boundary (e.g., waves, tides, groundwater, storm surge, setup, runup, etc.).

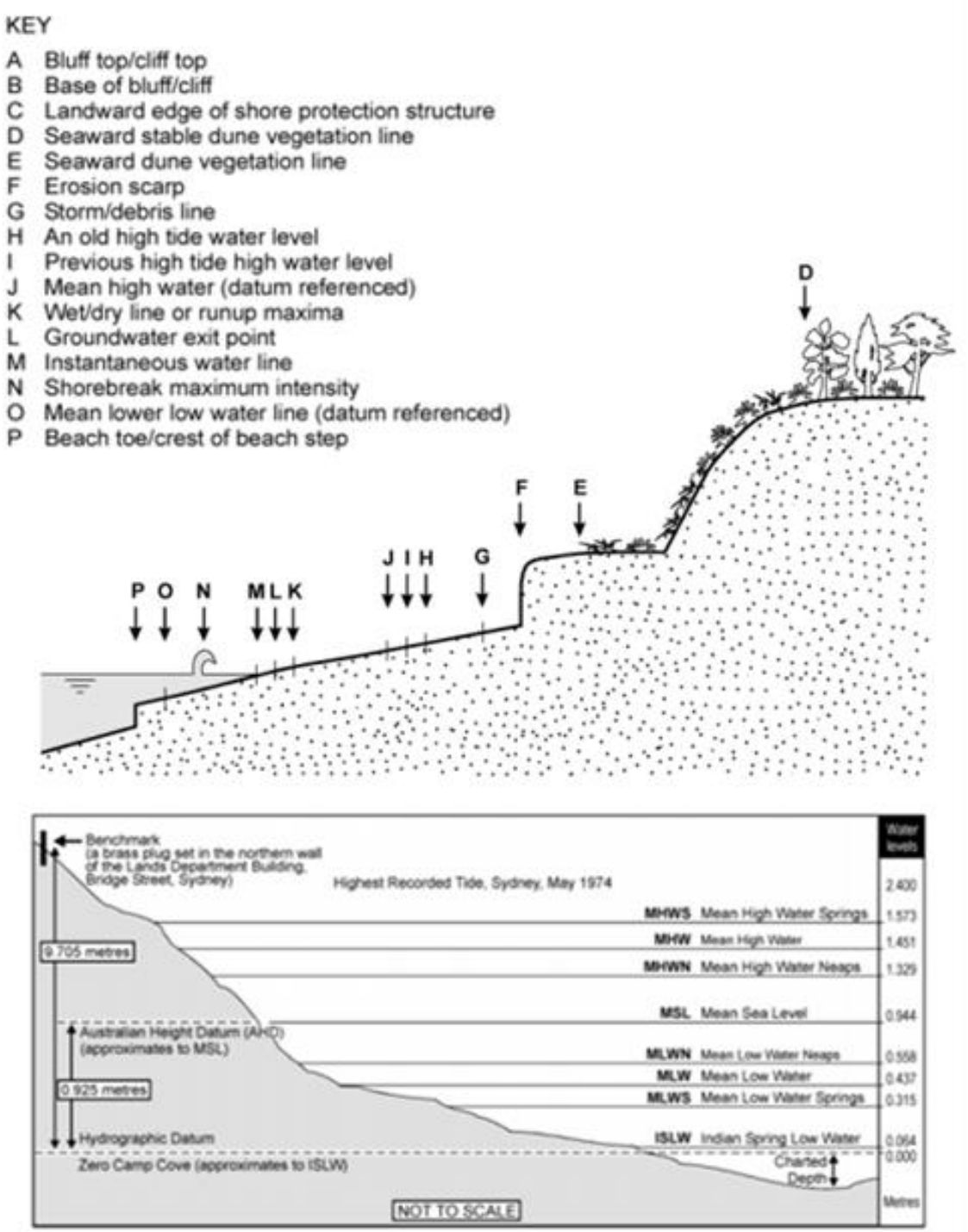

Figure 2.5 Shoreline definition and detection (Boak and Turner, 2005)

2.5 Beach States

Wave movement affects a wide variety of beach morphological characteristics and states. These states are quite different from one another, and the local wave and sediment features are mostly what govern them. As this research involves modelling of beach state variability, sand beach is the only beach type discussed herein.

The median grain size (D_{50}) of the sediment on the beach can be used to categories wave-dominated beach conditions quickly and easily. According to Soulsby (1997), there are three different types of beaches based on the features of the sediment: mixed (D_{50} = 0.1–250 mm), gravel (D_{50} = 2-250 mm), and sandy (D_{50} = 0.1–2.0 mm).

Dean (1973) who used Gourlay's (1968) dimensionless fall velocity to make a cross-shore sediment transport model that predicted how the beach would change, was the first to come up with a more complete and useful way to classify beaches. According to Wright and Short (1984) there are six different natural beach states based on the dean parameterisation (Figure 2.6). The hydrodynamic processes, sediment characteristics and morphology act as function of beach states. The beach state is dependent on the sediment characteristics, tide, wind conditions, immediate and antecedent wave conditions, and the antecedent beach state. The interaction between geological (e.g., sediment, beach slope) and hydrodynamic features (e.g., wave height, tide range) therefore determines a morphodynamic continuum of beach types which are classified according to their appearance. The beach states range from fully dissipative to highly reflective beaches. Fully dissipative beaches are more shallow and approach an almost flat slope and on the other side, highly reflective beaches have a steep slope. Reflective beaches consist of coarse sediment, whereas on dissipative beaches, there is much fine material.

Dissipative beaches are characterised by the high-energy end of the beach spectrum and long-period waves that break by spilling and dissipate progressively as they cross the surf zone with one or multiple linear bars. They are basically, the opposite of reflective states. The sediment material is relectively fine, and the beach has a wide surf zone with a low shore normal gradient, and little alongshore variations are typically present. These high energy conditions are typical for storm wave exposure and asssociated variability results in a highly dynamic coastal profile (Bosboom and Stive, 2015).

Reflective beaches are characterised by lower–energy waves that either surge or collapse on the steep beachface. The sediment material is coarse and characterised by a steep and narrow beach face with a berm and a narrow surf zone without bars. These beaches are the result of a period of mild wave conditions that transport sediment onshore (Bosboom and Stive, 2015). The reflective beach can be compared to a typical ‘summer’ profile as seen in Figure 2.4. In contrast to the dissipative beach where waves break, waves on a reflective beach will reach the beach face without breaking and surge onto the beach.

Intermediate beaches contain both dissipative and reflective aspects and have a complex morphology of all the beach states as stated by Wright and Short (1984). The intermediate beach state has four-sub states (Figure 2.6) with diverse morphological features. Respectively, the beach states correspond to winter and summer profiles as seen in Figure 2.4 and 2.6. To include the sediment characteristics in their conceptual model of morphodynamic beach states, Wright and Short (1984) used a dimensionless fall velocity Ω (Dean, 1973) for the classification , Equation 1.1.

Here, low values ($\Omega < 1$) correspond to reflective beaches, $1 < \Omega < 6$ intermediate beaches and $\Omega > 6$ dissipative beaches.

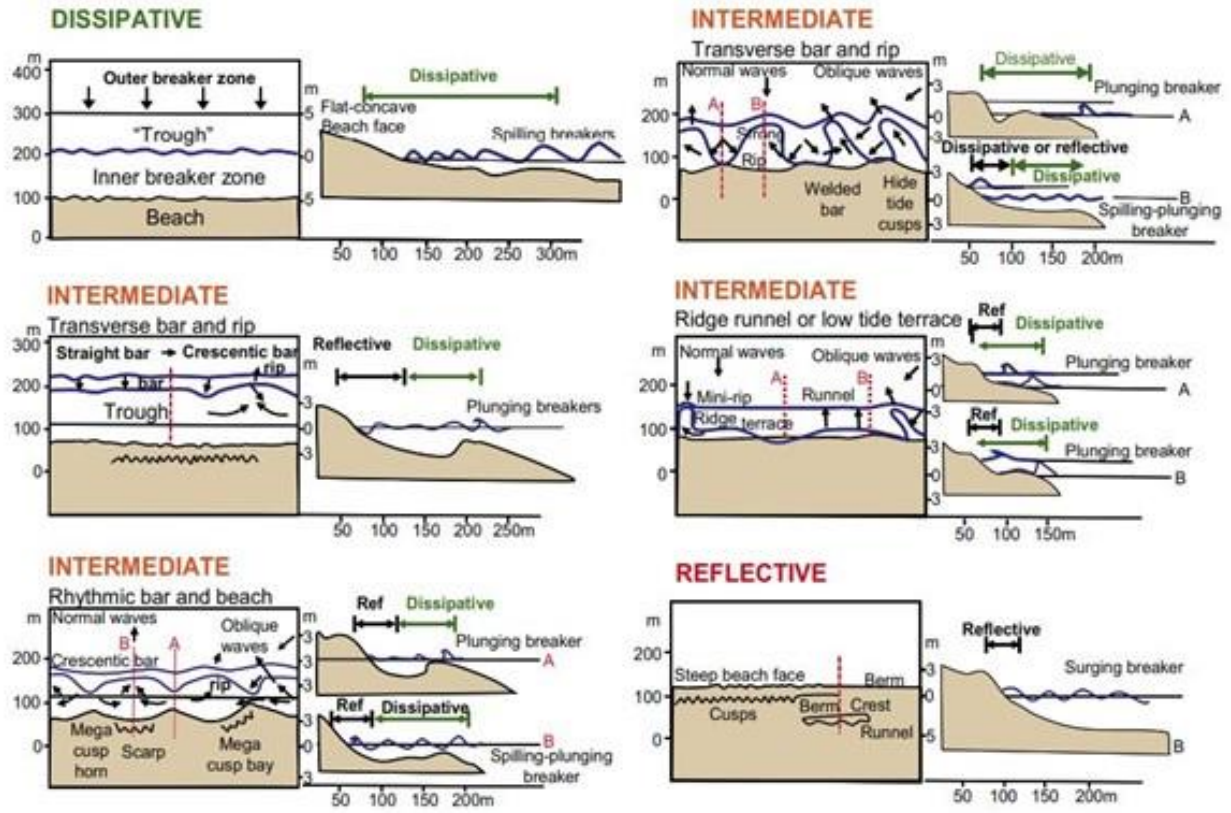

Figure 2.6 Wave dominated beach types, ranging from dissipative (top left), to four intermediate states characterised by bars moving further offshore toward the dissipative state, with reflective (lower right) (McLanchlan and Defeo, 2017).

2.5.1 Beach erosion

Coastal erosion and accretion, both of which have existed, help to shape the current coastlines. Thus, due to human activity, coastal erosion has significantly increased in recent years. Erosion is a growing problem around the world (Paskoff 1983; Bird 1985; Hanson and Lindh 1993; Van Rijin 2011; Komar 2018; Gonçalves and Ferreira 2022) causing loss of lives, property, and ecosystems. Erosion rates depend on many conditions around the beach. In terms of sediment types, sandy beaches are subject to higher erosion, which is a completely different physical process than inundation.

During storm events (erosive), erosion is also severe, the bottom sediments are mobilised within the breaker zone from a combination of the wave orbital velocity and the breaker-induced turbulence. A significant amount of offshore sediment is transported when there are high-energy wave conditions because of the turbulence and return flows caused by the breaking waves (Karunarathna et al., 2012). This causes shoreline recession, and the beach erodes. Theoretically, erosion brought on by offshore sediment movement during storms should be followed by a similar accretion as post-storm waves deposit the material back onshore, but this does not seem to be the case in most instances (Wright and Short, 1984; Hanson and Lindh, 1993; Gillie 1997; Karunarathna

et al., 2012). The beach can recover from an eroding storm event within days or maybe never at all (Karunarathna et al., 2014; Ranasinghe et al., 2012). Several factors influence the shape of the beach profile after a storm. The condition of the beach before the storm event is just as significant as the storm event parameters (wave height, wave period, wave direction, and storm duration). For the creation of a framework for modelling medium-term beach profile variability, the inclusion of antecedent beach states is crucial.

2.5.2 Beach Accretion

Beach accretion is the accumulation of sediment on the shoreline due to onshore sediment transfer during calm incident wave conditions, river discharge or alongshore drift deposition. During these times, as opposed to storm occurrences, weaker return flows that cannot carry significant amounts of sediment offshore deposit the sediment onshore. Beach accretion is influenced by several factors, including sediment features, the strength and direction of wave and current action, the slope and shape of the beach and the presence of coastal structures such as breakwaters.

2.6 Modelling of nearshore processes

Many studies in coastal areas involve morphodynamic modelling at some point, and some use an array of models to predict the change in morphodynamics due to natural or anthropogenic causes. Sometimes these models are run independently as they answer different questions related to the same problem.

A model is a simplified representation of a real system created for demonstration, descriptive, hindcasting, real-time monitoring, forecasting, or design purposes. Each method has its set of benefits and drawbacks, as well as simplifications and assumptions. Process representation within models is becoming both wider (as more processes are added) and deeper (as detailed physics replaces earlier parameterizations). Algorithms for wave-induced flows and sediment transport under shoaling waves are among the recent developments (Sherwood et al., 2022). Community and open-source models have become the norm. Observations of initial conditions (topography, land cover, and sediment characteristics) have become more detailed, and improvements in tropical cyclone and wave models provide forcing (winds, waves, surge, and upland flow) that are better resolved and more accurate, yielding adequate improvements in model skill. It is projected that future storm-impact models will increasingly resolve individual waves, apply data assimilation, and be used in ensemble modelling modes to predict uncertainties. Numerical models play crucial roles in estimating the beach profile hydrology and morphologies. Many studies have classified models according to the methods used such as physical models, statistical models, parametric or equilibrium models, analytical models, process based or numerical model, and behaviour based numerical models (e.g., Wolinsky, 2009; Reeve et al., 2016).

2.6.1 Modelling techniques

Various modelling techniques are used in coastal engineering to study various aspects of coastal systems. Models of coastal morphodynamic evolution differ considerably in terms of their complexity, computational requirements, stability, and time horizon for prediction. Each model has its pros and cons, simplifications, and underlying assumptions. Classifying models can therefore ensure that a model is selected adequately based on user requirements, the availability of calibration data, and generally accepted best practices. As more models are developed and combined, the classification of coastal models (De Vriend, 1997; Wolinsky, 2009; Reeve et al., 2016) becomes increasingly difficult. In general, models are classified according to their spatial (meters/km), temporal (short-term/long-term), or dimensional scales (e.g., profile, depth-averaged littoral area, 3D models). New developments are based on the coupling of distinct models, each of which can resolve distinct temporal/spatial dimensions and/or processes, as technology and process knowledge advance.

Roelvink and Reniers (2012) categorised coastal morphology models into three types, primarily due to their dimensionality: (a) one-dimensional (1D) cross-shore profile models (Roelvink and Brøker 1993; Schoonees and Theron 1995), including equilibrium shoreline models (Miller and Dean 2004; Yates et al. 2009, 2011); (b) 1D alongshore coastline models (Ashton et al. 2001; Ashton & Murray 2006; Davidson et al., 2013; Splinter et al. 2014; Vitousek et al. 2017); (c) two-dimensional (2D) and three-dimensional (3D) models (de Vriend et al. 1993, Nicholson et al. 1997). Vitousek et al. (2017) presented physics-based models to solve conservation equations for the mass and momentum of water and sediment and attempted to treat all the processes important to coastal evolution, whereas process-based models focus on a single dominant phenomenon. From the review of Sherwood et al. (2022), it is noted that all models rely on empiricism. Thus, in this research four models were discussed Equilibrium models, Process-based model, Data-driven model, and Hybrid models.

2.6.2 Equilibrium Models

Beaches are remarkably resilient, despite responding to and being spatially translated by eustatic and isostatic changes in sea level. The longevity and adaptation of beaches to sea level change (e.g., raised beaches) strongly suggests that beach systems are in a state of dynamic equilibrium. When a beach profile is considered over longer timescales (centuries), rather than short and medium timescales (months and years), it is common to find that ocean-facing beaches have a concave curve that becomes more gently sloped with distance offshore.

Bruun (1954) was the first to investigate the concept of the equilibrium profile, proposing a simple relationship in Equation. 2.3, for determining water depth (h) at a distance (x) from the shoreline, using a sediment dependent parameter (A). Dean (1977) confirmed this relationship with A being related to the sediment fall velocity (W_s) given in Equation. 2.4 as a result of fitting a linear relationship to the experimental data obtained by Moore (1982).

$$h = Ax^{\frac{2}{3}} \tag{2.3}$$

$$A = 0.067 w_s{}^{0.44} \tag{2.5}$$

Dean (1991) conducted additional research to support Bruun's (1954) relationship to physical principles. Several profiles representing laboratory and field scales were analysed, and it was determined that Equation 2.4 is a reasonable approximation. In addition, methods for quantifying the shoreline response due to elevated water levels and wave heights on both natural and seawall shorelines are presented. While this work supports its use for a wide range of problems, the mathematical form has several flaws (Reeve et al., 2011). For instance, the beach slope at the top is infinite as x tends to infinity, the beach depth increases infinitely offshore, and barred features are not captured.

There have been several efforts to combat the flaws. Some studies have developed the alternative form described in Equation 2.6. The equation asymptotically approaches the depth of closure (d_c) at the seaward boundary and has a slope of $d_c\,K$ at the shoreline where the depth of closure is defined as the seaward limit of significant cross-shore sediment transport (Bodge, 1992; Komar and McDougal, 1994). Pruszak (1993) discovered a best fit for profiles in the Baltic Sea by allowing the value of A to vary sinusoidally with time to extend the use of equilibrium profiles for barred coasts. Several other approaches have divided the profile into segments and specified different parameters for each of them (Inman et al.,1993; Wang and Davis, 1998). It is also noted that this approach of segmenting the beach can be used for beaches that have spatially varying sand sizes (Dean and Dalrymple, 2004).

$$h(x) = d_c\,(1 - e^{-kx}) \tag{2.6}$$

Although equilibrium profiles like Bruun's (1954) are easy to use, they have caused a lot of controversy. Ranasinghe and Stive (2009) concluded that the Bruun rule should only be applied to qualitative first-pass regional assessments and not at the local scale. The Bruun rule requires the specification of several input parameters that contain significant uncertainty. For example, using four different depth of closure formulations at Sydney, Australia, gave an uncertainty range that resulted in recession estimates from the Bruun rule varying by 500% (Ranasinghe et al., 2012).

Discussion of equilibrium models has thus far focused on the Bruun rule and cross-shore limitation, however, there are other equilibrium models for shoreline prediction. Davidson et al. (2013) created a one-dimensional behaviour-oriented model *(ShoreFor)* to represent the shoreline displacement induced by wave-driven cross-shore sediment transport. *ShoreFor* takes into consideration hysteresis effects, such as the fact that present shoreline modification is influenced by past conditions where the potential magnitude of shoreline alterations grows with incident wave strength and disequilibrium expressed in terms of time-evolving equilibrium and

instantaneous dimensionless fall velocities (Wright et al., 1985). The *ShoreFor* model was successfully employed to explore beach reaction at a variety of beach locations and timescales (Splinter et al., 2014). Despite their ease of use, the main disadvantages of these equilibrium models are their limited applicability to capture the impact of storms and other short-timescale events, such as initial development of post nourishment which appears to be a gap in the model. They are also inapplicable in areas with complex two-dimensional flows because wave transformation and sediment transport approaches are typically only valid for alongshore uniform coasts. However, they are still being developed to broaden their applicability and challenge these limitations. Other existing equilibrium models are Long-term shoreline change, Sediment budget model, Coastal vulnerability index etc., with each having its strengths and limitations.

2.6.3 Process-based Models

In coastal engineering, process-based models are commonly used to simulate the evolution of cross-shore beach profiles by explicitly taking into consideration the various morphodynamic processes that govern profile evolution. These models are based on physical laws and incorporate detailed physics of wave propagation, sediment transport, and the ensuing morphological changes, making them a more accurate and widely applicable modelling method (Omstedt, 2011; Pender and Karunarathna 2013; Jin et al., 2021).

The models are diverse, including 1D/2D, depth-resolving 2D/3D, and coastal profile area models such as Delft 3D, XBeach, and Mike 21. These models have been shown to be effective at simulating some form of cross-shore beach profile evolution. Process-based modelling is a well-established approach that includes the generation of nearshore currents (Warren and Bach, 1992; Lesser et al., 2004; Roelvink et al., 2009; Villaret et al., 2013).

Despite their accuracy and wider applicability, process-based models have several limitations. Firstly, they are computationally expensive, requiring lengthy computational times, especially for longer simulation timescales. Secondly, they have inadequate descriptions of non-linear process interactions, which result in accumulation of errors when simulating on longer timescales. Thirdly, detailed knowledge of the bathymetry, wave climate, and sediment properties of the beach is required for accurate modelling (Muller et al.,2011).

The high computational cost of process-based models is due to the detailed representation of physical processes included in the model. To reduce computational time, simplified parameterizations of certain processes may be used, but this compromises the accuracy of the model. Another way to reduce computational time is through parallel computing or using high-performance computing systems.

It is currently unknown what the implications of these model approximations are for the simulation of wave propagation, energy dissipation, and sediment transport in the sandbar area, as well as their effects on the morphological evolution of the sandbar. Identifying these limitations is crucial for further model development.

Inadequate description of non-linear process interactions is another limitation of process-based models. The non-linear interactions between waves, currents, and sediment transport are difficult to accurately capture in these models. This limitation can lead to errors in predictions, particularly on longer timescales (Roelvink, 2011; Cuddington et al., 2013; Roelvink et al., 2016).

Errors may also accumulate over time, resulting in discrepancies between model predictions and actual observations. This is particularly true when modelling over long timescales, as even small errors can accumulate and result in significant differences between the model and actual observations. It is important to validate the model predictions with observed data regularly to mitigate these errors.

2.6.4 Data-driven Models

Data-driven models, also known as reduced physics models, have become increasingly popular with the use of long-term morphodynamic datasets. These models are based on observational analysis and extrapolation and rely heavily on long and reliable datasets without prior knowledge of physical processes (Mouradi et al., 2020). Defects in system knowledge are no longer an impediment to prediction and can be learned by an algorithm, which is the principal advantage of this approach. These models are particularly useful for predicting long-term trends and changes in coastal systems, such as shoreline erosion and sediment transport.

At its most basic level, data-driven methods involve analysing a series of measurements to identify trends and cycles (Reeve et al.,2016). However, the use of manual methods of coastal monitoring, such as in-situ surveys, has been limited due to the significant amount of time and labour required to generate the data. This has led to the development of various techniques for monitoring coastal change, including remote sensing, aerial photography, and digital elevation models (e.g., Luijendijk et al., 2018; Vos et al., 2019; Castelle et al., 2021). This increase in data availability has made full data-driven models a more realistic option and paved the way for machine learning techniques. Goldstein et al. (2019) provide a comprehensive review of these machine-learning techniques for coastal applications. The machine-learning models fundamentally differ from statistical or empirical models in that there are no assumptions or hypotheses about the structure of the relationship in the data and instead, there is an automated search for rules and relationships (Goldstein et al., 2019). In machine leaning, no restrictive data assumptions are made, and residuals are not required to have a particular distribution.

Reichstein et al. (2019) proposes that future models should combine physical-based modelling and machine learning techniques. Such a combination will be the optimal method. Physical modelling provides dynamic understanding from the governing equations, whereas data-driven modelling results may uncover patterns not predicted by physical modelling (Fang 2021). However, data-driven models can be limited by the quality and availability of data.

Despite the growing popularity of data-driven models in numerous domains, there is still need for more research on how to evaluate and compare the performance of various data-driven models. Insufficient

knowledge exists regarding how to select the best data-driven model for a given task and how to optimise and fine-tune the parameters of these models to achieve the best results.

2.6.5 Hybrid models

Hybrid models are becoming increasingly popular in the field of modelling complex systems due to their ability to combine multiple modelling techniques to create a more accurate representation of a system. These models can provide a more comprehensive understanding of a system by incorporating several types of data and modelling approaches. These models are typically based on the concept of equilibrium, which assumes that a system is in a steady state and that any changes occur gradually over time. Hybrid models are particularly useful in cases where a system is too complex to be accurately represented by a single model or where multiple models are needed to capture several aspects of the system.

Compared to process-based models, which attempt to model every aspect of a system in detail, hybrid models are more computationally efficient and have been shown to be reliable on seasonal timescales to simulate shoreline behaviour (Yates et al, 2009; Splinter et al, 2017; Schepper et al., 2021). Hybrid models combine different modelling techniques, such as physical models, numerical models, and data-driven models, to create a more accurate representation of a complex system. By combining multiple types of data and modelling approaches, hybrid models can provide a more comprehensive understanding of these systems (Karunarathna and Reeve 2013).

For example, a hybrid model for a coastal system might combine a physical model that simulates wave and current behaviour with a numerical model that simulates sediment transport and a data-driven model that uses historical data to predict future morphodynamics. The physical model could be based on equations that describe wave propagation and the movement of water currents, while the numerical model could use mathematical models to simulate the transport of sediment. The data-driven model could use historical data on morphodynamics to develop a statistical model that predicts future morphodynamics based on environmental factors. The four models covered in this chapter are summarised in Table 2.1.

Table 2. 1 Summary of Models, Contributions, Limitations, and Knowledge Gaps

Models	Contribution	Limitations	Knowledge gap
Equilibrium model	Equilibrium models are valuable tools for predicting the behaviour of coastal systems and can provide useful information for coastal zone management	Equilibrium models do not account for the effects of storms and other extreme events, which can have a significant impact on the behaviour of the system.	The accuracy and reliability of equilibrium models in coastal areas can be improved by incorporating more detailed and accurate data on beach properties, wave climate, and sediment transport rates.
Process-based model	Process-based models can provide detailed information on the behaviour of a system and can be used to simulate complex processes that are not expected from physical modelling.	The accuracy of the model depends on the quality of the input data, the accuracy of the model parameters, and the validity of the assumptions made.	They are computationally expensive, requiring lengthy computational times, especially for longer simulation timescales.
Data-driven model	These models are particularly useful for predicting long-term trends and changes in coastal systems, such as shoreline erosion and sediment transport.	These models rely on historical data to make predictions, and if the data does not include extreme events, the model may not be able to accurately predict them.	Lack of information not represented by the available data.
Hybrid model	These models provide a more comprehensive understanding of a system by incorporating several types of data and modelling approaches.	Developing and implementing hybrid models can be expensive, as it requires specialised software and expertise from multiple fields.	The accuracy of hybrid model depends on several parameters

In summary, all the models (Table 2.1) require further examination to effectively close the existence gap that has been identified in the literature. These existence gaps are sufficiently addressed in empirical formulations. Empirical formulations are mathematical equations or models derived from experimental data, observations, or practical experience, as opposed to first principles or theoretical considerations. Typically, these formulas or models are derived by fitting data to a mathematical function or curve, which can then be used to anticipate future outcomes or draw inferences about the studied system.

2.7 Conclusion

This chapter provides a comprehensive review of the nearshore beach responses to hydrodynamics, and how the beach morphology is related to the forcing. It reviews various hydro-and morphodynamic parameters that have the potential to influence the equilibrium state of different types of beaches. Additionally, it explains

wave transformation from deep water to shallow regions and highlights the beach states that strongly depend on wave conditions and sediment transport processes. Several models have also been reviewed that show the importance of modelling beach state variabilities compared to field experiments, but these models also have limitations, as they do not specifically address beach states.

An empirical formulation has been proposed to overcome some of these limitations which consists of simple analytic solutions to predict the beach variabilities on different beach states. The model relies on free parameters that demonstrate a beach variability on a short timescale. The processes have been highly simplified to keep the computational time to a minimum. However, the model possesses quantitative skills like the beach model morphodynamic framework of Wright and Short (1984). The main benefit of this model is that it is more computationally efficient than other models, as it is based on the concepts of behavioural terms. The next chapter presents numerical model applied to facilitate easy empirical formulation generation.

Chapter 3: Beach Morphodynamic Modelling using XBeach.

3.1 Overview

This chapter presents details of XBeach (eXtreme Beach behaviour) coastal morphodynamic model and subsequent validation of the XBeach model using a large-scale experimental dataset. XBeach is a numerical model that simulates hydrodynamic and morphodynamic processes following the model structure shown in Figure. 3.1. The numerical model was validated using a Large-scale morphodynamic experimental data of beach profile evolution under sequences of alternating high-low energy wave condition. Section 3.2 provides a detailed description of the model numerical scheme and program structure. Section 3.3 details model physics and formulations, Section 3.4 describes the RESIST experiment and dataset while Section 3.5 presents the set-up of the XBeach model and a preliminary sensitivity analysis to choose the variables for the modelling exercise. The model results and simulation are compared with experiment as a form of validation to determine the model's accuracy in Section 3.6.

3.2 Numerical scheme and program structure

XBeach is a process-based model and an open-source numerical modelling system, which has been originally developed to investigate hurricane impact on sandy beaches (Roelvink et al., 2009, 2018; van Thiel de Vries, 2009, McCall et al., 2010). The system comprises a wave and roller module, non-linear shallow water equations (NLSWE) module and morphological module based on Soulsby-van Rijn (SvR) sediment transport equation. Surfbeat mode is based upon the wave action balance equations and solves for short wave only on the scale of wave grouping saving considerable computational time, skewness and asymmetry are parameterized.

Skewness and asymmetry are resolved by a non-hydrostatic method, which resolves all processes, including short-wave motions, but require additional computational time. This model has been used repeatedly by many researchers and companies worldwide for nearshore morphological studies on sandy beach and dune erosion, for example (Roelvink et al., 2019; van Dongeren et al., 2009; van Thiel de Vries 2009 McCall et al., 2010) calibrated and validated the model against laboratory experiments and field observations for the case of sandy beach dune and erosion, also in assessing flow properties in laboratory conditions (Ruffini et al., 2020).

However, XBeach has the ability to simulate the processes that occur mostly in the coastal zone during storm events matched with storm-impact regimes (Sallenger, 2000). By combining XBeach with a statistical

approach Pender and Karunarathna (2013) simulated long term behaviour on the sandy Narrabeen beach. This approach was extended to simulations of storm groups rather than single storm events only by Karunarathna et al. (2014). XBeach has been tested to simulate wave runup (Palmsten and Splinter, 2016; Lashley et al., 2018; de Ridder et al.,2021) as well as morphological changes in beach profiles (1D mode) (Dissanayake et al., 2014; Harley et al., 2011; Pender and Karunarathna, 2013; Vousdoukas et al., 2012) and domains (2D mode) (McCall et al., 2010; Williams et al., 2015). Recently (Rooijen et al., 2022) tested it on coastal canopies.

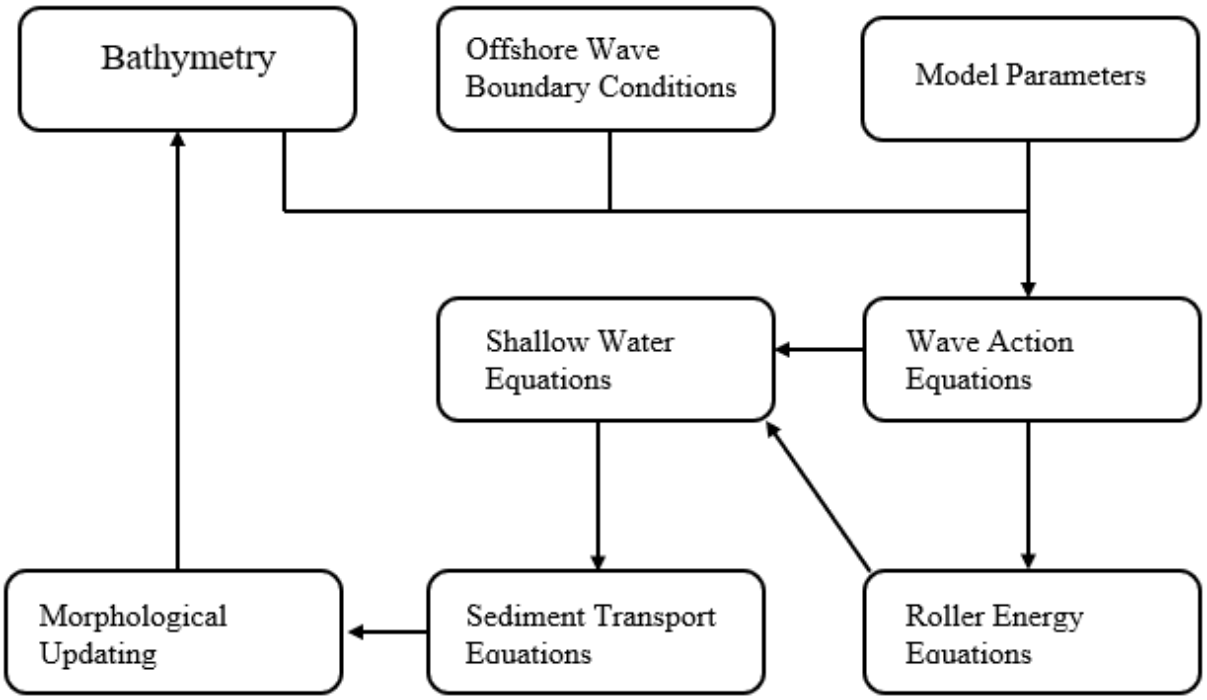

Figure 3.1 XBeach model setup

3.2.1 Functionalities

Optional functions to select in XBeach.

- Roller and wave dissipation model formula are applied for use when the wave energy varies on the wave group timescale. Time-varying wave action balance including refraction, shoaling and wave breaking. Depth-averaged shallow water equations that include time-varying wave forcing terms.
- Depth-averaged advection-diffusion equation to solve suspended transport and Soulsby – Van Rijn transport formulations. Bed updating algorithm including possibility of avalanching with separate criteria for critical slope at wet or dry points. Numerical scheme to improve long-wave run-up and backwash on the beach. Generalised Lagrangean Mean (GLM) approach to represent the depth-averaged undertow and its effect on bed shear stresses and sediment transport.

3.2.2 XBeach modules

In XBeach, the functionalities are divided amongst several modules. XBeach has four main modules as seen in Figure 3.2. These four modules have some functions which are associated with each it is like a circle going around and they communicate with each other during the XBeach simulation. The arrows show the connectivity of the modules, the arrow from the wave module indicates the use of output parameters from the wave module to the flow module and the morphology is determined using the output from flow and sediment transport modules. In a numerical time-step, each of the modules are called in sequence starting with the short-wave module for its computations.

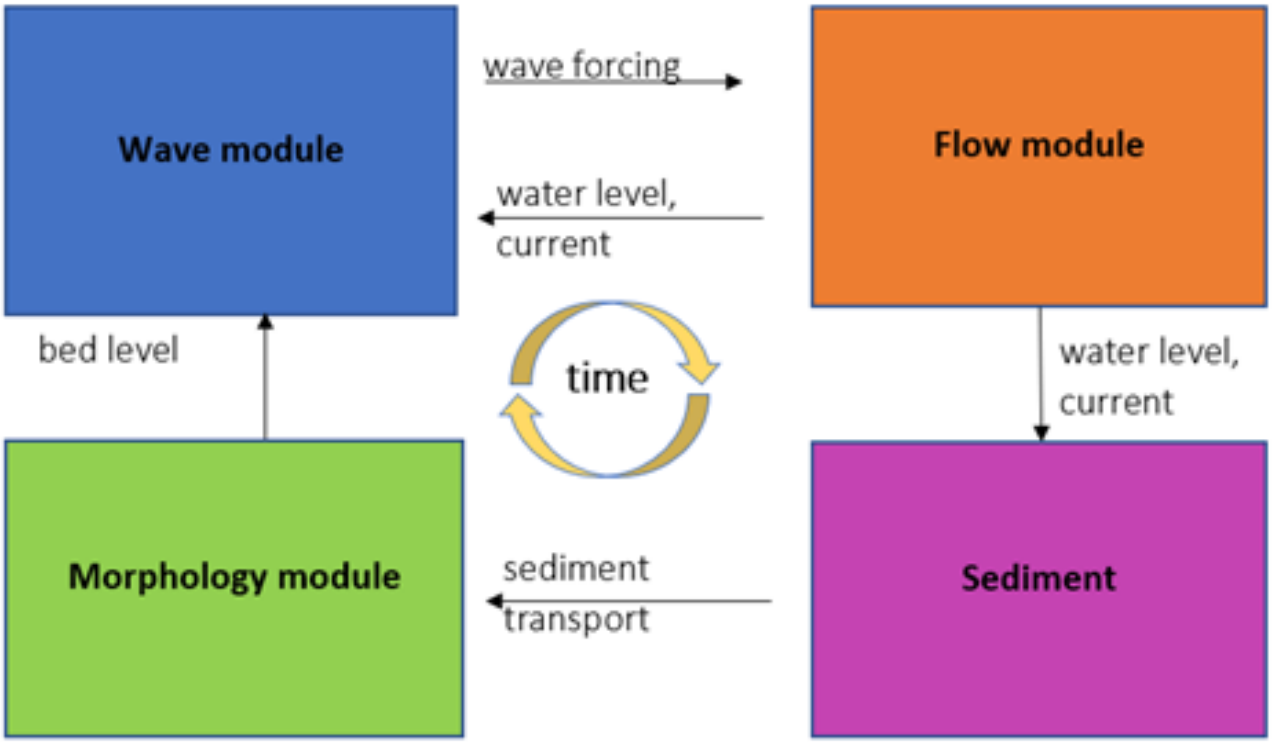

Figure 3.2 Modules in XBeach (Deltares 2015)

3.3 Model physics and formations

In XBeach, the first step is to define the site and related parameters as shown in Figure 3.1, which are bathymetry and offshore wave boundary conditions and the model parameters. The next step is the computation of wave action balance equation. In this step, the numerical model computes wave forcing in shallow water by solving the time dependent wave action balance equation. Roller energy equations are used to determine the surface stresses by taking the wave energy dissipation due to random wave breaking as a source term. The shallow water equations are solved using the momentum and mass conservation equations. By using the sediment formulations equilibrium sediment concentration is calculated. Finally, morphological

updating of the bathymetry is completed, and new bathymetry of the region is attained. The structure of XBeach shown in Figure 3.2 will be presented. The model description presented in this section is based on the publication of Roelvink et al. (2019) and the XBeach user manual. Chapter 4 illustrates the validation of XBeach against 1D flume data.

3.3.1 Coordinate system and grid set-up

XBeach uses a coordinate system in which x-axis is oriented towards the coast and the y-axis describes the longshore distance as seen in Figure 3.3. This coordinate system is defined in the world coordinates (x and y in Figure 3.3); the grid size in x- and y- direction may be variable but the grid must be curvilinear.

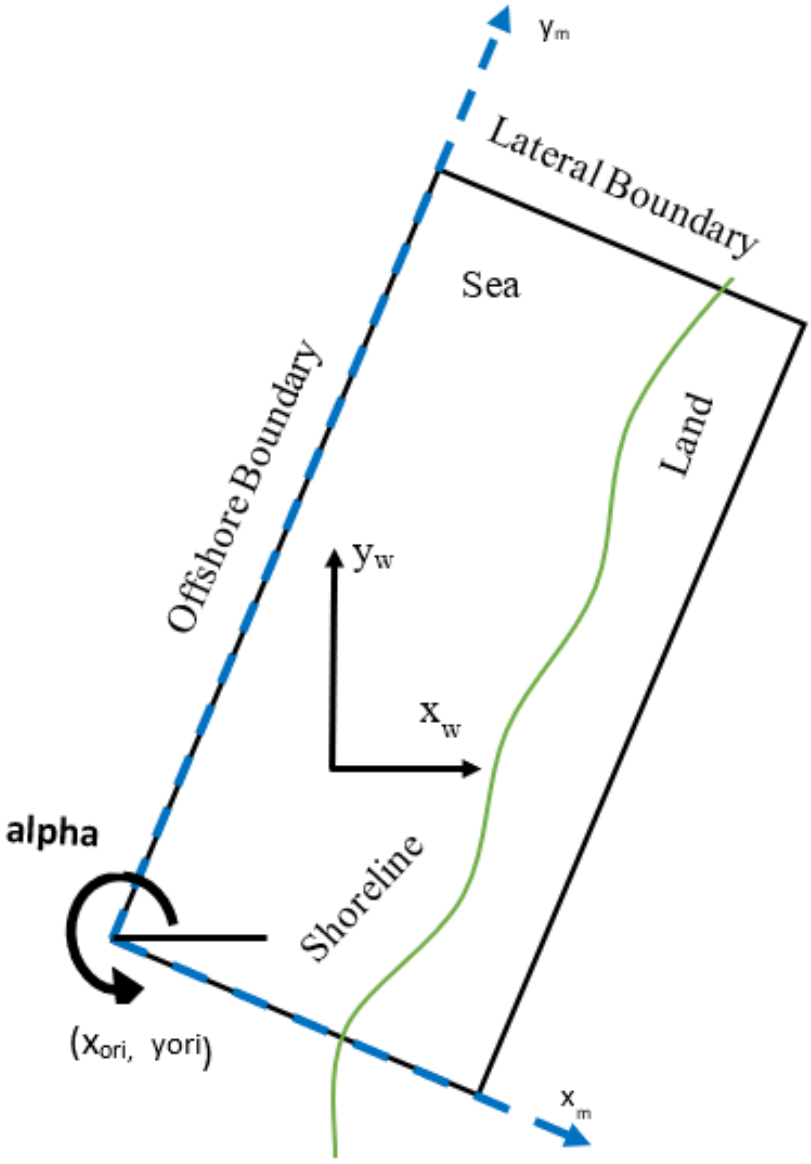

Figure 3.3 Coordinate system in XBeach (Roelvink et al., 2015)

Grids used in XBeach are staggered grids that mean bed levels, water levels, water depths and concentrations are defined in cell centres. Also, velocities and sediment transports are defined in cell interfaces. In the wave model, wave action, roller energy and radiation stresses are defined in cell centres, with the radiation gradients defined at the interfaces. In Figure 3.4, the grid system used in XBeach is shown.

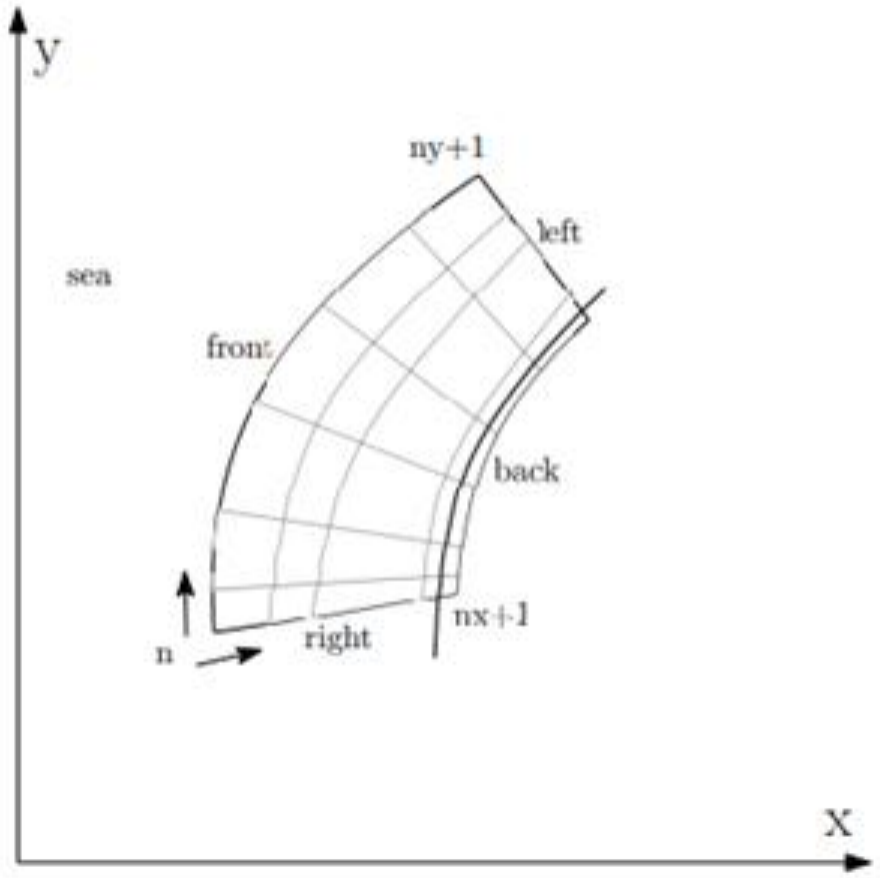

Figure 3.4 Curvilinear coordinates system of XBeach (Roelvink et al., 2015)

3.3.2 Hydrodynamics

The Xbeach model was originally developed as a short-wave averaged but wave-group resolving model which allows resolving of the short-wave variations on the wave group scale and the long waves associated with them this way, both short and long waves are accounted for, this principle is shown in Figure 3.5. Users can choose which timescales to resolve (Roelvink et al., 2015) Xbeach offers three different hydrodynamic modelling approaches which includes stationary (phase-averaged), Instationary (surfbeat) and non-hydrostatic (phase-resolving) (Roelvink et al., 2018)

- Stationary mode: The model solves wave-averaged formulations and wave action balance equation where the infra-gravity waves are excluded. This is useful for conditions where the incident waves are relatively small or short and infragravity motions would be small. The model equation is like HISWA (Holthuijsen et al., 1989) but wave growth and wave period variations are not included. In this mode,

the processes that are resolved by the model are, wave propagation, directional spreading, wave refraction, wave shoaling, wave breaking and a roller model (Roelvink and Reniers, 2011); these processes are usually dominant in nearshore areas of limited extent.

- Surfbeat mode: In this model, long waves (e.g., tides, storm surges and other infragravity) and currents are solved separately from the short waves using NLSWEs form derived based on a hydrostatic pressure assumption. The short waves amplitude variations are separately solved using a time-dependent wave action balance (Elsayed 2017, Deltares 2015a, Roelvink et al., 2010, 2017). This mode especially focusses on swash zone processes and is fully valid on dissipative beaches where the short waves are mostly dissipated by the time they are near the shoreline (Hoonhout, 2015). The short waves are enveloped on a group scale Figure 3.5 and the parameters are averaged over depth, leading to a 2DH model. No individual short waves must be resolved, which saves considerable computational time at the expenses that the phase of the short waves is not simulated (Roelvink et al., 2009). Intra-wave processes (e.g., wave asymmetry and skewness) are approximated.
- Non-hydrostatic mode: The model solves the non-linear shallow water equations including a non-hydrostatic pressure scheme, allowing the model to reproduce the propagation and decay of individual waves, a more complete hydrodynamic mode of Smit et al. (2010). The non-hydrostatic mode represents an extension of the surfbeat mode to provide Xbeach with capability to model nonlinear waves and wave breaking in the surf zone, but more computational expensive as it requires much higher spatial resolution and associated smaller time steps, and therefore not suitable for all modelling cases. Intra-wave processes (e.g., wave asymmetry and skewness) are resolved. In Figure. 3.5 XBeach non-hydrostatic solves the short and long waves while XBeach Surfbeat solves the short-wave envelope and the long waves.

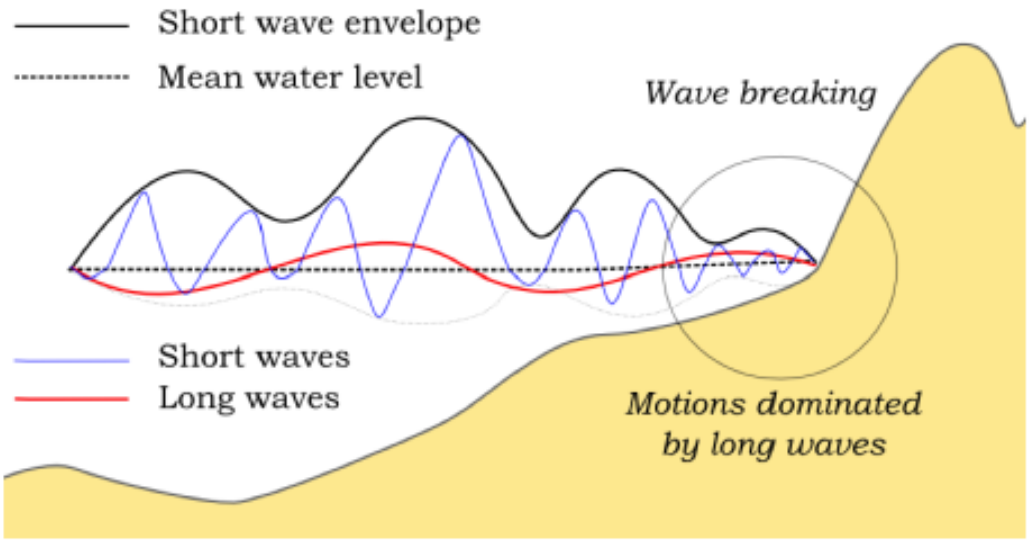

Figure 3.5 Principal sketch of the relevant wave processes (Roelvink et al.2015)

Short wave action balance

Short wave transformation is solved with the Short-Wave Action Balance equation. Short wave propagation is based on conservation of wave action, coupled with a roller energy balance, wave action is related to wave energy and wave amplitude. The directional distribution of the action density is considered, but frequency spectrum is parameterized and reduced to a single frequency parameter Holthuijsen et al., (1989) and Van Thiel de Vries (2009). This can be seen in Equation. 3.1.

The time dependent wave action balance equation both in x and y direction is show

$$\frac{\partial A}{\partial t} + \frac{\partial c_x A}{\partial x} + \frac{\partial c_y A}{\partial y} + \frac{\partial c\theta A}{\partial \theta} = -\frac{Dw + Df + Dv}{\sigma} \tag{3.1}$$

In which the wave action A is introduced as the wave energy density (potential and kinetic energy densities) in each directional bin S_w divided by the intrinsic wave frequency σ:

$$A(x, y, t, \theta) = \frac{S_w\,(x, y, t, \theta)}{\sigma(x, y, t)} \tag{3.2}$$

where θ represents the angle of incidence with respect to the x-axis, The intrinsic frequency is σ and group velocity $c_g$is obtained from linear dispersion relation. The intrinsic frequency is for example obtained with:

$$\sigma = \sqrt{gk \tanh kh.} \tag{3.3}$$

where:

A =Wave action term

c_x =Wave action propagation speed in x-direction

c_y =Wave action propagation speed in y-direction

c_θ =Wave action propagation in the directional space

σ = Intrinsic wave frequency

D_w = Wave breaking dissipation term

D_f = Bottom friction dissipation term

D_v = Vegetation dissipation term

where *t* is time (in sec). This equation solves the short-wave envelope on the wave group timescale as shown in Figure 3.5, where the blue line represents the short waves and black line represents the amplitude variations. However, this means that the wave height variations within the model vary with the wave group, also

considered the short-wave averaged approach. Due to the short-wave averaging the diffraction process is not included in the model because this is a process that occurs on the short-wave timescale. In this wave action balance the processes of shoaling and directional spreading are included. The wave dissipation terms used in the model are mainly for wave breaking (D_w), bottom friction $\left(D_f\right)$ and vegetation (D_v). In this study, energy dissipation due to vegetation is not taken into consideration. The propagation speed directional space (c_θ) is included in the wave action balance as follows:

$$c_\theta(x,y,t,\theta) = \frac{\sigma}{\sinh(2kh)}\left(\frac{dh}{dx}sin\theta - \frac{dh}{dy}\,cos\theta\right) + cos\theta\left(\frac{du}{dx}sin\theta - \frac{du}{dy}\,cos\theta\right) + sin\theta\left(\frac{dv}{dx}\,sin\theta - \frac{dv}{dy}\,cos\theta\right) \tag{3.4}$$

where:

c_θ =Propagation speed in the directional space

σ = Intrinsic wave frequency

k =Wave number

h =Local water depth

θ =Angle of incidence with respect to the x-axis

This equation includes both wave refraction due to differences in bottom depths (first term) and wave refraction due to currents (second term).

Through dissipation of short wave that interact with vertical elements that dampen the wave, dissipation due to vegetation is included. And the dissipation is defined as:

$$D_v = A_v \frac{pC_D\, b_v\, N_v}{2\sqrt{\pi}} \left(\frac{kg}{2\sigma}\right)^3 H_{rms}^3 \tag{3.5}$$

With:

$$A_v = \frac{(sinh^3 k\alpha h - sinh^3 k\alpha h) + 3(sinhk\alpha h - sink\alpha h)}{3kcosh^3 kh} \tag{3.6}$$

where:

k = Wave number

α = Relatively vegetation height (h_v/h)

C_D = Drag coefficient

b_v = Vegetation width

N_v = Vegetation density

Wave shape

As waves propagate towards a beach, non-linear effects start to play a significant role in wave induced transport. Besides the change in the shoaling zone, waves also change in shape. XBeach considers the wave energy of short waves as averaged over their length, and hence does not directly simulate the wave shape (Van Thiel Varies, 2009) As waves propagate from deep water towards a beach, the water surface elevation becomes increasingly nonlinear due to the amplification of the higher harmonics. However, the effects of wave non-linearity (skewness and asymmetry) are accounted for in the advection-diffusion equation of the sediment concentration (see Equation. 3.21). Skewness and Asymmetry are introduced in this equation in the form of u_a which is defined as:

$$u^a = (FacSK.SK - FacAs.As)u_{rms} \tag{3.7}$$

where:

$Sk\ and\ As$ = Skewness and Asymmetry respectively

$f_{Sk}\ and\ f_{As}$ = Calibration factors also referred to as facSk and facAs

U_{rms} = Orbital velocity due to short waves

To take non-linearity into account two wave forms are implemented:

1. A formulation of Ruessink et al. (2012) based on a parameterization with the Ursell number.
2. A formulation of Van Thiel de Vries (2009) based on the parameterized wave shape model of Rienecker and Fenton (1981).

The value for the skewness and asymmetry is calculated with the use of a Boltzmann sigmoid. The skewness and asymmetry are a function of ψ, and determined as follows:

$$S_k = B\cos(\psi) \tag{3.8}$$

$$A_s = B\sin(\psi) \tag{3.9}$$

B is determined as

$$B = p_1 + \frac{p_2 - p_1}{1 + \exp\frac{p_{3-\log(U_r)}}{P_4}} \quad (3.10)$$

And ψ is:

$$\psi = -90 + 90 \tanh(p_5 / U_r^{p6}) \quad (3.11)$$

This function is fitted to measurement data using the factors $p_1 \, to \, p_6$. A Sigmoid function is characterised by an S-shape. The top-asymptote in this function is defined by p_2 and the bottom asymptote is defined by p_1. The inflection point is found at a value point between $(p_1 + p_2)/2$.

The Ursell parameter (Ursell, 1953) indicates the non-linearity of gravity waves in shallow water and is defined as:

$$U = HL^3/h^3 \quad (3.12)$$

Wave breaking and dissipation.

The wave breaking formulation by Roelvink (1993) is used to account for the variations in wave energy due to breaking. The method of this wave breaking formulation is the use of the fraction of breaking waves (Q_b) multiplied by the dissipation per breaking event. The fraction of breaking wave is calculated using the ratio between the root mean squared error wave height (H_{rms}) and the maximum wave height (H_{max}). The maximum wave height is defined as the wave height where wave breaking starts to transpire. For defining this maximum wave height, a breaker index γ is used.

$$D_w = 2 * \left(\frac{\propto}{T_{rep}}\right) * Q_b * E_w \; and \; Q_b = 1 - \exp\left(-\left(\frac{H_{rms}}{H_{max}}\right)\right) \quad (3.13)$$

where:

D_w = Wave breaking dissipation term

$\propto$ = Wave dissipation coefficient

T_{rep} = Representative wave period

Q_b = Fraction of breaking waves

E_w = Energy of the wave

H_{rms} = Root-mean-square wave height

H_{rms} = Maximum wave height

n = Ratio of group velocity and phase velocity

Roller model

In Xbeach, when a wave breaks a turbulent wall of foam forms at the shoreward side of the wave. This circulation foam is known as 'surface roller'. The surface roller contributes to the total radiation stress, influencing the local sea level, and roller energy is described as propagation, generation, and dissipation of roller energy. The derivation of the roller radiation stress starts with the roller energy balance, where dissipation of the wave by breaking (D_w) is the energy input (Roelvink et al., 2009).

$$\frac{dE_r}{dt} = \frac{\partial E_r}{\partial t} + \frac{\partial E_r c \cos\theta}{\partial x} + \frac{\partial E_r c \cos\theta}{\partial y} = S - D_r \tag{3.14}$$

$$E_r = \frac{1}{2}\frac{\rho R(u^2 r + \omega^2 r)}{L} \tag{3.15}$$

$$D_r = 2\beta \frac{g}{c_g} E_r \tag{3.16}$$

where:

S = loss of organized wave motion due to wave breaking = D_w

E_r = roller kinetic energy

R = roller area

L = wavelength

β = coefficient

This roller model is basically an addition to the radiation stress in the breaker zone.

Turbulence

There is a high amount of turbulence within the water column when waves break. Which can cause an increased amount of suspended sediment when this turbulence reaches the bed. This allows transport of the turbulence from where the waves break to the bed causing the stirring up of sediment. This is also accounted for in XBeach with the use of a turbulence model. The model uses an exponential decay from the water surface to the bed to determine the turbulence near the bed:

$$k_b = \frac{k_s}{exp\left(\frac{h}{L_{mix}}\right) - 1} \tag{3.17}$$

where:

k_b =Turbulence variance at the bed

k_s =Wave-averaged turbulence energy

h = Local water depth

L_{mix} = Mixing length

Bottom friction

The short-wave dissipation by bottom friction (D_f) is encompassed in the model as follows:

$$D_f = \frac{2}{3\pi} * \rho f_w \left(\frac{\pi H_{rms}}{T_{m01}\, sinh\, kh}\right) 3 \tag{3.18}$$

where:

D_f = Short wave dissipation by bottom friction

ρ = Density

f_w = Short-wave friction coefficient

H_{rms} = Root-mean-square wave height

T_{mo1} = Mean wave period

k = Wave number

h = Local water depth

In this, f_w is the short-wave friction coefficient, and it is not related to the bed friction in the flow equations.

Radiation stresses

The radiation stresses in the model are as follows:

$$S_{xx,r}(x,y,t) = \int cos^2\theta S_r d\theta \tag{3.19}$$

$$S_{xy,r}(x,y,t) = S_{yx,r}(x,y,t) \int sin\theta cos^2\theta S_r d\theta \tag{3.20}$$

$$S_{yy,r}(x,y,t) = \int sin^2\theta S_r d\theta \tag{3.21}$$

where:

$S_{xx,r}$ = Radiation stress, x-component

$S_{xy,r}$ = Radiation stress shear component

$S_{yy,r}$ = Radiation stress, y-component

θ = Angle of incidence with respect to the x-axis

S_r = Radiation stress

In the model domain the radiation stress can also be considered as the variation in wave energy. Among other things, the radiation stress is influenced by the bottom friction, wave height, wave breaking and surface rollers. Gradients in radiation stress drive wave-driven currents like longshore currents, rip currents and undertow. These gradients also drive the long wave motions (bound and free) e.g., the surfbeat. These motions are solved by the shallow water equations.

Shallow water equations

To translate the forcing due to wave action into mean flow components shallow water equations are required and this includes undertow, long waves and wave set-up and set down. The depth averaged Generalised Lagrangian Mean formulation are used for this purpose. These equations are formulated in terms of the Lagrangian velocity, given by:

$$\frac{\partial u^L}{\partial t} + u^L * \frac{\partial u^L}{\partial y} + v^L * \frac{\partial u^L}{\partial y} - f v^L - v_h \left(\frac{\partial^2 u^L}{\partial x^2} + \frac{\partial^2 u^L}{\partial y^2} \right) = \frac{\tau_{sx}}{\rho h} - \frac{\tau_{bx}^E}{ph} - g * \frac{\partial \mathfrak{y}}{\partial x} + \frac{F_x}{\rho h} + \frac{F_{v,x}}{\rho h} \quad (3.22)$$

$$\frac{\partial v^L}{\partial t} + u^L * \frac{\partial v^L}{\partial y} + v^L * \frac{\partial v^L}{\partial y} - f u^L - v_h \left(\frac{\partial^2 v^L}{\partial x^2} + \frac{\partial^2 v^L}{\partial y^2} \right) \quad (3.23)$$

$$= \frac{\tau_{sy}}{\rho h} - \frac{\tau_{by}^E}{ph} - g * \frac{\partial \mathfrak{y}}{\partial y} + \frac{F_y}{\rho h} + \frac{F_{v,y}}{\rho h} \frac{\partial \mathfrak{y}}{\partial t} + \frac{\partial h u^L}{\partial x} + \frac{\partial h v^L}{\partial y} = 0$$

where:

u^L, v^L = Lagrangian velocities

f = Coriolis coefficient

$\tau_{sx}\tau_{sy}$ = Wind shear stresses in the x-and y-direction, respectively

$\tau_{bx}\tau_{by}$ = Bed shear stresses in the x-and y-direction, respectively

F_x, F_y = Wave-induced stresses in the x-and y-direction, respectively

$F_{v,x}, F_{v,y}$ = Stresses induced by vegetation

ρ = Density

g = Gravitational acceleration

h = Local water depth

The u^L and v^L are the Lagrangian velocities which consist of the Eulerian velocity in combination with the strokes drift velocity. Also τ_{bx} and τ_{by} are the bed shear stresses, F_x and F_y represents the wave induced stresses related to the gradients in radiation stresses, v_h is the horizontal viscosity and f is the effect of Coriolis.

Non-hydrostatic pressure correction

The non-hydrostatic module of XBeach uses the inclusion of a non-hydrostatic pressure correction term to resolve short waves and allows wave by wave modelling of the surface elevation and depth-averaged flow (McCall et al.,2014). The non-hydrostatic model accounts for all motions within the shallow water equations while from the mean of the dynamic pressure at the surface and at the bed, the depth-averaged dynamic pressure is computed by assuming the dynamic pressure at the surface to be zero and a linear change over depth (Roelvink et al., 2015). To calculate the normalized dynamic pressure at the bed, the role of advective and diffusive terms to the vertical momentum balance are presumed to be insignificant.

$$\frac{\delta w}{\delta t} + \frac{\delta q}{\delta z} = 0 \tag{3.24}$$

where:

w = Vertical velocity

z = Vertical coordinate.

The vertical velocity at the bed is set by the kinematic boundary condition.

3.3.3 Morphodynamic modelling

Sediment transport equations

The sediment transport in Xbeach can be computed in two modes which are, the suspended sediment rate and bed level changes. Modelling of the sediment concentrations in the water is performed using the depth-averaged advection diffusion scheme with a source-sink term based on equilibrium sediment concentration (Galappatti and Vreugdenhil, 1985).

$$\frac{\partial hC}{\partial t}+\frac{\partial hC(u^E-u_a sin\theta_m)}{\partial x}+\frac{\partial hC(v^E-u_a cos\theta_m}{\partial y}+\frac{\partial}{\partial x}\left[D_h h*\frac{\partial C}{\partial x}\right]+\frac{\partial}{\partial y}\left[D_h h*\frac{\partial C}{\partial y}\right] = \frac{hC_{eq}-hC}{T_s} \quad (3.25)$$

In this formulation the entrainment and deposition of sediment is determined by the difference between the equilibrium sediment concentration (C_{eq}) and the actual sediment concentration (C) which varies on the wave group time scale and (D_h) is the sediment diffusion coefficient. The entrainment of the sediment is represented by an adaptation time (T_S) given by a simple approximation based on the local water depth *(h)* and sediment fall velocity (w_s).

where:

C = Depth – averaged sediment concentration

C_{eq} = Equilibrium sediment concentration

D_h = Sediment diffusion coefficient

T_s = Adaptation time

h = Local water depth

w_s = Sediment fall velocity

u^E, v^E = Eulerian velocities

u_a = Onshore directed velocity.

The equation used to calculate T_S by using local water depth and sediment velocity is given in Equation. 3.26.

$$T_s = \max\left(f_{Ts}\frac{h}{w_s}, T_{s,min}\right) \quad (3.26)$$

where:

h: Total water depth

w_s: Sediment fall velocity

f_{Ts} : Correction and calibration factor

Sediment transport formulations

In Xbeach there are 2 sediment transport formulations available, Soulsby -Van Rijn: Van Thiel-Van Rijin. The total equilibrium sediment concentration is calculated in both using the following expression:

$$C_{eq} = \max\left(\min\left(C_{eq,b,}\ \frac{1}{2}\ C_{max}\right) + \min\left(C_{eq,s,}\ \frac{1}{2}\ C_{\max}\right),0\right) \quad (3.27)$$

where:

Subscripts b and s = bed load and suspended

Further details on these formulations may be found in the Xbeach Technical Reference Document (Roelvink et al., 2015). In XBeach, the sediment transport is modelled with the use of a depth averaged advection diffusion equation (Galappatti, 1983). XBeach allows the use of multiple sediment types, where each sediment type is calculated using its own grain size.

Morphological updating

For bottoming updating XBeach uses the sediment transport gradient to update the bed levels in the wet areas with the updating stated in (Equation 3.27). In this balance the net incoming or outgoing sediment in x- and y- direction determines the bed level change.

$$\frac{\partial z_b}{\partial t} + \frac{f_{mor}}{1-p}\left(\frac{\partial q_x}{\partial x} + \frac{\partial q_y}{\partial y}\right) = 0 \quad (3.28)$$

where:

f_{mor} = Morphological acceleration coefficient.

z_b = Bed level

P = Porosity

$q_x\ and\ q_y$ = Sediment rates in x- and y- direction respectively.

XBeach provides two methods with which morphology can be accelerated.

- All times are prescribed on input in morphological time. If you apply a morfac all input time series and other time parameters are divided internally by morfac. This means that each wave condition lasts 1/morfac times as short. The bottom changes multiplied with morfac, and this can be activated in XBeach with the keyword *morfacopt* = 1 which is applicable for short term simulations. And this method is only active if the water level changes that are now accelerated by morfac do not change the hydrodynamics excessively (Roelvink et al., 2015).

- With the keyword *morfacopt* = 0. The user can prevent the simulation time to be adapted to the *morfac* value by setting *morfacopt* to zero. The keywords *morstart* and *morstop* let the user enable the morphological processes in XBeach only for a particular period during the (hydrodynamic) simulation. These options can be useful if a spin up time is needed for the hydrodynamics.

In order to solve the dune erosion processes in XBeach an adjustable threshold is added. To activate the slumping and avalanching the model uses a critical slope (m_{cr}). When critical slope is surpassed, sediment is exchanged between the grid-cells, until the slope is less steep than the critical slope (Roelvink et al., 2009). In the model the values for the critical slope differ between wet or dry conditions default values are above water (~ 1.0) and below water (~0.15 -0.3). Cases of inundated areas, slumping occurs under less steep conditions, and this includes the total water level at a given location as a driver of dune erosion. This mechanism results in the following equations:

$$\left|\frac{\partial z_b}{\partial x}\right| > m_{cr} \tag{3.29}$$

where the estimated bed slope is

$$\frac{\partial z_b}{\partial x} = \frac{Z_{b,i+1,j} - Z_{b,i,j}}{\Delta x} \tag{3.30}$$

where:

Z_b = Bed level

m_{cr}= Critical bed slope

The bed change within one step is given by

$$\Delta z_b = \min\left(\left(\left|\frac{\partial z_b}{\partial x}\right| > m_{cr}\right)\Delta x, 0.05\Delta t\right), \frac{\partial z_b}{\partial x} > 0 \tag{3.31}$$

$$\Delta z_b = \text{mix}\left(-\left(\left|\frac{\partial z_b}{\partial x}\right| > m_{cr}\right)\Delta x, -0.05\Delta t\right), \frac{\partial z_b}{\partial x} < 0 \tag{3.32}$$

where:

ΔZ_b= Bed level change in one step

m_{cr}= Critical bed slope

Groundwater flow

In XBeach the effect of water infiltration/exfiltration of the groundwater flow in the swash zone is implemented by the principle of Darcy flow and this includes a vertical interaction flow between surface layer and ground water layer. To simulate the interaction between the surface water and groundwater, a vertical flow velocity (*w*) is introduced. For infiltration and exfiltration, the vertical velocity is given by:

$$w_{ex} = \frac{\eta_{gw-z_b}}{\Delta t} n_p \qquad (3.33)$$

$$w_{in} = -k_z \left(\frac{dp}{dz} + 1\right)$$

where:

n_p = Porosity

k_z = Vertical permeability

η_{gw} = Groundwater surface level

3.3.4 Boundary condition

In XBeach different boundary condition can be imposed on the flow condition and are to be stated on all sides of the domain where absorbing generating condition can be used front and back. It will be differentiated between the offshore and lateral boundaries. Generally, the offshore boundary is an artificial boundary, which wave, and flow conditions are stated. In the computational domain waves and currents will be generated which should pass through the offshore boundary to deep sea with minimal reflection. Options for the offshore and bayside flow boundary condition is shown in Table 3.1 the boundaries are set using the keywords 'front' and 'back'.

Table 3. 1 offshore & bayside flow inputs (Deltares, 2015)

Front & back	Abbreviated name	Description
0	abs 1d	Absorbing-generating (weakly reflective) boundary in 1D
1	abs2d	Absorbing-generating (weakly reflective) boundary in 2D
2	wall	No flux wall
3	wlevel	Water level specification (from file)
4	nonh_1d	Boundary condition for non-hydrostatic option

Lateral flow boundary conditions

Lateral boundaries are the boundaries perpendicular to the coastline. These boundaries are usually artificial depending on the limitation of the model domain. In XBeach, these boundaries can either be defined as Neumann boundaries or no-flux boundaries. These boundary conditions are activated using keywords "left = 0" or equivalently "left = neumann" in the settings part or "right =0" or equivalently "right = neumann". Table 3.2 shows the inputs required. The Neumann boundary condition has been shown to work well with stationary situation, where the coast can be assumed to be uniform outside the model domain (Roelvink, et al., 2015).

Table 3. 2 Lateral flow inputs (Deltares,2015)

Abbreviated name	Description
wall	No flux wall
neumann	Neumann boundary condition (constant water level gradient)
neumann_v	Velocity is determined by the adjacent cell
no_advec	Similar to neumann, but reduced terms

Wave boundary conditions

Wave conditions in XBeach can be implemented as spectral or non-spectral inputs as shown in Table 3.3, the spectral conditions are defined as either JONSWAP spectrum or SWAN spectrum in XBeach. The non-spectral are defined as a stationary or non-stationary bichromatic waves, for bichromatic waves the long wave /wave group period are stated. While for stationary the short-wave height, wave direction and representative wave group are stated. In table 3.3, second column are keywords applied in XBeach which forces as a boundary condition. At the offshore boundary, the wave energy density is prescribed as a function of y, θ and time. This function can be described based on spectral parameters.

Table 3. 3 Wave input (Deltares, 2015)

Instat	Abbreviated name	Type	Description
0	stat	Non-spectral	Stationary wave boundary condition (sea state)
1	bichrom	Special	Bichromatic (two wave component) waves

2	ts_1	Non - spectral	First-order time series of waves (generated outside XBeach), this option specifies free surface elevation and short-wave energy
3	ts_2	Non - spectral	Second-order time series of waves (generated outside XBeach), this option specifies free surface elevation and short-wave energy
4	jons	Spectral	Wave groups generated using a parametric (JONSWAP)spectrum
5	swan	Spectral	Wave groups generated using a SWAN 2D output file
6	vardens	Spectral	Wave groups generated using a formatted file
7	reuse	Special	Reuse of wave conditions
8	nonh	Non-spectral	Boundary conditions for non-hydrostatic option
9	off	Special	No wave boundary condition
40	stat_table	Non- spectral	A sequence of stationary conditions (sea states)
41	jons_table	Spectral	A sequence of time-varying wave groups

In this research, XBeach is used to develop a model of a 1D cross-shore beach profile to generate synthetic data on storm induced beach change. To examine the ability of XBeach to generate synthetic data, the 1D profile model was calibrated and validated with a set of experimental data collected during a large-scale laboratory testing programme.

3.4 Experimental data used to validate the 1D XBeach beach profile model

The present data were acquired from an experiment within the HYDRALAB + transnational access project: “Influence of storm sequencing and beach recovery on sediment transport and beach resilience (RESIST)”. The experiments took place in the enormous CIEM wave flume at Barcelona's Universitat Politècnica (UPC) (Eichentopf et al. 2020). The flume's dimensions were 100 m long, 3 m wide, and 4.5 m deep. The still water depth was 2.5 metres. The flume contained medium-grained sand with a settling velocity (ws) of 0.034 m/s

and a median sediment diameter (D_{50}) of 0.25 mm. A 1:15 slope was constructed for the initial profile. Eichentopf et al. (2019) provide a complete description of the experimental setting.

Figure 3.6 Snapshots of the wave flume. Waves arriving on the flume (Left) and swash zone (right) (Eichentopf et al., 2019)

3.4.1 Bichromatic Wave Cases

Two main frequencies make up a bichromatic wave condition (producing repeated wave groups); erosive and accretive wave conditions (Table 3.4). This section focuses on the erosive E1, E2 and the accretive A1, A2 wave conditions and their associated frequencies f_1 = 0.3041 and f_2 = 0.2365 H_z for E1, and f_1 = 0.3041 and f_2 = 0.0.2365 H_z for E2. For A1, f_1 = 0.2276 and f_2 = 0.1979 H_z and f_1 = 0.2018 and f_2 = 0.1755 H_z for A2. Wave group (Table 3.4) was defined as $T_{g\,=}$ 14.80 s and $T_{g\,=}$ 14.80 s for E1 and E2 respectively, A1, T_g = 33.68 s and T_g = 37.98 s for A2. For each of the waves, there were 3-4 short wave groups, and each was subjected to a peak period of $T_p = 1/f_p$ = 3.7 s for E1 and E2 having same peak period and 4.7 s and 5.3 s for A1 and

A2 respectively. Generally, $f_p = \frac{f_1 + f_2}{2}$. The period after which a wave phase repeats is T_r (the repetition period) = 2* T_g = 29.6 s for E1, E2 and 67.36 s for A1 75.96 s for A2. Not all the tests with wave condition E1, E2 and A1, A2 were analysed in-depth. Only two bichromatic conditions were used for the validation of the model E1 and A1. And two for calibration E2 and A2.

Table 3. 4 Wave parameters for Bichromatic wave cases from RESIST

Test case	Wave type	H_{rms} (m)	T_p(s) Ω (-)	$H_1(m)$	H_2(m)	f_1 (Hz)	f_2(Hz)	T_g(s)
B Benchmark	Random	0.30	4.0	2.21	n/a	n/a	n/a	n/a	n/a
E1 High energy 1	Bichromatic	0.42	3.7	3.34	0.320	0.320	0.3041	0.2365	14.80
E2 High energy 2	Bichromatic	0.32	3.7	2.54	0.245	0.245	0.3041	0.2365	14.80
A1 Low energy 1	Bichromatic	0.23	4.7	1.44	0.101	0.202	0.2276	0.1976	33.68
A2 Low energy 2	Bichromatic	0.19	5.3	1.05	0.085	0.171	0.2018	0.1755	37.98
A3 Low energy 3	Bichromatic	0.14	5.7	0.72	0.63	0.126	0.1877	0.1632	40.85

3.5 XBeach Model Setup for validation

- The XBeach model setup was done following several procedures as described below.

3.5.1 Setting up XBeach Cross-Shore Model Grid and Boundary Conditions

The focus of this Xbeach model set-up was to replicate the experimental set up in 3.4. A non-uniform grid was used in the XBeach model in order to be consistent with the profile of the wave flume used in the RESIST experiment. XBeach uses a coordinate system where the computational x-axis is oriented perpendicular towards the coast and y-axis is oriented alongshore. The numerical simulation were configured using a 1D approach (Surfbeat) to best represent the actual flume conditions. Surfbeat mode computes the propagation of the short wave averaged envelop and accompanying long-wave motion (Roelvink et al., 2009). Short waves

following a JONSWAP spectrum were produced at the offshore boundary. A 300 m long cross-shore domain was used with a constant grid spacing 0.5m. The grid spacing was gradually increased to 1m and kept constant until the model boundary.

The same sediment distribution and wave conditions were used as for the RESIST dataset. The initial bed (Figure 3.7) profile were based on the RESIST experimental beach setup. Following completion of this setup, the model was then run with a simulation time of 30 minutes, which is exactly the length of the wave sequences in the RESIST dataset.

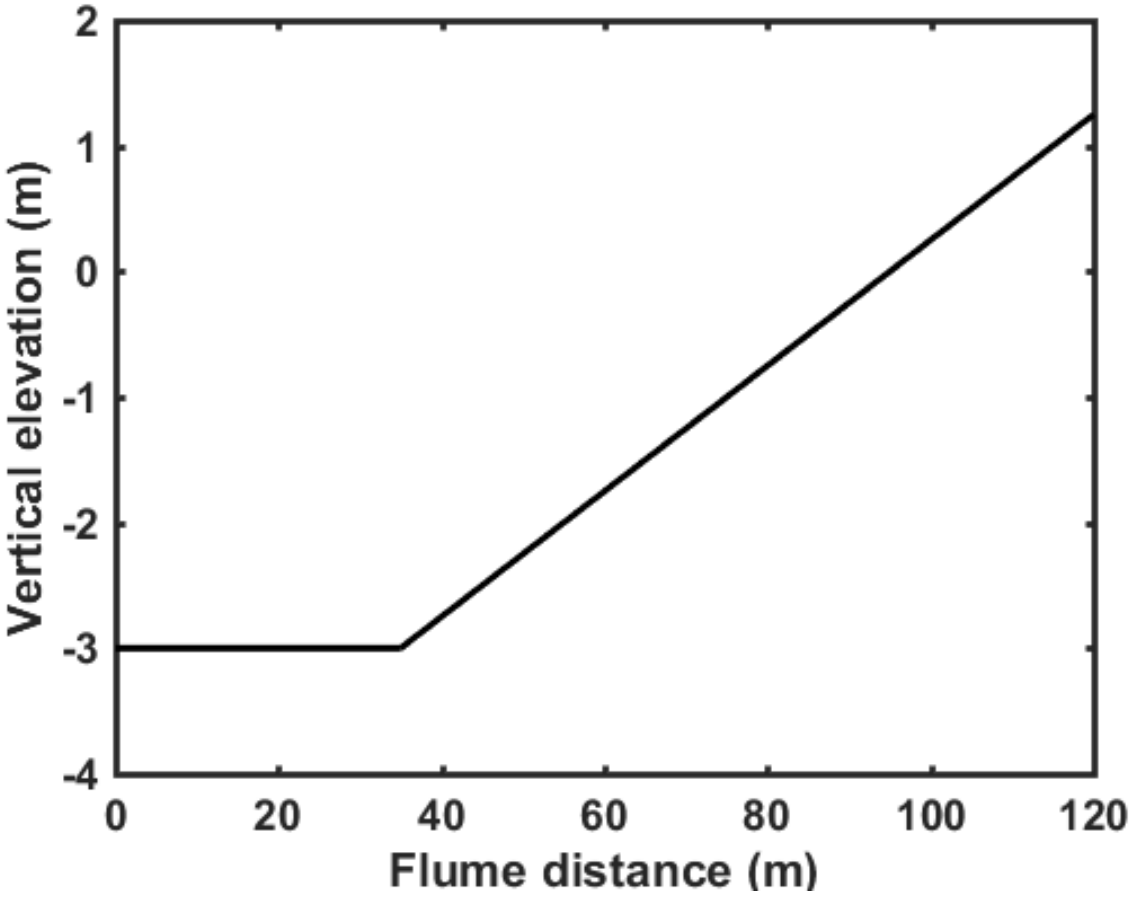

Figure 3.7 Model set-up which replicate the RESIST experiment beach profile

At the offshore boundary, a time series of wave forcing were imposed. For calculating the wave forcing, a JONSWAP spectrum was used to generate a bichromatic wave time series at a time step of 0.5 s resolution, which was used as the offshore wave boundary condition of the model. The JONSWAP spectrum equ. 3.34 and 3.35 was derived from the Joint Wave Observation Program for the North Sea (Hasselman et al., 1973) and is widely used in coastal engineering. The set of parameters in Table 3.5 were used to make the bichromatic waves at the given time interval.

Table 3. 5 Parameters used for JONSWAP spectrum

Parameter	Description
H_{m0}	The significant wave height;
T_p	The peak period of the spectrum;
θ	Main wave angle of incidence;
s	Measures for the directional spreading; and
gammajsp	Peak enhancement factor

$$S(f) = \frac{\alpha g^2}{(2\pi)^4 f^5}\ exp\ \left[-1.25\ \left(\left(\frac{f_p}{f} \right) \right)^4 \right] \Upsilon^{\mathrm{q}} \tag{3.34}$$

where

$$\alpha = 0.076\ \left(\frac{gF}{U_{10}^2} \right)^{-0.22} \quad f_p = \frac{3.5g}{U_{10}}\ \left(\frac{gF}{U_{10}^2} \right)^{-0.33} \tag{1.35}$$

where F = the fetch length and

$$q = exp\ \left(-\frac{(f - f_p)^2}{2\sigma^2 f_p^2} \right)$$

with

$$\sigma = \begin{cases} 0.07 & f \trianglelefteq f_p \\ 0.09 & f > f_p \end{cases}$$

The frequency at which the spectrum attains its maximum value is denoted by f_p. Where γ is the peak enhancement factor and has a mean value of 3.3 from the North Sea measurements.

Numerical simulations were first carried out using default values of the free model parameters to provide an estimate of model performance prior to calibration. Figure 3.8 shows an erosive wave condition with computational time of 14400 secs that was propagated to see the beach profile development at different time. As seen in Figure 3.8, as the time goes on, the profile kept developing until it attained equilibrium at 4hours.

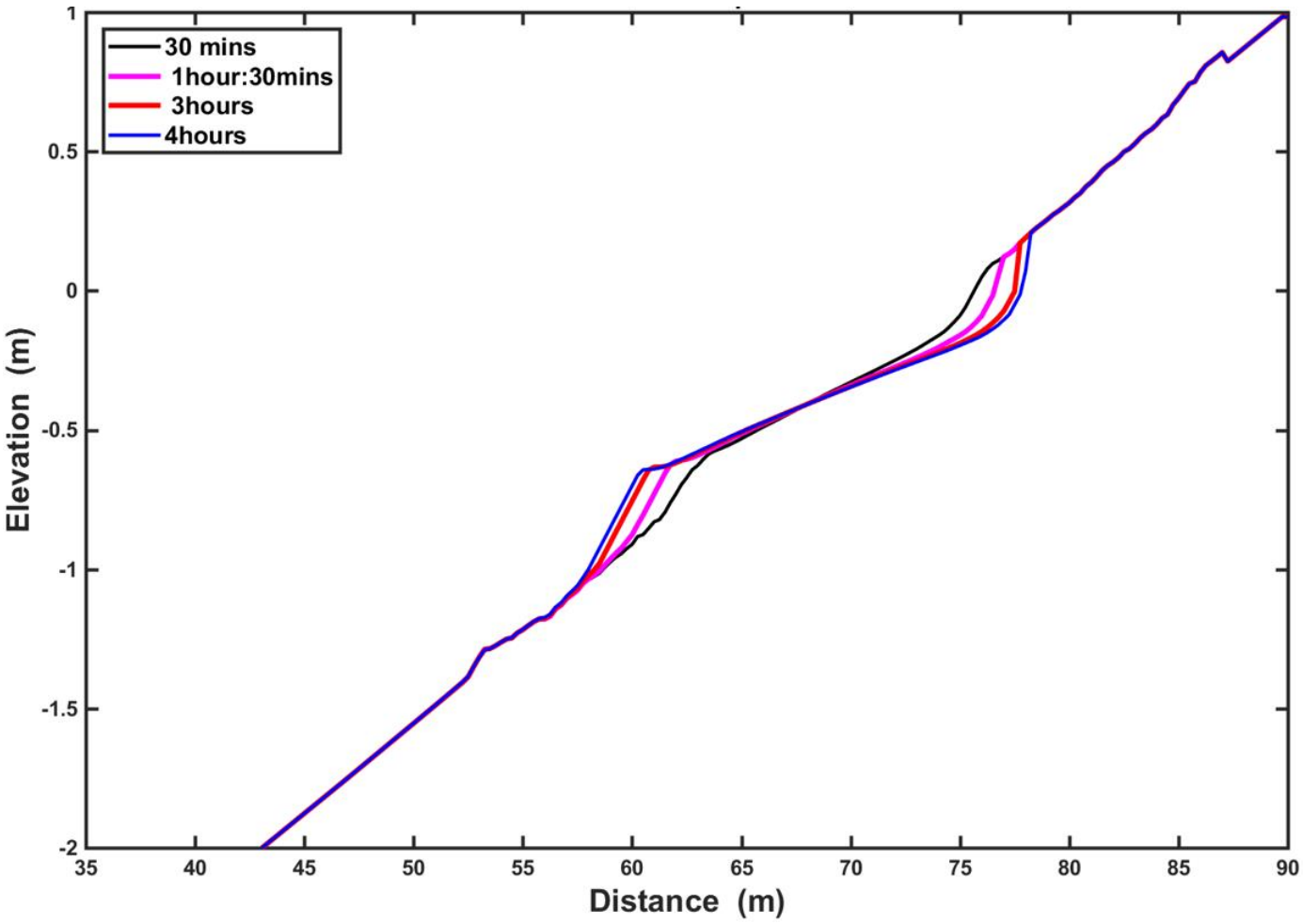

Figure 3.8 Beach development with same wave conditions on different time scale

3.5.2 Wave Input

Bichromatic wave input

The XBeach model is forced by the time-series bichromatic waves at the offshore model boundary as explained in Section 3.5.1. These timeseries were computed by XBeach, but were created in a seprate file in a readable format by the model from the JONSWAP analysis (Section 3.5.1). For the input wave timeseries, the parameters Hrms and Trep were specified in an input file. However, setting up an erosive and accretive wave condition in XBeach, a wave was propagated and compared with the measured wave height to ascertain the wave propagation and its breaking pattern (Figure 3.9). As the wave approaches the shoreline, wave height increases due to shoaling until the waves breaks. Using the relationship in equation 3.36, the wave height at breaking can be estimated by the product of depth at breaking and the breaking criterion or coefficient (γ). In this study, XBeach simulation produced an optimal breaking criterion or coefficient (γ) value of 0.55. The value of gamma depends on the slope of the beach and the physical processes that control the sediment transport and wave energy. Figure 3.9 shows an example of a steep slope.

The wave-breaking criterion is given as:

$$H_b = \gamma h_b \tag{3.36}$$

where:

H_b and h_b are the significant wave height and water depth at the breaking point respectively. γ is the breaking point index usually taken as 0.78.

To estimate the *hb* at which wave breaking occurs, the point of maximum shoaling wave height was extracted. An example case is shown in Figure 3.9, for the model conditions H_s 0.3 m, T_p 3.0 m with slope 1:10 on a steep beach. (Figure 3.9) Subsequently, for this example case *hb*= 0.4m. H_b is then calculated using, γ = 0.55 and h_b = 0.4m and Equation 3.36.

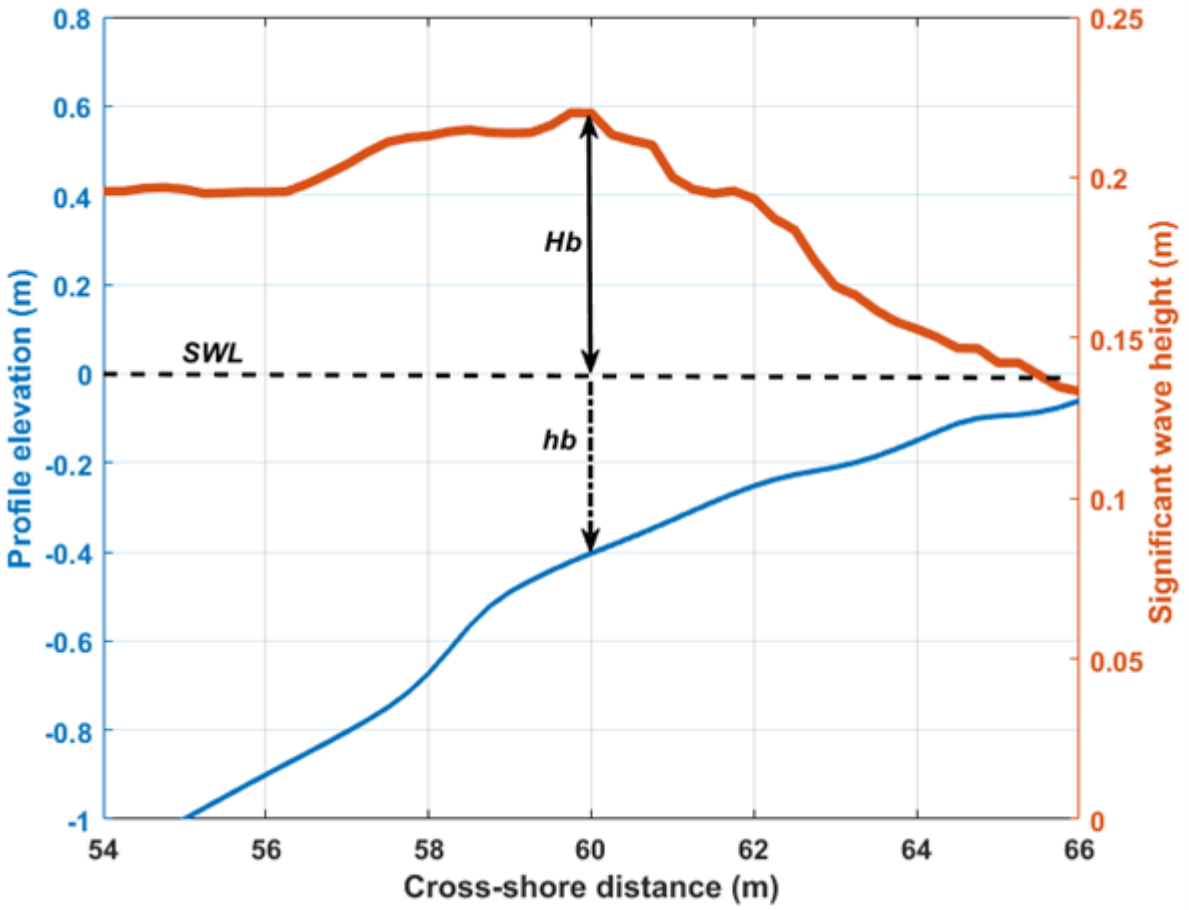

Figure 3. 9 Illustration of a wave propagation and its breaking point on a steep slope

Wave height comparison in surfbeat mode can be challenging because XBeach Surfbeat solves the variation in the short-wave envelope on wave group scale using the wave action balance equation (Figure 3.10a). This contrasts with combining surfbeat with other modes in XBeach, as surfbeat does not compute short waves.

The experimental set up deployed several wave gauges at various cross shore points, and to be concomitant with the setup, an envelope of time series was generated at each wave gauge using short wave measurements (e.g., Figure 3.10b).

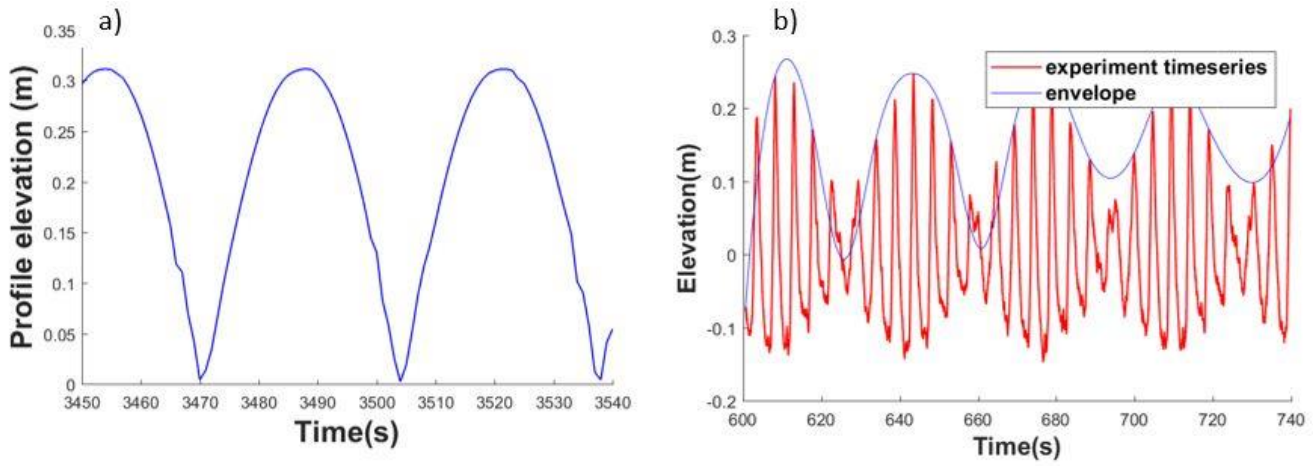

Figure 3. 10 (a) Snapshots of short-wave envelopes of bichromatic waves (light blue lines) and (b) short waves (red lines) used in RESIST experiments (red lines) with Hs 0.2 m Tp 4.7 s and 2.5 m water depth for both cases.

3.5.3 Input Variables

The XBeach model can run with most parameters in default settings. The user simply needs to provide the hydrodynamics and initial bed level. However, there are a few parameters in the XBeach model that can be utilised to calibrate the model. Table 3.6 below provides definitions for a few of the common input parameters used by XBeach. A number of these parameters in Table 3.6 have variable values which have to be 'turned' to attain good model results. These parameters are H_{rms}, T_{rep}, eps, C, gamma and alpha as defined in Table 3.6. The values of H_{rms} and T_{rep} depend on the wave input, e.g., bichromatic wave. The *eps* is the parameter that denotes the threshold water depth above which cells are classified as wet or dry. As a result, it distinguishes between wet and dry grid cells. The model's bed roughness can be changed by changing the C parameter for the Chezy friction coefficient. Wave breaking and dissipation are both impacted by the factor's alpha and gamma. The parameter alpha, gamma and gamma2 are all related to wave breaking and dissipation. Also, a threshold that determines when the breaking of waves starts. It is known as the parameter value increases, dissipation due to wave breaking decreases. In many studies it has been used as a calibration parameter to improve morphological changes due to wave breaking. (Daly et al., 2012; Williams et al., 2012; Harley et al., 2016; Jin et al., 2020).

Table 3. 6 XBeach input parameter

Parameter	**Description**	**Value**	**Units**
depfile	Name of input bathymetry file	Bed.dep	<file>
nx	Number of grid points in x-direction	103	
ny	Number of grid points in y-direction	2	
thetamin	Lower directional limit	-90	deg
thetamax	Upper directional limit	90	deg
nglobalvar	Number of global output variables (as specified by user)		
nmeanvar	Number of mean variables (as specified by user)		
tstart	Start time of simulation		s
tint	Time interval output global values	1	s
Hrms	Root mean square wave height		m
Trep	Alternative keyword for representative period		s
Tlong	Long wave/ wave group period		s
C	Chezy friction coefficient		
dtheta	Directional resolution	180	deg
dir0	Directional of wave propagation	270	deg
CFL	Courant number	0.9	
eps	Threshold water depth		m
gamma	Breaker parameter		
gammax	Maximum ratio of H/h		
Beta	Breaker slope coefficient		
n	Power in roelvink dissipation model		
alpha	Wave dissipation coefficient		

Model Output

The output requested from XBeach are the:

- Bed level (*zb*)
- Initial bed level (*zb0*)
- Water depth (*hh*)
- H_{rms} wave height based on instantaneous wave energy (H)
- Water level (*zs*)

The bed level was fixed in XBeach, thus *zb* and water depth were kept constants for all computational outputs.

3.5.4 Calibration of Free Model Parameters

Model parameters that produced the best model performance were investigated during the calibration processes. Table 3.7 below, shows the recommended default value and range of the selected parameters for model calibration. Most parameters were set to their default values as advised by the model XBeach manual (Roelvink et al., 2010), and other extensive scientific literature on the calibration of the XBeach model (Vousdoukas et al., 2012; Pender and Karunarathna, 2013; Dissanayake et al., 2014; Nederhoff et al., 2015; Elsayed and Oumeraci, 2017; Schambach et al., 2018; Simmions et al., 2019). The XBeach model was run with varying free parameters until a good agreement is reached between the RESIST measured profiles selected for calibration and the XBeach model. The wave conditions selected from the RESIST experiments to calibrate the model is shown in Table 3.7.

Table 3. 7 Free model parameters and their validity range, with the proposed defaults values

Parameter	Definition	Range	Default
eps	Threshold water depth about which cells are considered wet	0.001-0.1m	0.005m

facua	Calibration factor time averaged flows due to both wave skewness and wave asymmetry	0 – 1	0.1
form	Equilibrium sediment concentration formulation	van Thiel_vanRijn and soulsby_vanRijn	van Thiel_vanRijn
wetslp	Critical wet slope for avalanching	0.1 - 1	0.3
gamma	Random wave equivalent of the breaker index	0.4 – 0.9	0.55

Table 3. 8 RESIST wave cases and conditions selected for calibration.

Case	H_s (m)	T_p (s)
E2	0.32	3.7
A2	0.19	5.3

3.5.5 Sensitivity Analysis

The sensitivity of model outputs to the free model parameters was investigated by observing how the bed profile changed as their values were altered. This enhanced calibration. Parameter values were changed one at a time keeping all other parameters at their default values, simulation duration was 14400sec. Four model parameters were selected for the sensitivity analysis. These parameters were *wetslp, facua, gamma, and eps. Facua* is the model parameter that is used for tuning of the morphodynamics, it's the only parameter that directly influences the net cross-shore transport (Vousdoukas et al., 2012). *Gamma* is the wave breaking index, controlling the wave breaking height criteria in the wave breaking model formulation (Roelvink, et al., 2015). The *eps* is the parameter that denotes the threshold water depth above which cells are classified as wet or dry. *Wetslp,* the critical bed slope for the initiation of avalanching at the dry part of the profile.

Calibration parameter: *eps*

The *eps* is the parameter that denotes the threshold water depth above which cells are classified as wet or dry. In physical terms, the eps parameter represents the minimum water depth for XBeach calculations. Figure. 3.11 displays the model's output for sensitivity simulations with eps of 0.1, 0.003, 0.005, and 0.007 metres,

respectively. The model results showed that erosion inside the swash zone was sensitive to *eps* value, with a diminishing response for higher *eps* values.

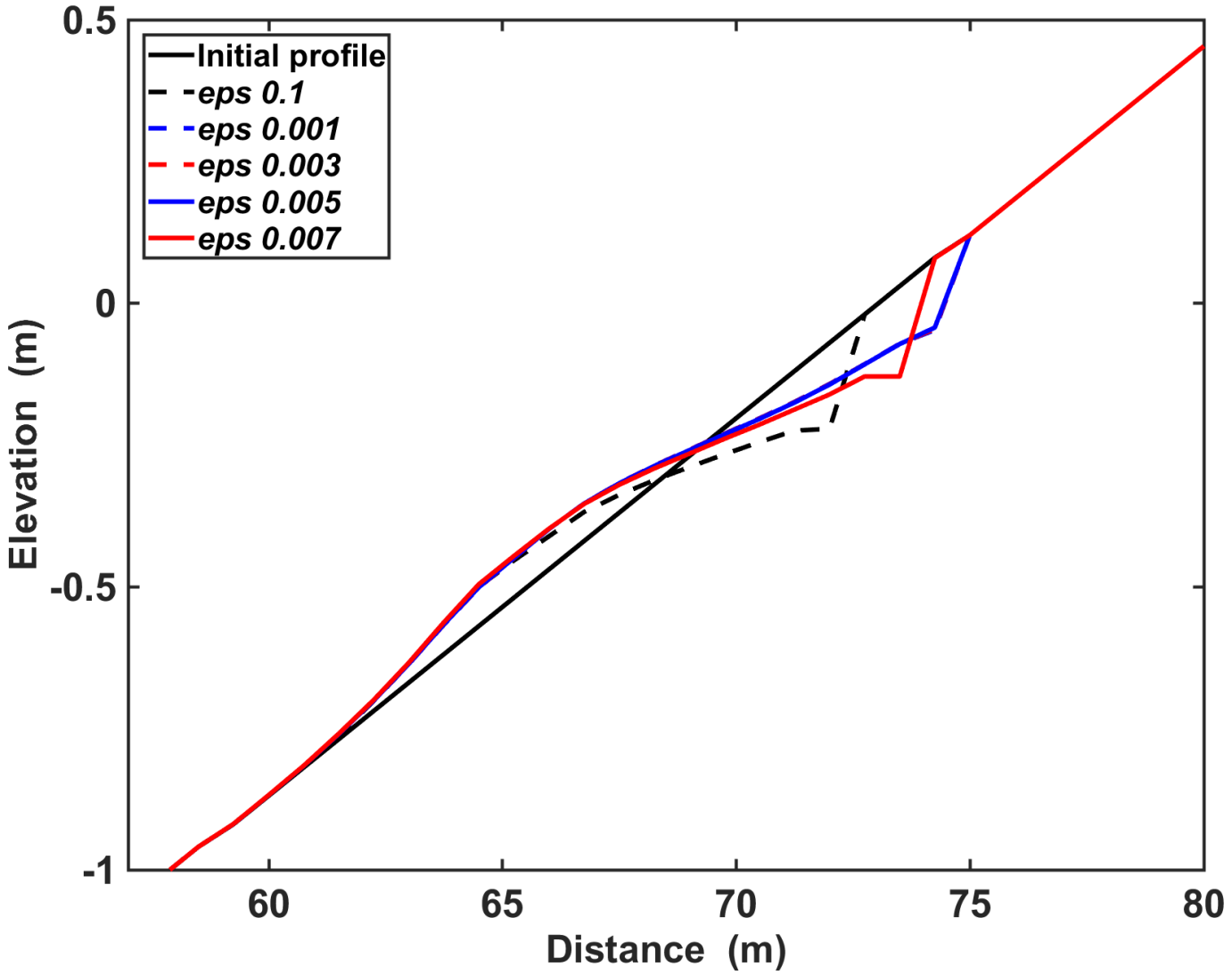

Figure 3.11 Sensitivity of model to different eps values calibrated for 14400 s, which was the duration for beach profile to reach equilibrium.

Calibration parameter: *facua*

facua is the calibration factor for short-wave averaged sediment transport due to both wave skewness and wave asymmetry. Several values were assigned to *facua* as 0.0, 0.2, 0.5, 0.7 and 1.0 m as shown in Figure. 3.12. The cross-shore profile evolution responded strongly to a changing *facua* value, a higher value resulted in less net offshore sediment transport and stronger onshore sediment transport components.

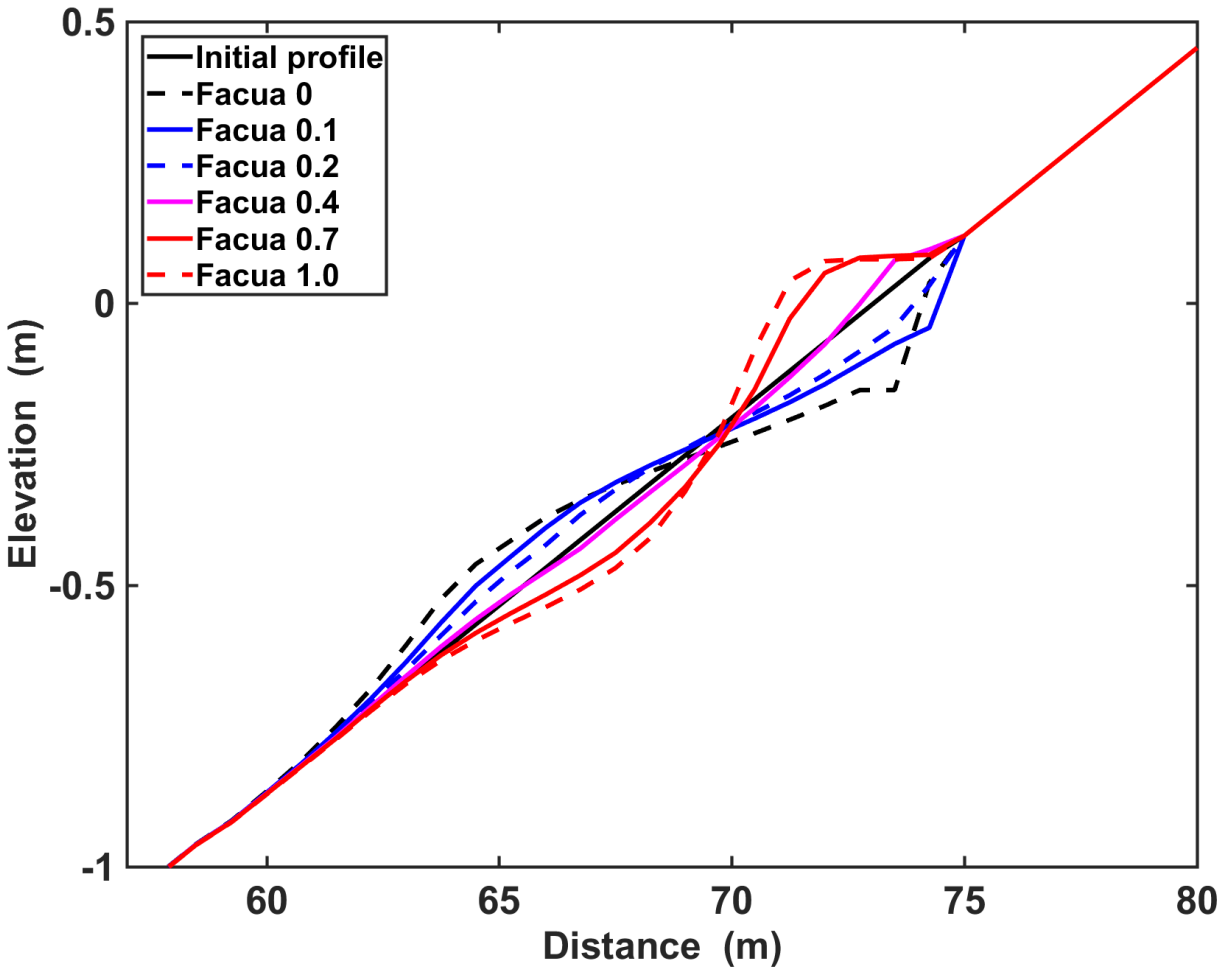

Figure 3.12 Effects of the sensitivity of the model to different facua value calibrated for 14400 s, which was the duration for beach profile to reach equilibrium

To test the sensitivity of the model to the parameterized wave asymmetry sediment transport component (facua), the first step was to increase the values. Higher values are suitable for dune erosion since they will lead to less net offshore sediment movement. The default setting is 0.1, however Nederhoff (2014) discovered that for New Jersey, a facua of 0.25 led to good agreement in morphological development during Hurricane Sandy. For modelling the dune and beach erosion in XBeach, the influence of wave skewness (facua) on the transport of sediment appears to be the parameter with the greatest sensitivity. Additionally, research on the effects of the storm in 2009 on the Australian coast found this parameter to be crucial (Splinter, Palmsten2012). The choice of facua values imposes onshore versus offshore wave-driven sediment transport. When there is a storm, it is assumed that the sediment is transported primarily offshore (*facua* = 0), and when there is calm (*facua* = 1), the sediment is transported towards the shore. To achieve the best possible balance between onshore and offshore sediment transport in the nearshore region during storm conditions, we calibrate XBeach for facua > 0, as indicated in Figure 3.14 for different values for accretive cases and facua between 0.25 and 0.5 was examined for erosive cases Figure. 3.13. Qualitatively, it can be argued that the facua parameter should be set to 0.5 for mild wave conditions and zero or extremely low values (as suggested by Van Thiel de Vries in 2009) for storm events. Other than facua, other parameters calibrated did not appear to be sensitive.

(A)

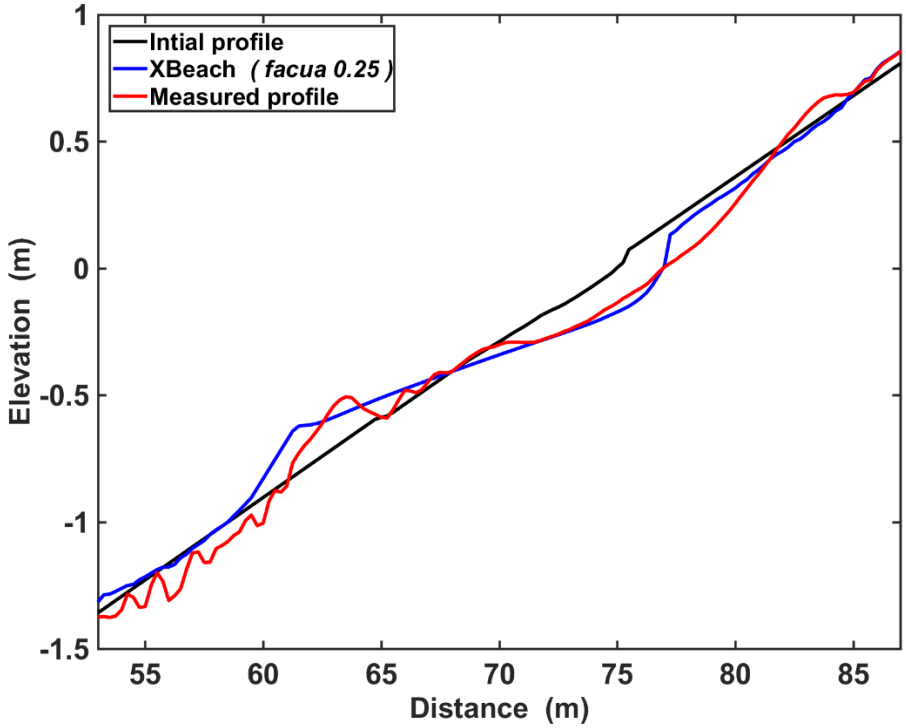

(B)

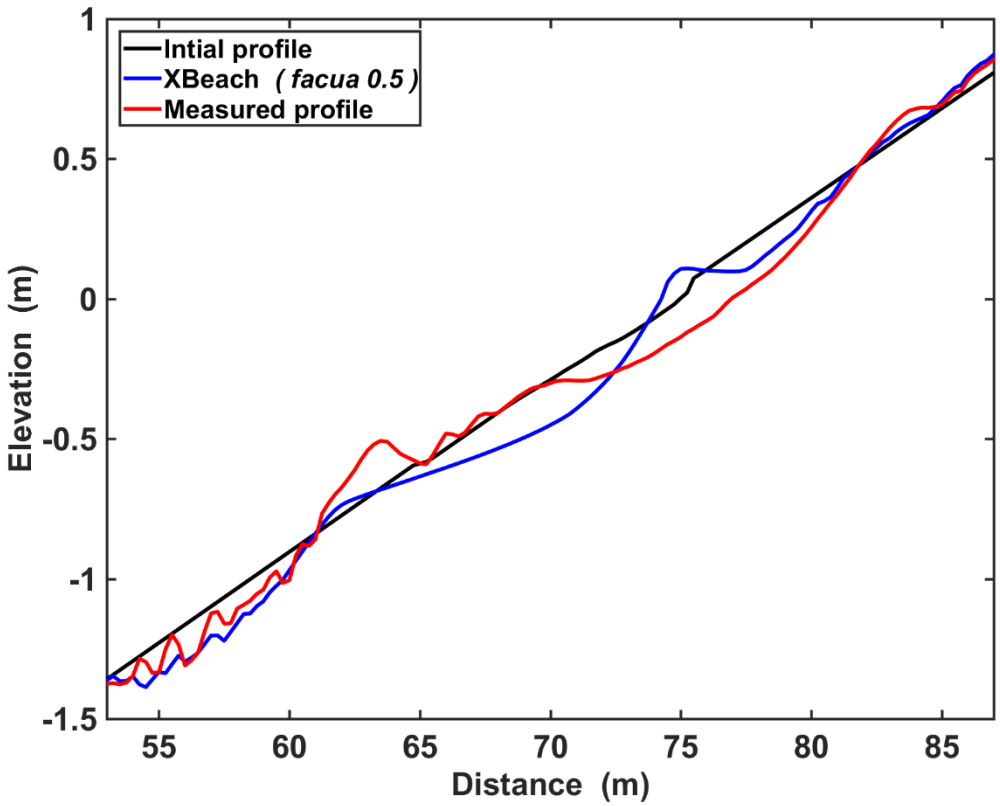

Figure 3.13 Post storm profiles with different facua parameters for erosive cases (a) Facua 0.25 (b) Facua 0.5 with Hs 0.32 m and Tp 3.7 s

(A)

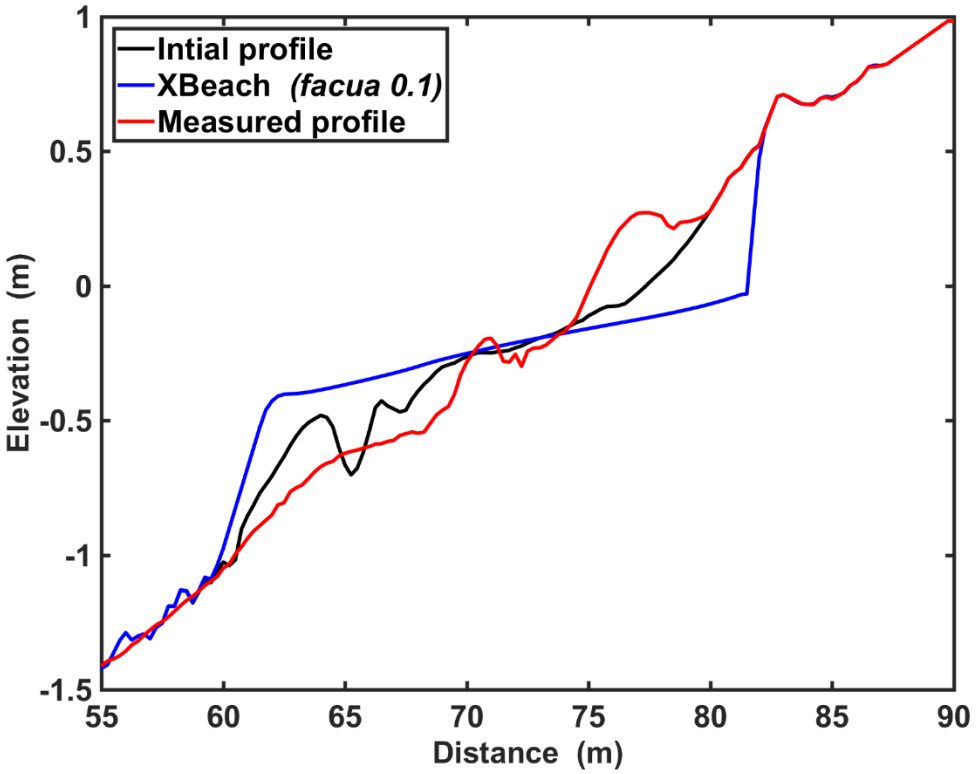
Intial profile
XBeach (facua 0.1)
Measured profile
Elevation (m)
Distance (m)
1
0.5
0
-0.5
-1
-1.5
55
60
65
70
75
80
85
90

(B)

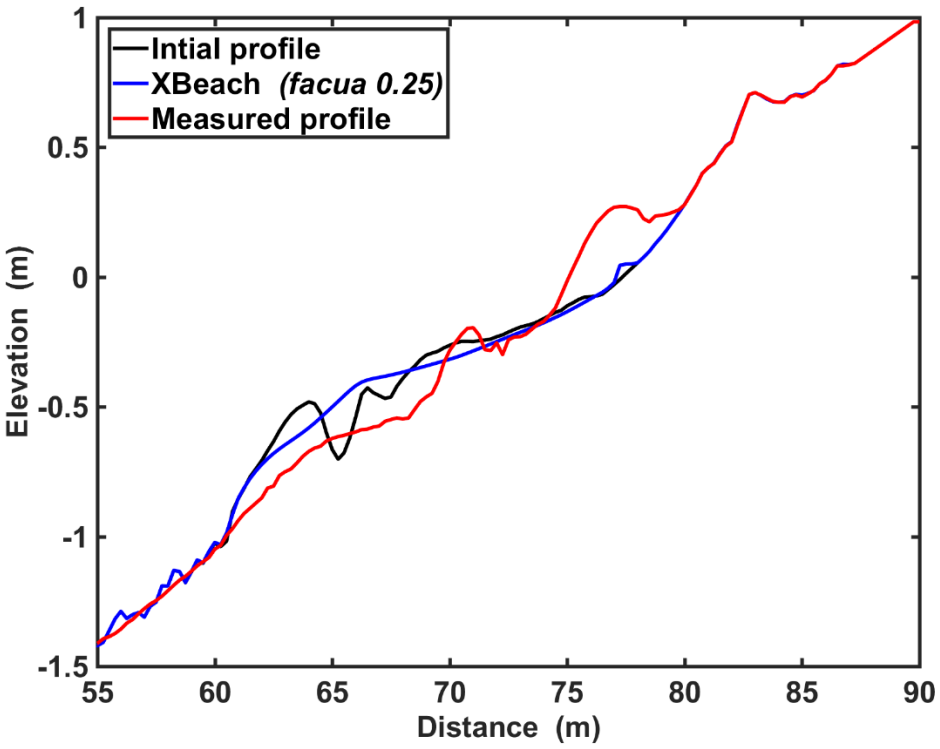
Intial profile
XBeach (facua 0.25)
Measured profile
Elevation (m)
Distance (m)
1
0.5
0
-0.5
-1
-1.5
55
60
65
70
75
80
85
90

(C)

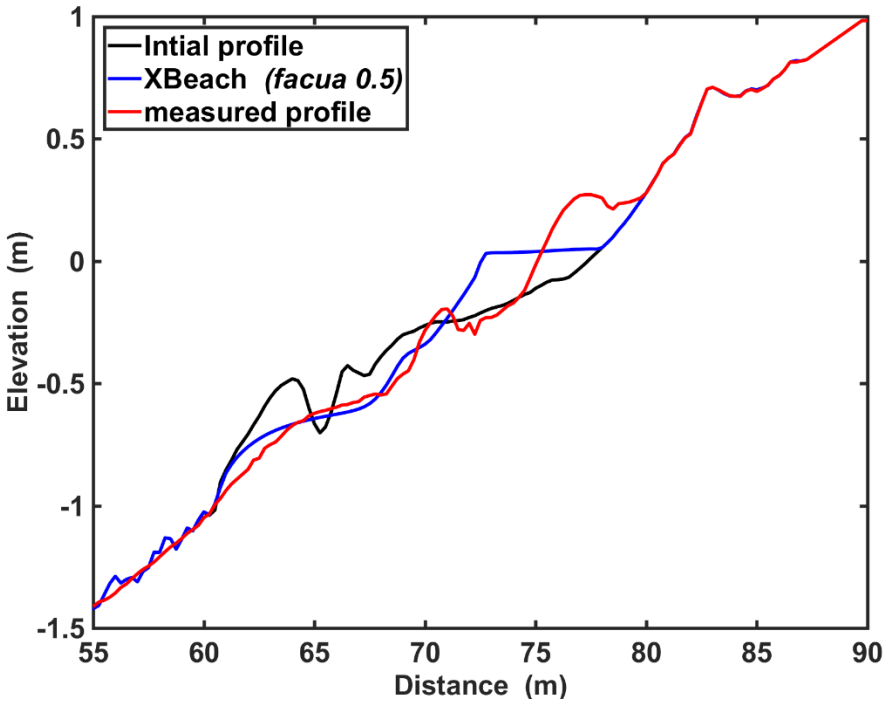

(D)

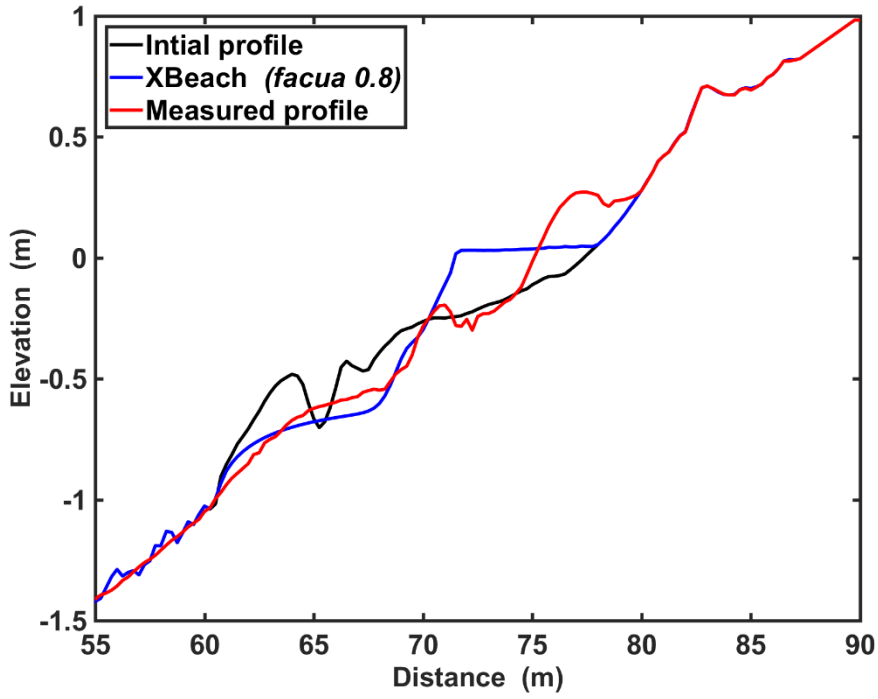

Figure 3.14 Post storm profiles with different facua parameters for accretive cases A2 (a) Facua 0.1 (b) Facua 0.25 (c) Facua 0.5 (d) Facua 0.8 with Hs 0.19 m and Tp 5.3 s

The best model performance for both erosive and accretive cases was obtained with the following parameter values: gamma = 0.55, facua = 0.5, wetslp = 0.2-0.4, eps = 0.1-0.007. Facua represents one of the most important parameters in XBeach as it is the only parameter mostly affecting the net cross-shore sediment transport.

3.6 Model validation

For the validation of the model, two experimental cases were selected: E1 representing a highly energetic storm and Al low energy conditions given in Table 3.9.

Table 3. 9 RESIST wave cases and conditions selected for validation.

Case	H_S (m)	T_P (s)
E1	0.42	3.7
A1	0.23	4.7

The results of the calibrated model were evaluated by comparing the results with the measured profiles. Within the context of coastal morphological modelling, a Brier Skill Score (BSS) is also a suitable and commonly used statistical indicator of accuracy. In the current study, a quantitative validation method was carried out by calculating the Brier Skill Score (BSS) (Vousdoukas et al. 2012; Sanuy and Jimenez 2019). The BSS applied to the compare the numerical results with laboratory results was computed with relation:

$$BSS = 1 - \left(\frac{\langle \| x_{p-} x_m \|^2 \rangle}{\langle \| x_b - x_m \|^2 \rangle} \right) \tag{3.37}$$

In which:

x_p is the predicted profile.

x_m is the measured profile

x_b is the initial profile.

The Brier Skill Score (BSS) represents how well the model predicts the bathymetry compared with the initial bathymetry. If the model is equal to the initial profile and no differences with the model, BSS is 0. When the

prediction for a certain moments is equal to the mesurements at that moment, the skill of the model is perfect and the score is 1 or close to 1 e.g., 0.8 – 1. When the model prediction is not as good as the initial profile, the (BSS) becomes negative. Table 3.10 shows the classification of BSS

Table 3. 10 Classification of Brier Skill Score (BSS) by Van Rijn et al.,2003

Score	**Classification**
<0	Bad
0.0 – 0.3	Poor
0.3 – 0.6	Reasonable
0.6 – 0.8	Good
0.8 – 1.0	Excellent

The qualitative assessment of each modelled results along with their measured profiles (Erosive and Accerative) are shown in Figure.3.15 and Figure 3.16. From the Figure below, the erosive case was captured well but the accreative case around (x ~75 m) there is berm formation above the water level, the model was unable to reproduce the measured profile.

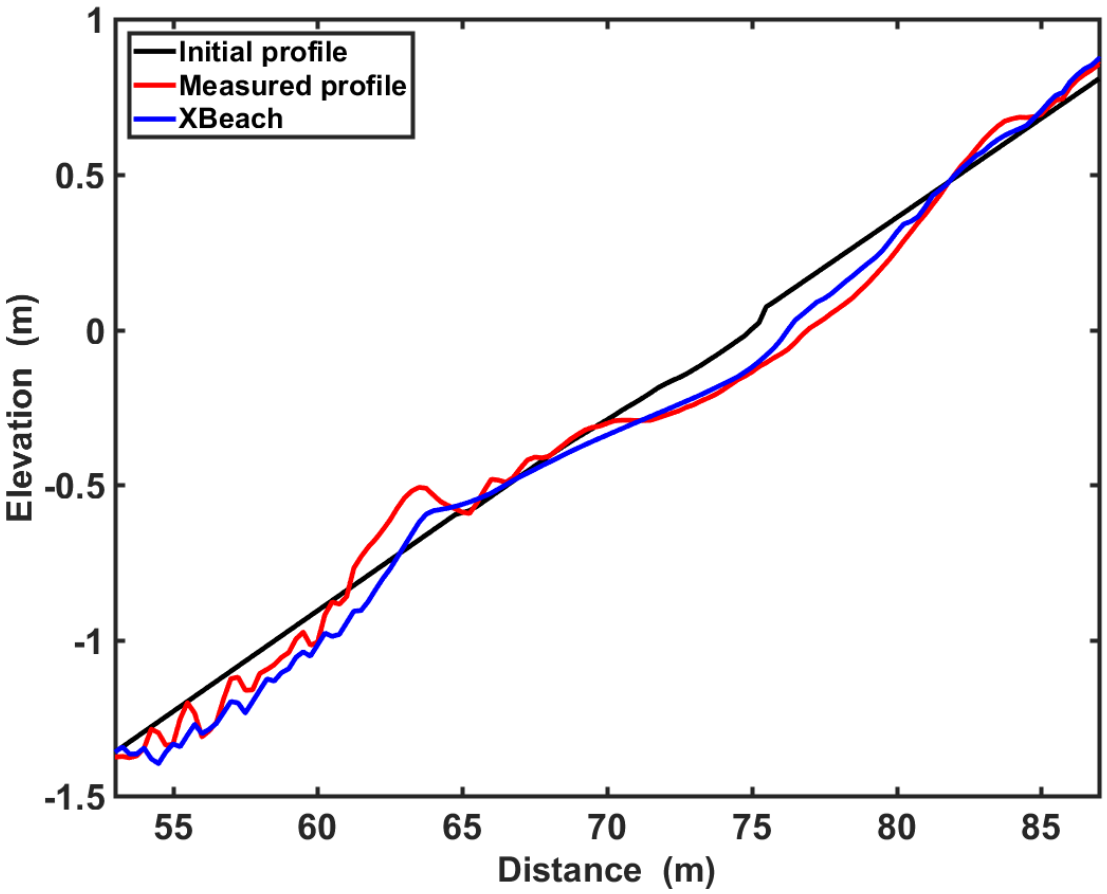

Figure 3.15 Comparison of the simulated profile with measured post-storm profile (erosive) for the storm case E1 with Hs = 0.42 m and Tp = 3.7 s Duration of 14400 s

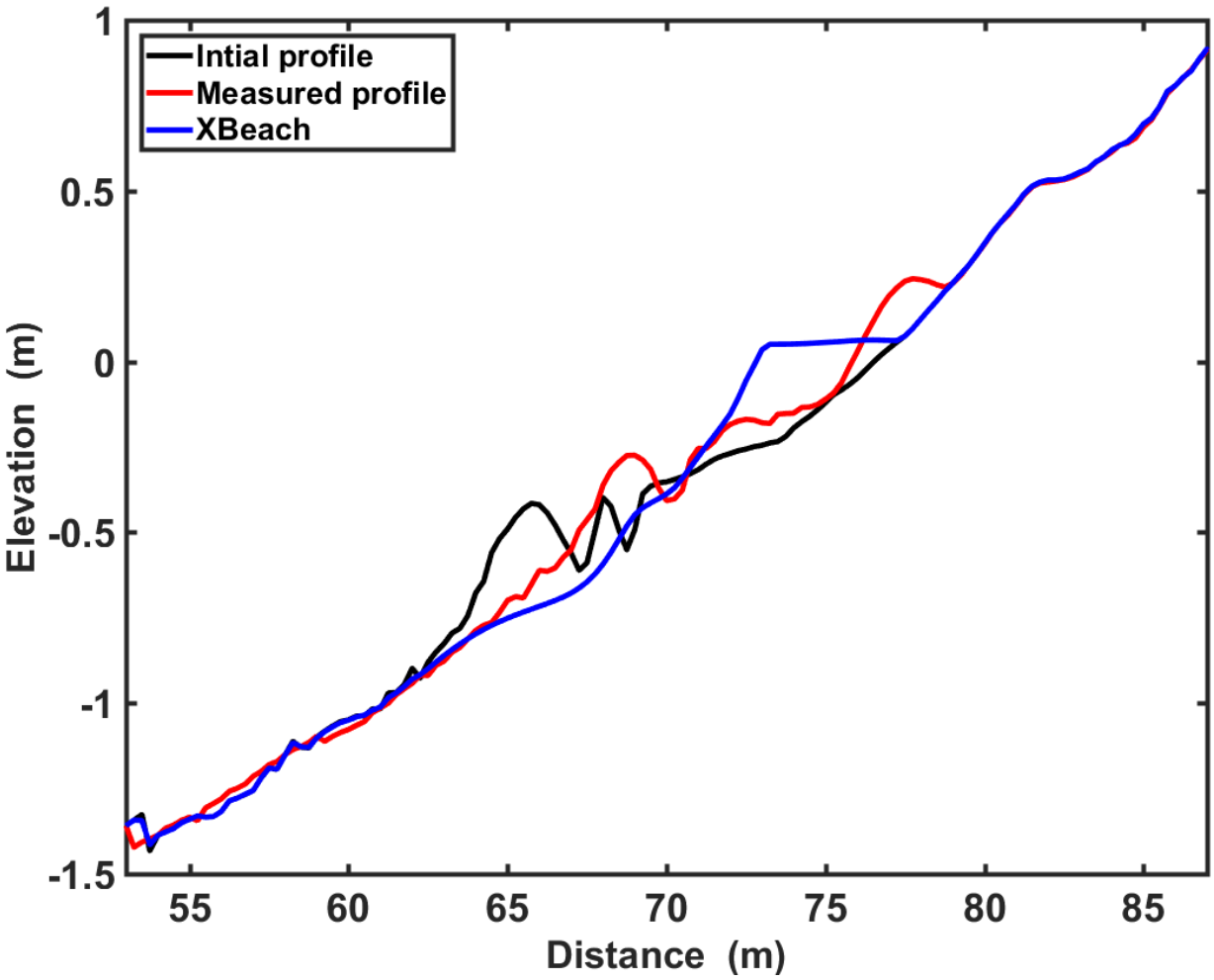

Figure 3.16 Comparison of the simulated profile with measured post-storm profile (accretive) for the storm case A1 with Hs = 0.23 m and Tp = 4.7 s

The model showed good agreement with the experimental data. The BSS for the comparison of post-storm profiles for E1 and A1 were 0.87 and 0.56, respectively. These BSS values correspond to an 'excellent' and 'good' classification respectively (van Rijn., 2003).

It should be noted that in XBeach surfbeat mode, waves are resolved at group scale. Wave asymmetry and skewness are incorporated using simplified empirical formulations and free parameters. As a result, some differences are expected between measured and simulated beach profiles.

3.7 Conclusion

XBeach numerical model set of a 1D beach profile was calibrated and validated against RESIST experimental beach profile evolution data. Key parameters *eps*, *wetslp*, *gamma* and *facua* were calibrated and sensitivity analysis has shown that an increased facua in the XBeach model is important to obtain satisfactory results. The best results were obtained when the value of facua was 0.5 which gave a good BSS value. According to Voukouvalas(2010) facua = 0 or lower than 0.5 indicates storm conditions, whereas facua =0.5 is suitable for medium wave conditions. The calibrated model captures beach profile change under both erosive and accretive

conditions satisfactorily. The validation of the model against erosive and accretive experimental conditions of E1 and A1 yielded 'excellent' and 'good' BSS values of between 0.87 and 0.56 respectively which gives confidence to use the model in this study for simulating beach profile response from both erosive and accretive conditions in modelling erosive profiles.

Chapter 4: Modelling Beach State Variability

4.1 Introduction

According to Wright and Short (1984), a beach profile can evolve around different states depending on their slope, sediment type and incident wave characteristics. Each individual beach state has a distinguished set of characteristics. This chapter is focused on investigating this beach state variability and developing a simple set empirical formulae which can predict beach profile state change under different wave conditions. A large synthetic dataset on beach profile change generated using the open source XBeach coastal model is used to develop the empirical formulae. It is anticipated that the empirical formulations will allow bypassing computationally costly numerical simulations to determine beach state variability of a given beach under different wave conditions.

Generally, there exist several parameters that influence the beach state change. One of such parameters is the dimensionless fall velocity (Dean 1973; Karus et al., 1991; Reeve et al., 2018). A detailed and efficient classification of beach types first proposed by Dean (1973) based on the dimensionless fall velocity of Gourlay (1968) was used to define the beach states in this study. This parameter is hereafter known as the Dean parameter (Ω) as stated in chapter 2 Equation .2.3.

Beach state variation corresponds to certain morphological features like shoreline change and inter-tidal bar and berm, which are the key morphological features of a beach profile. Beach states are extremely sensitive to wave energy variation (Wright & Short, 1984). Low energy beaches are associated with a large and wide berm (Wright & Short, 1984). According to Weir et al. (2006), the presence of berms has been linked to berm over wash, sediment accumulation on the berm crest and the horizontal sediment advection, and the subsequent dispersion of sediment transport along the beach (Alsina et al., 2005, 2018).

4.1.1 Beach Gradient and Sediment

Apart from the influence of waves on beach state variations, the slope of the beach face is a crucial parameter in coastal geomorphology and coastal engineering, as it is required for calculating the total height and excursion of wave run-up at the shoreline (Stockdon et al., 2006; Gomes da Silva et al., 2020; Vox et al., 2022). The beach-face slope parameter acts as an efficient substitute for surf-zone hydrodynamics and can provide information on wave set-up across the surf zone and the safety of beach swimmers in the absence of expensive surf-zone bathymetric data (Short et al., 1993; Stephens et al., 2011). Many physical parameters relate to the beach slope e.g., wave period, wave height, wave duration, wave direction, median grain size, etc. (Kim et al., 2014). Beaches are highly dynamic and complex, with sediments continually reworked and redistributed to attain equilibrium and a steady state under a highly variable hydrodynamic regime. (Splinter, et al., 2014). In this study, empirical formulae (Equations 4.2 and 4.3) derived by Wiegel (1964) for estimating beach slope as a function of grain size and wave energy were used. The beach face gradient therefore changes

under different sediment characteristics like grain size and sediment sorting (Bascom, 1951; Wiegel, 1964; Turner, 1995; Wilson et al., 2008; Reis and Gama, 2010); and swash infiltration/exfiltration on the equilibrium beach face (Turner and Masselink, 1998; Puleo et al., 2000; Baldock and Hughes, 2006). Five slopes (1/10, 1/20 1/30, 1/50, 1/100) were randomly selected and used to compute the grain sizes (D_{50}) for different beach states.

For dissipative beaches ($\Omega = 6$), the mean grain size is related to the beach slope (at mid-tide level) as in the empirically derived Equation 4.2 (Wiegel (1964).

$$D = -49.41 + 51.45\, S^{-0.01563} \tag{4.1}$$

where D is the mean grain size in phi, S is the beach slope in degrees. For the reflective beaches ($\Omega = 1$), the mean grain size for a given slope is defined by the Equation 4.3.

$$D = -41.68 + 44.71\, S^{-0.01991} \tag{4.2}$$

4.1.2 Fall Velocity

The fall velocity or settling velocity (w_s) of particles is referred to the velocity at which force due to gravity exceeds fluid forces and this depends on both the characteristics of particles and fluid. It is difficult to obtain a specific mathematical transcription of fall velocity because sediment particles are irregular in shape. Van Rijn (1993) derived a formula for spherical particles, and it is based on the kinematic viscosity and other properties of the particle and water density as shown in Equation 4.3:

$$w_s = 10\frac{v}{\overline{d}}\left[\left(1 + \frac{0.01\left(\frac{p_s}{p_w} - 1\right)gd^3}{v^2}\right)0.5 - 1\right] \tag{1.3}$$

where:

v = Kinematic viscosity $[m^2/s]$

d = Sphere diameter $[mm]$

p_s = Sediment density $[kg/m^3]$

p_w = Water density $[kg/m^3]$

g = Acceleration due to gravity $[m/s^2]$

Using the five main slopes that were selected and Equation 4, the Fall velocities were then computed correspondingly (1/10 ~ 0.0519 m/s; 1/20 ~ 0.0633 m/s; 1/30 ~ 0.0503 m/s; 1/50 ~ 0.0369 m/s; 1/100 ~ 0.0218 m/s).

4.1.3 Numerical simulation scenarios for wave conditions

Numerical simulations of beach profile change were carried for a range of different beach slopes (m= 1:10, 1:20, 1:30, 1:50, 1:100), sediment sizes (median grain diameter d_{50} = 0.35, 0.43, 0.34, 0.26, 0.18 mm) under a range of incident wave conditions (Hs = 0.1, 0.2, 0.3, 0.4 and 0.5 m; Tp = 1.0, 2.0, 3.0 s). D_{50} values, appropriate for each seabed slope, were used. A numerical wave channel with an offshore water depth of 3.0 m is developed using XBeach non-hydrostatic model, calibrated validated as presented in Chapter3. The initial (pre-storm) beach profile for all beach slopes was taken as a plane beach (Figure. 4.1). Different water level variations, representative of high and low tidal evaluations (0.15 m and 0.25 m) were analysed.

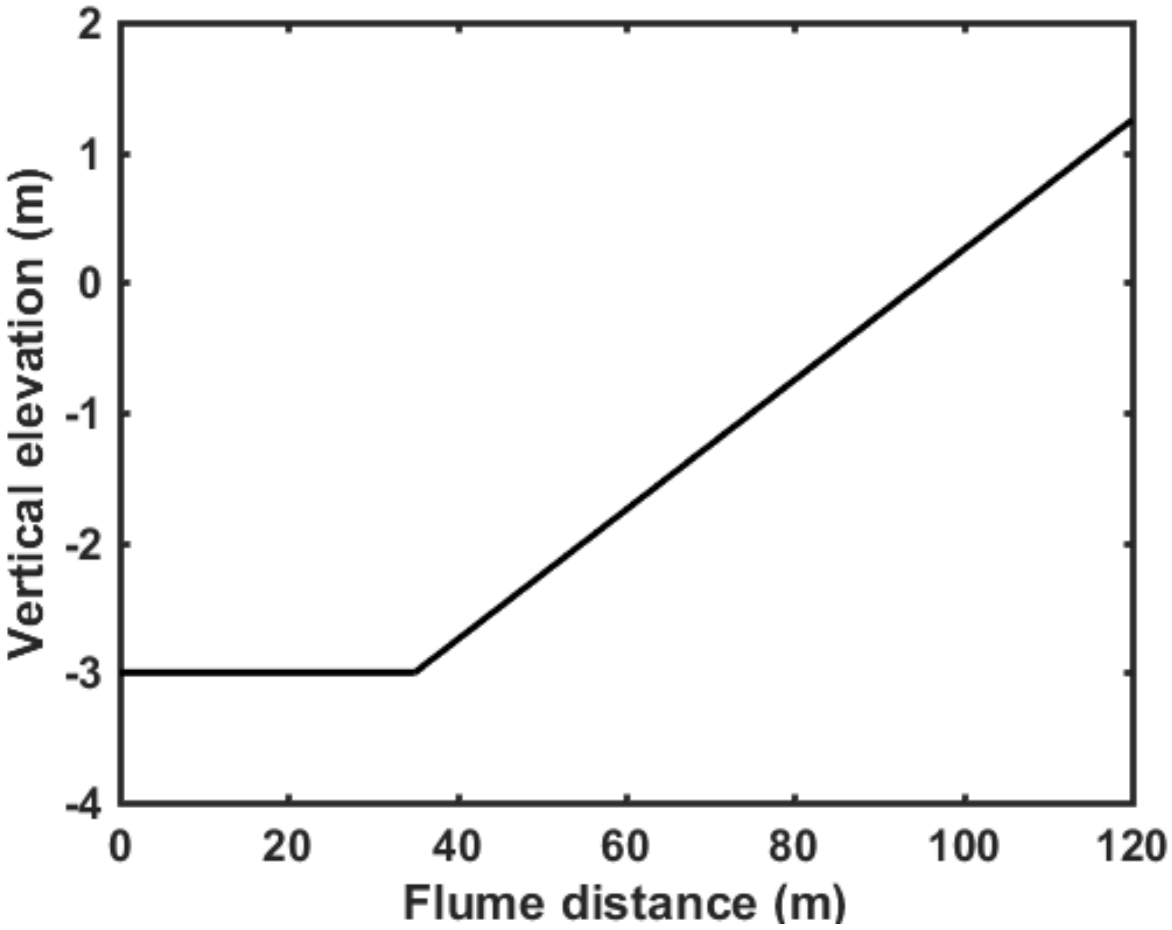

Figure 4.1 Cross-shore numerical wave flume developed using XBeach non-hydrostatic model

A wide range of scenarios were developed by combining wave conditions and beach characteristics covering accretive and erosive wave conditions with different range of Ω values. About 300 conditions were simulated and were grouped depending on their Ω values for the 3 different beach states. In all, six variables were used. Water depth is kept constant and Ω factor gives three beach conditions. XBeach non-hydrostatic is computationally expensive because of the large number of simulations, thus a high-performance computer (HPC) was used for all simulations. The morphodynamic change of the beach under different wave conditions was obtained by simulating the wave conditions on a time range of 5 to 200 hours. To achieve this, waves could propagate until an equilibrium state of the beach was attained, i.e., until the changing rate of the beach profile becomes small, as seen in Figure.4.2. The profile changes became negligible after the fourth hour, signifying that equilibrium has been attained. To see changes it was measured every hour.

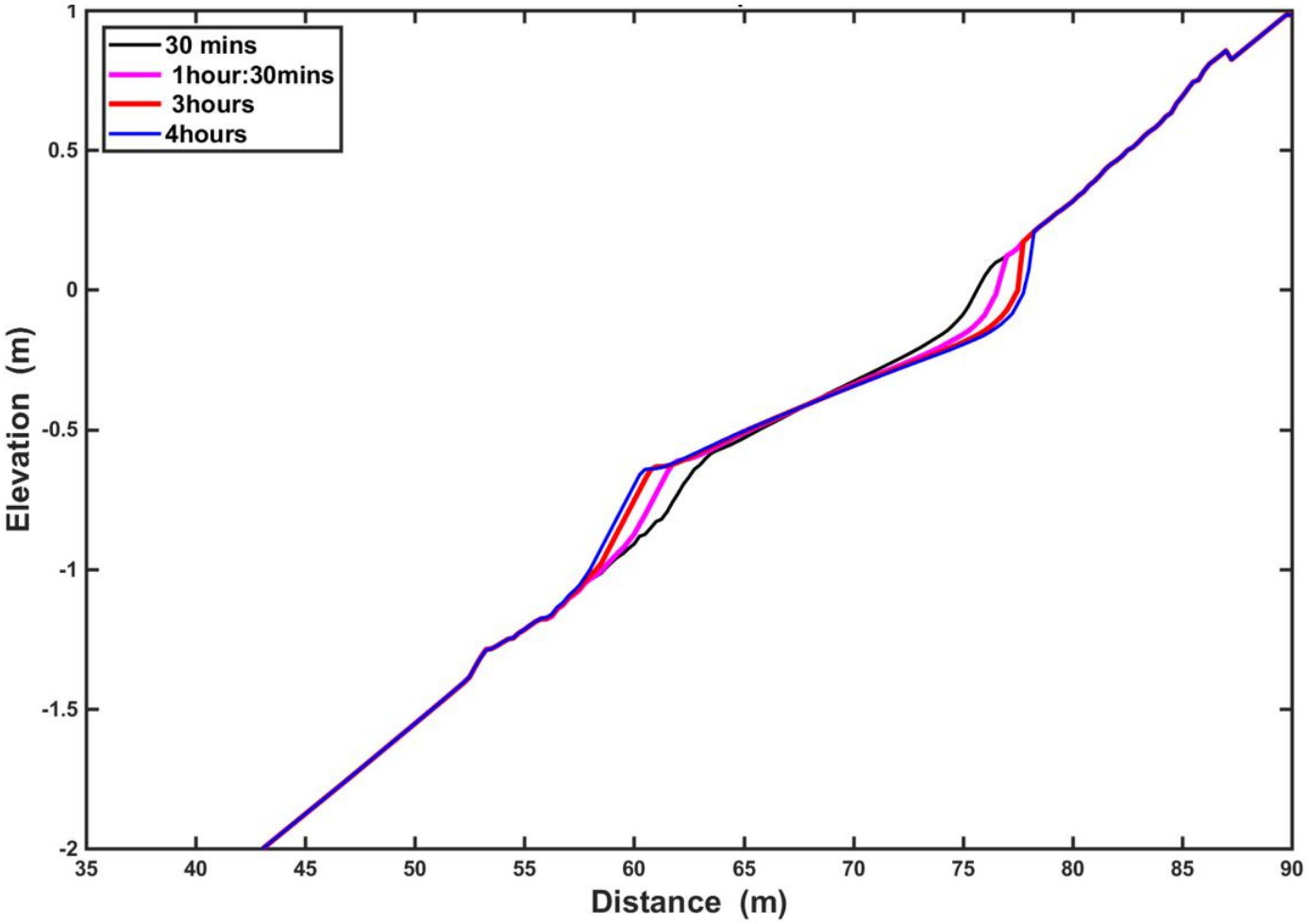

Figure 4.2 Beach profile change to equilibrium state

4.1.4 Influence of beach state variation on beach profiles

Figure. 4.3 shows the change in beach profile shape of a beach with 1:20 slope under different Ω values representing reflective, intermediate, and reflective beach states. In the dissipative state, sediment is transported offshore from the upper shore face, reducing the beach slope, forming a prominent subtidal bar

and a rectilinear profile. This could be seen in nature during a storm event when the upper portion of the beach erodes and the profile changes. For reflective and intermediate profiles, the development of concave and shallow concave profiles was observed. For the intermediate state where Ω ~1.9 (Figure. 4.3), the beach gradient becomes steeper as the beach evolves, and sediment is transported onshore to form an upper berm that is clearly nurtured. Little berm formation was observed for profiles with a low Ω value, i.e., reflective state, the beach was not as nourished as in the intermediate, which appears to be a typical beach profile reconstruction by a fair-weather wave following a strong event (storm). Shoreline change is common in all the profiles because the beaches developed into berms or bars and 0m is the still water level (SWL) used as a reference point.

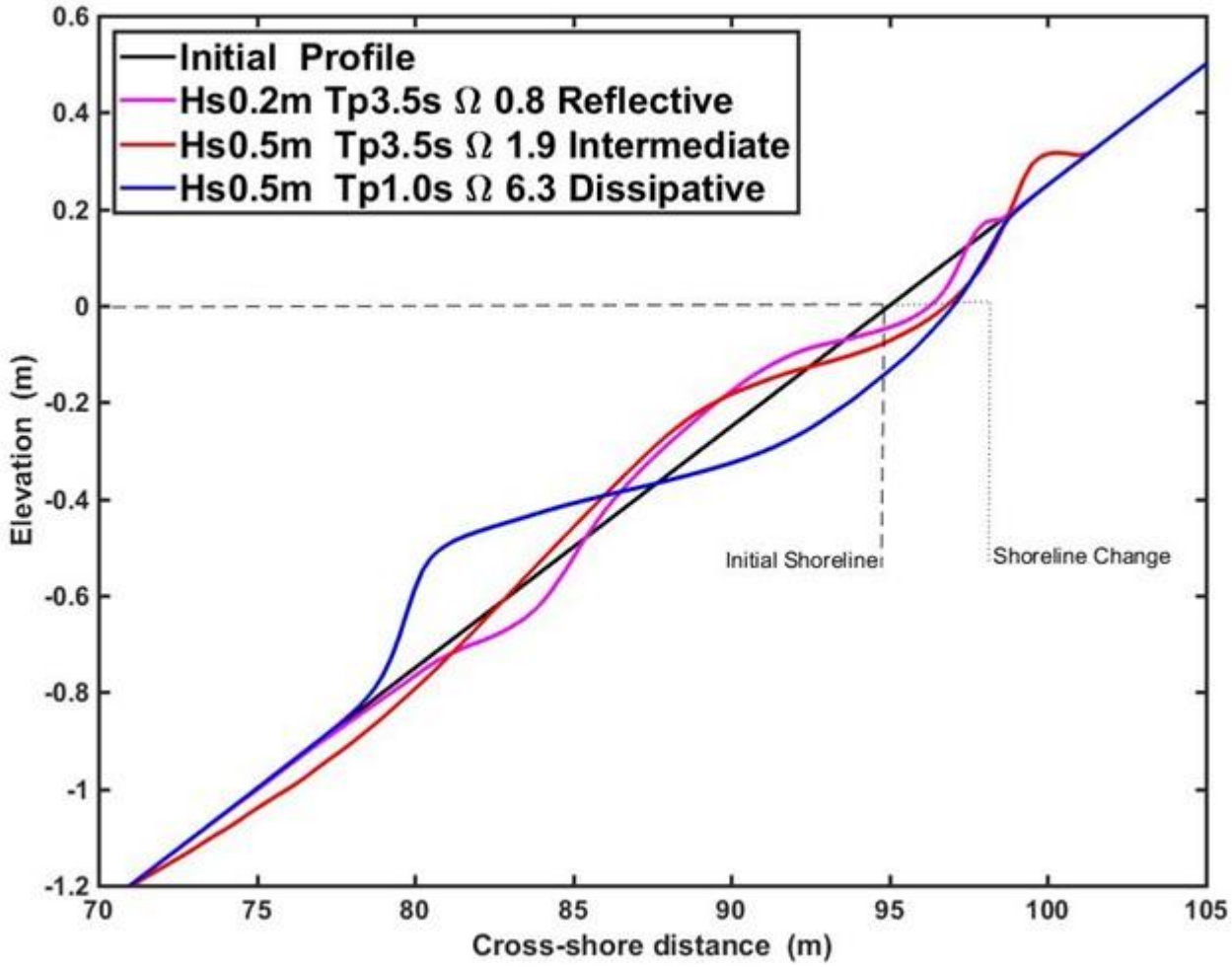

Figure 4.3 Cross-shore profile change under varying Ω values on a 1:20 slope beach profile

Figure. 4.4 shows a sample of profile variability under different wave condition and its corresponding Ω value. For Ω 0.9 on slope 1:20, a prominent berm formation just below the shoreline can be seen while the bar was less prominent in slope 1:10 for Ω 0.5. Larger wave periods tend to cause more erosion than short waves for the same wave height which can be attributed to larger energy carried by longer waves. A small amount of sediment is transported onshore in both cases to form an upper beach berm above the shoreline.

(A)

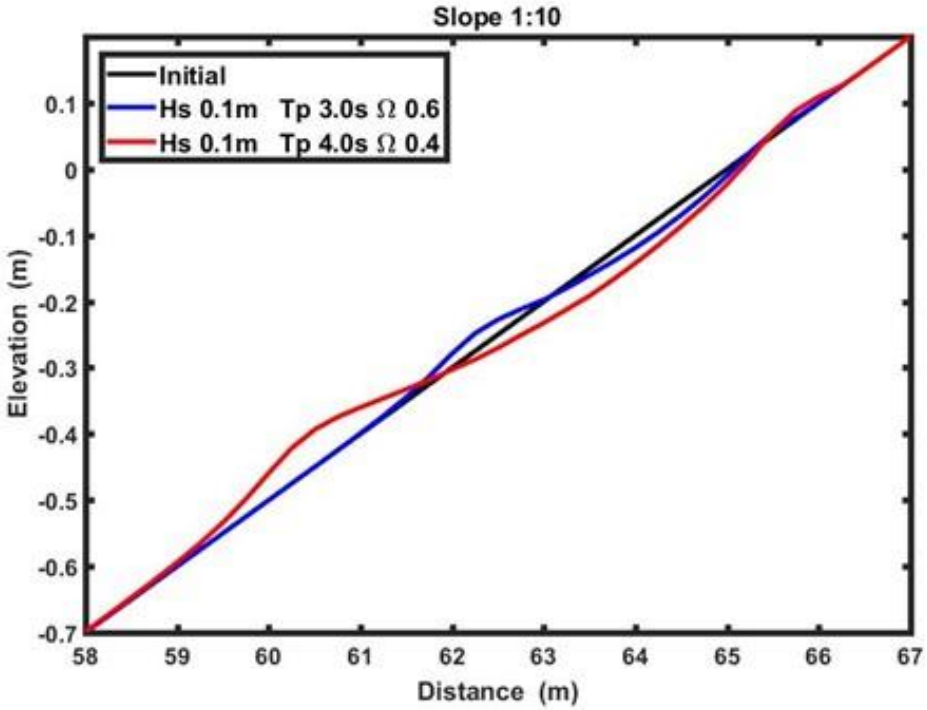

(B)

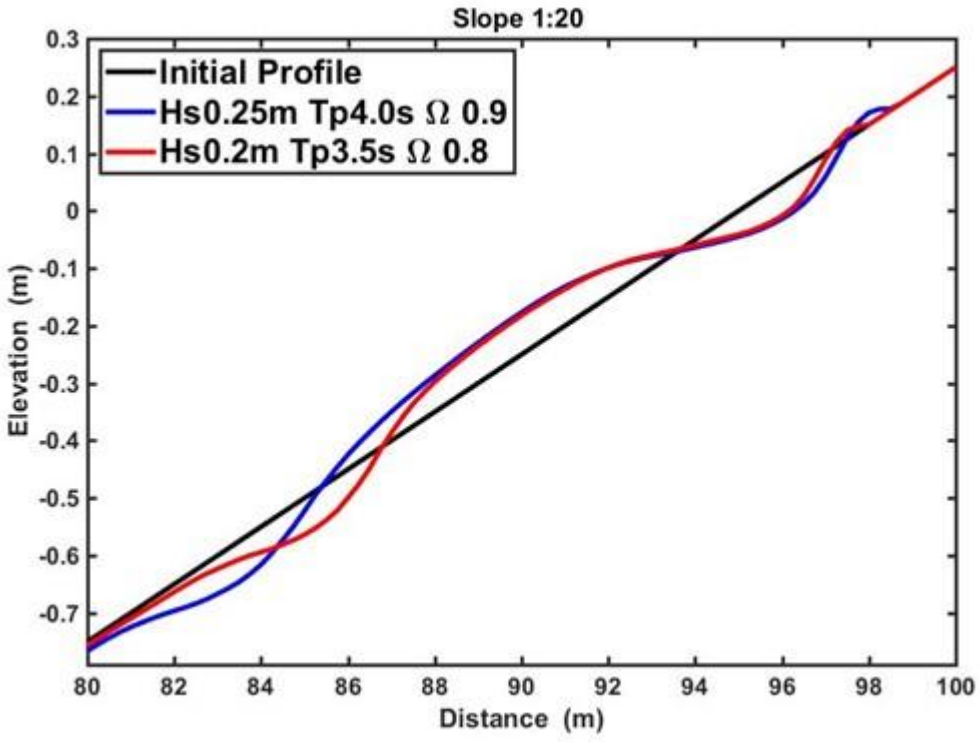

Figure 4.4 Cross-shore profile change under varying wave conditions and **Ω** values on reflective beach state (a) 1:10 profile, (b) 1:20 profile

Figure. 4.5 illustrates the profile variability of an Intermediate beach state under different wave conditions. Depending on the value of the Ω parameter, the beach may undergo either erosion or deposition. High wave energy, for instance, can lead to the erosion of the beach face and offshore bar, resulting in a wide and gentle beach, as shown in Figure. 4.5. Conversely, low wave energy can cause sediment deposition, leading to the formation of a narrower and steeper beach.

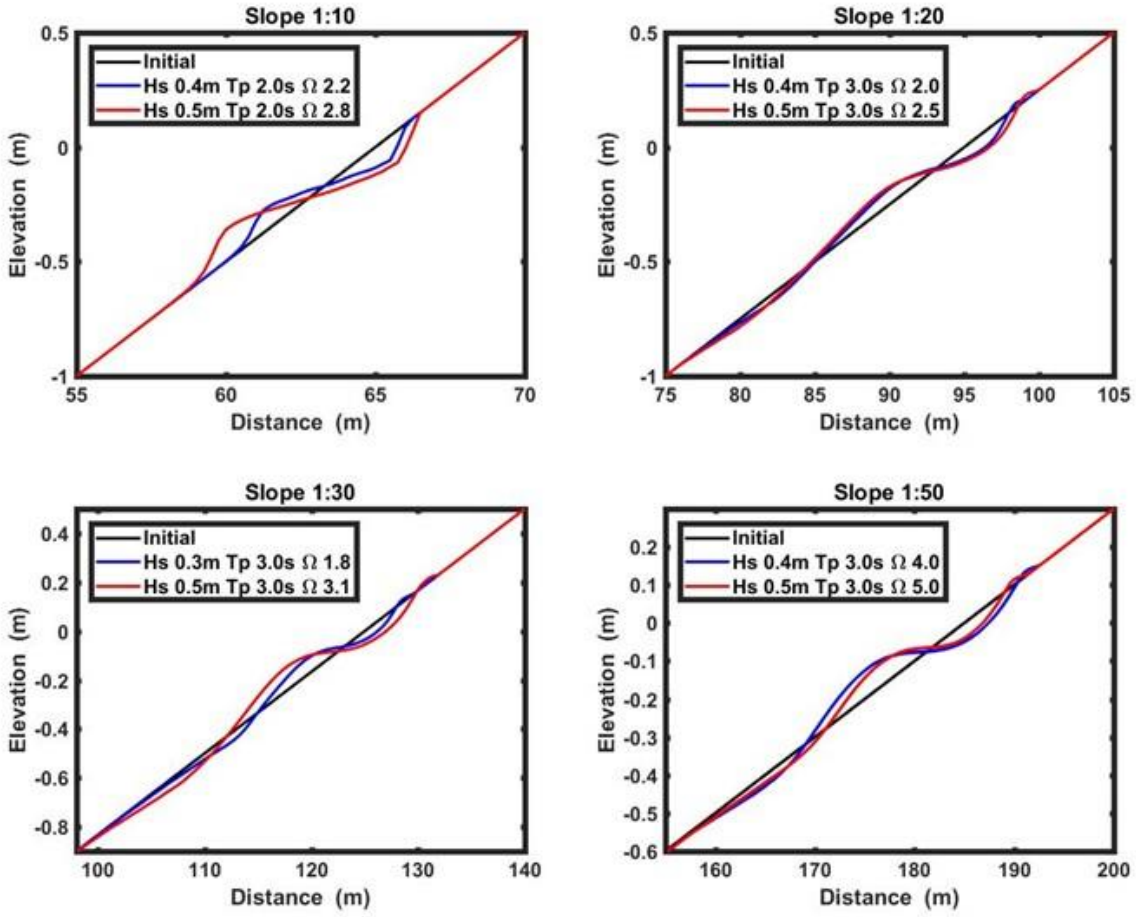

Figure 4.5 Cross-shore profile change under varying wave conditions and omega values on intermediate beach state (a) 1:10 profile, (b) 1:20 profile, (c) 1:30 profile, and (d) 1:50 profile

Figure 4.6 displays the profile evolution of a dissipative beach state under various wave conditions. The observed beach condition is consistent with the findings presented by Wright and Short (1984) regarding dissipative beach states. Notably, all profiles exhibit a distinct development of an intertidal berm.

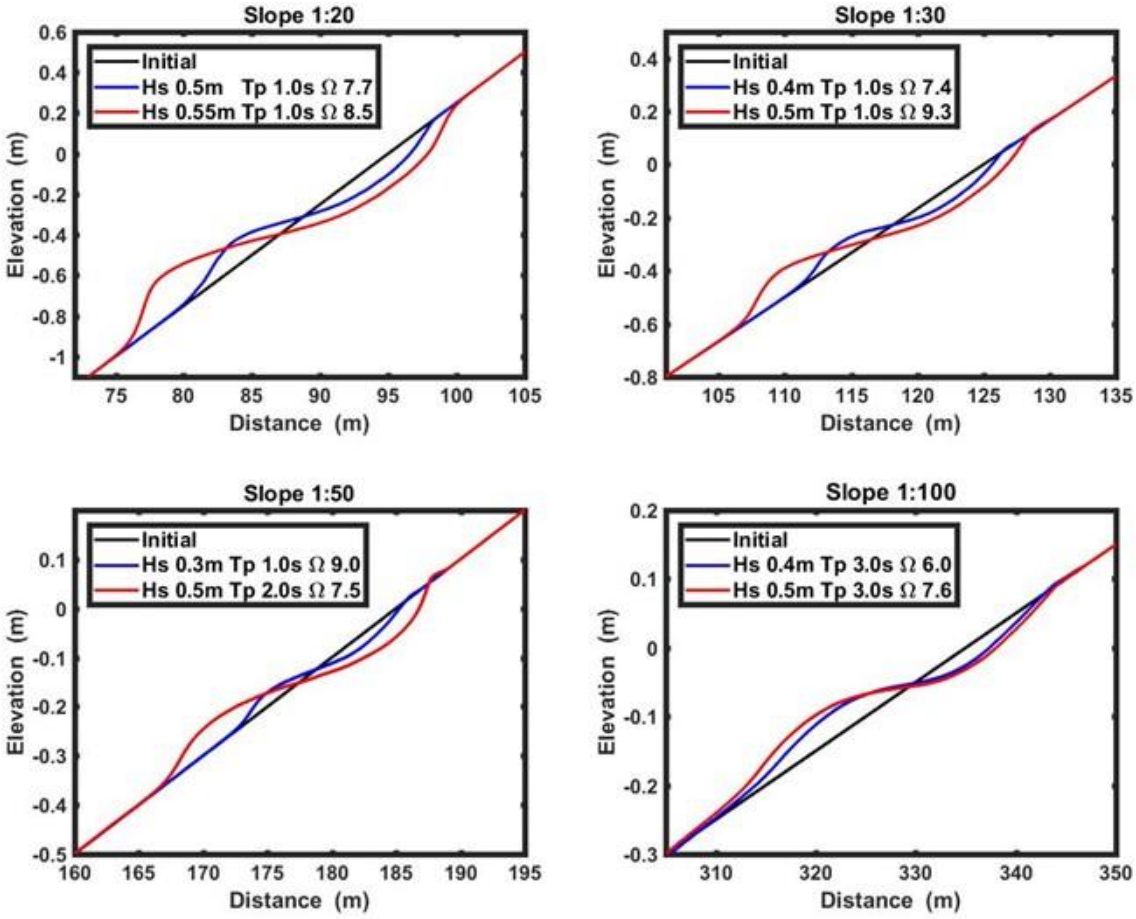

Figure 4.6 Cross-shore profiles change under varying wave conditions and Ω values on dissipative state (a) 1:20 profiles, (b) 1:30 profile (c) 1:50 profile (d) 1:100 profile.

4.1.5 Development of empirical formulations to model key cross-shore profile features.

Numerical simulations aimed at predicting beach state variability are often expensive and time-consuming. To overcome this challenge, this section describes the development of empirical formulations based on the numerical simulations presented above. The fundamental goal of this research is to develop empirical relationships that may accurately anticipate beach profile changes in response to incoming wave conditions. Once developed, these formulations can serve as reliable predictors of beach state variability. The formulations will establish relationships between hydrodynamic and beach parameters (H_s, T_p, beach slope ($tan\beta$), wave steepness (H_s/L_0) L_0 is the deep-water wavelength and key cross-shore features (shoreline position, berm length, berm height and berm crest level below still water line). Figure 4.7 gives schematics of key beach profile features considered in this study. The reference lines used were the still water and the initial profile.

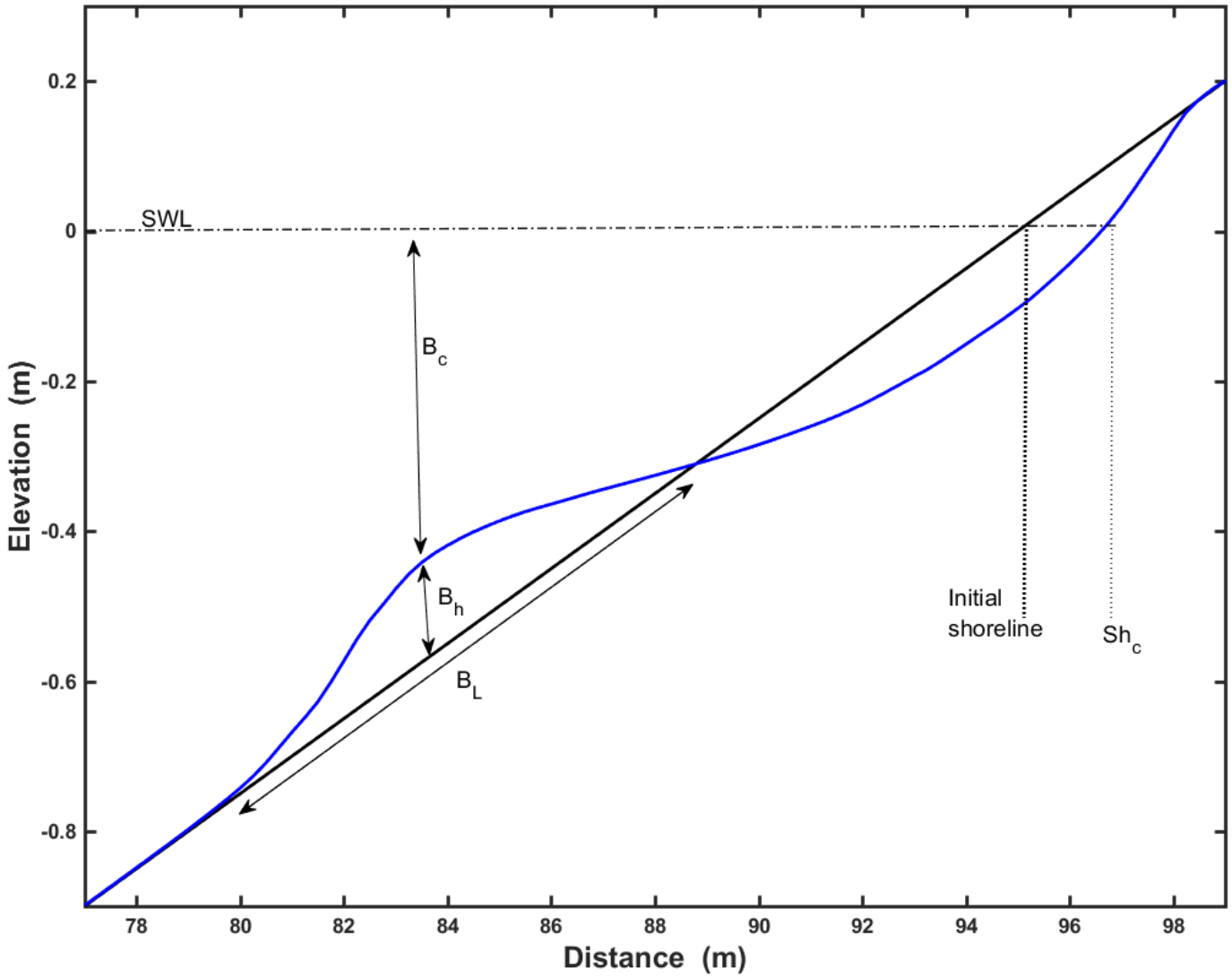

Figure 4.7 Schematics of key cross-shore profile parameters: Shoreline change (sh_c); berm height (B_h); berm length (B_L); and berm crest below still water level (B_c)

The first step in developing empirical formulation and analysing the parameters was to generate a set of non-dimensional parameters involving key profile features. In most engineering applications, results are made non-dimensional to minimize measurement errors (Komurcu et al.,2007). Buckingham's Pi theorem is used to develop non-dimensional parameters. Following the above analysis, a non-dimensional Equation (E_f) (4.4) was derived and uniquely presented for the different parameters of bar formations and shoreline change (Equations 4.5 to 4.8). However, in this study sandbar will be referred to as underwater berm formation because of its visual shape and model used in validation. In These non-dimensional parameters incorporate the tanβ, water depth and wave steepness and the values of shoreline change, berm height, berm crest, or berm length.

$$E_{f=}(\eta)^{0.5}(H_s/L_o)/Tan\beta \quad (4.4)$$

where:

η = Derived parameters

H_s/L_o = Wave steepness

$Tan\beta$ = Gradient

Parameters	**non-dimensional parameter**	
Berm height	$(\frac{B_h}{h})^{0.5}(H_s/L_o)/Tan\beta$	(4.5)
Berm crest	$(\frac{B_c}{h})^{0.5}(H_s/L_o)/Tan\beta$	(4.6)
Berm length	$(\frac{B_L}{h})^{0.5}(H_s/L_o)/Tan\beta$	(4.7)
Shoreline change	$(\frac{Sh_c}{h})^{0.5}(H_s/L_o)/Tan\beta$	(4.8)

4.2 Results and Discussion

This section presents a detailed analysis of beach state variability and its impact for various beach states. A series of comparisons were conducted on different beach states to evaluate whether a relationship between non-dimensional beach parameters and the **Ω** parameters can be found. The results obtained from these analyses provide comprehensive insights into the variability of beach states and the extent to which they are affected by the **Ω** parameters.

4.2.1 Relationships between non-dimensional beach parameters and the Dean's parameter for reflective beach states

Figure. 4.8 show non-dimensional beach parameters are shown against **Ω** values for reflective beach state. A general trend of all four beach profile parameters increasing linearly with the increase of Dean's parameter can be seen, irrespective of the beach slope.

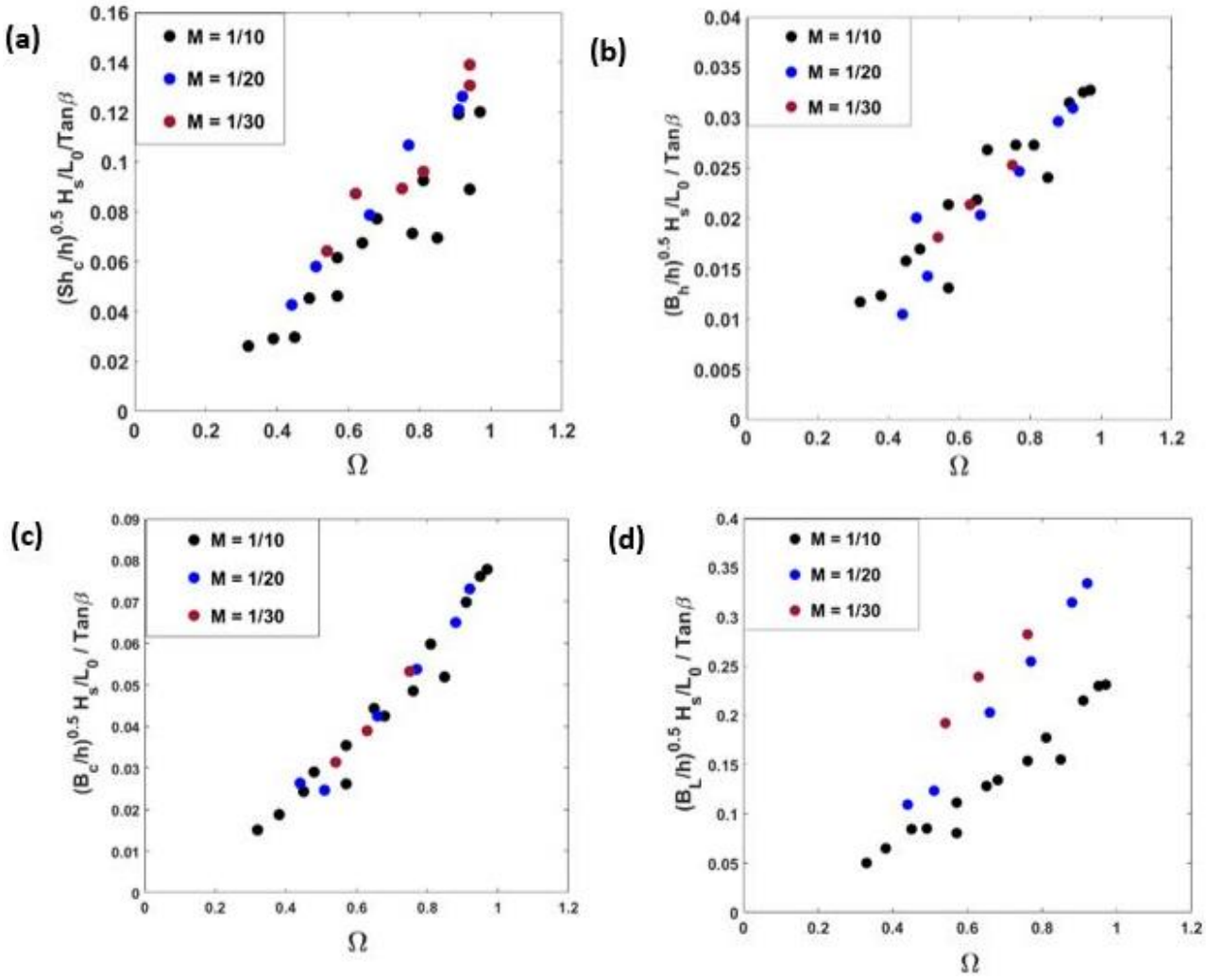

Figure 4. 8 Comparison of derived parameters (a) shoreline change (b) berm height (c) berm crest (d) berm length versus Dean's parameter on reflective beach states

4.2.2 Relationships between non-dimensional beach parameters and the Dean's parameter for intermediate beach state

Figure. 4.9 show non-dimensional beach parameters are shown against Ω values for intermediate beach state. Results show a general trend of increase in all four beach profile parameters with increase of Ω can be seen although data is scattered slightly for larger Ω.

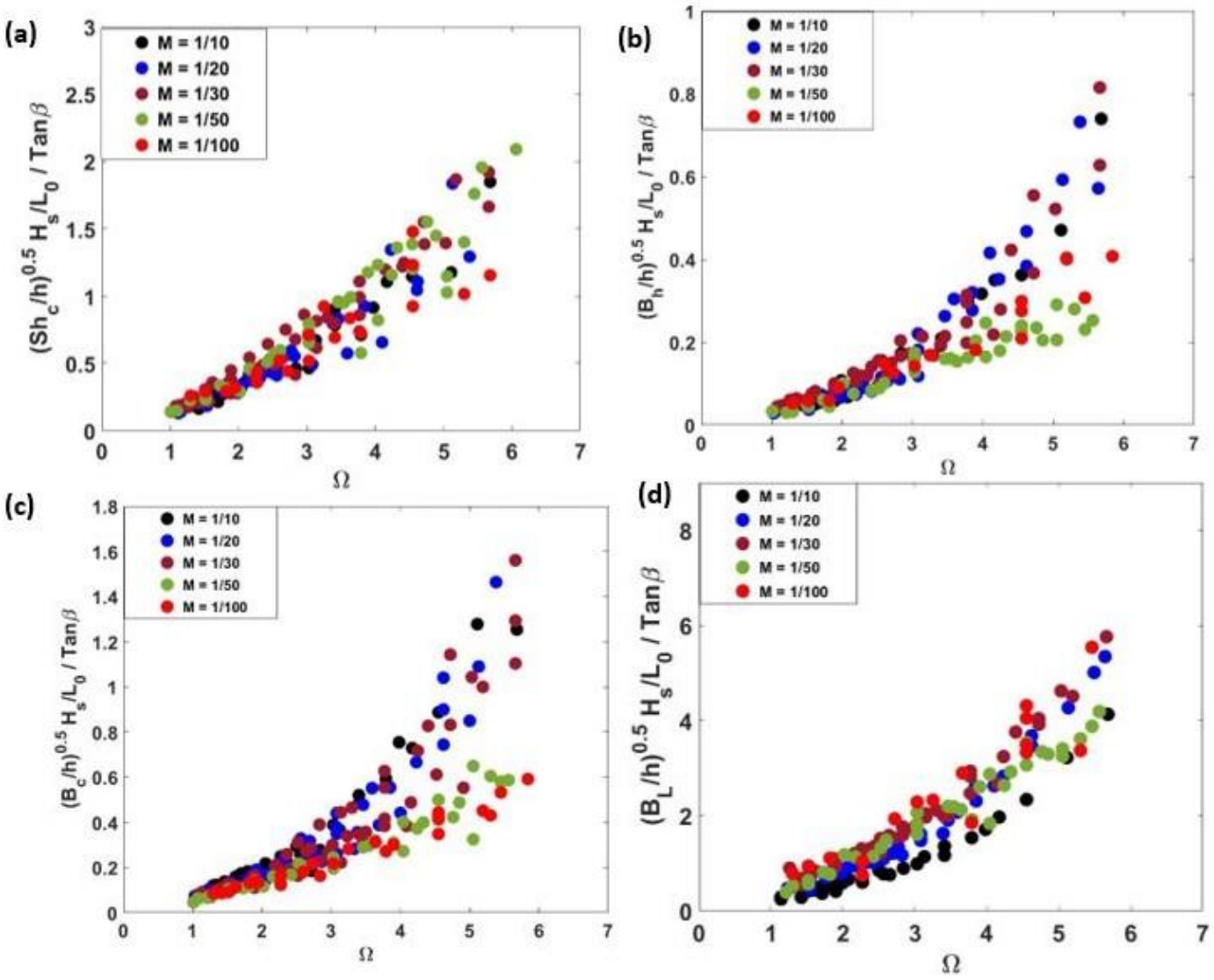

Figure 4.9 Relationship of derived parameters (a) shoreline change (b) berm height (c) berm crest (d) berm length versus Dean's parameter on intermediate beach states

4.2.3 Relationships between non-dimensional beach parameters and the Dean's parameter for dissipative beach state

Figure. 4.10 show non-dimensional beach parameters are shown against Ω values for dissipative beach state. Results show a general trend of increase in all four beach profile parameters with increase of Ω can be seen although data is scattered slightly for larger Ω. Shoreline and berm crest parameters show some scatter while the variability berm height and berm length are much conformant with Ω although an overall trend of all of them increase with increase in Ω can be seen.

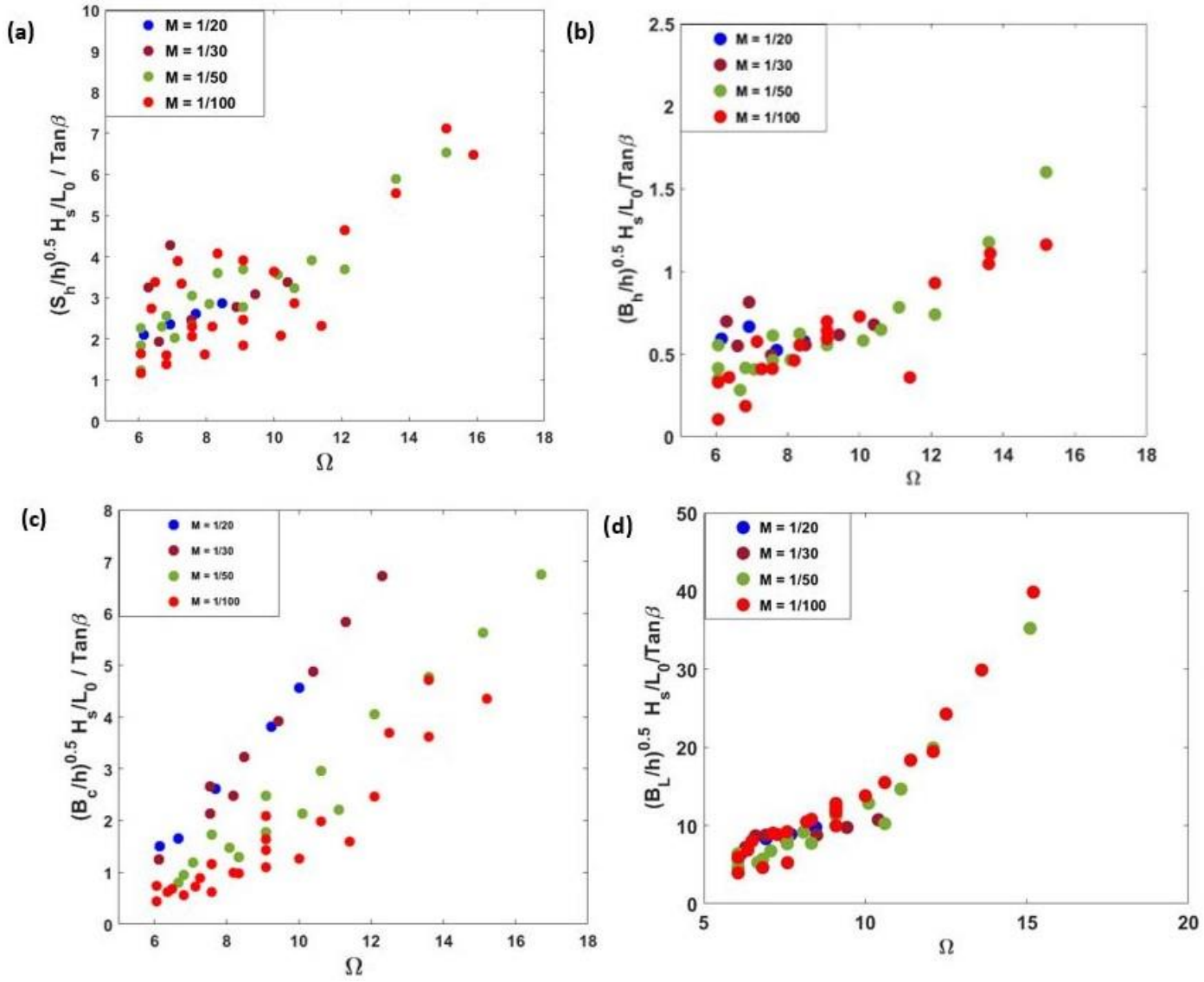

Figure 4.10 Relationships of derived parameters (a) shoreline change (b) berm height (c) berm crest (d) berm length versus Dean's parameter on dissipative beach states

For all the parameters derived, the magnitude of shoreline change shows reflective beach state is less pronounced with no apparent increase in shoreline variability compared to dissipative beach state. The relation between the sh_c and Ω shows high correlations. The results revealed that high dispersion in sh_c occurs with increasing Ω values. Erosion was recorded for these higher states. The first hypothesis is that XBeach has the tendence of eroding the shoreline particularly for higher states. Furthermore, during the validation and calibration, the experimental data used was not fine sand, thus I calibrated and validated against a situation where the beach is moving within the first two low states, from intermediate to reflective, rather than dissipative to reflective. Thus, the model eroded the beach more in its dissipative state.

Amongst the parameters used to simulate the B_h, wave height and wave period were noted to control evolution of the berm heights. In consistence to the formulation in the Dean number (Dean, 1973), it was noticed that

an increase in wave periods was linked to onshore sediment transport while lower wave periods moved the beach towards dissipative state. It is also observed that intermediate beach states produced more berms (Figure. 4.9), but the higher berm heights were noted in dissipative states. For B_h, the shape of the beach is important for all beach state. The higher the Ω value for each beach state the higher the B_h. Ninety percent of the berms calculated are less than 0.2 m in height, and 65% are less than 1m in height. For instance, 46% of the berm in dissipative are greater than 2 m in height. Berms occur where there is a significant steep gradient in sediment transport.

There is large variability in B_C which most of the time happened in the dissipative state. Gentle beaches have lower berm crests while steeper beaches have higher berm crests. A combination of the berm lengths for all the three beach states that were assessed revealed similar trend with the Ω values.

4.3 Beach states and wave propagation

For different beach states the wave propagation and breaking were investigated to identify wave breaking location with respect to berm formation. The berm height and berm location are important parameters to describe the berm.

From each numerical simulation, wave height distribution across the cross-shore profile and wave breaking point were extracted. Some sample results on dissipative, intermediate, and reflective beach states are shown and discussed below.

In reflective beach state, wave breaking typically occurs remarkably close to the shoreline when the incoming waves interact with the seabed as the water depth becomes shallow near the shoreline. Unlike dissipative beach states, reflective beach states often lack a prominent berm, as seen in Figure 4.11. However, wave breaking can still occur on the berm under less energetic wave conditions with smaller wave heights H_s of 0.1 m, longer periods T_p of 3.0 s, and a slope of 1:10. The lack of a prominent berm in a reflective beach state can cause the shoreline to be more dynamic. The point of maximum shoaling wave height was extracted and estimated as h_b at which breaking occurs.

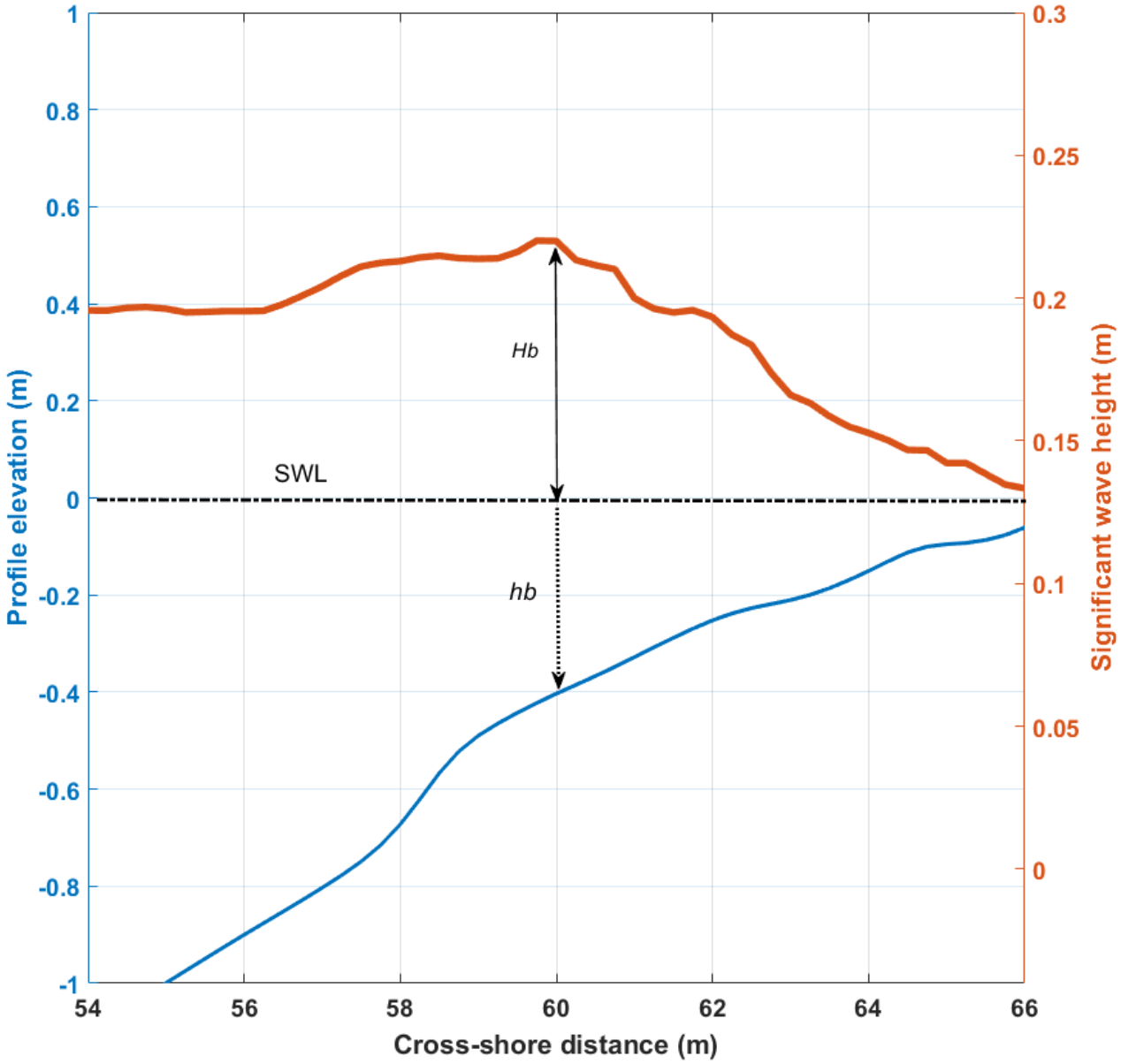

Figure 4.11 Wave propagation and its breaking point on a reflective beach state Hs 0.1 m Tp 3.0 s, on a slope of 1:10

For the intermediate beach state (as presented in Figure. 4.12), characterized by a significant wave height H_s of approximately 0.5 m, a peak wave period T_p of around 3.0 s, and a slope of 1:20, the wave breaking location (defined as the maximum wave height-to-water depth ratio) is shown with respect to the position of the berm at breaking. Under these wave conditions, sediment from an offshore berm begins to migrate towards the shore, resulting in the formation of a new berm closer to the shoreline as the offshore berm erodes. As illustrated in Figure. 4.12, the wave breaking occurs at the edge of the newly formed berm, highlighting the important role of the berm in controlling wave breaking and sediment transport on intermediate beaches.

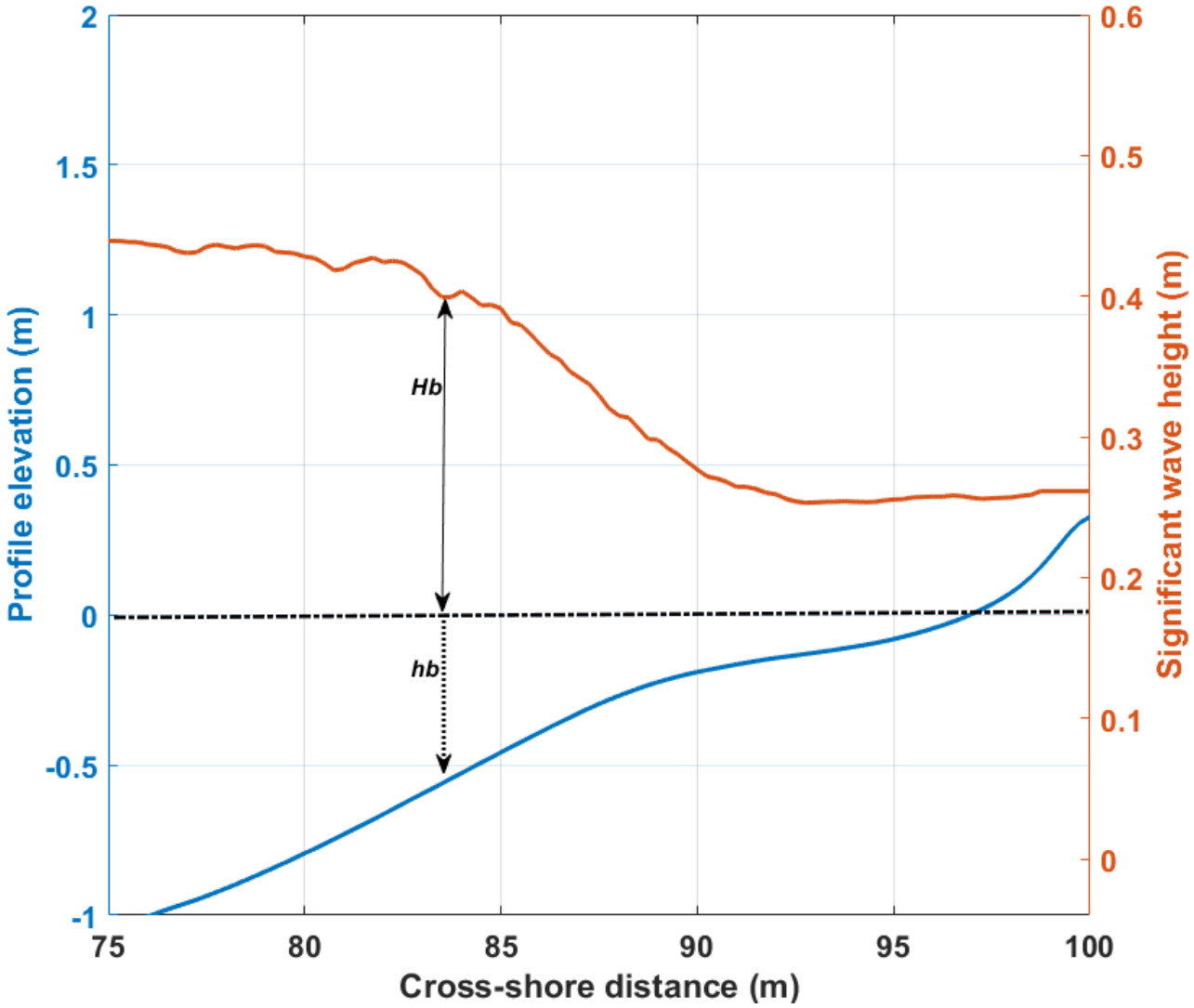

Figure 4.12 Wave propagation and its breaking point on intermediate beach state Hs 0.5 m Tp 3.0s, on a slope of 1:20

Figure. 4.13 illustrates a dissipative beach state with a significant wave height H_s of around 0.4 m, a peak wave period T_P of approximately 2.0 s, and a slope of 1:50. As shown in the figure, the waves are breaking on the berm, which is notably higher compared to the reflective and intermediate beach states. This is due to the unique wave characteristics of a dissipative beach. The height of the berm on a dissipative beach is notably higher compared to reflective and intermediate beach states, emphasizing the significant role of the berm in dissipating wave energy before it reaches the shoreline.

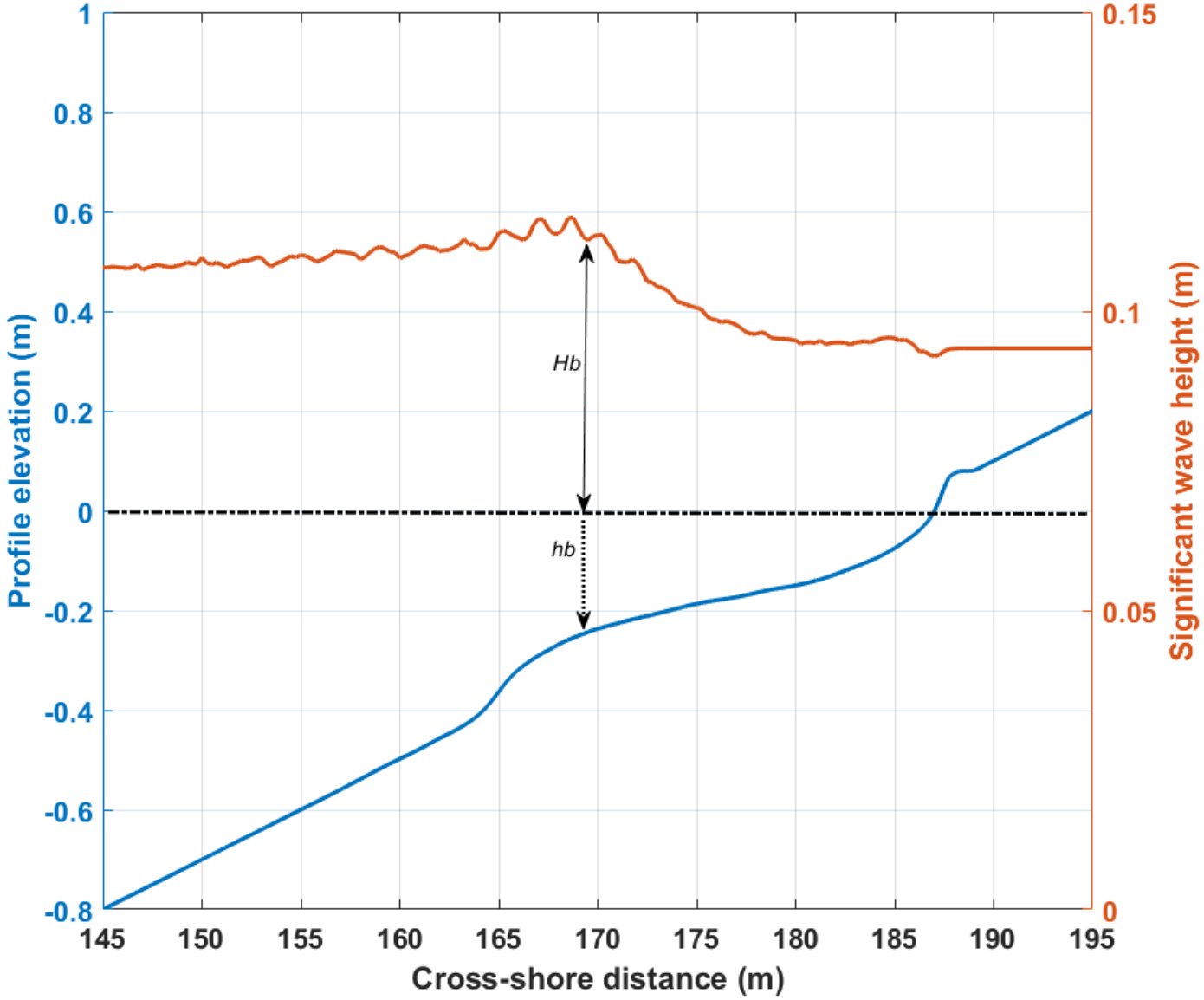

Figure 4.13 Wave propagation and its breaking point on dissipative beach state Hs 0.4 m Tp 2.0 s, on a slope of 1:50

4.4 Empirical formulations to predict key cross-shore profile parameters

The beach state at a specific beach is not a constant; beaches can undergo a sequence of beach states changes. A regression analysis was conducted between the formulation of the four non-dimensional beach parameters (shoreline change, berm height, crest, and length) and the Ω value which can serve as empirical formulations to predict beach profile shape under all three beach states.

Figure 4.14 and Equation 4.9 shows the trend line connecting shoreline position and Ω. The R^2 value is 0.9118, indicating a good fit. The data scatter is higher for larger Ω values however, R^2 value is 0.9118, indicating an overall good fit.

$$(\frac{Sh_c}{h})^{0.5}(H_s/L_o)/Tan\beta \quad = 0.1277\ \Omega^{1.4695} \tag{4.6}$$

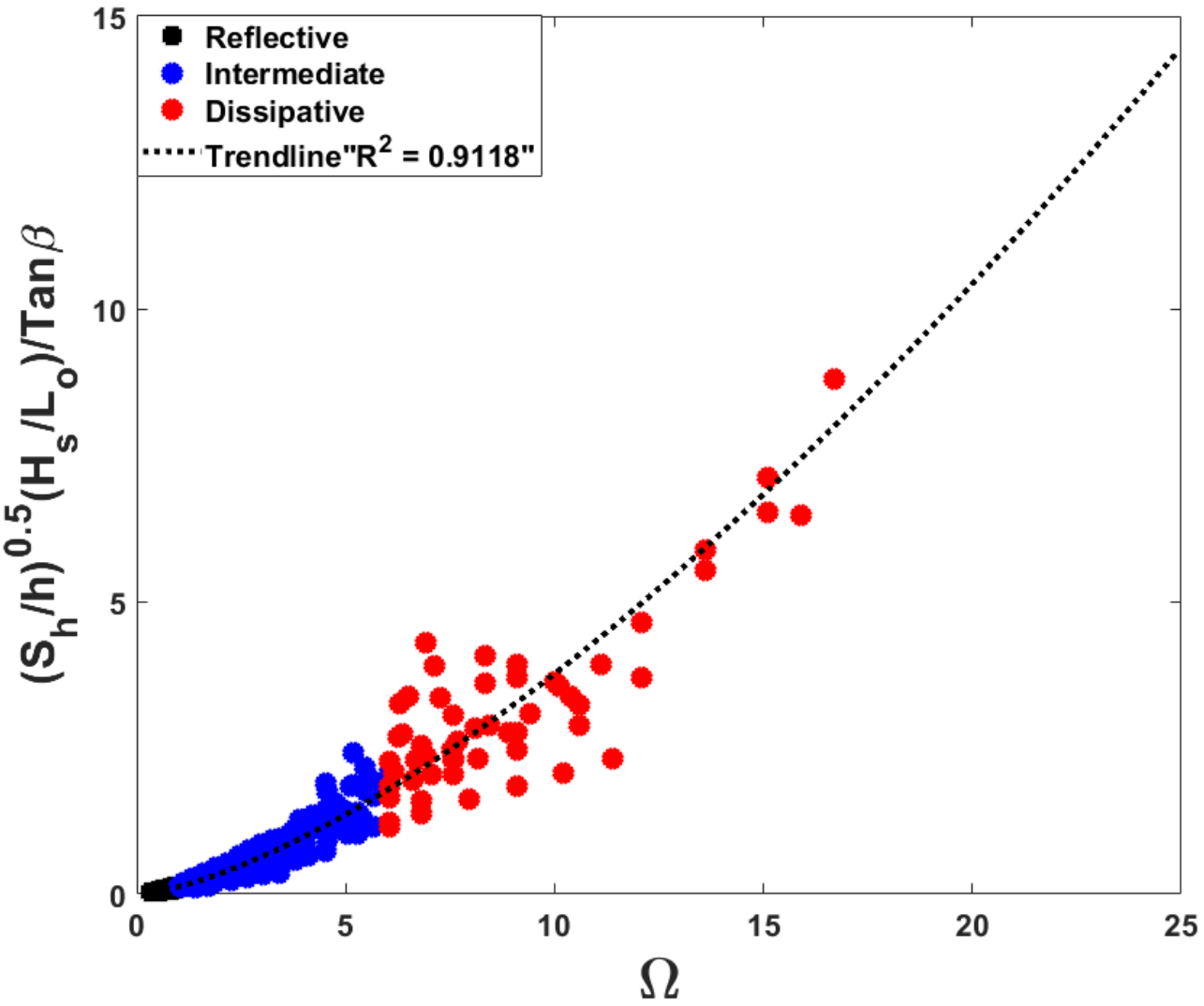

Figure 4.14 Trend of variability of non-dimensional shoreline change against Dean's parameter Ω for all three beach states

Figure 4.15 and Equation 4.10 show the trend line between berm height and Ω. The R^2 value is 0.7914, indicating an overall good fit although once again, a larger deviation of the data from the trend line can be seen at larger Ω values.

$$(\frac{B_h}{h})^{0.5}(H_s/L_o)/Tan\beta \quad =0.0387\ \Omega^{1.261} \tag{4.10}$$

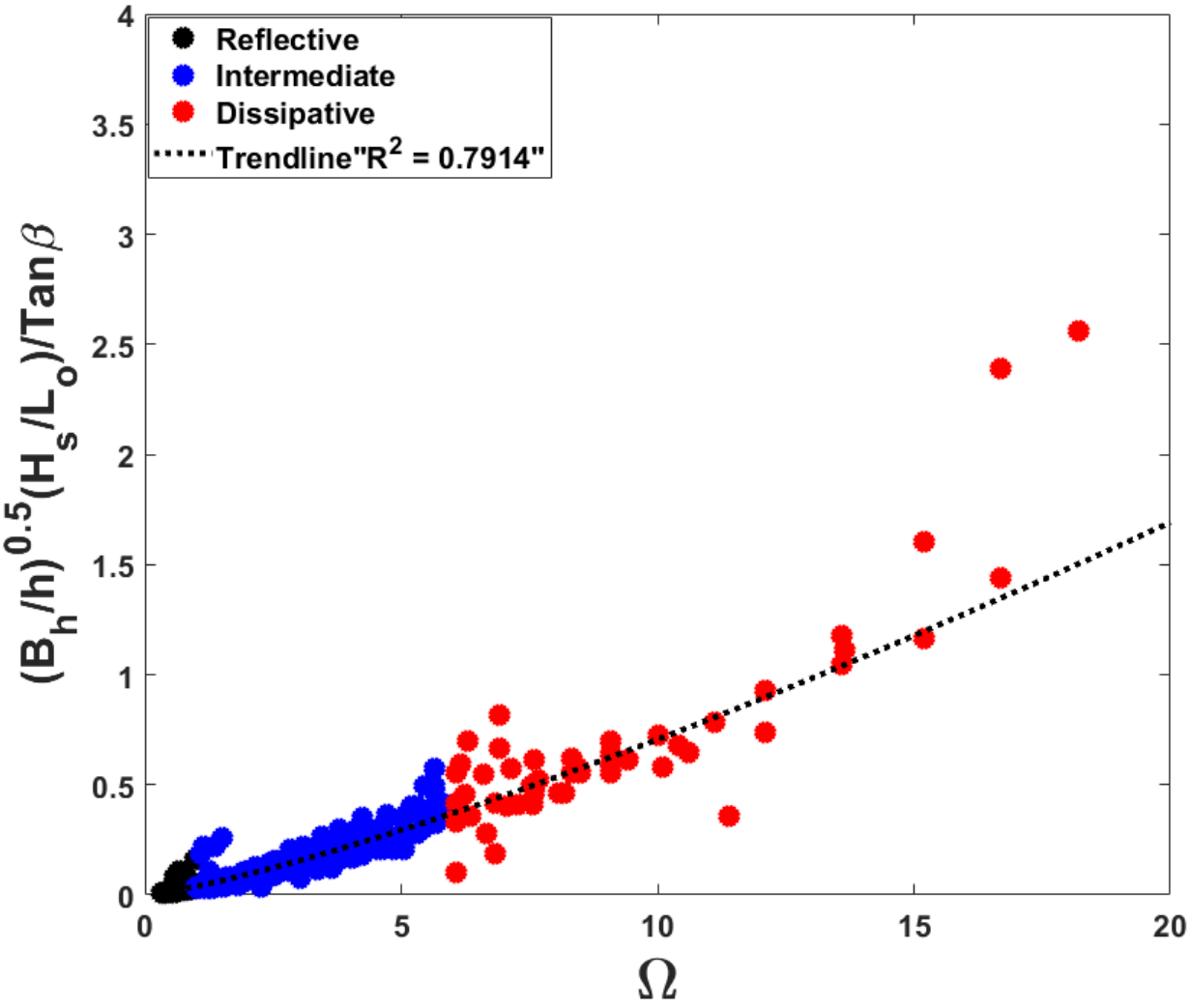

Figure 4.15 Trend of variability of non- dimensional berm height against Dean's parameter Ω for all three beach states

Figure 4.16 depicts different beach states and shows a trend line that predicts the relationship between the equation and Ω value. Figure 4.16 and Equation 4.13 demonstrate that the trend line between berm crest and Ω values has a strong correlation, with an R^2 value of 0.9001 indicating a good fit. Although there is a greater data scatter for larger Ω values, but the R^2 value is 0.9001, which shows good fit.

$$(\frac{B_c}{h})^{0.5}(H_s/L_o)/Tan\beta \ = 0.0626\ \Omega^{1.5124} \qquad (4.11)$$

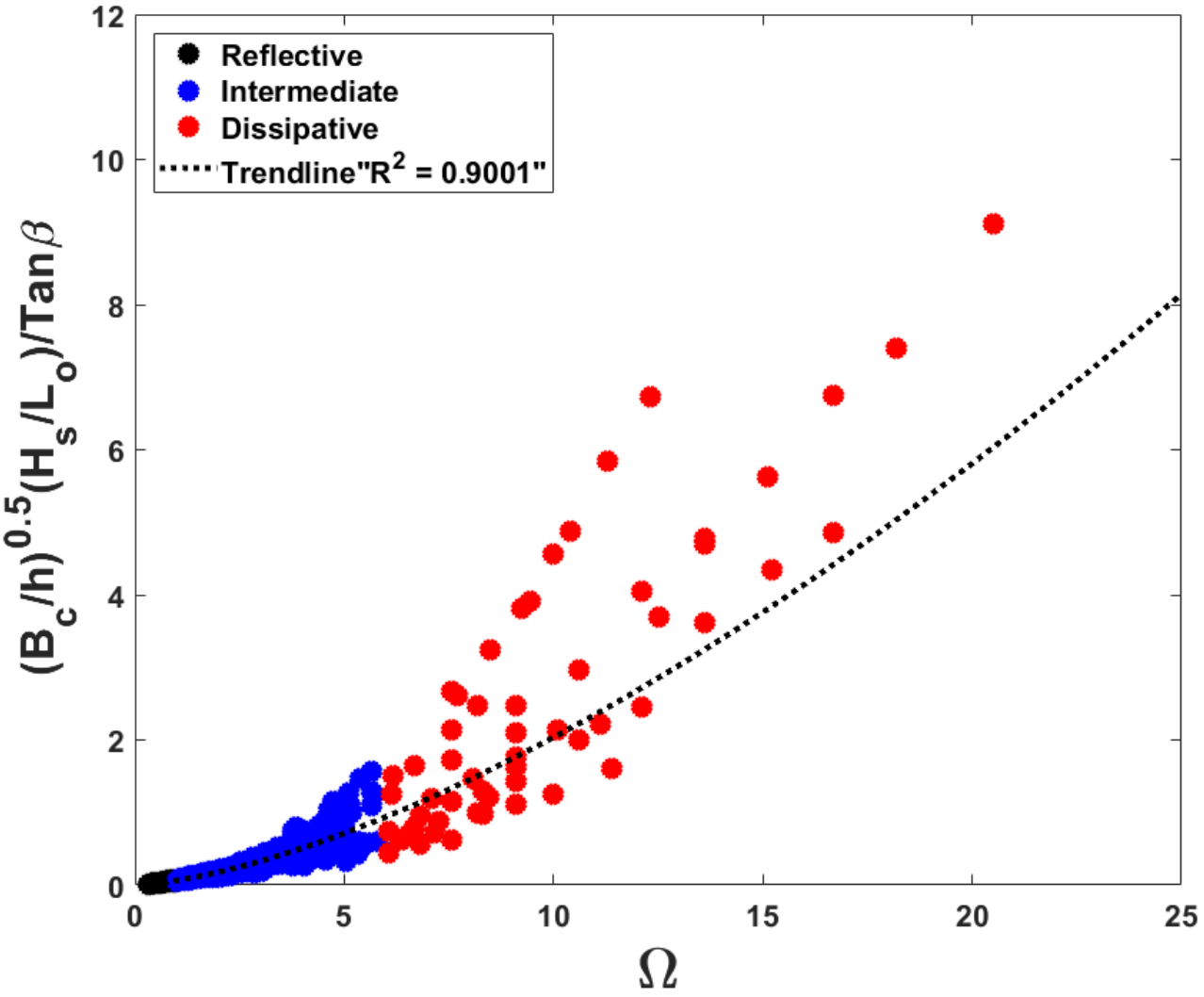

Figure 4. 16 Trend of variability of non-dimensional berm crest against Dean's parameter Ω for all three beach states

The trend line connecting the berm length and Ω values is shown in Figure 4.17 and Equation 4.14. The R^2 value is 0.9528, indicating that the fit is satisfactory. The data scatter increases with increasing Ω values, but the R^2 of 0.9528 indicates a good fit overall.

$$(\frac{B_L}{h})^{0.5}(H_s/L_o)/Tan\beta \ = 0.2825\ \Omega^{1.6588} \qquad (4.12)$$

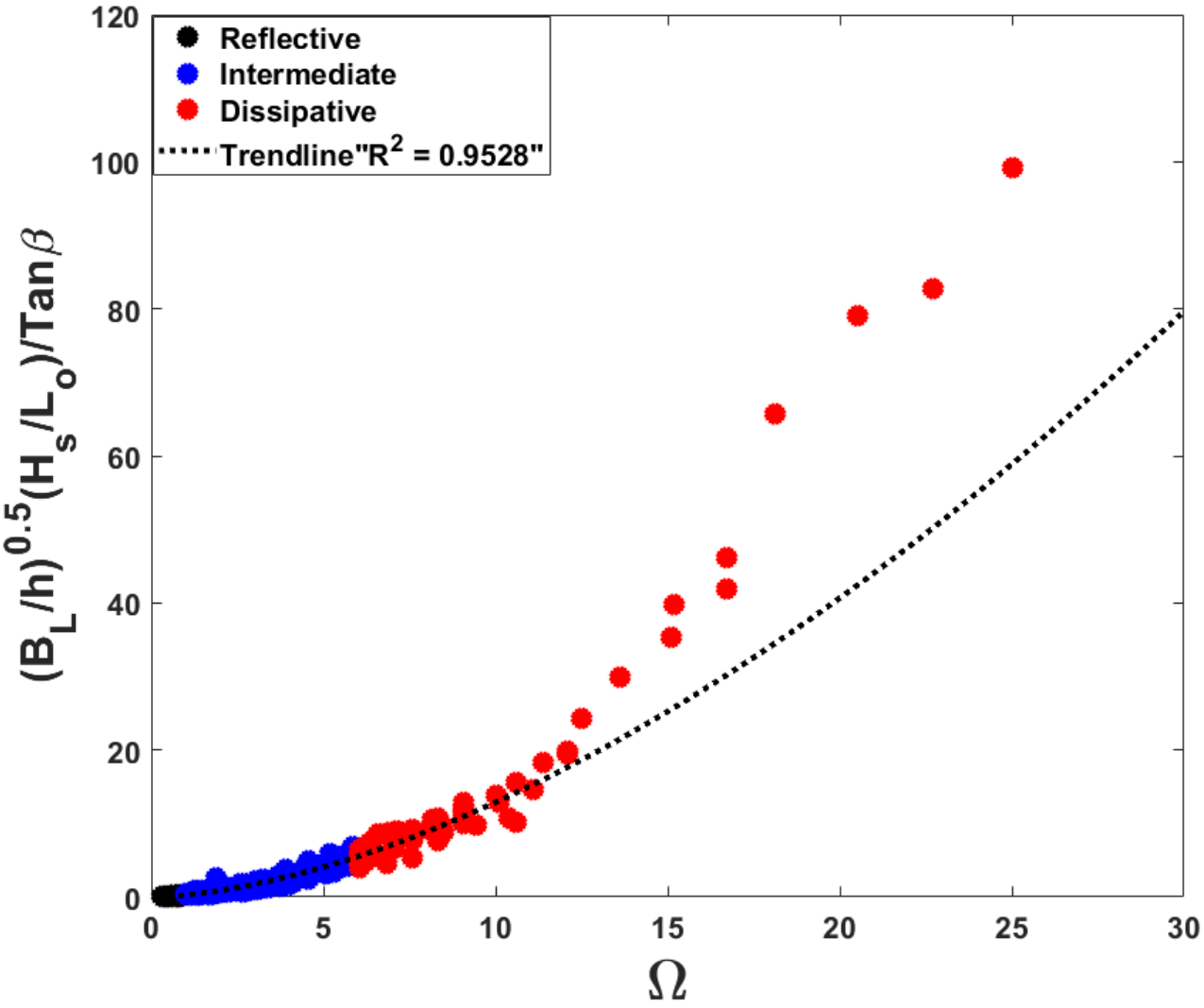

Figure 4. 17 Trend of variability of non-dimensional berm length against Dean's parameter Ω for all three beach states

4.5 Influence of water level on empirical models of beach state change

Water level variations due to astronomical tides can be an important factor in determining beach profile (Bernard et al., 2009) and hence beach variability, although water level variation was neglected in the numerical simulations used for building our parametric beach profile shape equations. To investigate the impacts of water level variations on the beach state variability empirical models, an additional set of numerical simulations on beach profile change were conducted and the results were compared with the results obtained for MSL.

Numerical simulations were performed using static hypothetical Low Water Levels (LWL) of -0.15 m and -0.25 m, and High Water Levels (HWL) of +0.15 m and +0.25 m on a 1:20 beach slope and numerous incident wave conditions. The previous simulations carried out under MWL was consistently used as the reference point. The attention was focused on shoreline change, berm length and berm height but did not incorporate

the berm crest height from free surface due to the changing water level. The simulations were done with respect to the water depths to determine water level that corresponds to the water depth used in the experiment. It was noticed that the water level of ±0.15 m with 3 m water depth used in the experiment which also yields a beach slope of 1:20, aligning more closely with field cases for comparative purposes. ±0.15 m water level variation around MSL closely corresponds to Low water Level (LWL) and High Water Level (HWL) of microtidal variations in real world, with tidal range of less than 2 m in full scale. To check the performance of the empirical models meso and macrotidal beaches, the simulations were done with ±0.25 m water level change around MSL. Figures 4.18 to 4.20 the performance of the parametric models with different low and high water level with respect to the MSL. All the three beach states were observed where the transitions between beach state zones are marked with the Ω values. Plots of different beach states for different water variation can be seen in Appendix B.

Figure 4.18 demonstrates the effects of water level variabilities on berm height at different beach states. There is no significant change in the non-dimensionalised berm height because of HWL, MWL and LWL for intermediate and reflective beaches, while there seems to be some reduction of the berm height due to changes in water for dissipative beaches. Slight change was recorded in the dissipative beach state for HWL and MWL with a percentage difference of only 3.7% with respect to MSL scenario.

When water level change around MSL is ±0.25 m, a much clearer reduction of the non-dimensionalised berm heights particularly for HWL, can be seen on dissipative beaches. Visually, between 0.15 m and 0.25 m, the spacing in berm height between MWL and HWL is approximately 1 m, which could be influenced by the alteration of wave breaking patterns and sediment transport. It was noticed that as the water level fluctuates from low to high, berm height decreases. This means water depth increases at the berm location. Given that wave breaking depends on water depth, i.e., waves break easily on shallower areas, this result suggests the wave break point may then be shifted towards the shore or to much shallower area with the increase in water level. This can cause waves to break closer to the shore, leading to more intense turbulence, suspension of sediment and erosion. This proximity of wave breaking near the shore during HWL contributes to increased sediment transport from the beach, resulting in berm accretion and sediment deposition in nearshore areas. Conversely during LWL, reduced wave breaking intensity and offshore wave propagation limit sediment transport towards the coast, resulting in sediment deposition and beach accretion. The calculated percentage difference in non-dimensional berm height between HWL and MWL was 5.2%. Figure 4.18 therefore attributes that the influence of water levels on berm height on beaches is a key factor in understanding beach morphodynamics in macro-tidal beaches. Berm height variation with water level change was found to be particularly prominent in dissipative beach states, highlighting the sensitivity of these coastal environments to changes in water levels. In Figure 4.18, the berm height varied between 70 and 110 m, erosion becoming more aggressive in beach section with 0.25 m water level. Indicating that this model could be more valid for micro-tidal beaches than macro-tidal beach but will have to trade with caution. Table 4.1 shows measurements of

different berm height on different water levels using the empirical formulation for berm height. More detailed measurements and percentage difference for all parameters can be found in Appendix C.

Table 4. 1 Berm heights at different beach states and water levels for MWL, LWL and HWL values

	Dissipative Berm height			**Intermediate Berm height**			**Reflective berm height**		
Water Level (m)	MWL	LWL	HWL	MWL	LWL	HWL	MWL	LWL	HWL
0.15 m	1.66	1.66	1.59	0.08	0.07	0.09	0.014	0.014	0.014
0.25 m	1.65	1.65	1.56	0.09	0.09	0.06	0.01	0.01	0

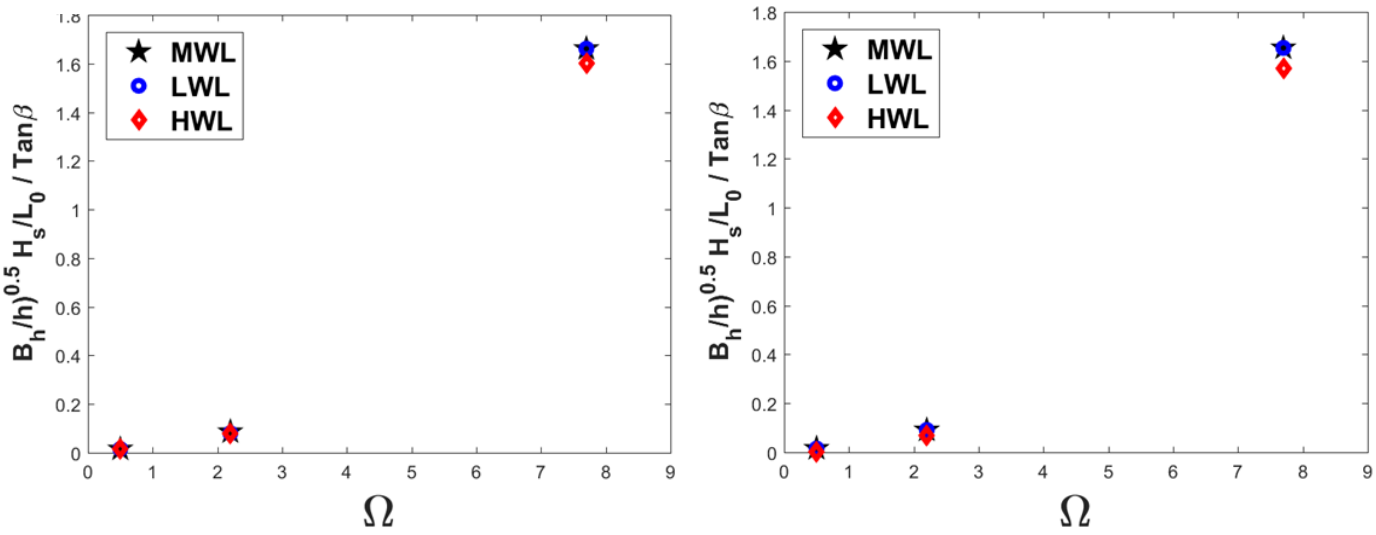

Figure 4. 18 Variability of non-dimensional berm height on different water level against Dean's parameter Ω for all three beach states 0.15 m (left) and 0.25 m (right) water level

The non-dimensional berm length was under different water levels were compared with those under MSL, which are shown in Figure. 4.19 for the three beach states. In contrast to berm height, berm length increases with increasing water levels. Figure 4.19 shows changes of the berm length between 0.15 m and 0.25 m. Berm length slightly increased when water levels were increased from 0.15 m to 0.25m. This is much clearer for dissipative beaches. The berm length is seen to increase with the water level. This implies that the wave breaking that was observed away from the berm because of decreasing berm height as explained earlier leads to the building of the berm. Sediment transported or eroded from Sediment transported or eroded from the beach builds the berm in the cross-shore. The calculated difference between HWL and MWL was determined to be 2.8% and 6.6% respectively. Thus, the % difference is very small for water level ±0.15 emphasizing that the empirical formulation can be satisfactory used for micro/meso tidal beaches.

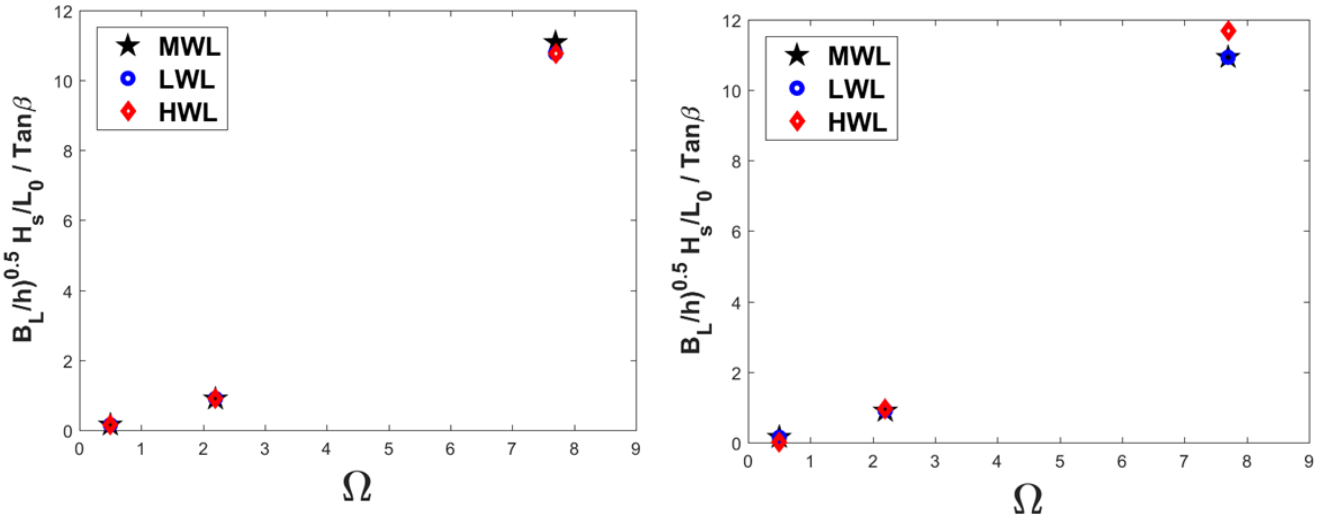

Figure 4.19 Variability of non-dimensional berm length on different water level against Dean's parameter Ω for all three beach states (left) 0.15 m and (right) 0.25 m water level

Changes in water levels will increases submersion and erosion rate as well as shoreline positions. Figure 4.20 shows response of shoreline to changing water levels. For different water levels shoreline change is negligible. This observation highlights unique relationship between the beach state and shoreline change. It suggests that shoreline changes could be due to the energy of the beach and not water levels. Nonetheless, this is peculiar to my model. The calculated difference between HWL and MWL was determined to be 5.2% and 5.2%, respectively.

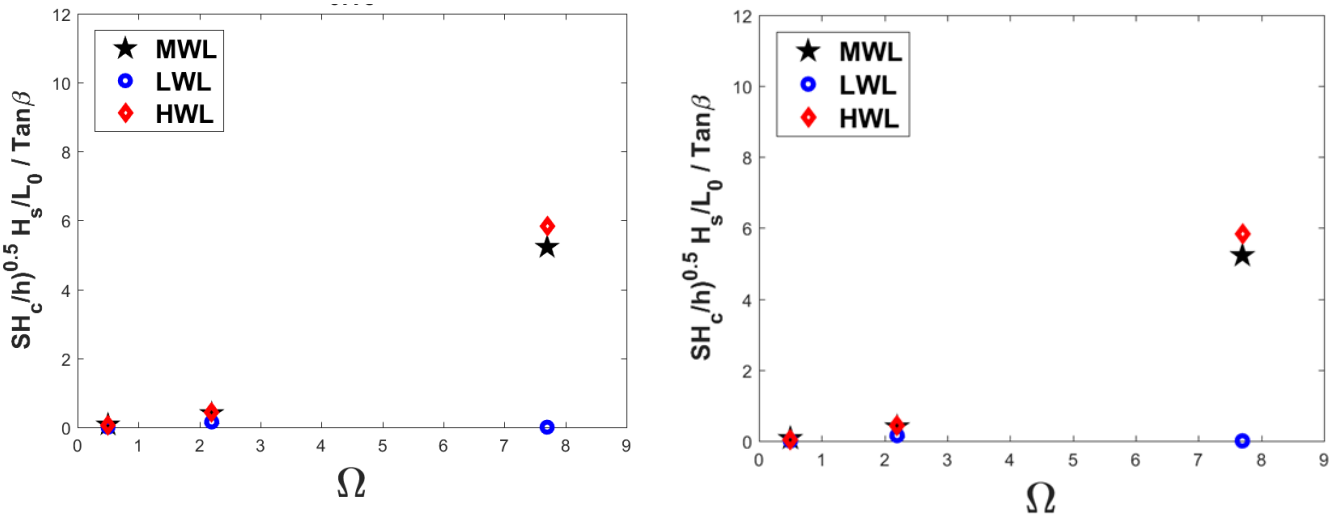

Figure 4. 20 Variability of non-dimensional shoreline change on different water level against Dean's parameter Ω for all three beach states (left) 0.15 m and (right) 0.25 m water level

4.6 Conclusion

In this chapter, the performance of the empirical formulations that characterise the shape of a beach profile for tide-induced static water level change was examined and compared with those under MSL values Although these empirical formulations provide a simple, cost-effective method of determining beach state variability, without having to run expensive and time consuming and costly numerical models, they can be satisfactorily used to determine beach profile shape for both micro and meso tidal beaches under all beach states. On macro-tidal beaches also, the parameters show only less than 10% deviation from the MSL.

Chapter 5: Application and validation of the empirical formula for beach state change prediction

The empirical beach state change formula presented in Chapter 4 will be applied and tested on three field sites with distinctly different characteristics in terms of beach slope, sediment properties and incident wave conditions (Narrabeen - Collaroy beach, Australia; Hasaki beach, Japan; and Duck beach, North Caroline USA) in this Chapter. It will also be tested against the laboratory testing of gravel beach change carried out by Polidoro (2018).

5.1 Site descriptions

5.1.1 Narrabeen – Collaroy Beach, Australia

The Narrabeen-Collaroy (herein referred to as Narrabeen beach) is a 3.6 km long sandy beach situated in New South Wales (NSW), Australia, located 20 km north of Sydney (Karunarathna et al., 2016). It is bounded by two headlands Narrabeen Head in the north and Collaroy and Long Reef point in the south (Figure. 1a & 1b). Surveys of five representative subaerial cross-shore beach profile lines have been done monthly since 1976 and are identified as PF1, PF2, PF4, PF6 and PF8 (Figure 1c). The beach profile PF4 was selected for this study (Figure.1d) as it is the least impacted by longshore sediment transport due to being the pivotal point of inter-annual scale beach rotation Ranasinghe et al., (2004). Also, it experiences ranges of beach states depending on the antecedent wave conditions (Wright & Short, 1984), although it is predominantly at intermediate state, tending towards more dissipative and reflective under higher and lower wave conditions (Wright et al., 1985), respectively.

Narrabeen beach is characterised by fine to medium quartz and carbonate sands with $D_{50} \sim 0.3 – 0.4$ mm with approximately 30% carbonate fragments shells and algae detritus. The spring tide range is 1.6 m (2 m maximum), and average wave height is 1.6 m, with 20% of the waves exceeding 2 m, 5% exceeding 3 m, 1% exceeding 4 m and a very few may reach 8 m (Short and Trenaman, 1992,). Narrabeen beach's morphodynamic response is highly variable and extremely rapid due to frequent storm wave conditions. Because of the open nature of the beach, erosion and accretion occur any time of the year (Ranasinghe et al., 2004, Karunarathna et al., 2014). In determining the beach morphodynamic variability, storm duration as well as the maximum significant wave height plays an important role (Dolan and Davis 1994; Karunarathna et al., 2014).

This site was selected due to the large morphological dataset available freely online. Narrabeen beach has some of the world's best survey quality and long-time data sets from 1976 to present which incorporates both underwater hydrographic and above water beach profile surveys.

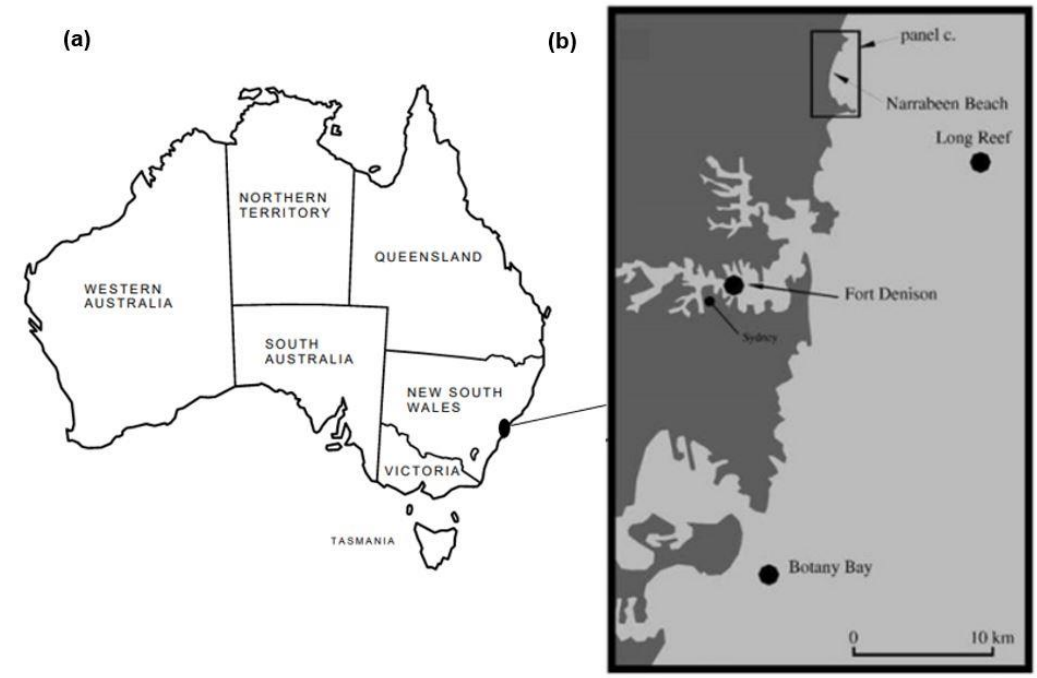

Figure 5.1(a) Map of Australia (b) location of Narrabeen beach and wave measuring points long reef and Botany Bay (c) Satellite image of Collaroy - Narrabeen Beach showing locations of five historical cross-

section profile lines (d) Profile of interest. For more interpretation, the reader is referred to (http://narabeen.wrl.unsw.edu.au/)

5.1.2 Hasaki Beach, Japan

The Hasaki beach is a microtidal beach located in eastern Japan exposed to the Pacific Ocean. It is wide a sandy beach and characterised by a longshore uniform beach (Dastgheib et al., 2022; Banno et al., 2020; Kuriyama et al., 2008) the medium grain size of the foreshore sediment is 0.18 mm with a porosity of 39.5% (Katoh & Yanagishima, 1995). The mean high water (MHW), mean water level (MWL) and mean low water (MLW) at Hasaki beach are 1.25 m, 0.65 m, and -0.20 m, respectively based on the datum level at Hasaki (Tokyo Peil -0.69m) (Kuriyama,2002). The morphodynamics of Hasaki beach is dominated by the nearshore bar-trough system. The cross-shore beach profile at HORS is known for its seasonal disparity in storms and calmer periods, i.e., fall/winter or September to March (shoreline moves seaward) and spring/summer or April to August (shoreline moves landward). In contrast, the sandbar moves periodically seaward during winter and landward during summer. The shoreline or bar-trough system progradation or erosion is dependent on the season. Along the cross-shore and the along shore profiles are nearly uniform despite the morphological changes (Kuriyama 2002; Suzuki and Kuriyama 2007; Malek et al.,2020 Suzuki et al., 2020). Basically, Hasaki beach has a single bar and a mean beach slope of 1/50 from -60 m to 200 m seaward and 1/20 in the deeper region (Kuriyama, 2002). Beach profiles have been measured weekly at the Hasaki Oceanographic Research Station (HORS) pier, which is 427 m long, with a deck of 3.3 m in width and 6.9 m above the low water level supported by single pilings (Figure, 5.2).

(a) **(b)**

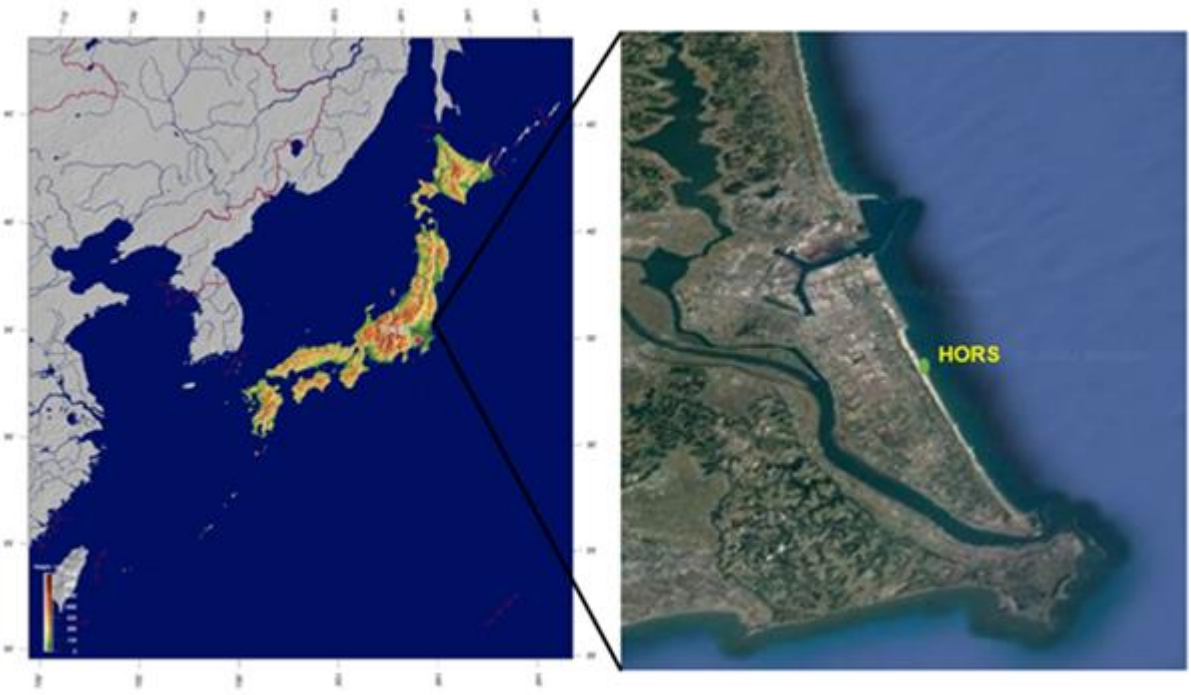

(c)

Figure 5.2 (a) Site location of the Hasaki Oceanographical Research Station (HORS) Japan, (b) View of the beach

5.1.3 Duck Beach

Duck Beach is located on the east coast of the United States, North Carolina, which has been the home of the U.S. Army Corps of Engineers field Research Facility (Figure 5.3). This Field Research Facility (FRF) established in 1977(Birkemeier and Holland, 2000) on the beach is oriented – 20.3^0 north-northwest to the true north. For over 27 years, hundreds of surveys have been collected by the FRF as part of monitoring the beach.

The sediments at Duck beach typically include a medium-to-fine sand mixture with a grain size decreasing from 1 mm on the foreshore to 0.125 mm in the offshore zone. In the offshore region (~ 1 km from shore), the sediments are uniform and fine (Birkemeier and Holland, 2000; Horrillo-Caraballo et al., 2016; Zhang and Larson, 2021). The area is characterized by regular shore-parallel contours, a moderate slope, and bars in the surf zone. An outer storm bar is present at about 4.5 m of depth, relative to the mean water level, and an inner bar is present between 1.0 and 2.0 m of depth relative to the mean water level (Horrillo-Caraballo et al., 2016).

Based on the offshore wave buoy data wave energy varies with season and high during the fall and winter and lower in the spring and summer (Zang et al., 2002). According to Horrillo-Caraballo and Reeve (2010), sand

is removed from the beach face and deposited further offshore forming sand bars during high energy wave condition (winter) and shoreward during lower energy condition (summer), due to predominant transport of sediment towards the land. In both conditions of high energy and milder conditions, a smoother beach profile with relatively flattened bars can also form (Holland,1998).

Figure 5.3 Duck beach location and overview of the Field Research Facility (FRF) pier, and the observation tower (Left). Holman and Manson (2020)

5.1.4 Laboratory Experiment with Gravel Beach (hereafter known as Polidoro experiments)

To verify the accuracy of empirical formulation, the model was validated based on experimental data from Polidoro (2019). The experiments were conducted in a large wave flume measuring 100 m long, 2.0m deep and 1.8m wide with a 30 m long flat bathymetry, leading to two slopes of 1:30 (31m long) and 1:75 (33m long) respectively at HR Wallingford, as presented in Figure. 5.4. In this experiment, a two-dimensional (2D) physical model study was carried out to investigate the variability of a gravel beach in various combinations of different wave conditions. The wave conditions were based broadly around a framework of measured conditions (wave height, wave steepness and wave period). For each wave condition, an in-line array of six wave gauges was used to measure both the incident wind and swell waves. The physical model presented diverse beach profile patterns based on the effects of bimodal wave spectrum. Using the profiles obtained from this 2D physical model study, pre- and post-storm beach profiles were selected for analyses such as shoreline changes of a steep beach were evaluated. A large range of input conditions to examine the response of shingle/steep beaches was used in the experiment. A detailed description of each test series is given by

(Polidoro et al., 2018). In these profiles, only profiles generated by unimodal wave condition were selected for comparison as the empirical formula was derived from unimodal conditions. DoC was not calculated in the experiment. However, twice the water depth was considered as the DoC, to be consistent with the empirical model.

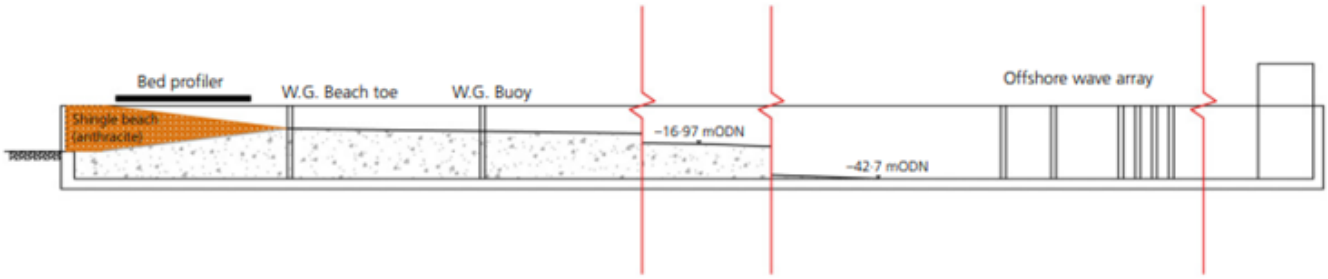

Figure 5.4 Flume set-up (HR Wallingford Modelling Hall)

5.2 Data Selection

5.2.1 Narrabeen Beach

The annual wave climate of Narrabeen can be classified as moderate to high energy with an average significant wave height (H_s) of 1.6 m and peak wave period (T_p) of 10s (Turner et al., 2016). Storm conditions in Narrabeen beach were typically categorised using the peak-over threshold method where the offshore significant wave heights exceeded a 95% threshold (Lord and Kulmar, 2000; Simmons and Splinter, 2022). Correspondingly, we defined storm-wave conditions at a threshold of significant wave height $H_s > 3$ m which is the 95% threshold. For this study we analysed the cross-shore beach profiles carried out at Profile 4 (Figure 5.1d), situated in the central part of Narrabeen.

Figure 5.5a represents the mean profile and Figure 5.5b represent the historical cross-shore profile survey data measured from 10 m elevation above shoreline at Profile 4.

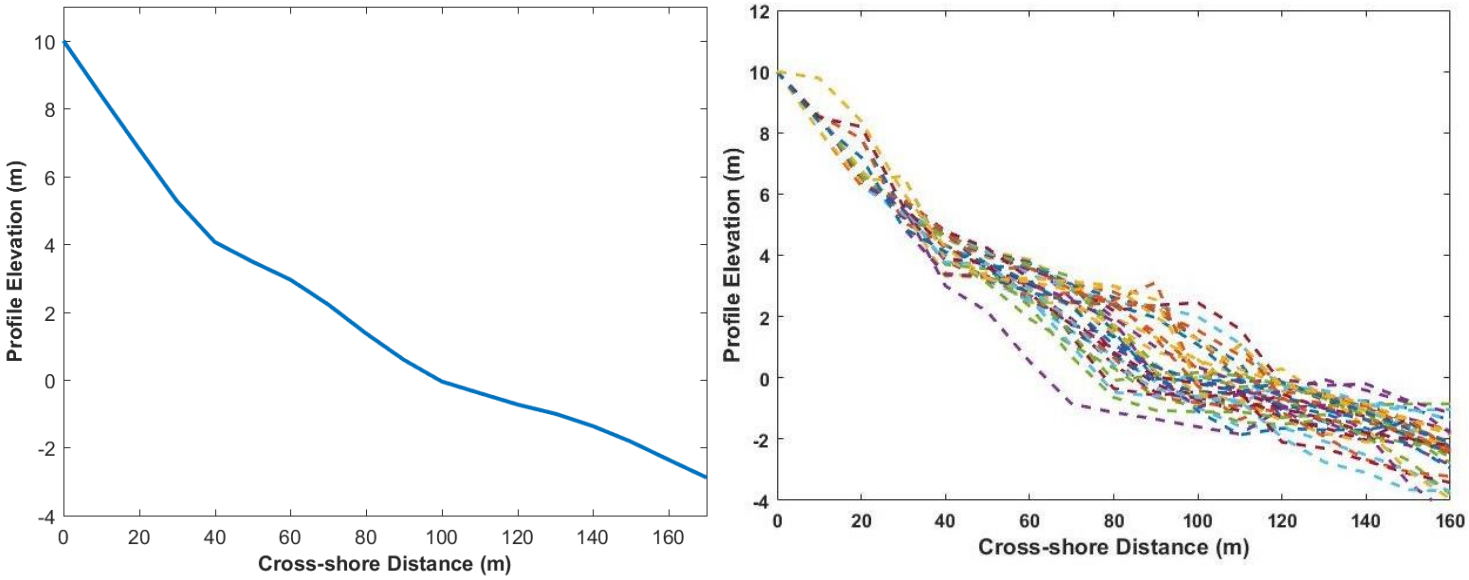

Figure 5. 5 (a) Mean profile of selected site (b) Cross-shore survey data at Profile 4 Narrabeen Beach

The key data selected for the analysis of Narrabeen beach include pre- and post-storm cross-shore beach profiles at different wave conditions between 1982 and 1992. Profiles selected are profiles with a single storm in between two measured profiles, 14 cases were selected. All cases cover mostly dissipative states with few intermediate states. Figure 5.6 shows some of the selected pre and post storm profiles. The sub-tidal beach slope (tanβ) was derived from the averaged of all the sections of all profiles below low tide (-4 m to 0) (see Figure 5.5a).

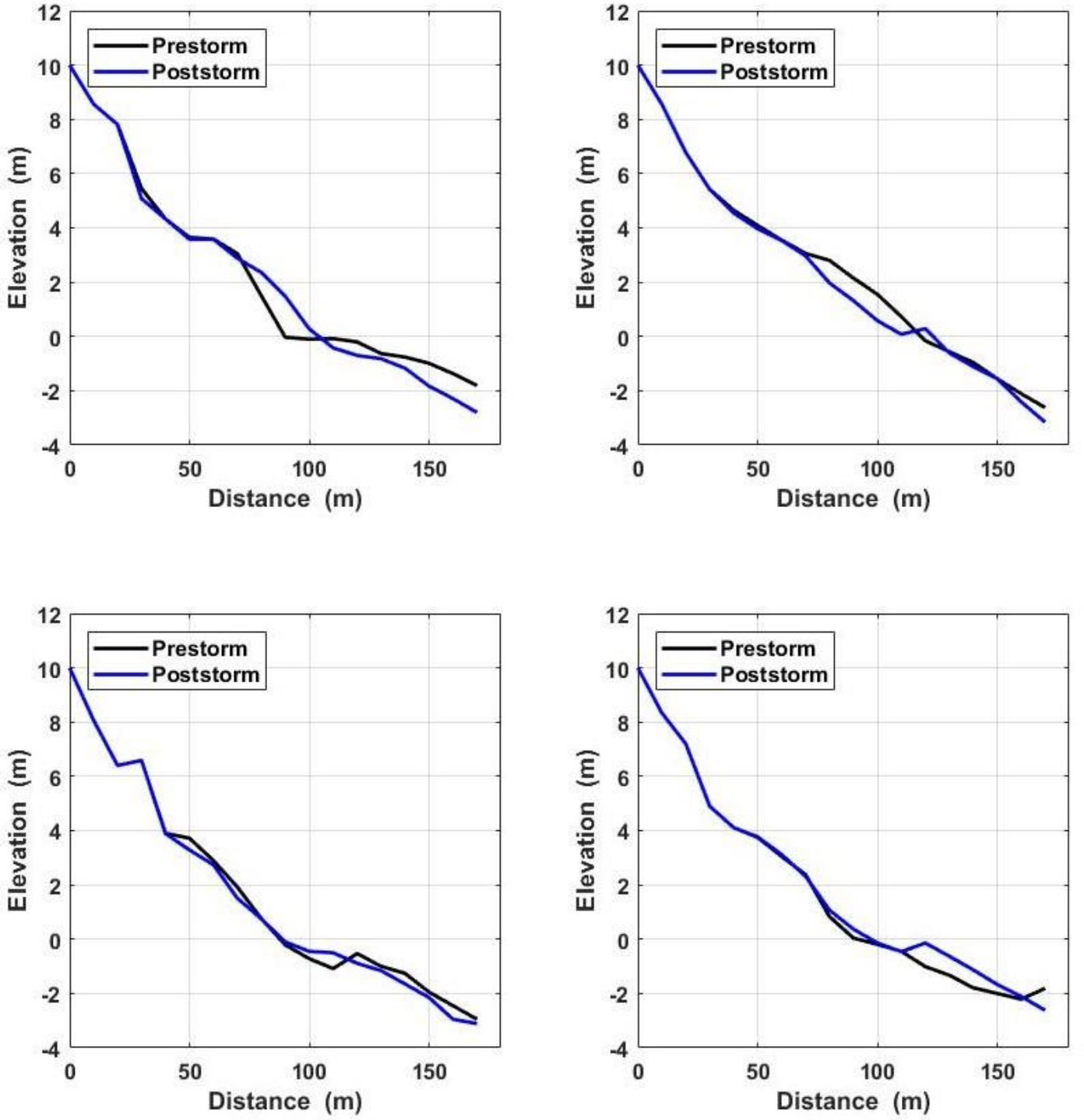

Figure 5.6 Some selected pre and post -storm profiles at Narrabeen beach

In this study, the non-dimensional parameters used exclude the water depth which is substituted with the DoC given that the depth of closure is an important parameter. The DoC (h_c) were estimated using Hallermeier (1981). Hallermeier (1981) defined the depth of closure of a beach as the seaward limit to any significant change in the elevation of the beach profile for a given time interval. Beyond this point of the cross-shore profile, waves have no significant effect on the sediment transport. Hallermeier (1981), suggested that the depth of closure, h_c, can be calculated using the following formulation.

$$h_c = 2.28\, H_{e,t} - 68.5\left(\frac{H_{e,t}^2}{\mathrm{g}T_{e,t}^2}\right) \quad (5.1)$$

where:

h_c = Predicted depth of closure over years, referenced to mean low water

$H_{e,t}$ = Nearshore significant wave height that exceeds only 12 hours per year.

$T_{e,t}$ =Associated wave period.

g =the acceleration due to gravity.

For all the field measured data, DoC was estimated as half of the water depth because in the experiment used for the model calibration the DoC was calculated as water depth. From the empirical formulation h_o was replaced by twice the DoC and calculated the wavelength at the DoC however, L_o was replaced by L value, given that L value is usually smaller than L_o

All storms selected are in the same order of magnitude above 3m threshold. For storm selection, storms above the 3m threshold of Narrabeen beach were selected as seen in Table 5.1. For the calculation for fall velocity and other non-dimensional statistics, H_s and T_p values from the averaged storms were used. D_{50} for Narrabeen was taken as 0.35 mm (Karunarathna 2012, Short and Trembanis, 2004).

The fall velocity or settling velocity (w_s) of particles is referred to as velocity at which force due to gravity exceeds fluid forces and this depends on both the characteristics of particles and fluid. It is difficult to obtain a specific mathematical transcription of fall velocity because some particles are irregular in shape. Van Rijn (1993) derived a formula for spherical particles, and it's based on the kinematic viscosity and other properties of the particle and water density as shown in Equation 4. The fall velocity was calculated as 0.0519 m/s which is comparable to 0.045 ms^{-1} as reported by Wright et al., 1984.

Table 5.1 Narrabeen beach profiles and storm conditions selected for comparison

Profile Start	Profile end	Storm start	Storm end	Hs	Tp	Ω	
21/07/1980	14/08/1980	23/07/1980	23/07/1980	3.17	9.5	6.43	Dissipative
30/04/1981	28/05/1981	22/05/1981	24/05/1981	3.37	10.5	6.16	Dissipative
02/08/1981	25/08/1981	10/08/1981	11/08/1981	3.43	9.8	6.74	Dissipative
23/09/1981	17/10/1981	28/09/1981	28/09/1981	3.31	11.20	5.69	Intermediate
27/11/1981	22/12/1981	14/12/1981	15/12/1981	3.64	9.40	7.46	Dissipative
09/03/1982	28/03/1982	09/03/1982	09/03/1982	3.76	8.40	8.62	Dissipative
31/05/1983	16/06/1983	04/06/1983	08/06/1983	3.30	12.0	5.3	Intermediate
18/01/1984	16/02/1984	10/02/1984	11/02/1984	3.22	10.0	6.2	Dissipative
01/03/1985	04/04/1985	04/03/1985	05/03/1985	3.38	9.20	7.17	Dissipative
04/08/1985	29/08/1985	19/08/1985	20/08/1985	3.15	11.10	5.47	Intermediate
28/03/1986	23/04/1986	05/04/1986	06/04/1986	3.85	10.0	7.42	Dissipative
12/09/1986	17/10/1986	15/09/1986	18/09/1986	3.36	11.0	5.89	Intermediate
25/06/1987	29/07/1987	12/07/1987	13/07/1987	3.57	10.70	6.43	Dissipative
04/08/1988	31/08/1988	23/08/1988	24/08/1988	3.58	8.50	8.12	Dissipative
05/10/1988	27/10/1988	13/10/1988	13/10/1988	3.06	9.60	6.14	Dissipative

5.2.2 Hasaki Beach

Seventeen years of wave and beach profile and wave data are used. Long-term and seasonal profile variability were carefully analyzed using the pre and post storm profiles. In Hasaki beach, offshore bar and intertidal berm are very prominent. I considered only the nearshore berm which changes the beach profile into different states like dissipative, intermediate and reflective. Only cross-shore sediment transport was considered because longshore transport is negligible at the Hasaki beach (Kato and Udo, 2020).

Similarly, to what was presented in section 5.2.1, storms at Hasaki beach were defined with the significant wave height exceeding the 95% threshold and lasting for at least 6h where H_s exceeds 3 m. Table 5.2, shows some selected storm profiles and wave condition used for validation.

The average sub-tidal slope of 0.015 m was calculated from the mean (Figure 5.7b) of all the subtidal pre- and post-storm profiles (Figure 5.7a). Figure 5.8 shows some of the selected pre and post storm profiles. For Hasaki beach, DoC was calculated as 6.5 m and fall velocity as 0.0257 (m/s) using Equation (4.4) Hallermeier (1981).

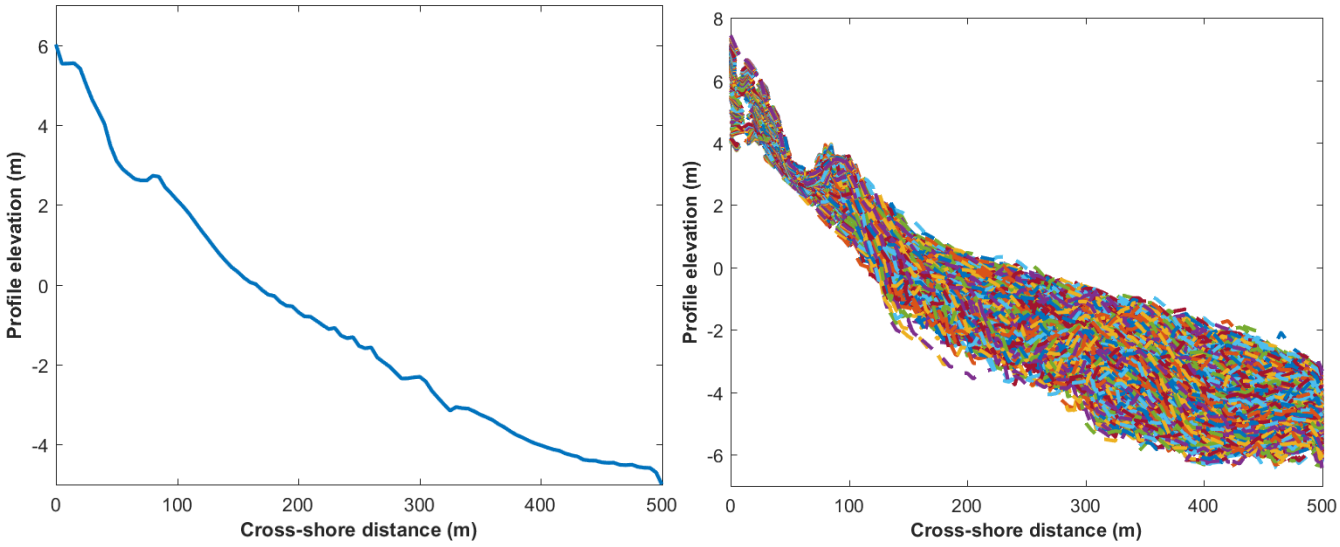

Figure 5.7 (a) Mean beach profile, the elevation is based on the Hasaki datum level (b) Selected profiles 1993-2010

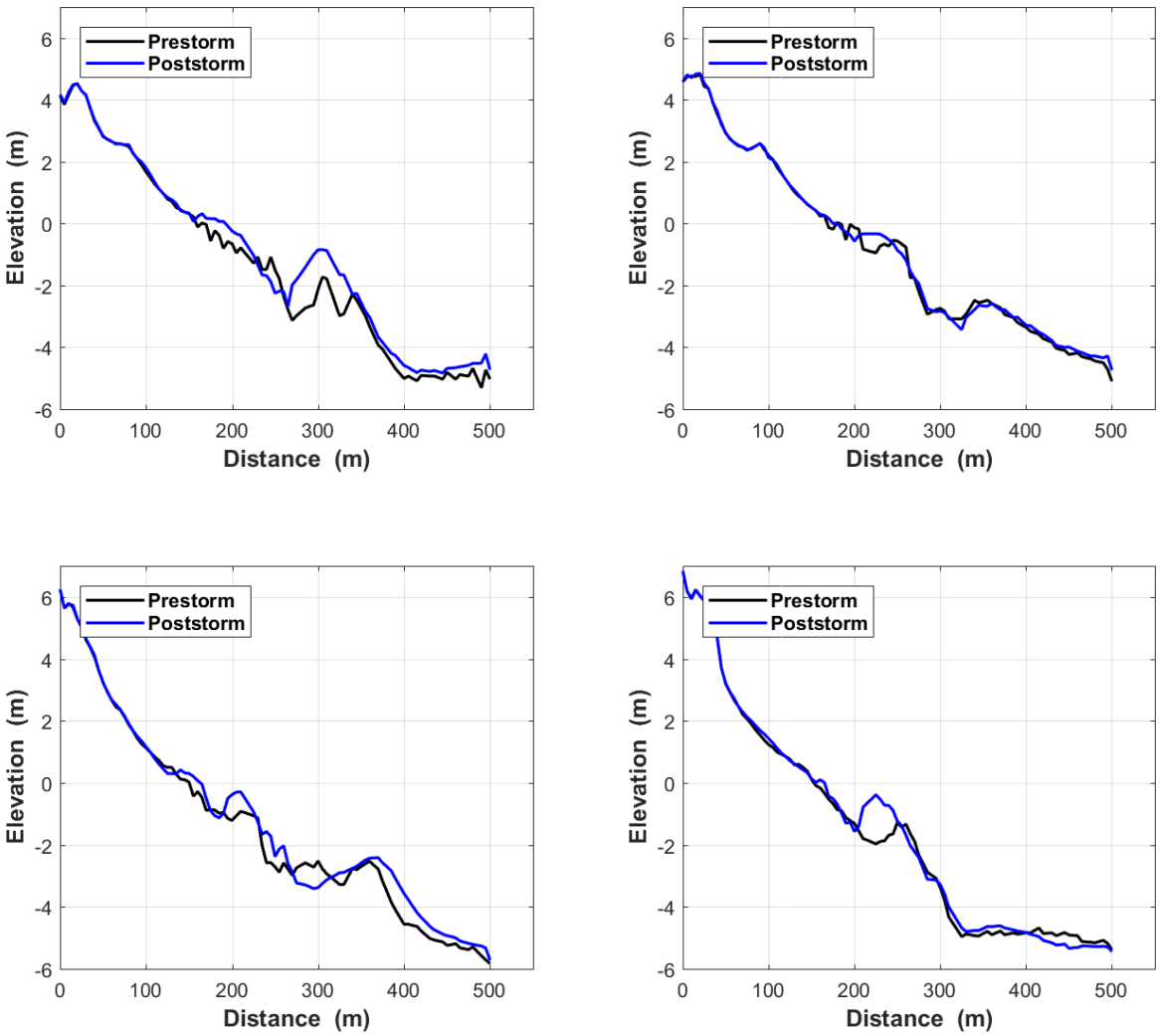

Figure 5.8 Few selected pre- and post - storm from Hasaki beach

Table 5. 2 Hasaki beach profiles and storm conditions selected for comparison

Profile Start	**Profile end**	**Storm start**	**Storm end**	H_s	T_p	**Ω**	
23/01/1995	30/01/1995	27/01/1995	27/01/1995	2.77	11.9	9.1	Dissipative
05/02/1996	12/02/1996	08/02/1996	08/02/1996	2.77	11.9	9.7	Dissipative
12/01/1998	12/01/1998	15/01/1998	16/01/1998	2.9	9.4	12	Dissipative
02/11/1998	09/11/1998	07/11/1998	08/11/1998	2.94	10.1	11.3	Dissipative
01/04/2002	01/04/2002	06/04/2002	07/04/2002	3.11	10.9	11.1	Dissipative
22/07/2002	29/07/2002	24/07/2002	25/07/2002	3.05	11.2	10.6	Dissipative
25/11/2002	02/12/2002	25/11/2002	27/11/2002	3.28	19.8	6.4	Dissipative
10/04/2006	17/04/2006	14/04/2006	16/04/2006	3.96	8.8	17.5	Dissipative
03/09/2007	10/09/2007	06/09/2007	07/09/2007	3.09	9.4	12.8	Dissipative
12/11/2007	19/11/2007	14/11/2007	14/11/2007	2.96	10.8	10.7	Dissipative
07/04/2008	14/04/2008	08/04/2008	10/04/2008	3.53	8.7	15.8	Dissipative
12/05/2008	19/05/2008	14/05/2008	15/05/2008	2.86	10.6	10.5	Dissipative
02/06/2008	09/06/2008	03/06/2008	04/06/2008	3.01	10.1	11.6	Dissipative

5.2.3 Duck Beach

Since 1981, there have been cross-shore beach profile measurements carried out at four locations at Duck Beach. The data collected covers pre- and post-storm profiles. The data set used in this study covers the period between 1981 and 2000. In this study, profile location 62 was selected for analysis because it offers a good point of comparison with other techniques that have used measurements from the profile (e.g., Gunawardena et al., 2008; Li et al., 2005; Horrillo-Caraballo & Reeve,2010) the profile measurement is shown in Figure 5.9a. Storm conditions as shown in Table 5.3, were charaterised by using a long-term series of wave data extracted from Horrillo-Caraballo et al., (2016).

A sub-tidal slope of 0.013 m was calculated from the mean (Figure 5.9b) of all the subtidal pre- and post-storm profiles (Figure 5.9a). Figure 5.10 shows some of the selected pre and post storm profiles. DoC was calculated using Equation (5.1). For Duck beach, DoC was 9.5 m and fall velocity was 0.0218(m/s)

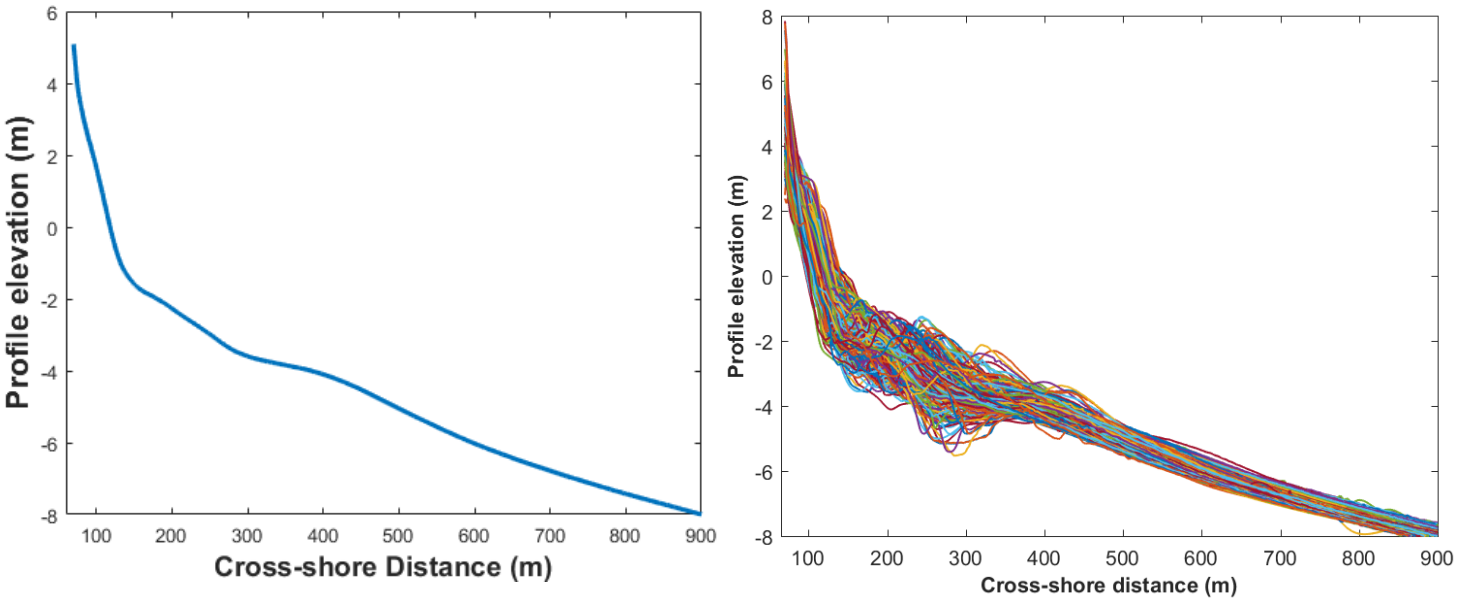

Figure 5.9 (a) Mean profile (b) Composite plot of measured beach profile 62 at Duck, NC, USA

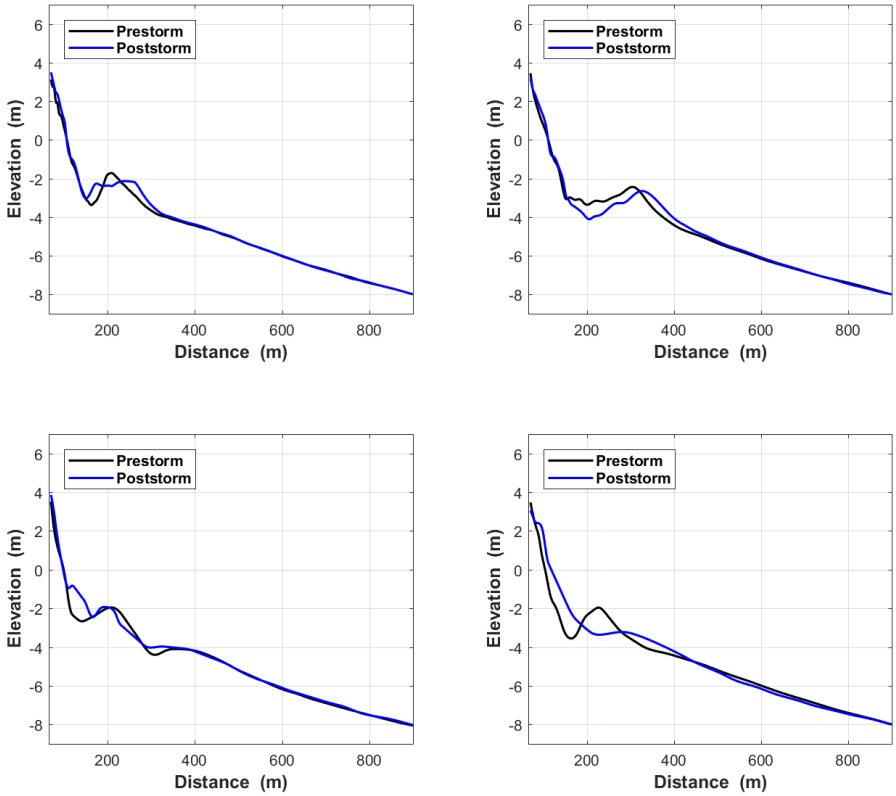

Figure 5.10 Some selected pre and post-storm from Duck beach

Table 5.3 Duck beach profiles and storm conditions selected for comparison

Profile Start	Profile end	Storm start	Storm end	H_s	T_p	Ω	
31/08/1987	28/09/1987	04/09/1987	05/09/1987	2.36	7.3	12.5	Dissipative
22/04/1991	24/05/1991	18/05/1991	19/05/1991	2.72	6.9	15.3	Dissipative
23/08/1991	23/09/1991	20/09/1991	20/09/1991	2.55	7.3	13.5	Dissipative
04/08/1993	02/09/1993	31/08/1993	31/08/1993	4.81	12.2	15.3	Dissipative
27/06/1996	24/07/1996	12/07/1996	13/07/1996	3.04	8.8	13.4	Dissipative
23/03/1999	19/04/1999	26/03/1999	28/03/1999	3.41	11.8	11.2	Dissipative
29/01/2001	26/02/2001	22/02/2001	22/02/2001	2.67	7.7	13.4	Dissipative

5.2.4 Polidoro Experiment

Three cases from Polidoro experiments were selected for this study. Each pre-and post-storm profile selected Figure 5.12 corresponds to different unimodal storm wave condition as in Table 5.4.

Figure. 5.11 shows the initial profile selected for all profiles. The profile measurement covers the intertidal and subtidal of the beach.

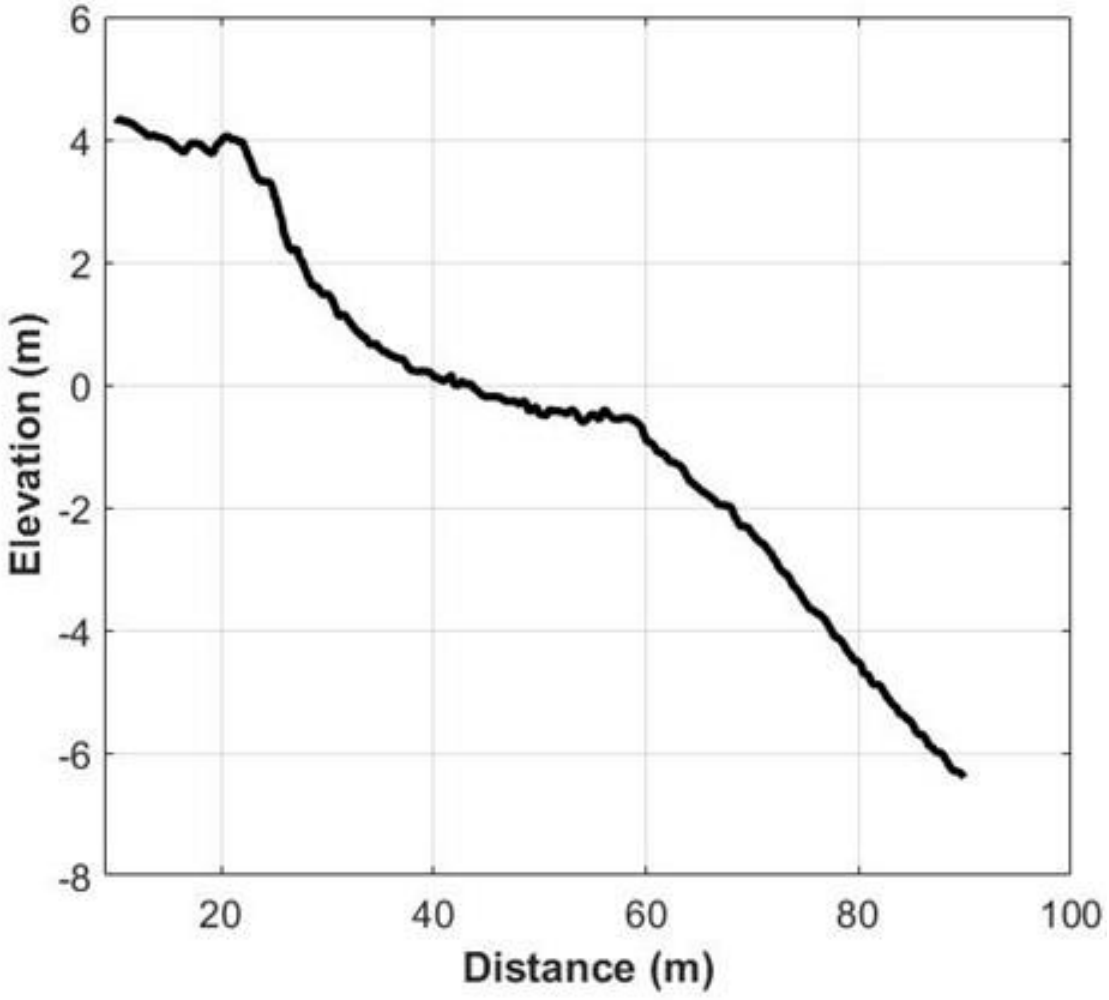

Figure 5.11 Initial Profile

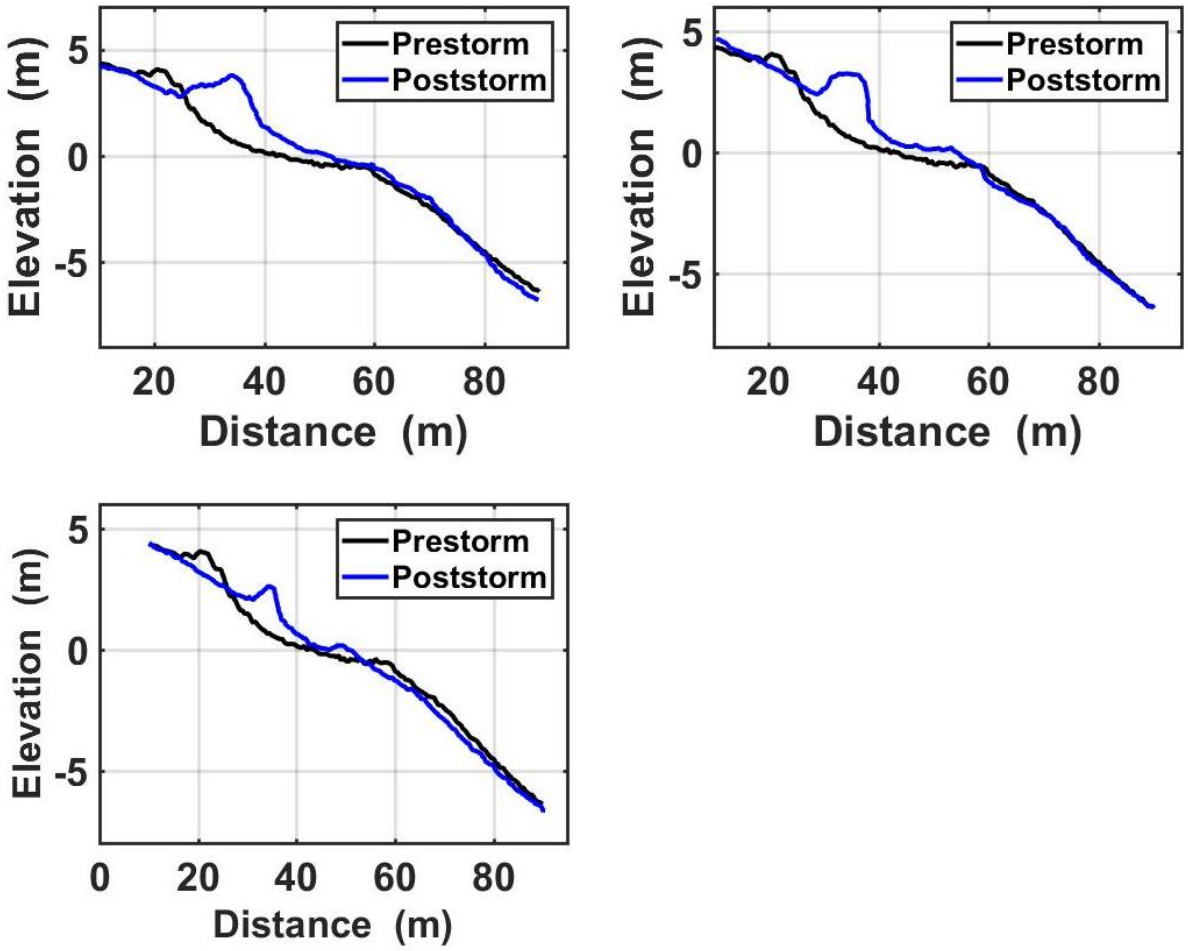

Figure 5.12 Selected pre and post storm from the Polidoro's experiment

Table 5. 4 Overview of selected wave conditions from Polidoro flume experiments

Profile	H_s **(m)**	T_p **(s)**	**Ω**	
1	**3.0**	**7.18**	**0.9**	**Reflective**
2	**3.0**	**8.26**	**0.8**	**Reflective**
3	**3.0**	**9.54**	**0.7**	**Reflective**

5.3 Results and Discussion

In this section, detailed results on the comparison of the empirical formulation for beach state variabililty at all sites are presented and discussed. This methodology involved careful data selection and analysis, leading to the identification of key parameters relevant to the empirical formulation. Table 5.5 provides a comprehensive summary of all the selected data, including sediment fall velocity, W_s, which is dependent on the median grain diameter D_{50} as seen in the Table.

Table 5.5 Summary of beach characteristics for selected beaches and experiment data

Beach Characteristic	**Narrabeen Beach**	**Hasaki Beach**	**Duke Beach, NC**	**Polidoro experiment**
D_{50}	0.35 mm	0.2 mm	0.2 mm	15 mm
Fall velocity	0.0519(m/s)	0.0257(m/s)	0.0218(m/s)	0.4487(m/s)
Profile data period (year)	1982 – 1992	1993 – 2010	1981 – 2006	
Profile type	Sandy Wave dominated Mean slope-composite	Sandy Wave dominated Mean slope – steep, composite	Sandy Wave dominated Mean slope - steep	Gravel beach Steeper slope
Approximate sub-tidal mean profile gradient	0.053	0.015	0.013	Slope1:7
Wave conditions	High energy, all year-round storms	Seasonal storms – sea summer	Seasonal storms	
Beach state	Intermediate	Dissipative	Dissipative	Reflective

5.3.1 Comparison of Narrabeen beach profile variability with Empirical formulation

To compare the empirical formulations for shoreline change, berm crest, berm height, and berm length were first calculated from the measured pre- and post-storm Narrabeen beach profiles. Cases of profile change where only one storm occurred between the pre- and post -storm profile measurements were considered in this analysis as the occurrence of multiple storms between profile measurements induce unnecessary complication into the analysis. Shoreline change was obtained by finding the difference in shoreline positions (shoreline at still water level) between pre and post – storm profiles for all profiles. The non-dimensional shoreline position parameter was then calculated. The Ω corresponding the storm occurred between pre- and post-storm profiles was calculated using measured storm data. The comparison of these results with the empirical formula is shown in Figure 5.13. The results show that 60% of the measured data lies within the 95% confidence interval while the empirical formulation overestimates the shoreline change in 40% of the cases. This discrepancy may be attributed to the fact the empirical formulation did not consider storm duration. Differences in the duration of actual storm events compared to the simulation used to develop the empirical model can significantly affect the predicted shoreline change. If the numerical simulation used to develop the empirical model does not accurately represent the temporal characteristics of the actual storm events, the empirical formulation may not align with the Narrabeen changes. For example, shorter storm durations in the simulation may underestimate the erosion or accretion effects on the shoreline compared to long-duration storms experienced in the field. Differences in wave energy distribution over time, such as variations in wave height, period, and direction, can further contribute to the discrepancies observed.

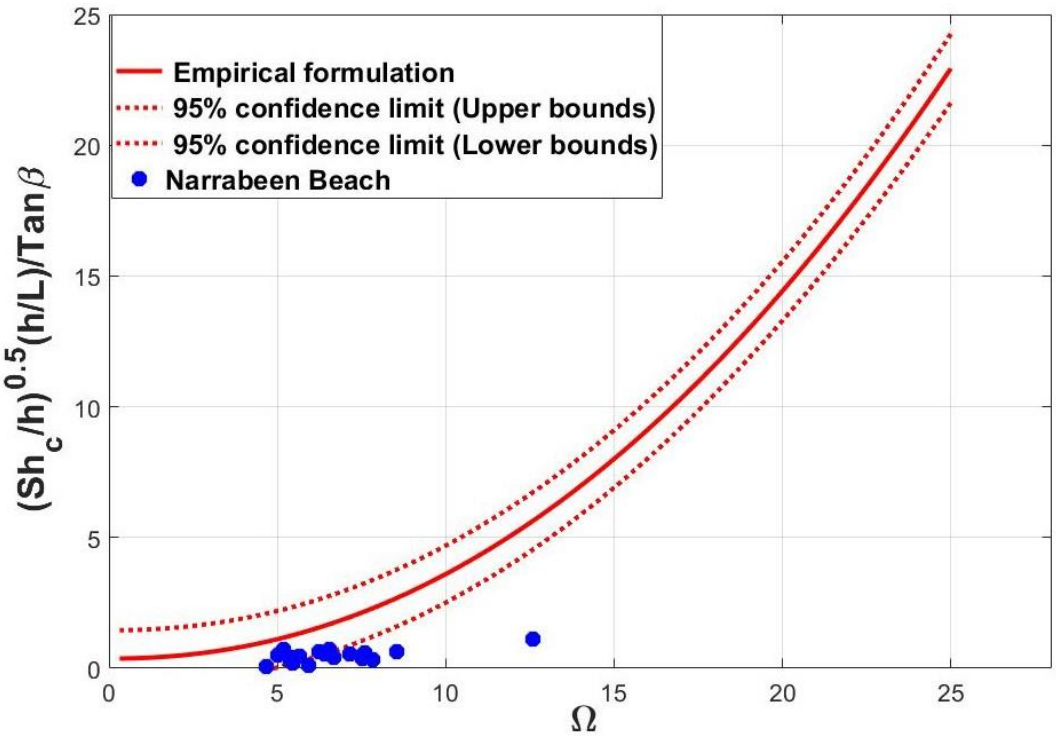

Figure 5.13 Comparison of empirical formulation with shoreline change profiles at Narrabeen Beach

Figure 5.14 gives a comparison of berm height change at Narrabeen beach against the empirical formulation. Berm height is considered as the maximum elevation of the beach profile with respect to the initial profile. The figure shows that the empirical formulation satisfactorily captures the berm height change at Narrabeen beach except at a few cases with large Ω values, the berm height was under-predicted.

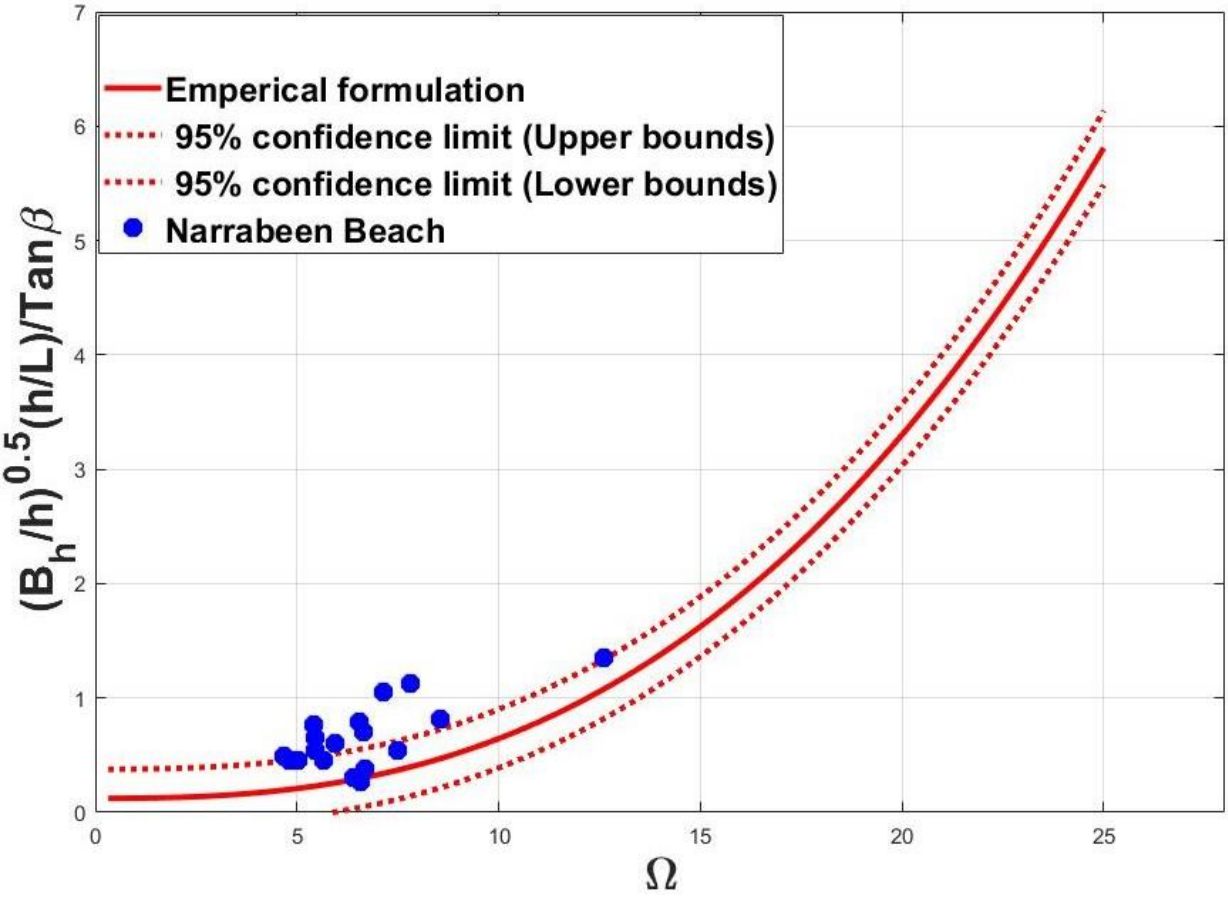

Figure 5.14 Comparison of empirical formulation with berm height at Narrabeen Beach

A comparison between the measured berm crest and empirical formulation is shown in Figure 5.15. The vertical distance between the berm crest and the still water level (SWL) was called the berm crest. The figure shows that 77% of the measured data lies within the 95% confidence interval of the empirical formulation. The berm crest at Narrabeen beach is submerged at all times within the sub- tidal zone (Karunarathna et al., 2016). The results further show that as Ω increases the accuracy of prediction by the empirical formulation decreases. However, the empirical model shows high accuracy in determining the berm crest for omega values ranging from 4 – 9 as seen in Figure 5.15.

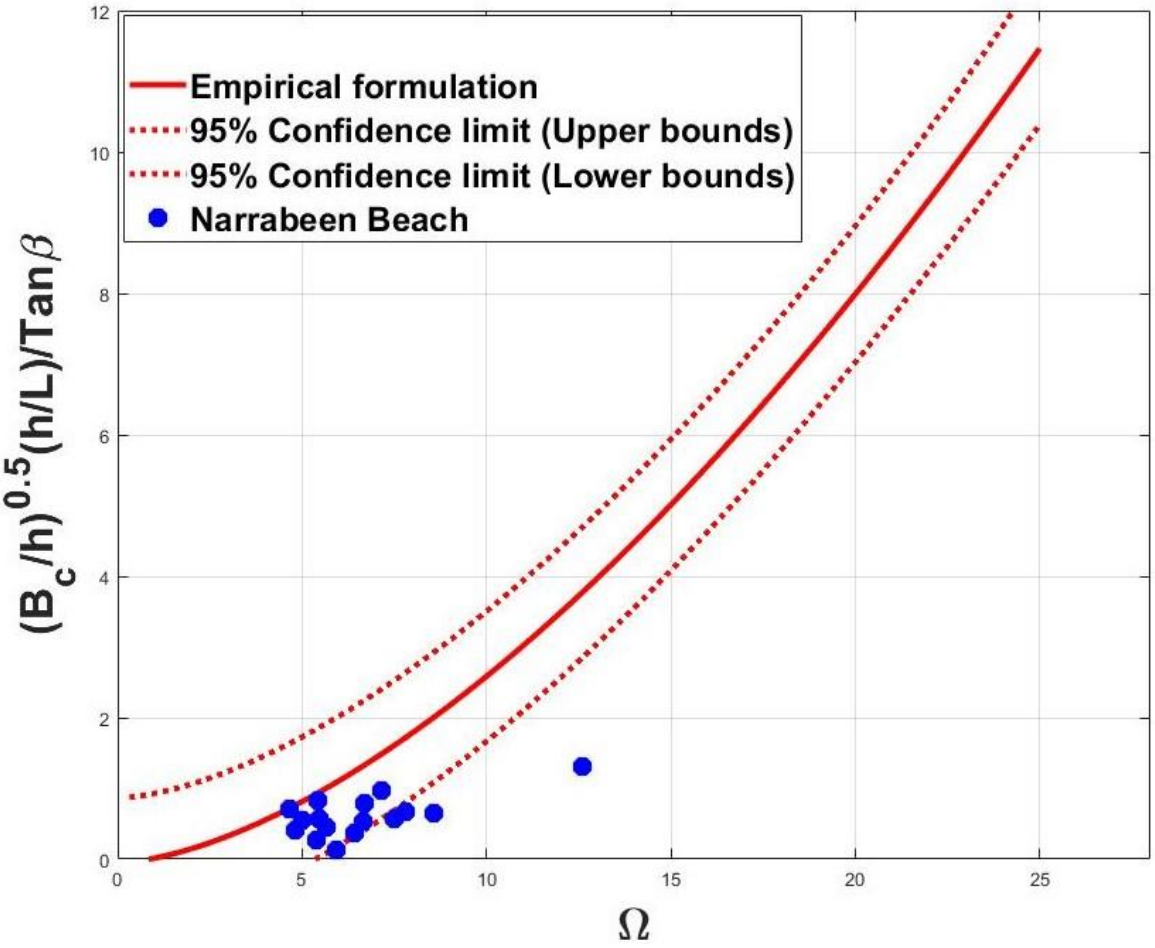

Figure 5.15 Comparison of empirical formulation with berm crest at Narrabeen Beach

As presented in chapter 4, the cross-shore horizontal distance between the start and the end points of the berm was considered as the berm length. As noted in Figure 5.16, for comparison between the measured berm length and empirical formulation, 80% of the measured data lie within the 95% confidence interval of the empirical formulation. The berm length at Narrabeen beach is mostly estimated for Ω values corresponding to the intermediate and dissipative beach states. The results further show that as Ω increases the accuracy of prediction of berm length by the empirical formulation decreases, though minimally. The empirical model shows high accuracy in determining the berm length for Ω values ranging from 5 – 8 as seen in Figure 5.16.

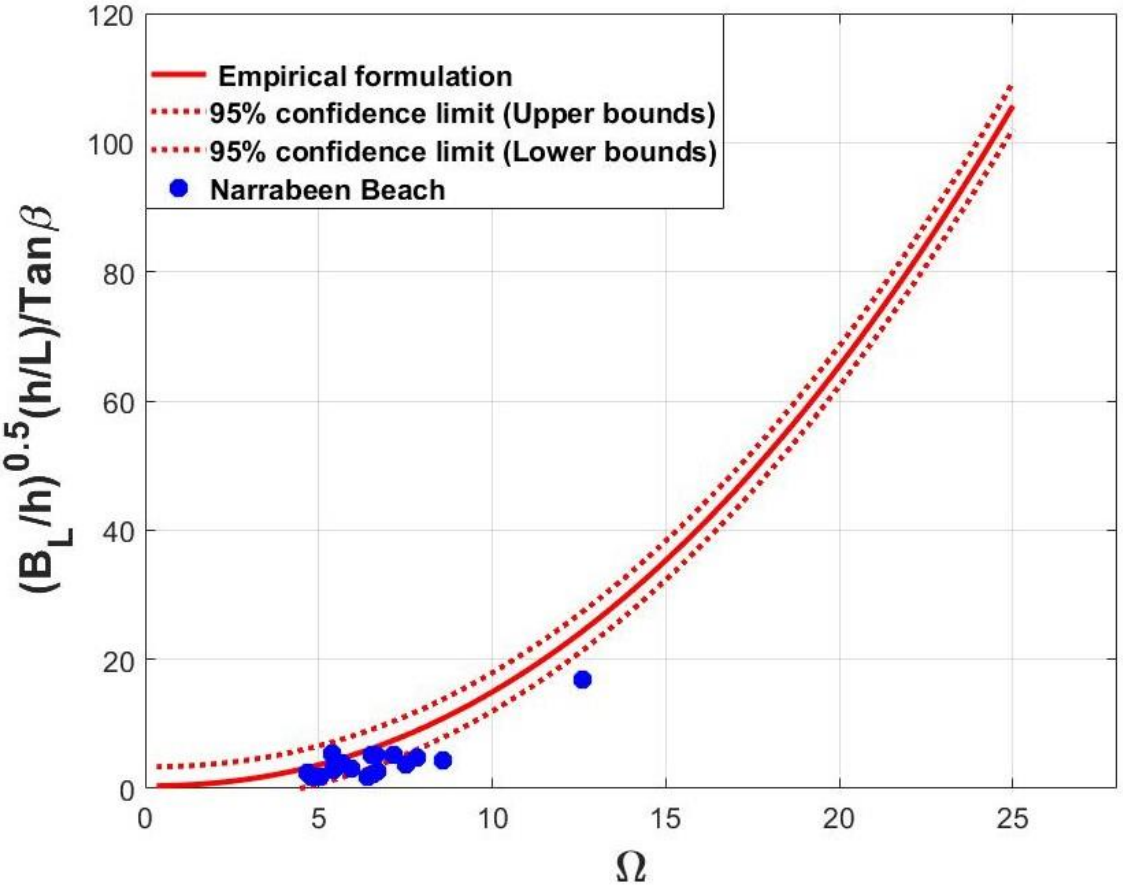

Figure 5.16 Comparison of empirical formulation with berm length at Narrabeen Beach

5.3.2 Comparison of Hasaki beach profile variability with Empirical formulation

In this section, the empirical formulations for the four parameters stated in the previous section were compared with the measure's values at Hasaki beach. At Hasaki, profiles remained in a dissipative state (Ω ~ 6 to 16) during the storm conditions considered in this comparison. Like Narrabeen, only cases of profile change where one storm occurred between pre storm and post- storm measurements were considered. Shoreline change was obtained by finding the difference in shoreline positions between pre- and post-storm profiles. The Ω corresponding the storm occurred between pre- and post-storm profiles was calculated using measured storm data. The comparison of these results with the empirical formulation is shown in Figure 5.17. The result shows that shoreline change at Hasaki beach is overestimated by the empirical formulation. This could be due to several factors, e.g., the beach's shape, the storm duration and tidal variations.

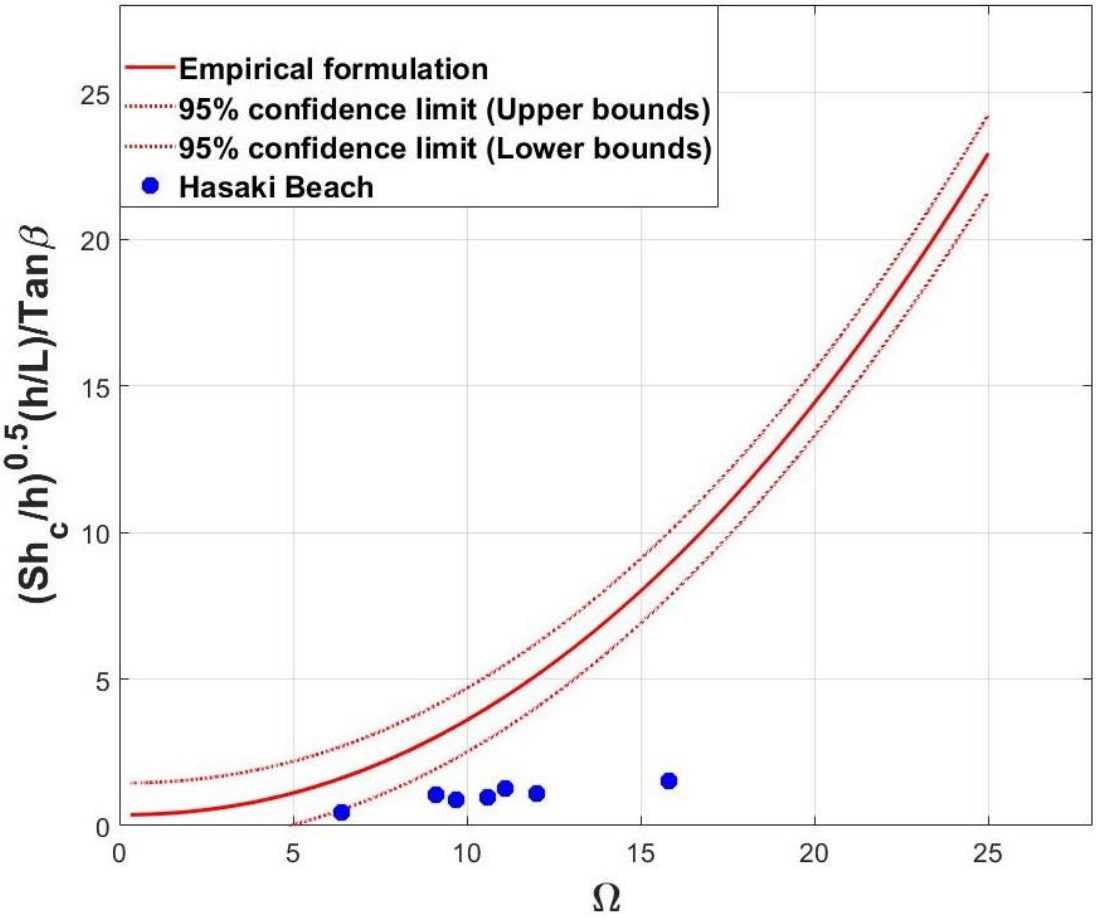

Figure 5.17 Comparison of empirical formulation with shoreline change at Hasaki Beach

The results (Figure 5.18) revealed that the empirical formulation overestimates the berm height parameter at Hasaki. The empirical formulation was only able to predict 5% of the berm height in correlation with the measured storm data. This could be because of continuous degradationof sediment by energetic waves within the considered zone causing much faster erosion of the berm and subsequently reduction in berm height. Figure 5.18 indicates that for highly dissipative cases the sediment moves offshore when a berm height is considered in the model. This may have made it incompatible and thus underestimated the berm height.

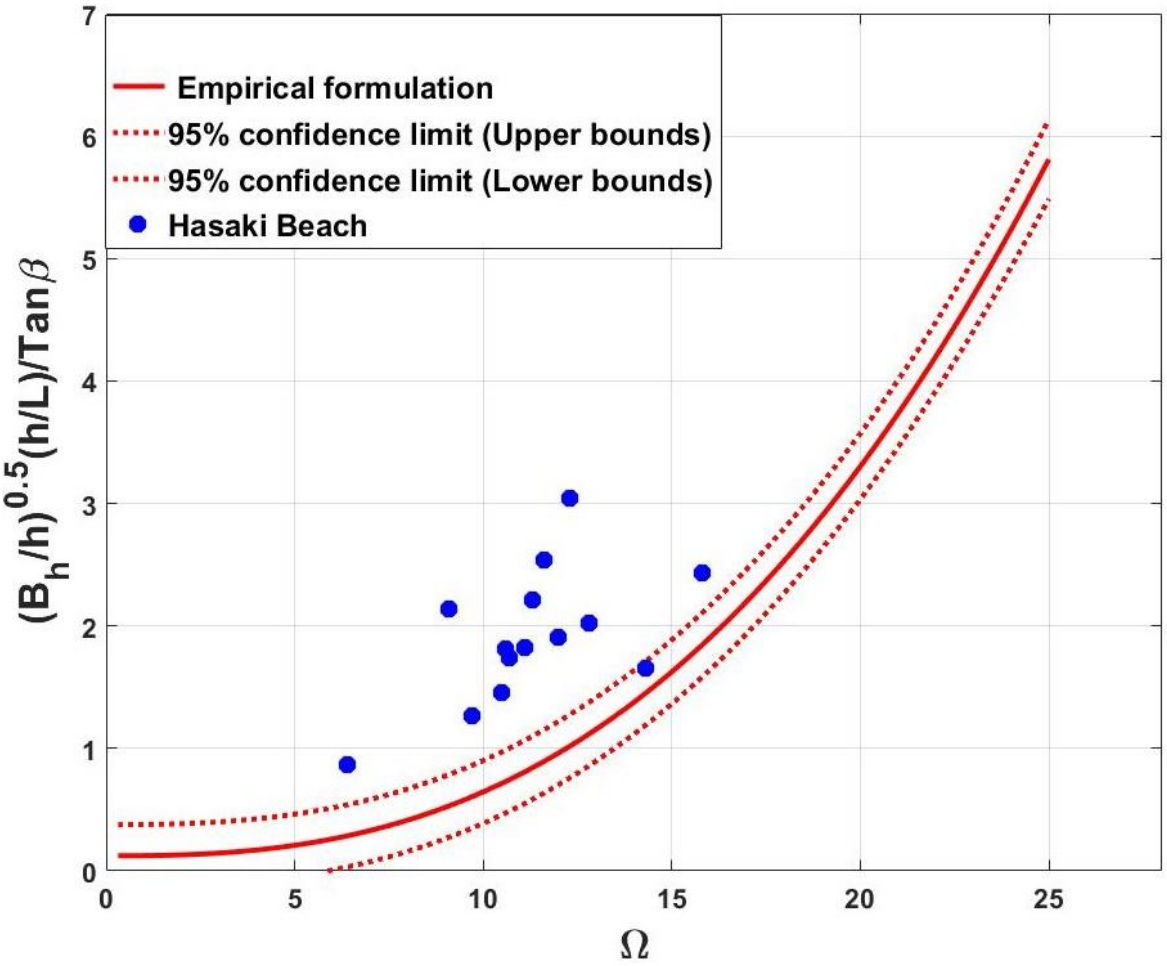

Figure 5.18 Comparison of empirical formulation with berm height at Hasaki Beach

A comparison between empirical formulation berm crest and measured berm crest parameter is given in Figure 5.19. The figures show fair agreement between empirical formulation and measured values where approximately 40% of berm crest was within the formulation. The results further show that due to changes in sediment supply and wave energy the berm crest can change over time. As indicated in Figure 5.19, the berm crest at Hasaki beach tends to move from dissipative to ultra dissipative state with ($\Omega \sim 6$ -16).

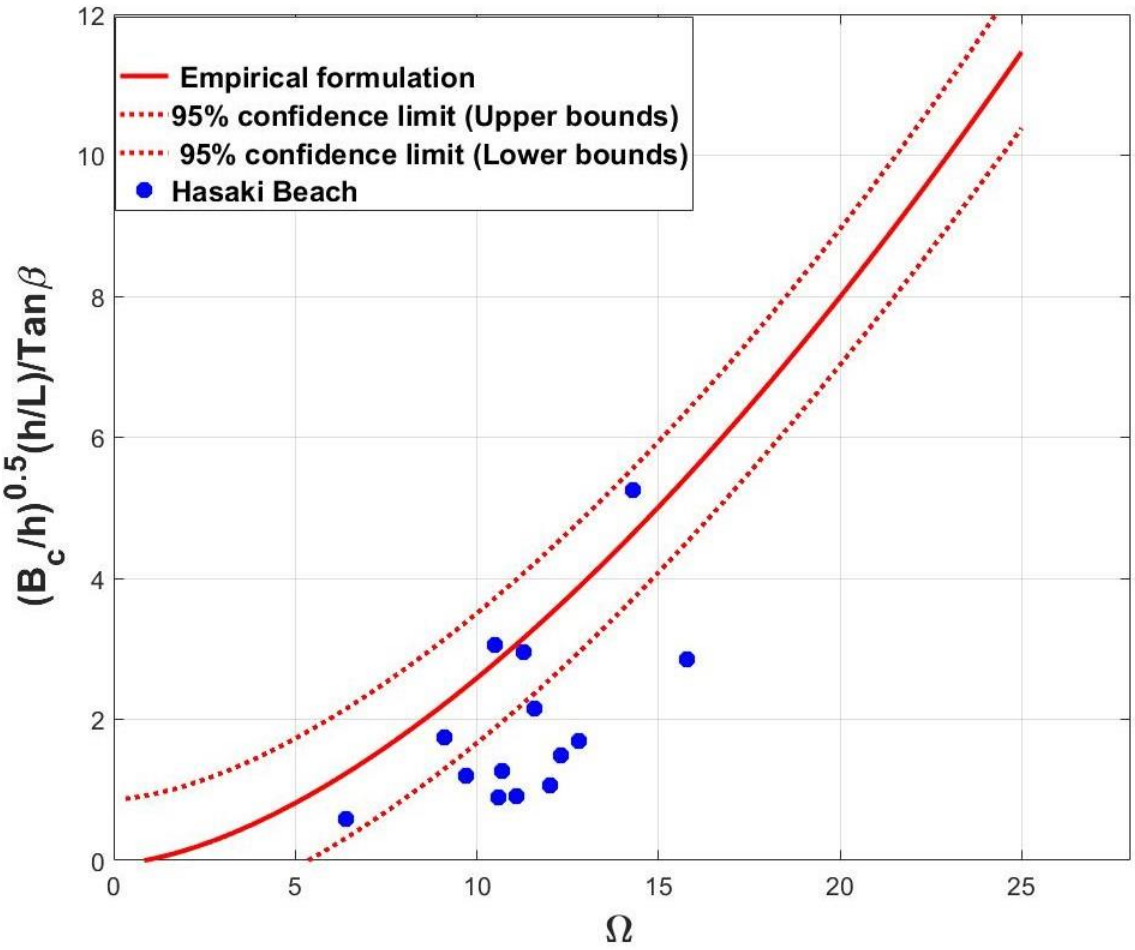

Figure 5.19 Comparison of empirical formulation with berm crest at Hasaki Beach

Some discrepancies between the measured berm length and empirical formulation remain unresolved. Virtually, the measured storm data remains poorly fit within the 95% confidence interval to the formulation. The berm length at Hasaki beach is mostly estimated for Ω >6 which is mostly dissipative beach state. The results further show that as Ω increases the accuracy of prediction by the empirical formulation decreases. The empirical model shows low accuracy in determining the berm length for Ω values ranging from 9 – 15 as seen in Figure 5.20.

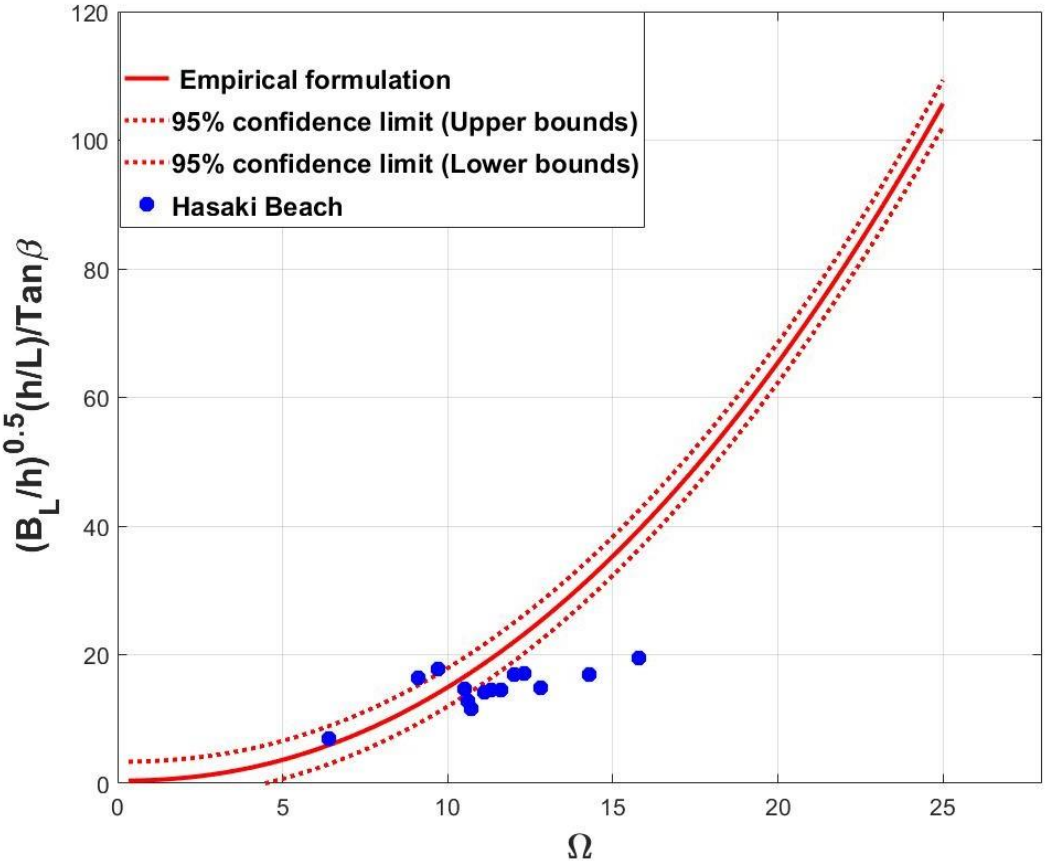

Figure 5.20 Comparison of empirical formulation with berm length at Hasaki Beach

Overall, the ability of the empirical formulations to predict the four cross-shore beach profile proxies at Hasaki beach is limited. This can be attributed to a few characteristics of Hasaki beach: (i) the Ω values in this beach is extremely high indicating a very highly dissipative beach; (ii) careful look at the beach prifle change (Figure. 5.7) indicates that the highest profile change takes place in the subtropical areas; (iii) no indication of formation of an inter-tidal berm/bar but a prominent subtidal bar and (iv) numerical model results used to develop the empirical model tends to over-predict intertidal beach for very dissipative beaches.

5.3.3 Comparison of Duck beach profile variability with Empirical formulation

At Duck beach, the pre–storm and post–storm profiles were also used to calculate shoreline change, berm height, berm crest and berm length from the measured data. From the selected profiles provided in Table 5.3, not all profiles have berm formation therefore only profiles with berm formation were selected. Duck beach is characterised by dynamic inner bars. Most profiles showed more than one inner bar. During the profile selection, the inner bar (seaward) was more prominent than nearshore underwater inner bar(berm). The difference in shoreline positions (shoreline at still water level) between pre- and post-storm profiles was used

to calculate shoreline change for all selected profiles. Ω was calculated from the pre- and post storm profiles of the measured storm data. Shorelinechange from the storm data were compared with the empirical formulation Figure 5.21. The results show that empirical formulation significantly overestimated the shoreline change. This could be attributed to the fact that the numerical simulations used to develop the empirical model have a tendency to erode the beach more when in dissipative states. The presence of the pier could have also influenced the shoreline change by obstructing sediment distribution.

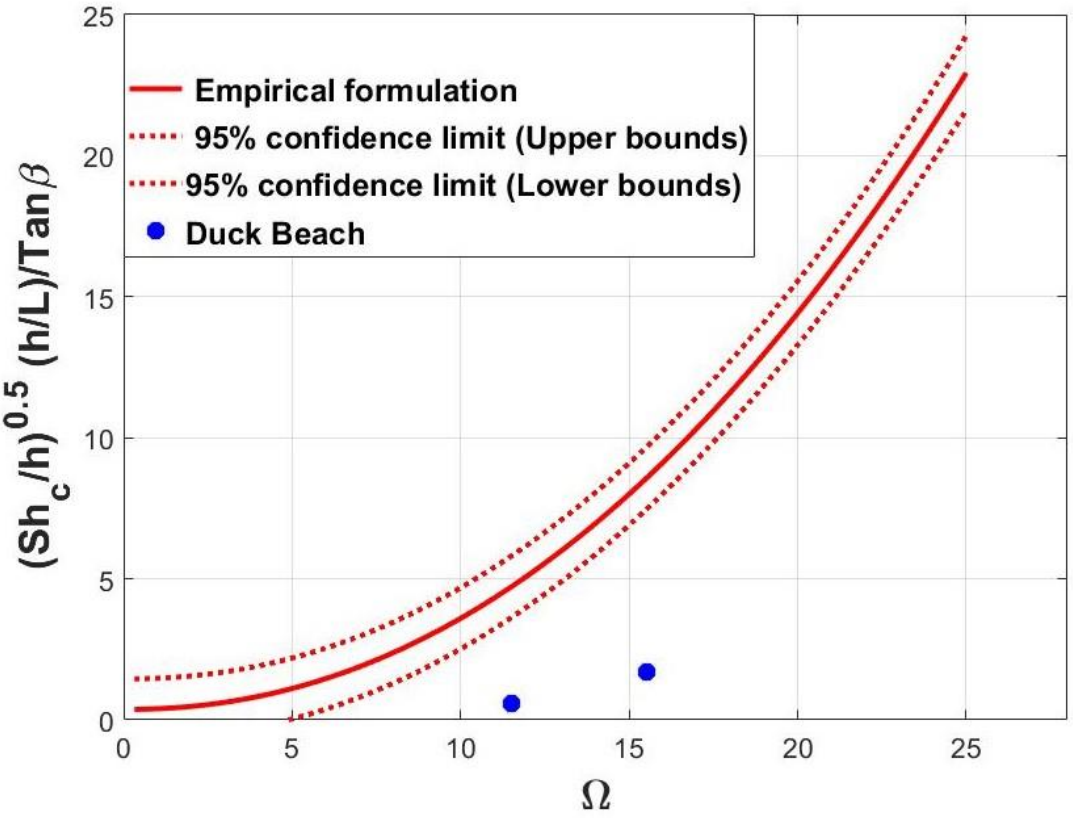

Figure 5.21 Comparison of empirical formulation with shoreline change profiles at Duck Beach

Figure 5.22 presents the comparison between the empirical formulation of berm height at Duck beach. The figure shows that the empirical formulation was not able to capture the berm height development at Duck beach except in some limited cases. This could be because of berm location and the wave energy which can be affected by changes in the water depth at Duck beach. In the empirical formulation berm was formed close to the shoreline position. Ω values calculated were quite dissipative at Duck beach.

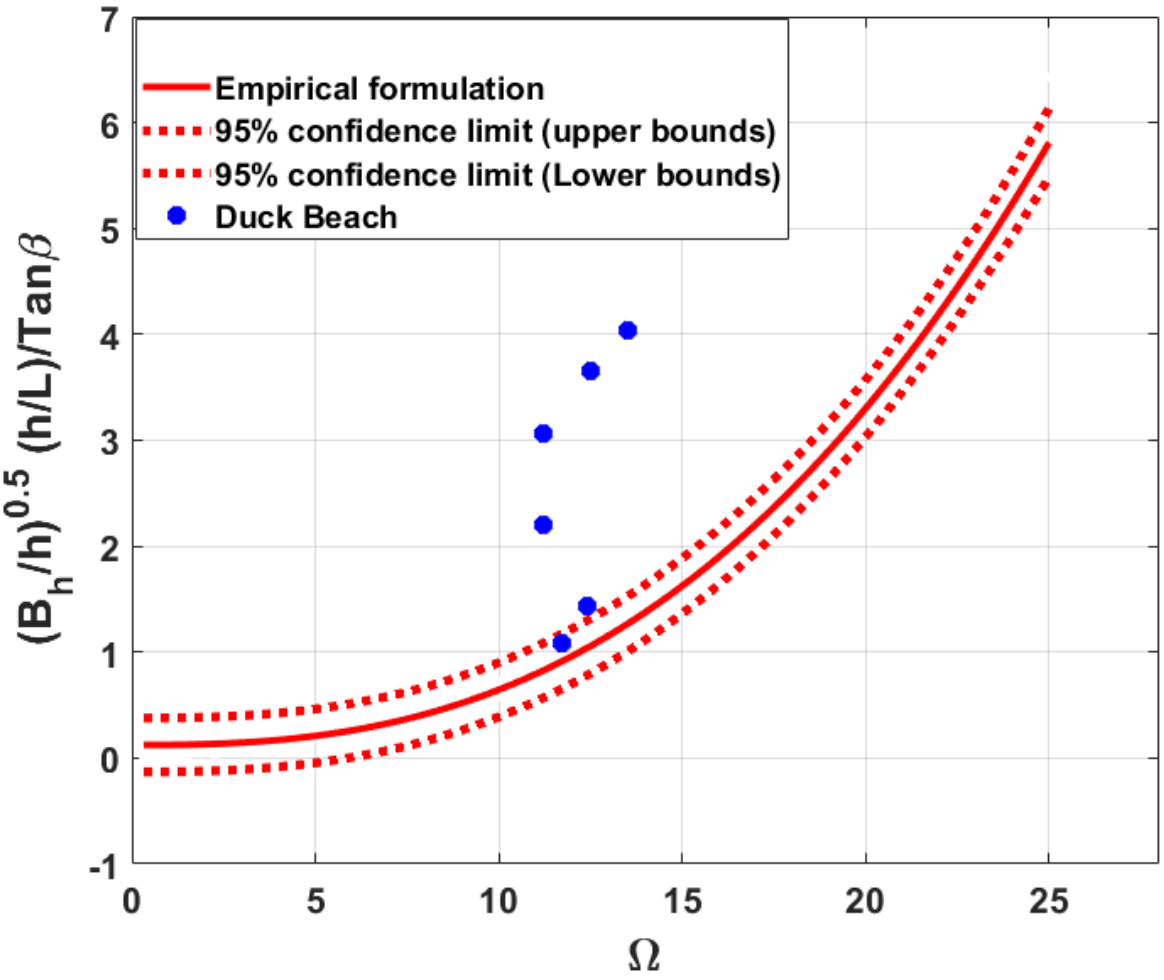

Figure 5.22 Comparison of empirical formulation with berm height at Duck Beach

At Duck beach it was noticed that 5 out of the 8 berm crest parameter values (Figure 5.23) are within the 95% confidence interval, which suggests high accuracy of the model in predicting berm crest height on this beach.

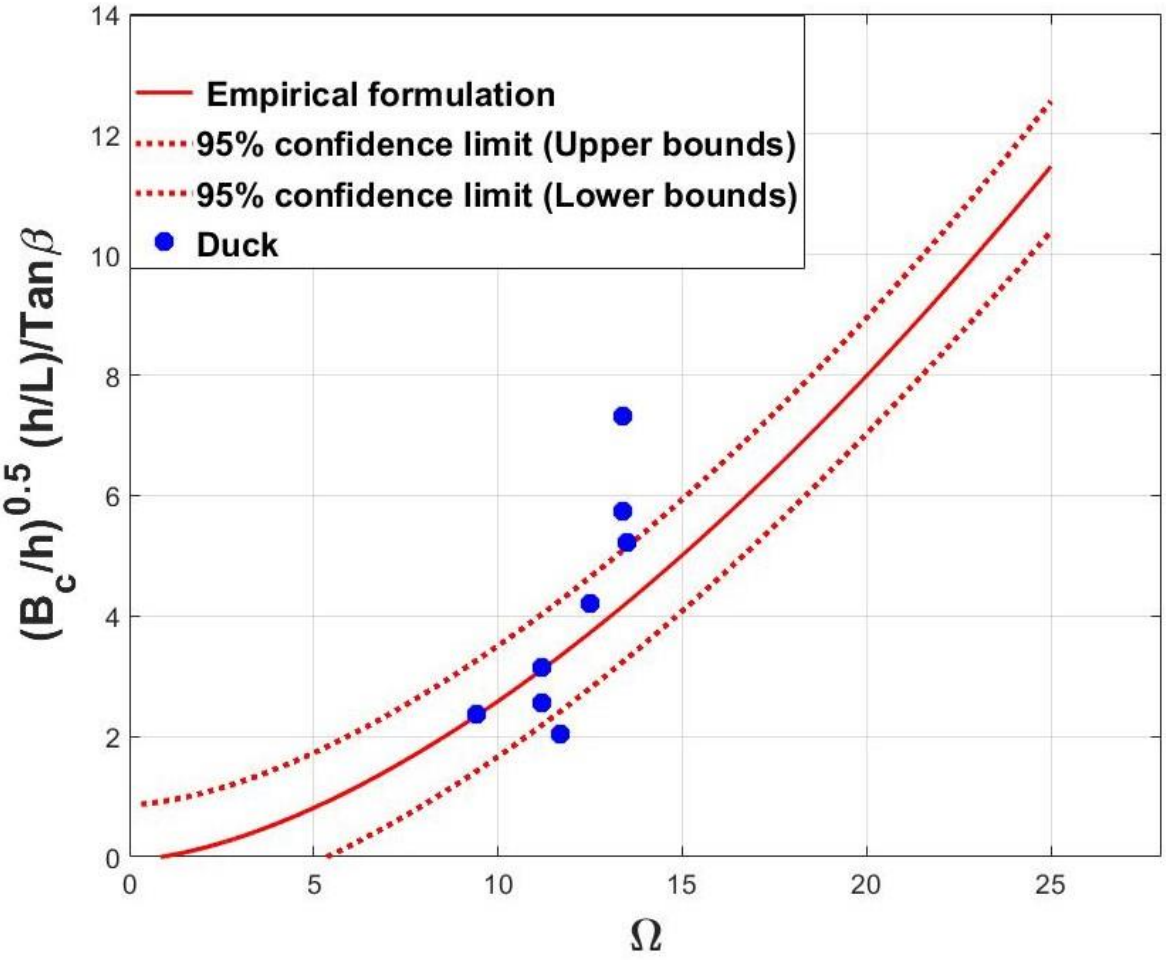

Figure 5.23 Comparison of empirical formulation with berm crest at Duck Beach

The empirical formulation significantly overestimated the berm length at Duck (Figure 5.24). This discrepancy could be because of the dissipative nature of Duck beach, an energetic beach, where the sediment transport rate can be high, and sand bar can be easily transported further offshore. The berm length seems to be changing continuously due to continuous erosion by storm waves. Given that most of the profiles were chosen pre-storm and post-storm, storms could cause the berm to move offshore quite rapidly.

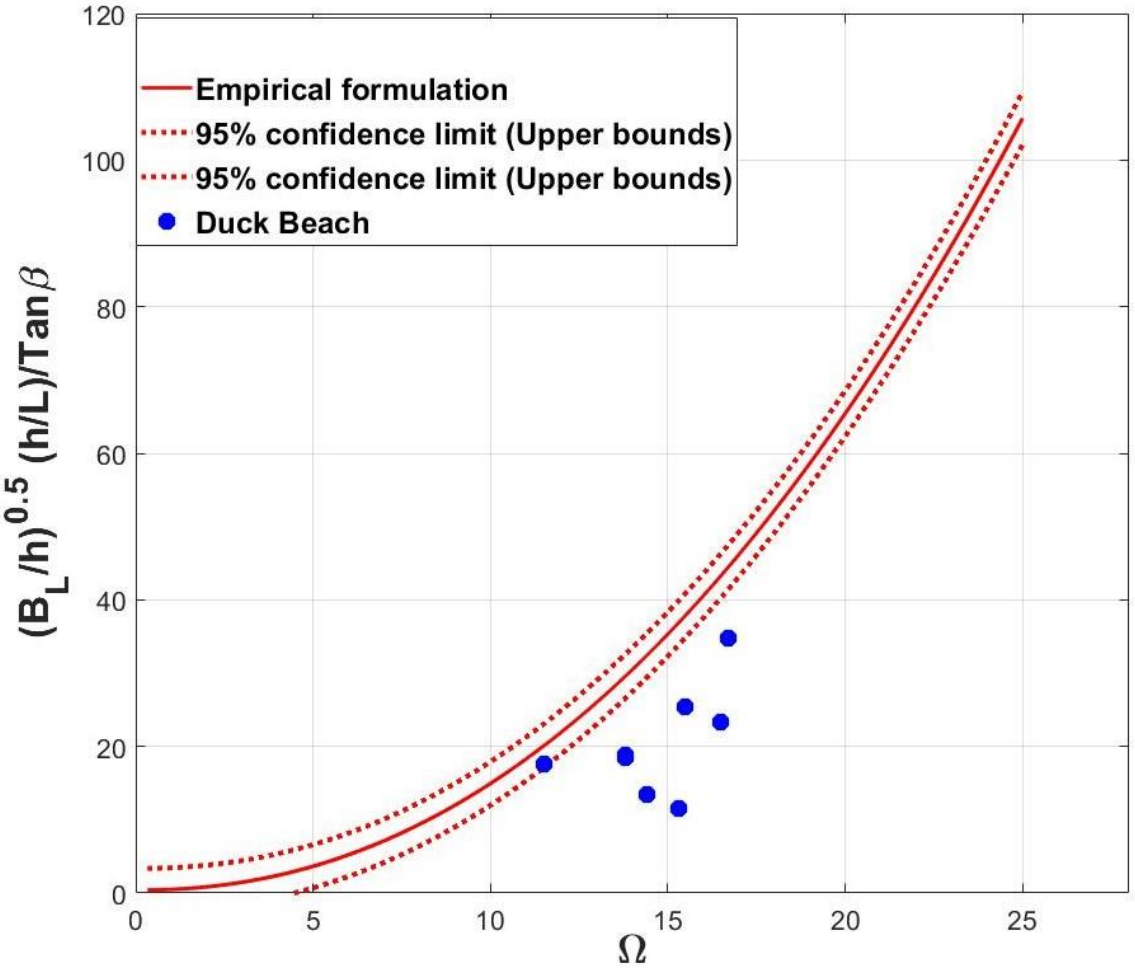

Figure 5.24 Comparison of empirical formulation with berm length profiles at Duck Beach

5.3.4 Comparison of Polidoro experiment with Empirical formulations

For this chapter, the main goal is to validate the empirical formulation of the morphodynamic parameters against measured data for dissipative, intermediate, and reflective beaches. However, pre-storm and post-storm profiles were only available for intermediate and dissipative beaches as in the cases of Narrabeen, Hasaki and Duck beaches. It was challenging to obtain field data of pre-storm and post-storm profiles for reflective beaches. Therefore, to assess the performance of the empirical formulation on reflective beaches, experimental data reported by Polidoro et al., (2018) was used.

Here, the initial profile was used as the pre-storm profile. Except berm crest, a perfect prediction of all the parameters (shoreline change, berm height, berm length) Table 5.6. The berm crest was poorly fitted because the berm height was at the still water level.

Growth and onshore movement of Berm height in Polidoro's experiment is predicted by the model. The amount of berm height growth with the empirical formulation with respect to (Ω) value 0.4 is the same as

experiment data Table 5.6. Berm height in the experiment were calculated from the near shore same as the measured data. Difference in wave height between the empirical formulation (H_s = 0.5 m) and experiment (H_s = 0.3 m). Shoreline change remains in the reflective state with the empirical formulation and is zero. The variability of the berm length and the berm height is of the same order in the experiment with (Ω) 0.9. The comparison as shown in Table 5.6, was assessed using Root mean square error (RMSE).

RMSE is a commonly used accuracy metric for predictive models. It is calculated as the square root of the average squared difference between predicted and observed values. The Equation for RMSE is

$$RMSE = \sqrt{\frac{\sum_{i=1}^{n}(x_i - y_i)2}{n}} \tag{5.2}$$

where

x_i = Observed value

y_i = Predicted value

n = number of data points

For shoreline change the RMSE was calculated using only 3 data points from Polidoro's experiment, and the value obtained was 0.024429. Based on limited data, only the difference was calculated for berm height and berm length. Values obtained for these variables were -0.00088 and 0.719366, respectively.

The value for shoreline change indicates the average difference between the empirical formulation and experiment shoreline change value, based on the limited data. A lower RMSE value suggests that the model is more accurate in predicting shoreline change.

Table 5. 6 Comparison of empirical formulation with Polidoro et al., (2018) experimental data on shoreline change, berm height and berm length on a reflective beach

Parameters	**Ω**	**Polidoro's experiment**	**Empirical formulation**	**Variance**	**RMSE**
$(sh_c/h_o)^{0.5}\ (H_s\ /L_O)\ /Tan\beta$	0.9	0.087039	0.119041	-0.032	0.024429
$(sh_c/h_o)^{0.5}\ (H_s\ /L_O)\ /Tan\beta$	0.8	0.091049	0.096184	-0.00514	0.024429
$(sh_c/h_o)^{0.5}\ (H_s\ /L_O)\ /Tan\beta$	0.7	0.079561	0.106762	-0.0272	0.024429
$(B_h/h_o)^{0.5}\ (H_s\ /L_O)\ /Tan\beta$	0.9	0.12563	0.126515	-0.00088	
$(B_L/h_o)^{0.5}\ (H_s\ /L_O)\ /Tan\beta$	0.9	1.059321	0.339955	0.719366	

5.3.5 Comparison of XBeach model with a profile at Hasaki Beach

Transferring numerical analysis from lab-scale experiments to field applications involves a systematic approach to ensure accuracy and applicability under real-world conditions. The process begins with thorough documentation of lab-scale experiments, capturing key parameters such as wave height, wave period, sediment size, and beach slope. Then, the empirical formulation from this experiment using dimensional analysis based on the Buckingham theorem for real-world application was modified. This guarantees an accurate representation of physical process scaling. Representative field sites and data collected on environmental conditions were used to establish baseline conditions. Small-scale pilot tests are conducted at these sites to validate the numerical analysis, compare predictions with observed data, and refine the formulation as needed. Sensitivity analysis identifies critical variables impacting accuracy. After achieving satisfactory pilot results, the refined formulation is implemented at all field sites, deploying continuous monitoring systems to collect real-time data on beach state variables. This data facilitates ongoing updates and refinements to the

formulation, ensuring reliability over time. Error propagation and uncertainty quantification analyses provide confidence intervals for predictions. The entire process is meticulously documented, ensuring a comprehensive understanding and providing a valuable reference for future research and applications.

To demonstrate the empirical formulation's real-world applicability, data from Hasaki Beach, a dissipative beach, was calibrated, and a profile with one storm in between was calibrated (Hs 2.83, Tp 11.9 s). I chose Hasaki Beach to compare with XBeach because Hasaki Beach profiles are much more complete compared to Narrabeen Beach and Duck Beach, where some profiles are incomplete. The goal was to compare the Hasaki Beach results to the empirical formulation's predictions. Model parameters that produced the best model performance were investigated during the calibration processes. Table 5.7 below, shows the recommended default value and range of the selected parameters for model calibration. The XBeach model was run with varying free parameters until a good agreement is reached between Hasaki measured profile selected for calibration and the XBeach. The wave conditions selected from the Hasaki data to calibrate the model is shown in Table 5.8

Table 5.7 Model parameters and their validity range, with proposed default values

Parameter	**Definition**	**Range**	**Default**
wetslp	Critical wet slope for avalanching	0.1 - 1	0.3
Gamma	Random wave equivalent of the breaker index	0.4 – 0.9	0.55

Table 5.8 Wave cases and conditions selected for calibration

	$\boldsymbol{Hs}\ (\boldsymbol{m})$	$\boldsymbol{Tp}\ (\boldsymbol{s})$
Calibration	2.83	11.9

(A)

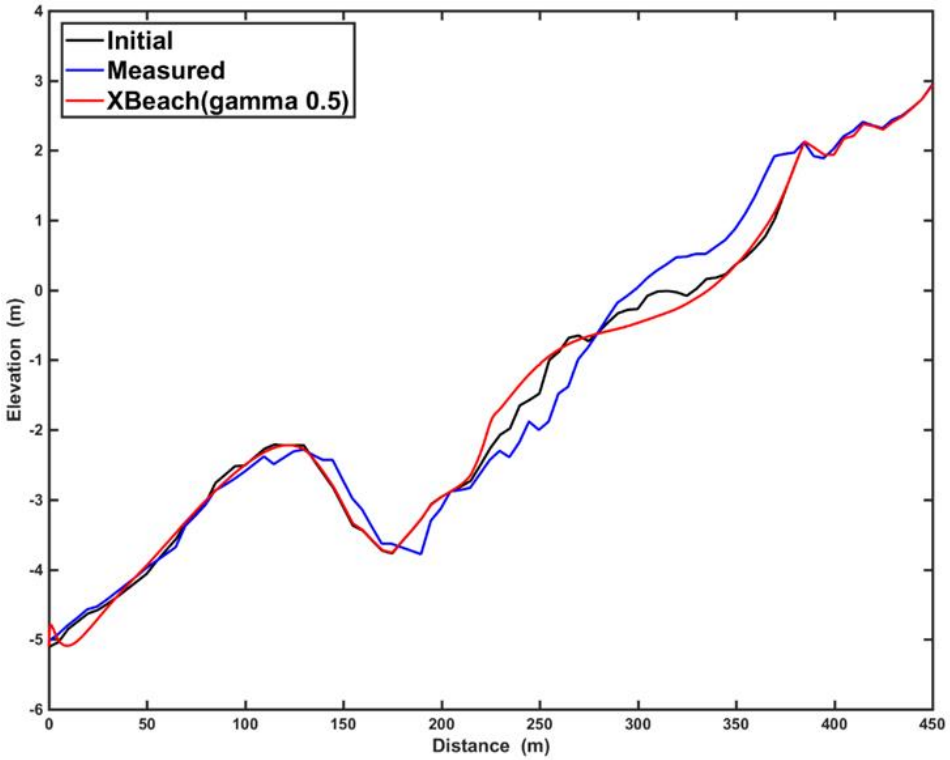
Initial
Measured
XBeach(gamma 0.5)
Elevation (m)
Distance (m)

(B)

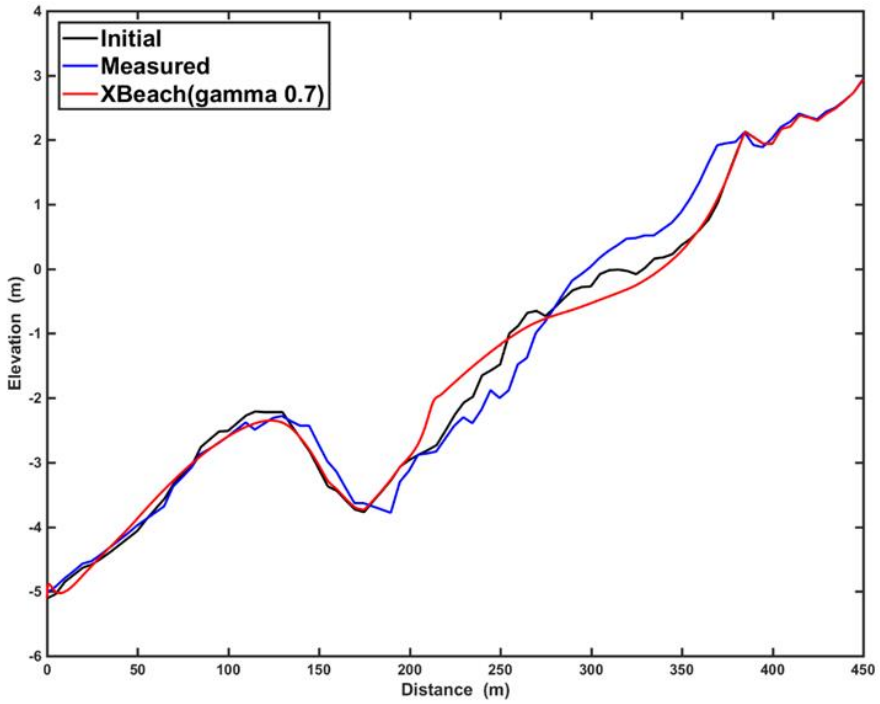
Initial
Measured
XBeach(gamma 0.7)
Elevation (m)
Distance (m)

(C)

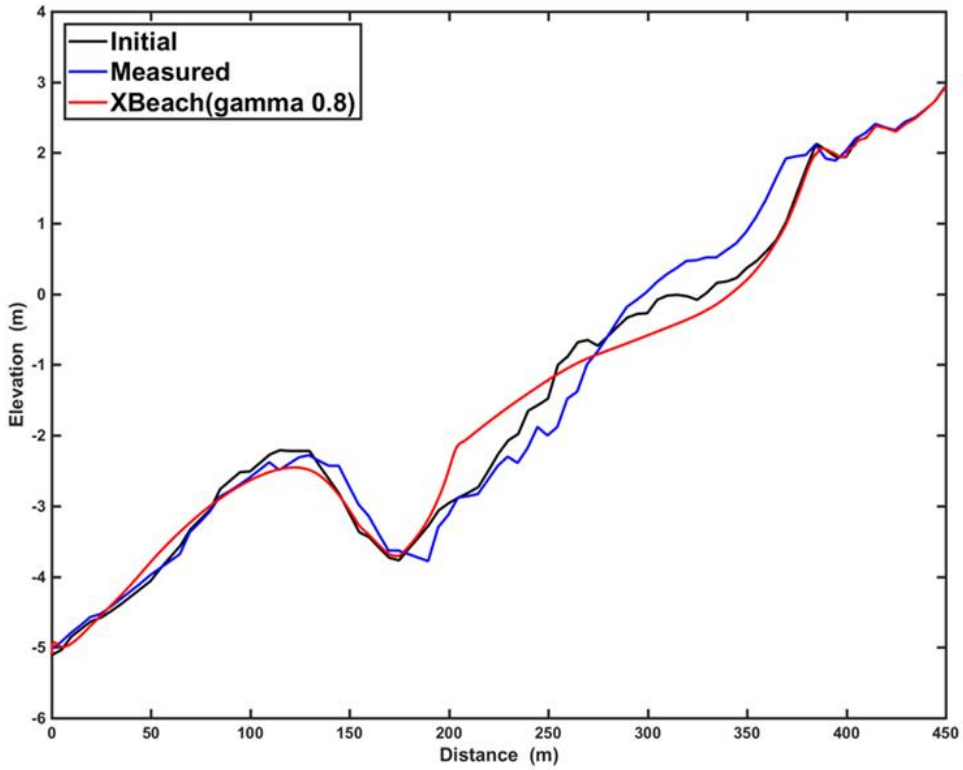

Figure 5.25 Post storm profiles with different gamma parameters (a) gamma 0.5 (b) gamma 0.7 and (c) gamma 0.8 with Hs 2.83 m and Tp 11.9 s

The best model performance was obtained with the following parameter value wetslp = 0.3 and gamma = 0.5. Gamma represents one of the most important parameters in XBeach.

For the validation of the model, a profile with one storm in between was selected. Wave conditions used for validation are shown in Table 5.9

Table 5.9 Wave cases and conditions selected for validation.

	***Hs* (m)**	***Tp* (s)**
Validation	2.77	11.1

The qualitative assessment of the model result along with the measured profile are shown in Figure 5.26. From the figure below, the post storm was not captured well, and the model was unable to reproduce the measured profile perfectly.

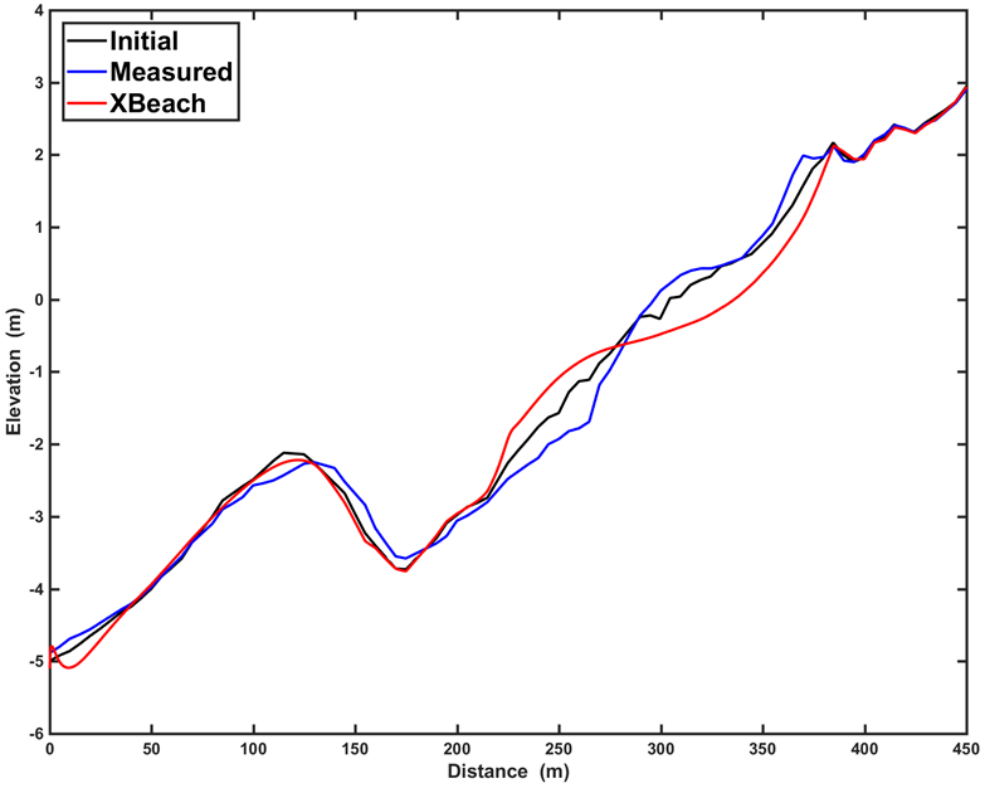

Figure 5.26 Comparison of simulated profile with measured post-storm profile with Hs = 2.77 m and Tp = 11.1 s

The variability and impact of the model performance were evaluated in detail through statistical analysis, revealing important insights into its applicability to real-world conditions. The model's performance was specifically validated using data from Hasaki Beach, where it demonstrated slight validity. This validation was quantified using the Brier Skill Score (BSS), as shown in Equation 3.7. The BSS is a widely accepted metric for assessing the accuracy of predictive models in coastal engineering.

In the case of Hasaki Beach, the model showed reasonable agreement with observed data but tended to overestimate shoreline changes. Notably, the upper berm observed between 350 to 400 meters on the measured profile was not accurately simulated by the model, highlighting a significant limitation. The BSS value for the post-storm profile comparison was 0.4, which falls within the range classified as reasonable according to van Rijn (2003).

This reasonable classification indicates that while the model captures some aspects of beach state variability, it does not fully replicate all observed features, particularly in more complex beach profiles. The successful validation through statistical analysis, despite some overestimations and limitations, underscores the model's general accuracy and reliability in representing the beach state variability of dissipative beaches like Hasaki. However, the overestimation of shoreline changes and the inability to simulate the upper berm suggest that further refinements and adjustments are necessary for improving the model's predictive capability.

To address these limitations, future work could focus on incorporating additional physical processes and finer-scale sediment transport mechanisms into the model. Enhanced data collection methods, such as high-resolution topographic surveys and advanced remote sensing technologies, could provide more detailed inputs and validation data. Moreover, the incorporation of machine learning techniques might help identify and correct systematic biases in the model, leading to more accurate predictions. By continuously refining the model and incorporating feedback from field observations, it is possible to enhance its robustness and applicability to a broader range of beach environments. Such improvements would not only increase the model's predictive accuracy but also provide more reliable tools for coastal management and mitigation strategies in response to dynamic coastal processes.

Limitations of using the empirical formulation

The cross-shore model as presented has several limitations.

- First, the cross-shore profile biased developed only on a single storm accounting only for cross-shore processes is insufficient on most beaches when considering increasing time scales (i.e., toward long timescale) where the relative importance of other processes, such as longshore processes.
- The model predicts beach profile proxies like shoreline change, berm height, berm crest elevation, and berm length, providing insights into beach morphology and coastal dynamics. However, its predictive capacity may be limited for full profile change due to complex factors like wave conditions, sediment transport processes, tidal variations, and coastal geomorphology.
- The empirical formulation is based on specific conditions and parameters, demonstrating its efficacy and reliability. However, its applicability may be limited when extrapolated to scenarios beyond those considered. Factors like input parameters, environmental factors, and system dynamics could affect accuracy and predictive capability. Future research should focus on expanding the model's applicability to diverse scenarios.
- Finally, as an empirical model, the model provides a developed coastline based on empirical relationships drawn from observed data but does not produce a dynamic representation of shoreline dynamics. Understanding this distinction is critical for efficiently using the model's findings and recognizing its limitations in portraying the dynamic character of coastal settings.

5.4 Conclusion

Using measured field data from three beaches (Narrabeen Beach Australia, Hasaki Beach, Japan and Duck Beach, USA), and one experiment done by Polidoro, the performance of the empirical formulations of four key beach parameters (shoreline change, berm height, berm crest, berm width) were validated. Three steps were followed to validate the empirical formulation. First, suitable pre- and post-storm profiles were selected, and the mean profile slope was calculated, which was used as the pre-storm. Secondly, four beach parameters above were determined. The results were compared with the empirical formulations of the four parameters.

Specifically, the empirical formulation is able to satisfactorily capture the beach profile change at the intermediate Narrabeen beach measured data. In reflective beaches the results indicate that the empirical formulation can be accurately predict berm height, berm length and shoreline change at 95% confidence interval. On the Intermediate beach the results show that the formulation on the average value can predict 70% on berm height ,90% on berm crest, berm length 90% and shoreline change 60% For dissipative beach, results show that empirical formulation is not able capture the beach change satisfactorily, except in a few limited cases.

Figure 5.27 to Figure 5.30 show a summary of all validation cases. The results show that empirical models work better for intermediate and reflective beaches but overestimates all quantities in highly dissipative beaches. One important fact should be noted here. In the data used for the development of the empirical model, the pre-storm profile was always taken as a plane beach where is in the data used for validation, the pre-storm profile was the actual profile shape before the storm. This may be one important issue on very dissipative beaches where the pre-storm profile can significantly deviate from a plain beach shape hence contributing to the discrepancies between empirical model and measures values. This also highlights the importance of antecedent beach profile shape on beach change during storms.

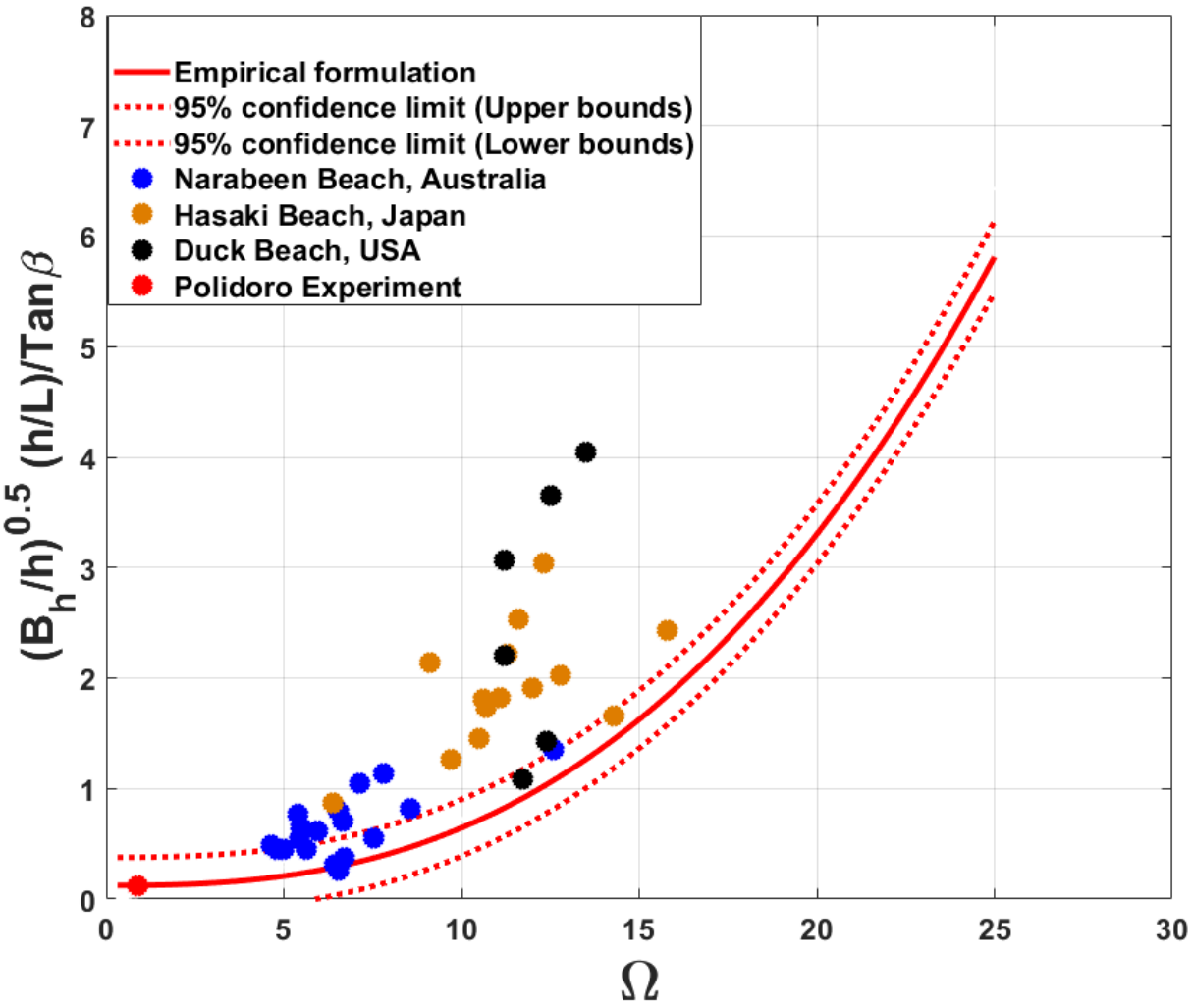

Figure 5.27Presentation of analysed data sets and empirical formulation with respect to Berm height

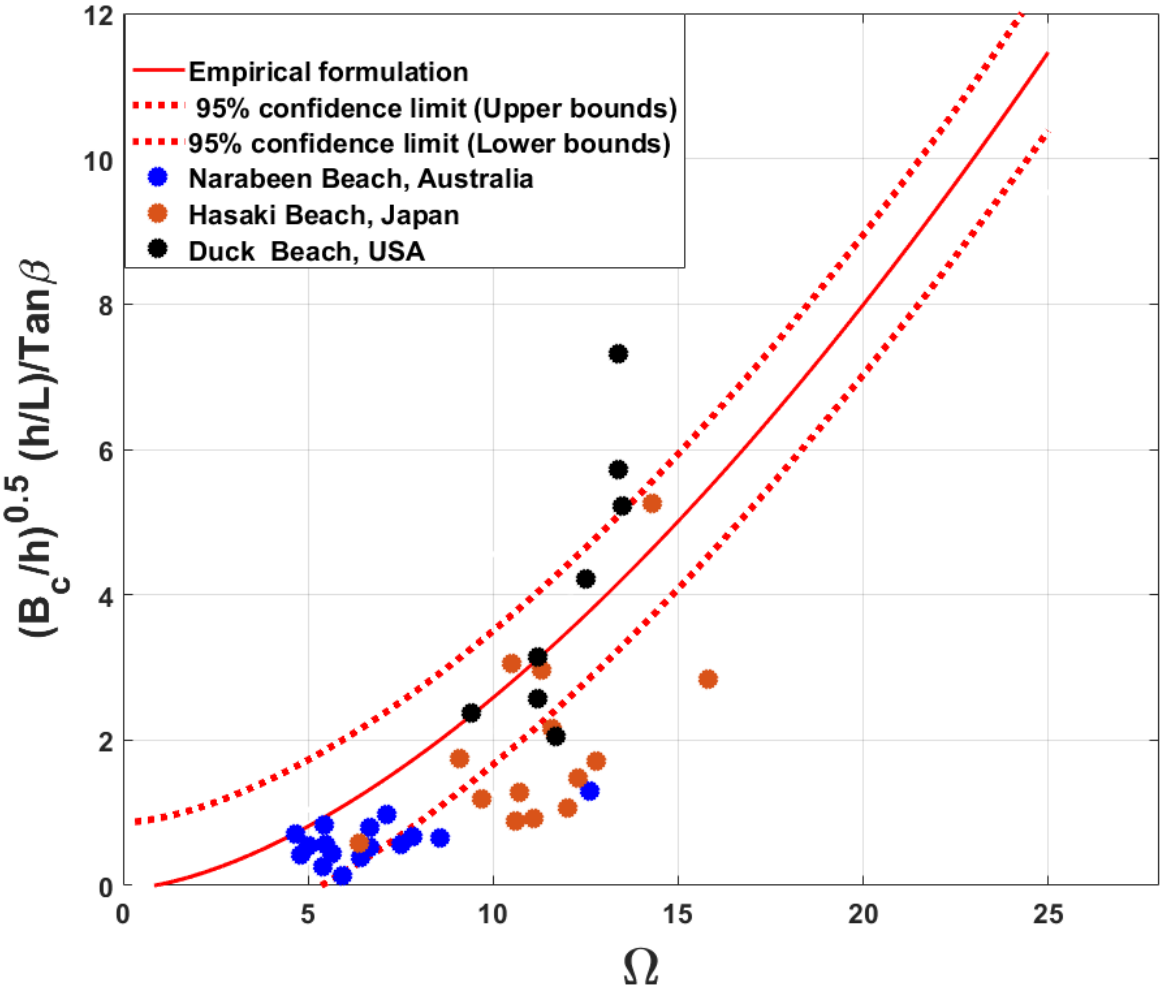

Figure 5.28 Presentation of analysed data sets and empirical formulation with respect to Berm Crest

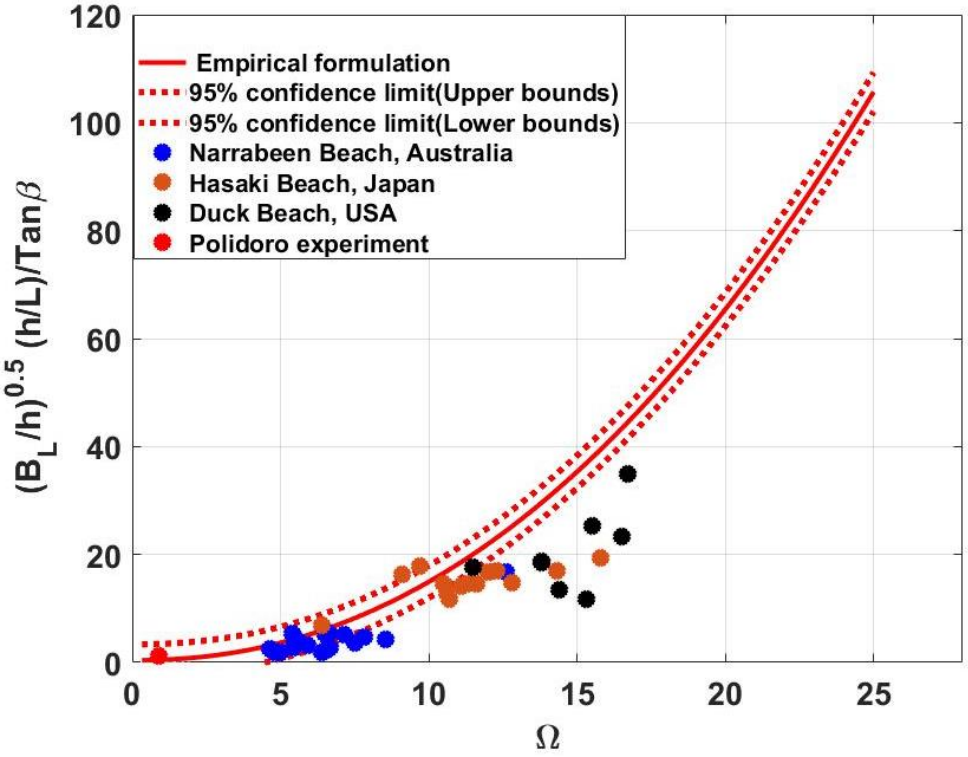

Figure 5.29 Presentation of analysed data sets and empirical formulation with respect to Berm length

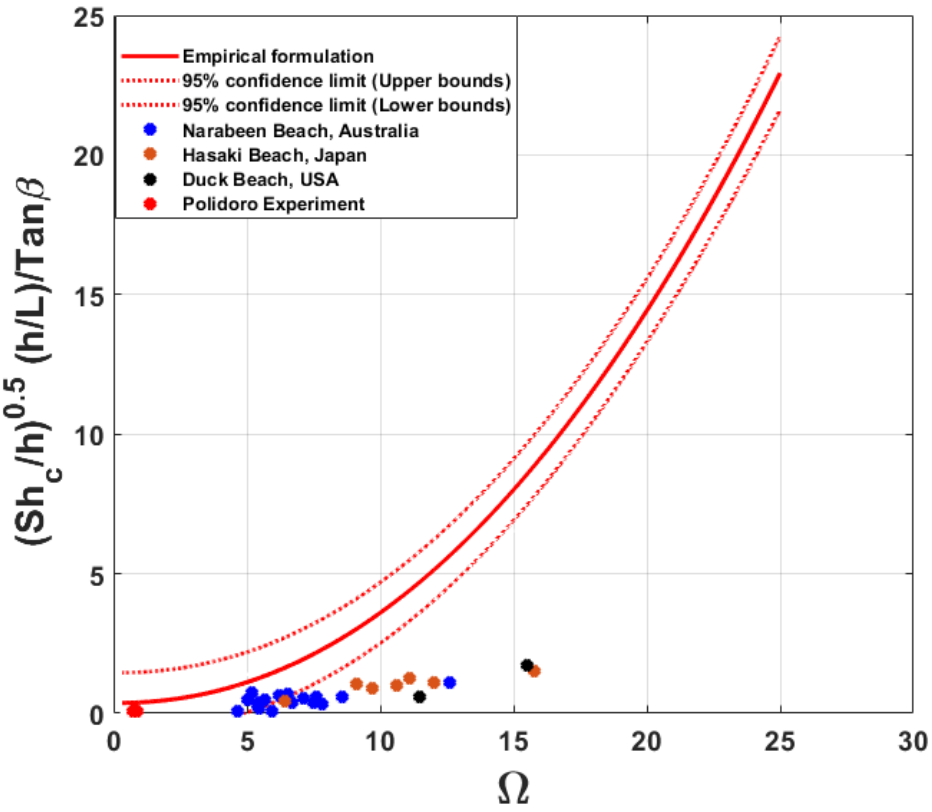

Figure 5.30 Presentation of analysed data sets and empirical formulation with respect to shoreline change

Chapter 6: Conclusion and Future Research

6.1 Conclusion

The main aim of this study is to develop a new empirical beach state model that can recognise beach state variability due to varying wave climates without the need to use computationally expensive process-based models. This study revealed how the beach states evolve over different physical parameters that drive the beach processes. The process-based morphodynamic XBeach numerical model was calibrated and validated using a life-scale laboratory beach profile measurement. This numerical model was then used to create a database from which an empirical beach model was developed.

After validation of the empirical model, an equilibrium profile was generated by simulating various beach conditions, and this equilibrium beach profile was subsequently used as the initial beach profile to analyse the response of different storm events to the three beach states. In this work, the initial beach profile was needed because it needed to be adjusted to a long-term balance between incoming and outgoing sediments due to the changing wave conditions. Furthermore, an equilibrium profile would allow for the assessment of the impact of severe coastal events such as a storm. Besides, understanding the dynamics of beach profiles could contribute to maintaining a stable and aesthetically acceptable beach profile which is critical for tourism and recreation. Initial beach profile is critical for adapting coastal areas to rising sea levels and changing climate patterns, as well as designing methods to reduce climate change's impact on erosion and flooding.

The present research has led to novel insights on different beach states. These insights involved various aspects, some of which are the morphodynamic changes of beaches with different slopes and the sediment characteristics from a large number of incident wave conditions. Different scenarios have been verified based on Dean’s parameter (Ω) which relates to beach profile changes, characteristics and is compared with the empirical formulation.

This study not only introduces a novel empirical model, but also increases our understanding of beach morphodynamics, slope-related changes, and sediment properties under various wave circumstances. These findings have important implications for coastal management and decision-making. This model can help design early warning systems for coastal hazards, which is a critical step towards making communities more robust to coastal risks. By putting together real-time data and predictions, the model can help figure out how the beach might change in the future. This helps people get ready for and deal with impending dangers like storms and high tides. By simulating several scenarios, the model can determine which places are vulnerable to erosion or flooding. The model predicts the evolution of beach conditions over time, which helps

policymakers make long-term land-use decisions that consider changes in coastal conditions. However, the main conclusions are presented as follows.

6.2 Response of different beach states to a large number of storm conditions

Different hydrodynamic and morphological scenarios were modelled in response to different beach states. Storm waves were identified from incident wave conditions at different Ω values which are linked to beach states; dissipative, intermediate, and reflective beach states.

In this study, the beaches which were initially planner (pre-storm profile) evolved to form different shapes and points. Several beach features were observed as the Ω value changes i.e., subtidal berm formation, upper beach changes, etc., but shoreline remained unchanged with the three beach states. Furthermore, it was evident that the intermediate beach state produces a steeper mean profile that promotes beach face accretion as sediment is transported onshore to form upper berm forcing the upper berm to distinctly build. This is a typical beach profile reconstruction by fair weather waves following erosion by a strong storm. The result further showed that the beaches in dissipative states with high Ω value led to beach-faced erosion and those in the reflective states with low Ω value were erosive as well as having no backshore beach. The erosion on the reflective beach state resulted from the calibrated numerical model used. The main idea of these results was to obtain a relationship between Ω value and beach response. All the simulated results responded well with different beach states. One key observation was that, for a given wave height, a large Ω value corresponded to smaller wave period.

6.3 Validation using the synthetic beach profile change.

From the numerical results, when wave height increases, the Ω value increases and when Ω value increases the beach tends to move from reflective state to intermediate state and to dissipative state. Different features of the beach were observed, but particular focus was put on describing the response of the nearshore underwater berm formation and shoreline change. Features of the beach were related to Dean's parameter by looking at the berm height (B_h), berm crest (B_c), berm length (B_L), and shoreline change (sh_c). The selected parameters were non-dimensionalised to compare with the Ω value, a good non-dimensional equation was developed based on the empirical formulation. This was validated on different beach states for different parameters and a good trendline with goodness-of-fit of 0.8 for different parameters as measured R^2 and the trendline can serve as a predictor for a given Ω value.

6.4 Validating the empirical formulation against different water level

Numerical simulations were performed using static hypothetical Low Water Levels (LWL) of -0.15 m and -0.25 m, and High Water Levels (HWL) of +0.15 m and +0.25 m on a 1:20 beach slope and numerous incident wave conditions. MWL was used as the reference point. ±0.15 m water level variation corresponds to microtidal variations in the real world, with tidal range of less than 2 m in full scale while ±0.25 m water level corresponds to meso and macrotidal beaches.

The results were obtained from shoreline change, berm length and berm height but did not incorporate berm crest due to the changing water level. The results from different water levels show that (sh_c) is negligible which highlights unique relationship between the beach state and shoreline change. The Percentage difference between HWL and MWL was calculated to be 5.2% and 5.2%, respectively. (B_h) % difference was calculated between HWL and MWL and was determined to be 3.7% for ±0.15 m and 5.2% ±0.25 m. (B_L), % difference determined between HWL and MWL were 2.8% and 6.6% respectively.

From the results, the % difference is small for water level ±0.15 emphasizing that the empirical formulation can be satisfactory used for micro/meso tidal beaches. Although these empirical formulations provide a simple, cost-effective method of determining beach state variability, without having to run expensive and time consuming and costly numerical models, they can be satisfactorily used to determine beach profile shape for both micro and meso tidal beaches under all beach states. On macro-tidal beaches also, the parameters show only less than 10% deviation from the MSL.

6.5 Validating the empirical formulations against beach state change at field sites under different characteristics.

The empirical formulations were validated against beach profile measurements from three sites around the world, and an experiment which are distinctly different in terms of beach characteristics and incident wave conditions.

The results of empirical formulations of the four parameters satisfactorily captured the beach profile change at the intermediate beach state when compared with the field measurements. Furthermore, the results reflective beach states indicate that the empirical formulation can accurately predict (B_h), (B_L), and (sh_c), at a confidence interval of 95%.

On intermediate beaches, the results show that the formulation can predict approximately (B_c) and (B_L) by about 90% (B_h) by 70% and (Sh_c) by 60%. For dissipative beaches, the empirical formulation was not able to capture the beach changes satisfactorily, except in a few limited cases. It can be concluded that the empirical model works better for intermediate and reflective beaches but overestimates all quantities in highly

dissipative beach states. Then implementation of the new empirical formulation in real-world situations provides shoreline managers with a realistic, cost-effective, and user-friendly tool for monitoring and addressing changes in beach conditions. This enhances the development of adaptable, well-informed, and environmentally sustainable strategies for managing coastal areas.

6.6 Recommendation for Further studies

Having extensively studied beach state variability in this study, it is essential to suggest the following for further research:

1. Using the empirical formulation on other beach types such as gravel or mixed sand and gravel beaches this will allow comparison for different beaches.
2. Adopt and implement the empirical model on other parameters rather than the four used in this study to authenticate its efficiency.
3. Application of this model should emphasise on the study of upper berm formation. The empirical model was robustly and successfully implemented to assess the dynamics of underwater berms. It would significantly contribute to scientific methodology if it could evaluate the changes in the upper beach such as the profile length, berm crest or elevation.
4. Further research could build on this work to explore other aspects of beach state variability and improve the accuracy of the empirical formulation by testing the model in several areas with different data sets.

References

Aagaard, T., Greenwood, B., & Hughes, M. (2013). Sediment transport on dissipative, intermediate, and reflective beaches. Earth-Science Reviews, 124, 32-50.

Aagaard, T., Nielsen, J., & Greenwood, B. (1998). Suspended sediment transport and nearshore bar formation on a shallow intermediate-state beach. Marine Geology, 148(3-4), 203-225.

Alsina, J. M., Baldock, T. E., Hughes, M. G., Weir, F., & Sierra, J. P. (2007). Sediment transport numerical modelling in the swash zone. In Coastal Dynamics 2005: State of the Practice (pp. 1-14).

Alsina, J. M., Van der Zanden, J., Caceres, I., & Ribberink, J. S. (2018). The influence of wave groups and wave-swash interactions on sediment transport and bed evolution in the swash zone. Coastal engineering, 140, 23-42.

Altomare, C., Laucelli, D. B., Mase, H., & Gironella, X. (2020). Determination of semi-empirical models for mean wave overtopping using an evolutionary polynomial paradigm. Journal of Marine Science and Engineering, 8(8), 570.

and Predictive Models: University of Tokyo Press, Tokyo.

Angnuureng, D. B., Almar, R., Senechal, N., Castelle, B., Addo, K. A., Marieu, V., & Ranasinghe, R. (2017). Shoreline resilience to individual storms and storm clusters on a meso-macrotidal barred beach. Geomorphology, 290, 265-276.

Ashton, A. D., & Murray, A. B. (2006). High-angle wave instability and emergent shoreline shapes: 1. Modeling of sand waves, flying spits, and capes. Journal of Geophysical Research: Earth Surface, 111(F4).

Ashton, A., Murray, A. B., & Arnoult, O. (2001). Formation of coastline features by large-scale instabilities induced by high-angle waves. Nature, 414(6861), 296-300.

Babanin, A. (2011). Breaking and dissipation of ocean surface waves. Cambridge University Press.

Bagnold, R. A. (1954). Experiments on a gravity-free dispersion of large solid spheres in a Newtonian fluid under shear. Proceedings of the Royal Society of London. Series A. Mathematical and Physical Sciences, 225(1160), 49-63.

Baldock, T. E., & Hughes, M. G. (2006). Field observations of instantaneous water slopes and horizontal pressure gradients in the swash-zone. Continental Shelf Research, 26(5), 574-588.

Banno, M., Nakamura, S., Kosako, T., Nakagawa, Y., Yanagishima, S. I., & Kuriyama, Y. (2020). Long-term observations of beach variability at Hasaki, Japan. Journal of Marine Science and Engineering, 8(11), 871.

Barbier, E. B., Hacker, S. D., Kennedy, C., Koch, E. W., Stier, A. C., & Silliman, B. R. (2011). The value of estuarine and coastal ecosystem services. Ecological monographs, 81(2), 169-193.

Bascom, W. N. (1951). The relationship between sand size and beach-face slope. Eos, Transactions American Geophysical Union, 32(6), 866-874.

Battjes, J. A. (1974). Surf similarity. In Coastal Engineering 1974 (pp. 466-480).

Battjes, J. A., & Janssen, J. P. F. M. (1978). Energy loss and set-up due to breaking of random waves. In Coastal engineering 1978 (pp. 569-587).

Beck, M. W. (2014). Coasts at risk: an assessment of coastal risks and the role of environmental solutions. A joint publication of United Nations University-Institute for Environment and Human Security (UNU-EHS), The Nature Conservancy (TNC) and the Coastal Resources Center (CRC) at the University of Rhode Island Graduate School of Oceanography, 80.

Beuzen, T., Harley, M. D., Splinter, K. D., & Turner, I. L. (2019). Controls of variability in berm and dune storm erosion. Journal of Geophysical Research: Earth Surface, 124(11), 2647-2665.

Bird, E. C. (1985). Coastline changes. A global review.

Bird, E. C. F. (1983). Factors influencing beach erosion and accretion: a global review. In Sandy Beaches as Ecosystems: Based on the Proceedings of the First International Symposium on Sandy Beaches, held in Port Elizabeth, South Africa, 17–21 January 1983 (pp. 709-717). Dordrecht: Springer Netherlands.

Bird, E. D. F. (1976). Coasts. Australian National University.

Birkemeier, W. A. (1985). Time scales of nearshore profile changes. In Coastal Engineering 1984 (pp. 1507-1521).

Birkemeier, W. A., & Holland, K. T. (2000). The US Army Corps of Engineers Field Research Facility: More than Two Decades of Coastal Research.

Boak, E. H., & Turner, I. L. (2005). Shoreline definition and detection: a review. Journal of coastal research, 21(4), 688-703.

Bodge, K. R. (1989). A literature review of the distribution of longshore sediment transport across the surf zone. Journal of Coastal Research, 307-328.

Bodge, K. R. (1992). Representing equilibrium beach profiles with an exponential expression. Journal of coastal research, 47-55.

Borribunnangkun, K., & Suzuki, T. (2019). Statistical analysis of undertow on a barred beach. Journal of Japan Society of Civil Engineers, Ser. B3 (Ocean Engineering), 75(2), I_707-I_712.

Bosboom, J., & Stive, M. J. (2015). Coastal dynamics 1, 0.5 edn. VSSD, Delft.

Bosboom, J., & Stive, M. J. (2021). Coastal dynamics.

Brocchini, M., & Baldock, T. E. (2008). Recent advances in modeling swash zone dynamics: Influence of surf-swash interaction on nearshore hydrodynamics and morphodynamics. Reviews of Geophysics, 46(3).

Bruun, P. (1954). Coast erosion and the development of beach profiles (Vol. 44). US Beach Erosion Board.

Butt, T., & Russell, P. (1999). Suspended sediment transport mechanisms in high-energy swash. Marine Geology, 161(2-4), 361-375.

Carter, R. W. G. (2013). Coastal environments: an introduction to the physical, ecological, and cultural systems of coastlines. Elsevier.

Castelle, B., & Harley, M. (2020). Extreme events: impact and recovery. In Sandy beach morphodynamics (pp. 533-556). Elsevier.

Castelle, B., Marieu, V., Bujan, S., Splinter, K. D., Robinet, A., Sénéchal, N., & Ferreira, S. (2015). Impact of the winter 2013–2014 series of severe Western Europe storms on a double-barred sandy coast: Beach and dune erosion and megacusp embayments. Geomorphology, 238, 135-148.

Castelle, B., Masselink, G., Scott, T., Stokes, C., Konstantinou, A., Marieu, V., & Bujan, S. (2021). Satellite-derived shoreline detection at a high-energy meso-macrotidal beach. Geomorphology, 383, 107707.

Chen, C., Bu, J., Zhang, Y., Zhuang, Y., Chu, Y., Hu, J., & Guo, B. (2019). The application of the tasseled cap transformation and feature knowledge for the extraction of coastline information from remote sensing images. Advances in Space Research, 64(9), 1780-1791.

Chen, C., Liang, J., Xie, F., Hu, Z., Sun, W., Yang, G., ... & Zhang, Z. (2022). Temporal and spatial variation of coastline using remote sensing images for Zhoushan archipelago, China. International Journal of Applied Earth Observation and Geoinformation, 107, 102711.

Chowdhury, P., & Behera, M. R. (2017). Effect of long-term wave climate variability on longshore sediment transport along regional coastlines. Progress in Oceanography, 156, 145-153.

Clark, D. B., Feddersen, F., & Guza, R. T. (2010). Cross-shore surfzone tracer dispersion in an alongshore current. Journal of Geophysical Research: Oceans, 115(C10).

Coasts at Risk: An Assessment of Coastal Risks and the Role of Environmental Solutions. (n.d.). https://www.conservationgateway.org/ConservationPractices/Marine/crr/library/Pages/coastsatrisk.

Cohn, N., Ruggiero, P., de Vries, S., & García-Medina, G. (2017, June). Beach growth driven by intertidal sandbar welding. In Proceedings of coastal dynamics (Vol. 1, No. 99, pp. 12-16).

Crowell, M., Leatherman, S. P., & Buckley, M. K. (1991). Historical shoreline change: error analysis and mapping accuracy. Journal of coastal research, 839-852.

Cuddington, K., Fortin, M. J., Gerber, L. R., Hastings, A., Liebhold, A., O'connor, M., & Ray, C. (2013). Process-based models are required to manage ecological systems in a changing world. Ecosphere, 4(2), 1-12.

da Silva, P. G., Coco, G., Garnier, R., & Klein, A. H. (2020). On the prediction of runup, setup and swash on beaches. Earth-Science Reviews, 204, 103148.

Dalrymple, R. A., & Kirby, J. T. (1988). Models for very wide-angle water waves and wave diffraction. Journal of Fluid Mechanics, 192, 33-50.

Daly, C., Roelvink, D., van Dongeren, A., de Vries, J. V. T., & McCall, R. (2012). Validation of an advective-deterministic approach to short wave breaking in a surf-beat model. Coastal Engineering, 60, 69-83.

Dastgheib, A., Martinez, C., Udo, K., & Ranasinghe, R. (2022). Climate change driven shoreline change at Hasaki Beach Japan: A novel application of the Probabilistic Coastline Recession (PCR) model. Coastal Engineering, 172, 104079.

Davidson, M. A., Splinter, K. D., & Turner, I. L. (2013). A simple equilibrium model for predicting shoreline change. Coastal Engineering, 73, 191-202.

Davidson-Arnott, R., Bauer, B., & Houser, C. (2019). Introduction to coastal processes and geomorphology. Cambridge university press.

de Ridder, M. P., Smit, P. B., van Dongeren, A. R., McCall, R. T., Nederhoff, K., & Reniers, A. J. (2021). Efficient two-layer non-hydrostatic wave model with accurate dispersive behaviour. Coastal Engineering, 164, 103808.

de Vriend, H. J. (1997). Evolution of marine morphodynamic modelling: Time for 3-D?. Ocean Dynamics, 49(2), 331-341.

de Vriend, H. J., Zyserman, J., Nicholson, J., Roelvink, J. A., Pechon, P., & Southgate, H. N. (1993). Medium-term 2DH coastal area modelling. Coastal engineering, 21(1-3), 193-224.

Dean, R. G. (1973, January). Heuristic models of sand transport in the surf zone. In First Australian Conference on Coastal Engineering, 1973: Engineering Dynamics of the Coastal Zone (pp. 215-221). Sydney, NSW: Institution of Engineers, Australia.

Dean, R. G. (1977). Equilibrium beach profiles: US Atlantic and Gulf coasts.

Dean, R. G. (1991). Equilibrium beach profiles: characteristics and applications. Journal of coastal research, 53-84.

Dean, R. G., & Dalrymple, R. A. (2004). Coastal processes with engineering applications. Cambridge University Press

Di Leonardo, D., & Ruggiero, P. (2015). Regional scale sandbar variability: Observations from the US Pacific Northwest. Continental Shelf Research, 95, 74-88.

Dissanayake, P., Brown, J., & Karunarathna, H. (2014). Modelling storm-induced beach/dune evolution: Sefton coast, Liverpool Bay, UK. Marine Geology, 357, 225-242.

Dissanayake, P., Yates, M. L., Suanez, S., Floc'h, F., & Krämer, K. (2021). Climate change impacts on coastal wave dynamics at Vougot Beach, France. Journal of Marine Science and Engineering, 9(9), 1009.

Dolan, R. O. B. E. R. T., Hayden, B. P., May, P., & May, S. (1980). The reliability of shoreline change measurements from aerial photographs. Shore and beach, 48(4), 22-29.

Dolan, R., & Davis, R. E. (1994). Coastal storm hazards. Journal of Coastal Research, 103-114.

Doornkamp, J. C., & King, C. A. (1971). Numerical analysis in geomorphology: an introduction. (No Title).

Dubarbier, B., Castelle, B., Ruessink, G., & Marieu, V. (2017). Mechanisms controlling the complete accretionary beach state sequence. Geophysical Research Letters, 44(11), 5645-5654.

Dunkin, L. M. (2010). Variability in Long-Wave Runup as a Function of Nearshore Bathymetric Features (No. DOE TEES 64644-1). Texas A & M Univ., College Station, TX (United States). Texas A & M Engineering Experiment Station.

Dyke, P. P. (2007). Modeling coastal and offshore processes. Imperial College Press.

Eichentopf, S., Karunarathna, H., & Alsina, J. M. (2019). Morphodynamics of sandy beaches under the influence of storm sequences: Current research status and future needs. Water Science and Engineering, 12(3), 221-234.

Einstein, H. A. (1950). The bed-load function for sediment transportation in open channel flows (No. 1026). US Department of Agriculture.

Elsayed, S. M., & Oumeraci, H. (2017). Effect of beach slope and grain-stabilization on coastal sediment transport: An attempt to overcome the erosion overestimation by XBeach. Coastal Engineering, 121, 179-196.

Elsayed, S. M., Gijsman, R., Schlurmann, T., & Goseberg, N. (2022). Nonhydrostatic numerical modeling of fixed and mobile barred beaches: Limitations of depth-averaged wave resolving models around sandbars. Journal of waterway, port, coastal, and ocean engineering, 148(1), 04021045.

Ercanlı, Ç., Savaşır, G., & Tokuç, A. (2021). Climate Change Adaptation in Coastal Cities. In Encyclopedia of Sustainable Management (pp. 1-6). Cham: Springer International Publishing.

Falqués, A., Ribas, F., Mujal-Colilles, A., & Puig-Polo, C. (2021). A New Morphodynamic Instability Associated with Cross-Shore Transport in the Nearshore. Geophysical Research Letters, 48(13), e2020GL091722.

Fang, F. (2021). Numerical and data-driven modelling in coastal, hydrological and hydraulic engineering. Water, 13(4), 509.

Fernandez Luque, R., & Van Beek, R. (1976). Erosion and transport of bed-load sediment. Journal of hydraulic research, 14(2), 127-144.

Fredsoe, J., & Deigaard, R. (1992). Mechanics of coastal sediment transport (Vol. 3). World scientific publishing company.

Galappatti, G., & Vreugdenhil, C. B. (1985). A depth-integrated model for suspended sediment transport. Journal of Hydraulic Research, 23(4), 359-377.

Galappatti, R. (1983). A depth integrated model for suspended transport. Communications on hydraulics, 1983-07.

Gallagher, E. L., Elgar, S., & Guza, R. T. (1998). Observations of sand bar evolution on a natural beach. Journal of Geophysical Research: Oceans, 103(C2), 3203-3215.

Galvin Jr, C. J. (1968). Breaker type classification on three laboratory beaches. Journal of geophysical research, 73(12), 3651-3659.

Gillie, R. D. (1997). Causes of coastal erosion in Pacific island nations. Journal of Coastal Research, 173-204.

Goldstein, E. B., Coco, G., & Plant, N. G. (2019). A review of machine learning applications to coastal sediment transport and morphodynamics. Earth-science reviews, 194, 97-108.

Gonçalves, S. C., & Ferreira, S. M. (Eds.). (2022). Sandy Beaches as Endangered Ecosystems: Environmental Problems, Possible Assessment and Management Solutions. CRC Press.

Gourlay, M. R. (1992). Wave set-up, wave run-up and beach water table: Interaction between surf zone hydraulics and groundwater hydraulics. Coastal engineering, 17(1-2), 93-144.

Gourlay, M. R., & Meulen, T. (1968). Beach and dune erosion tests (I). M0935.

Grasso, F., Michallet, H., Barthélemy, E., & Certain, R. (2009). Physical modeling of intermediate cross-shore beach morphology: Transients and equilibrium states. Journal of Geophysical Research: Oceans, 114(C9).

Haller, M. C., Honegger, D., & Catalan, P. A. (2014). Rip current observations via marine radar. Journal of waterway, port, coastal, and ocean engineering, 140(2), 115-124.

Hallermeier, R. J. (1980). A profile zonation for seasonal sand beaches from wave climate. Coastal engineering, 4, 253-277.

Hanson, H., & Kraus, N. C. (1989). GENESIS: Generalized model for simulating shoreline change, Report 1 technical reference. US Army Corps of Engineers Waterways Experiment Station.

Hanson, H., & Lindh, G. (1993). Coastal erosion: An escalating environmental threat. Ambio, 188-195.

Harley, M. D., Turner, I. L., Kinsela, M. A., Middleton, J. H., Mumford, P. J., Splinter, K. D., ... & Short, A. D. (2017). Extreme coastal erosion enhanced by anomalous extratropical storm wave direction. Scientific reports, 7(1), 6033.

Harley, M. D., Turner, I. L., Short, A. D., & Ranasinghe, R. (2011). A reevaluation of coastal embayment rotation: The dominance of cross-shore versus alongshore sediment transport processes, Collaroy-Narrabeen Beach, southeast Australia. Journal of Geophysical Research: Earth Surface, 116(F4).

Harley, M. D., Valentini, A., Armaroli, C., Perini, L., Calabrese, L., & Ciavola, P. (2016). Can an early-warning system help minimize the impacts of coastal storms? A case study of the 2012 Halloween storm, northern Italy. Natural Hazards and Earth System Sciences, 16(1), 209-222.

Hasselmann, K., Barnett, T. P., Bouws, E., Carlson, H., Cartwright, D. E., Enke, K., ... & Walden, H. (1973). Measurements of wind-wave growth and swell decay during the Joint North Sea Wave Project (JONSWAP). Ergaenzungsheft zur Deutschen Hydrographischen Zeitschrift, Reihe A.

Hoefel, F., & Elgar, S. (2003). Wave-induced sediment transport and sandbar migration. Science, 299(5614), 1885-1887.

Holman, R. A., & Mason, C. (2020). The Field Research Facility Research Tower. Journal of Coastal Research, 137-140.

Holthuijsen, L. H. (2010). Waves in oceanic and coastal waters. Cambridge university press.

Holthuijsen, L. H., Booij, N., & Herbers, T. H. C. (1989). A prediction model for stationary, short-crested waves in shallow water with ambient currents. Coastal engineering, 13(1), 23-54.

Hoque, M. A., Asano, T., & Neshaei, M. A. L. (2002). Effect of reflective structures on undertow distribution. In Ocean Wave Measurement and Analysis (2001) (pp. 1042-1051).

Horikawa, K. (1988). Nearshore Dynamics and Coastal Processes: Theory. Measurement,

Horn, D. P., & Mason, T. (1994). Swash zone sediment transport modes. Marine geology, 120(3-4), 309-325.

Horrillo-Caraballo, J. M., & Reeve, D. E. (2010). An investigation of the performance of a data-driven model on sand and shingle beaches. Marine Geology, 274(1-4), 120-134.

Horrillo-Caraballo, J. M., Karunarathna, H., Pan, S. Q., & Reeve, D. (2016). Performance of a data-driven technique applied to changes in wave height and its effect on beach response. Water Science and Engineering, 9(1), 42-51.

Inman, D. L., Elwany, M. H. S., & Jenkins, S. A. (1993). Shorerise and bar-berm profiles on ocean beaches. Journal of Geophysical Research: Oceans, 98(C10), 18181-18199.

Itzkin, M., Moore, L. J., Ruggiero, P., Hovenga, P. A., & Hacker, S. D. (2022). Combining process-based and data-driven approaches to forecast beach and dune change. Environmental Modelling & Software, 153, 105404.

Jackson, D. W., Short, A. D., Loureiro, C., & Cooper, J. A. G. (2022). Beach morphodynamic classification using high-resolution nearshore bathymetry and process-based wave modelling. Estuarine, Coastal and Shelf Science, 268, 107812.

Jackson, D., & Short, A. (Eds.). (2020). Sandy beach morphodynamics. Elsevier.

Jin, H., Do, K., Chang, S., & Kim, I. H. (2020). Field observation of morphological response to storm waves and sensitivity analysis of XBeach model at beach and crescentic bar. Journal of Korean Society of Coastal and Ocean Engineers, 32(6), 446-457.

Jin, H., Do, K., Shin, S., & Cox, D. (2021). Process-Based model prediction of coastal dune erosion through parametric calibration. Journal of Marine Science and Engineering, 9(6), 635.

Kaczmarek, L. M., Ostrowski, R., Pruszak, Z., & Rozynski, G. (2005). Selected problems of sediment transport and morphodynamics of a multi-bar nearshore zone. Estuarine, Coastal and Shelf Science, 62(3), 415-425.

Kamphuis, J. W. (2020). Introduction to coastal engineering and management (Vol. 48). World Scientific.

Karunarathna, H., & Reeve, D. E. (2013). A hybrid approach to model shoreline change at multiple timescales. Continental Shelf Research, 66, 29-35.

Karunarathna, H., Horrillo-Caraballo, J. M., Ranasinghe, R., Short, A. D., & Reeve, D. E. (2012). An analysis of the cross-shore beach morphodynamics of a sandy and a composite gravel beach. Marine Geology, 299, 33-42.

Karunarathna, H., Horrillo-Caraballo, J., Kuriyama, Y., Mase, H., Ranasinghe, R., & Reeve, D. E. (2016). Linkages between sediment composition, wave climate and beach profile variability at multiple timescales. Marine Geology, 381, 194-208.

Karunarathna, H., Pender, D., Ranasinghe, R., Short, A. D., & Reeve, D. E. (2014). The effects of storm clustering on beach profile variability. Marine geology, 348, 103-112.

Kato, K., & Udo, K. (2020). CROSS-SHORE MODEL APPLICATION TO HASAKI BEACH, JAPAN: EVALUATION OF PARAMETER SETTING. Coastal Engineering Proceedings, (36v), 23-23.

Katoh, K. (1995). Changes of sand grain distribution in the surf zone. Proc. Coastal Dynamics' 99, Am. Soc. of Eng., New York, 410, 335-364.

Kim, H., Hall, K., Jin, J. Y., Park, G. S., & Lee, J. (2014). Empirical estimation of beach-face slope and its use for warning of berm erosion. Journal of Measurements in Engineering, 2(1), 29-42.

Kim, J. H., Lee, J., Cheong, T. J., Kim, R. H., Koh, D. C., Ryu, J. S., & Chang, H. W. (2005). Use of time series analysis for the identification of tidal effect on groundwater in the coastal area of Kimje, Korea. Journal of Hydrology, 300(1-4), 188-198.

Kobayashi, N. (2016). Coastal sediment transport modeling for engineering applications. Journal of Waterway, Port, Coastal, and Ocean Engineering, 142(6), 03116001.

Komar, P. D. (1998). The 1997-98 El Niño and erosion on the Oregon coast. Shore & Beach, 66(3), 33-41.

Komar, P. D. (2018). Beach processes and erosion—an introduction. Handbook of coastal processes and erosion, 1-20.

Komar, P. D., & McDougal, W. G. (1994). The analysis of exponential beach profiles. Journal of Coastal Research, 59-69.

Kömürcü, M. İ., Özölçer, İ. H., Yüksek, Ö., & Karasu, S. (2007). Determination of bar parameters caused by cross-shore sediment movement. Ocean engineering, 34(5-6), 685-695.

Kraus, N. C., Larson, M., & Kriebel, D. L. (1991, June). Evaluation of beach erosion and accretion predictors. In Coastal sediments (pp. 572-587). ASCE.

Kriebel, D. L., & Dean, R. G. (1993). Convolution method for time-dependent beach-profile response. Journal of Waterway, Port, Coastal, and Ocean Engineering, 119(2), 204-226.

Kroon, A., & Masselink, G. (2002). Morphodynamics of intertidal bar morphology on a macrotidal beach under low-energy wave conditions, North Lincolnshire, England. Marine geology, 190(3-4), 591-608.

Kuriyama, Y. (2002). Medium-term bar behavior and associated sediment transport at Hasaki, Japan. Journal of Geophysical Research: Oceans, 107(C9), 15-1.

Kuriyama, Y., Ito, Y., & Yanagishima, S. (2008). Medium-term variations of bar properties and their linkages with environmental factors at Hasaki, Japan. Marine Geology, 248(1-2), 1-10.

Kuroiwa, M., Matsubara, Y., Kuchiishi, T., Kate, K., & Noda, H. (2002, May). Prediction of Undertow and Beach Profile Change Over Barred Beach. In ISOPE International Ocean and Polar Engineering Conference (pp. ISOPE-I). ISOPE.

Kuroiwa, M., Noda, H., Son, C. B., Katoh, K., & Taniguchi, S. (2001). Numerical prediction of bottom topographical change around coastal structures using quasi-3D nearshore current model. In Coastal Engineering 2000 (pp. 2914-2927).

Larson, M., & Kraus, N. C. (1993). Dynamics of longshore bars. In Coastal Engineering 1992 (pp. 2219-2232).

Larson, M., Erikson, L., & Hanson, H. (2004). An analytical model to predict dune erosion due to wave impact. Coastal Engineering, 51(8-9), 675-696.

Larson, M., Kraus, N. C., & Department of the army. US Army corps of engineers. (1989). SBEACH: Numerical model for simulating storm-induced beach change. Report 1, Empirical foundation, and model development.

Lashley, C. H., Roelvink, D., van Dongeren, A., Buckley, M. L., & Lowe, R. J. (2018). Nonhydrostatic and surfbeat model predictions of extreme wave run-up in fringing reef environments. Coastal Engineering, 137, 11-27.

Le Cozannet, G., Bulteau, T., Castelle, B., Ranasinghe, R., Wöppelmann, G., Rohmer, J., ... & Salas-y-Mélia, D. (2019). Quantifying uncertainties of sandy shoreline change projections as sea level rises. Scientific reports, 9(1), 42.

Lee, G. H., Nicholls, R. J., & Birkemeier, W. A. (1998). Storm-driven variability of the beach-nearshore profile at Duck, North Carolina, USA, 1981–1991. Marine geology, 148(3-4), 163-177.

Lerma, A. N., Castelle, B., Marieu, V., Robinet, A., Bulteau, T., Bernon, N., & Mallet, C. (2022). Decadal beach-dune profile monitoring along a 230-km high-energy sandy coast: Aquitaine, southwest France. Applied Geography, 139, 102645.

Lesser, G. R., Roelvink, J. V., van Kester, J. T. M., & Stelling, G. S. (2004). Development and validation of a three-dimensional morphological model. Coastal engineering, 51(8-9), 883-915.

Lippmann, T. C., & Holman, R. A. (1989). Quantification of sand bar morphology: A video technique based on wave dissipation. Journal of Geophysical Research: Oceans, 94(C1), 995-1011.

Lippmann, T. C., & Holman, R. A. (1990). The spatial and temporal variability of sand bar morphology. Journal of Geophysical Research: Oceans, 95(C7), 11575-11590.

Liu, J., Liu, N., Zhang, Y., Qu, Z., & Yu, J. (2019). Evaluation of the non-use value of beach tourism resources: A case study of Qingdao coastal scenic area, China. Ocean & coastal management, 168, 63-71.

Longuet-Higgins, M. S. (1970). Longshore currents generated by obliquely incident sea waves: 1. Journal of geophysical research, 75(33), 6778-6789.

Lord, D., & Kulmar, M. (2001). The 1974 storms revisited: 25 years experience in ocean wave measurement along the south-east Australian coast. In Coastal Engineering 2000 (pp. 559-572).

Luijendijk, A., Hagenaars, G., Ranasinghe, R., Baart, F., Donchyts, G., & Aarninkhof, S. (2018). The state of the world's beaches. Scientific reports, 8(1), 6641.

Luque, R. F., & van Beek, R. (1974). The Effect of Shallow-Water Waves on the Stability and Bearing Capacity of Sea Beds. Society of Petroleum Engineers Journal, 14(04), 330-336.

MALEK, M. A., SUZUKI, T., HIGA, H., & NAKAMURA, Y. (2020). Analyze the Coastal Storm Impulse (COSI) Parameter and Beach Erosion at Hasaki Coast, Japan. Journal of Japan Society of Civil Engineers, Ser. B3 (Ocean Engineering), 76(2), I_1061-I_1066.

Martínez, M. L., Intralawan, A., Vázquez, G., Pérez-Maqueo, O., Sutton, P., & Landgrave, R. (2007). The coasts of our world: Ecological, economic, and social importance. Ecological economics, 63(2-3), 254-272.

Masselink, G., & Hughes, M. G. (2003). Introduction to Coastal Geomorphology and Processes. Arnold: London, UK, 354.

Masselink, G., & Kroon, A. (2009). Morphology and morphodynamics of sandy beaches. Coastal Zones and Estuaries. Encyclopedia of Life Support Systems, 221-243.

Masselink, G., & Short, A. D. (1993). The effect of tide range on beach morphodynamics and morphology: a conceptual beach model. Journal of coastal research, 785-800.

Masselink, G., Hughes, M., & Knight, J. (2014). Introduction to coastal processes and geomorphology. Routledge.

Masselink, G., Scott, T., Poate, T., Russell, P., Davidson, M., & Conley, D. (2016). The extreme 2013/2014 winter storms: hydrodynamic forcing and coastal response along the southwest coast of England. Earth Surface Processes and Landforms, 41(3), 378-391.

Matias, A., Masselink, G., Castelle, B., Blenkinsopp, C. E., & Kroon, A. (2016). Measurements of morphodynamic and hydrodynamic overwash processes in a large-scale wave flume. Coastal Engineering, 113, 33-46.

McCall, R. T., De Vries, J. V. T., Plant, N. G., Van Dongeren, A. R., Roelvink, J. A., Thompson, D. M., & Reniers, A. J. H. M. (2010). Two-dimensional time dependent hurricane overwash and erosion modeling at Santa Rosa Island. Coastal Engineering, 57(7), 668-683.

McCall, R. T., Masselink, G., Poate, T. G., Roelvink, J. A., Almeida, L. P., Davidson, M., & Russell, P. E. (2014). Modelling storm hydrodynamics on gravel beaches with XBeach-G. Coastal Engineering, 91, 231-250.

McLachlan, A., & Defeo, O. (2017). The ecology of sandy shores. Academic press.

Mentaschi, L., Vousdoukas, M. I., Pekel, J. F., Voukouvalas, E., & Feyen, L. (2018). Global long-term observations of coastal erosion and accretion. Scientific reports, 8(1), 12876.

Miller, H. C. (1999). Field measurements of longshore sediment transport during storms. Coastal engineering, 36(4), 301-321.

Miller, J. K., & Dean, R. G. (2004). A simple new shoreline change model. Coastal Engineering, 51(7), 531-556.

Moore, L. J. (2000). Shoreline mapping techniques. Journal of coastal research, 111-124.

Morton, R. A., Paine, J. G., & Gibeaut, J. C. (1994). Stages and durations of post-storm beach recovery, southeastern Texas coast, USA. Journal of Coastal Research, 884-908.

Mouradi, R. S., Goeury, C., Thual, O., Zaoui, F., & Tassi, P. (2020). A Predictive Data-Driven Approach Based on Reduced Order Models for the Morphodynamic Study of a Coastal Water Intake. In Advances in Hydroinformatics: SimHydro 2019-Models for Extreme Situations and Crisis Management (pp. 849-866). Springer Singapore.

Muller, M. C., Roelvink, D., Luijendijk, A., de Vries, S., & de Vries, J. V. T. (2011). Process-based modeling of coastal dune development. Coastal Engineering Proceedings, (33), 33-33.

Murray, A. B. (2007). Reducing model complexity for explanation and prediction. Geomorphology, 90(3-4), 178-191.

Nederhoff, C. M., Lodder, Q. J., Boers, M., Den Bieman, J. P., & Miller, J. K. (2015). Modeling the effects of hard structures on dune erosion and overwash: A case study of the impact of Hurricane Sandy on the New Jersey coast. In The Proceedings of the Coastal Sediments 2015.

Nguyen, H. D., Hamma, W., Stan, M. I., TRAN, V. T., AŞTEFĂNOAIEI, R., BUI, Q. T., ... & IANOŞ, I. (2020). IMPACTS OF URBANIZATION AND TOURISM ON THE EROSION AND ACCRETION OF EUROPEAN, ASIAN, AND AFRICAN COASTAL AREAS AND POSSIBLE SOLUTIONS. Urbanism. Architecture. Constructions/Urbanism. Arhitectura. Constructii, 11(2).

Nicholls, R. J., Wong, P. P., Burkett, V., Codignotto, J., Hay, J., McLean, R., ... & Saito, Y. (2007). Coastal systems and low-lying areas.

Nicholson, J., Broker, I., Roelvink, J. A., Price, D., Tanguy, J. M., & Moreno, L. (1997). Intercomparison of coastal area morphodynamic models. Coastal Engineering, 31(1-4), 97-123.

Nielsen, P. (2009). Coastal and estuarine processes (Vol. 29). World Scientific Publishing Company.

Omstedt, A. (2011). Guide to process-based modeling of lakes and coastal seas. Berlin: Springer.

Palmsten, M. L., & Holman, R. A. (2012). Laboratory investigation of dune erosion using stereo video. Coastal engineering, 60, 123-135.

Palmsten, M. L., & Splinter, K. D. (2016). Observations and simulations of wave runup during a laboratory dune erosion experiment. Coastal Engineering, 115, 58-66.

Paskoff, R. (1983). L'érosion des plages. Penn ar Bed (Brest), (114), 131-144.

Passeri, D. L., Hagen, S. C., Medeiros, S. C., Bilskie, M. V., Alizad, K., & Wang, D. (2015). The dynamic effects of sea level rise on low-gradient coastal landscapes: A review. Earth's Future, 3(6), 159-181.

Peach, L., da Silva, G. V., Cartwright, N., & Strauss, D. (2023). A comparison of process-based and data-driven techniques for downscaling offshore wave forecasts to the nearshore. Ocean Modelling, 182, 102168.

Pedrozo-Acuña, A., Simmonds, D. J., Chadwick, A. J., & Silva, R. (2007). A numerical–empirical approach for evaluating morphodynamic processes on gravel and mixed sand–gravel beaches. Marine Geology, 241(1-4), 1-18.

Pender, D., & Karunarathna, H. (2013). A statistical-process based approach for modelling beach profile variability. Coastal Engineering, 81, 19-29.

Phillips, M. S., Blenkinsopp, C. E., Splinter, K. D., Harley, M. D., & Turner, I. L. (2019). Modes of berm and beach face recovery following storm reset: Observations using a continuously scanning lidar. Journal of Geophysical Research: Earth Surface, 124(3), 720-736.

Pierson Jr, W. J. (1955). Wind generated gravity waves. In Advances in geophysics (Vol. 2, pp. 93-178). Elsevier.

Plant, N. G., & Holman, R. A. (1999). Extracting morphologic information from field data. In Coastal Engineering 1998 (pp. 2773-2784).

Plant, N. G., Aarninkhof, S. G., Turner, I. L., & Kingston, K. S. (2007). The performance of shoreline detection models applied to video imagery. Journal of Coastal Research, 23(3), 658-670.

Plant, N. G., Freilich, M. H., & Holman, R. A. (2001). Role of morphologic feedback in surf zone sandbar response. Journal of geophysical research: Oceans, 106(C1), 973-989.

Poelhekke, L., Jäger, W. S., Van Dongeren, A., Plomaritis, T. A., McCall, R., & Ferreira, Ó. (2016). Predicting coastal hazards for sandy coasts with a Bayesian Network. Coastal Engineering, 118, 21-34.

Polidoro, A. (2019). The effect of grain size distribution and bimodal sea states on coarse beach sediment dynamics. Open University (United Kingdom).

Polidoro, A., Pullen, T., Eade, J., Mason, T., Blanco, B., & Wyncoll, D. (2018, December). Gravel beach profile response allowing for bimodal sea states. In Proceedings of the Institution of Civil Engineers-Maritime Engineering (Vol. 171, No. 4, pp. 145-166). Thomas Telford Ltd.

Pritchard, D., & Hogg, A. J. (2005). On the transport of suspended sediment by a swash event on a plane beach. Coastal Engineering, 52(1), 1-23.

Pruszak, Z. (1993). The analysis of beach profile changes using Dean's method and empirical orthogonal functions. Coastal Engineering, 19(3-4), 245-261.

Puleo, J. A., Beach, R. A., Holman, R. A., & Allen, J. S. (2000). Swash zone sediment suspension and transport and the importance of bore-generated turbulence. Journal of Geophysical Research: Oceans, 105(C7), 17021-17044.

Ranasinghe, R., & Stive, M. J. (2009). Rising seas and retreating coastlines. Climatic change, 97, 465-468.

Ranasinghe, R., Holman, R., de Schipper, M., Lippmann, T., Wehof, J., Duong, T. M., ... & Stive, M. (2012). Quantifying nearshore morphological recovery time scales using argus video imaging: Palm Beach, Sydney and Duck, North Carolina. Coastal Engineering, 2012, 1-7.

Ranasinghe, R., McLoughlin, R., Short, A., & Symonds, G. (2004). The Southern Oscillation Index, wave climate, and beach rotation. Marine Geology, 204(3-4), 273-287.

Reeve, D. E., Karunarathna, H., Pan, S., Horrillo-Caraballo, J. M., Różyński, G., & Ranasinghe, R. (2016). Data-driven and hybrid coastal morphological prediction methods for mesoscale forecasting. Geomorphology, 256, 49-67.

Reeve, D., Chadwick, A., & Fleming, C. (2018). Coastal engineering: processes, theory, and design practice. Crc Press.

Reichstein, M., Camps-Valls, G., Stevens, B., Jung, M., Denzler, J., Carvalhais, N., & Prabhat, F. (2019). Deep learning and process understanding for data-driven Earth system science. Nature, 566(7743), 195-204.

Reis, A. H., & Gama, C. (2010). Sand size versus beachfaceslope—an explanation based on the constructal law. Geomorphology, 114(3), 276-283.

Rienecker, M. M., & Fenton, J. D. (1981). A Fourier approximation method for steady water waves. Journal of fluid mechanics, 104, 119-137.

Robertson, B., Hall, K., Zytner, R., & Nistor, I. (2013). Breaking waves: Review of characteristic relationships. Coastal Engineering Journal, 55(01), 1350002.

Roelvink, D. (2011). A guide to modeling coastal morphology (Vol. 12). world scientific.

Roelvink, D., & Costas, S. (2019). Coupling nearshore and aeolian processes: XBeach and duna process-based models. Environmental Modelling & Software, 115, 98-112.

Roelvink, D., McCall, R., Mehvar, S., Nederhoff, K., & Dastgheib, A. (2018). Improving predictions of swash dynamics in XBeach: The role of groupiness and incident-band runup. Coastal Engineering, 134, 103-123.

Roelvink, D., Reniers, A. J. H. M., Van Dongeren, A. P., Van Thiel de Vries, J., Lescinski, J., & McCall, R. (2010). XBeach model description and manual. Unesco-IHE Institute for Water Education, Deltares and Delft University of Tecnhology. Report June, 21, 2010.

Roelvink, D., Reniers, A., Van Dongeren, A. P., De Vries, J. V. T., McCall, R., & Lescinski, J. (2009). Modelling storm impacts on beaches, dunes and barrier islands. Coastal engineering, 56(11-12), 1133-1152.

Roelvink, J. A., & Brøker, I. (1993). Cross-shore profile models. Coastal Engineering, 21(1-3), 163-191.

Roelvink, J. A., & Stive, M. J. F. (1989). Bar-generating cross-shore flow mechanisms on a beach. Journal of Geophysical Research: Oceans, 94(C4), 4785-4800.

Roelvink, J. D., Walstra, D. J. R., van der Wegen, M., & Ranasinghe, R. (2016). Modeling of coastal morphological processes. Springer Handbook of Ocean Engineering, 611-634.

Roelvink, V. D., Van Dongeren, A., McCall, R., Hoonhout, B., Van Rooijen, A., Van Geer, P., ... & Quataert, E. (2015). XBeach technical reference: Kingsday release. Model description and reference guide to functionalities.

Ruessink, B. G., Kuriyama, Y., Reniers, A. J. H. M., Roelvink, J. A., & Walstra, D. J. R. (2007). Modeling cross-shore sandbar behavior on the timescale of weeks. Journal of Geophysical Research: Earth Surface, 112(F3).

Ruessink, B. G., Ramaekers, G., & Van Rijn, L. C. (2012). On the parameterization of the free-stream non-linear wave orbital motion in nearshore morphodynamic models. Coastal engineering, 65, 56-63.

Ruffini, G., Briganti, R., Alsina, J. M., Brocchini, M., Dodd, N., & McCall, R. (2020). Numerical modeling of flow and bed evolution of bichromatic wave groups on an intermediate beach using nonhydrostatic XBeach. Journal of Waterway, Port, Coastal, and Ocean Engineering, 146(1), 04019034.

Sallenger Jr, A. H. (2000). Storm impact scale for barrier islands. Journal of coastal research, 890-895.

Sallenger Jr, A. H., & Holman, R. A. (1985). Wave energy saturation on a natural beach of variable slope. Journal of Geophysical Research: Oceans, 90(C6), 11939-11944.

Samaras, A. G., Gaeta, M. G., Miquel, A. M., & Archetti, R. (2016). High-resolution wave and hydrodynamics modelling in coastal areas: operational applications for coastal planning, decision support and assessment. Natural hazards and earth system sciences, 16(6), 1499-1518.

Sanuy, M., & Jiménez, J. A. (2019). Sensitivity of storm-induced hazards in a highly curvilinear coastline to changing storm directions. The Tordera Delta Case (NW Mediterranean). Water, 11(4), 747.

Sanuy, M., & Jiménez, J. A. (2021). Probabilistic characterisation of coastal storm-induced risks using Bayesian networks. Natural Hazards and Earth System Sciences, 21(1), 219-238.

Saravanan, S., & Chandrasekar, N. (2015). Wave refraction pattern and littoral sediment transport along the SE Tamilnadu coast, India. Journal of Coastal Research, 31(2), 291-298.

Sardain, A., Sardain, E., & Leung, B. (2019). Global forecasts of shipping traffic and biological invasions to 2050. Nature Sustainability, 2(4), 274-282.

Schambach, L., Grilli, A. R., Grilli, S. T., Hashemi, M. R., & King, J. W. (2018). Assessing the impact of extreme storms on barrier beaches along the Atlantic coastline: Application to the southern Rhode Island coast. Coastal Engineering, 133, 26-42.

Schepper, R., Almar, R., Bergsma, E., de Vries, S., Reniers, A., Davidson, M., & Splinter, K. (2021). Modelling cross-shore shoreline change on multiple timescales and their interactions. Journal of Marine Science and Engineering, 9(6), 582.

Schoonees, J. S., & Theron, A. K. (1995). Evaluation of 10 cross-shore sediment transport/morphological models. Coastal Engineering, 25(1-2), 1-41.

Schwartz, R. K. (2012). Bedform, texture, and longshore bar development in response to combined storm wave and current dynamics in a nearshore helical flow system. Journal of Coastal Research, 28(6), 1512-1535.

Senechal, N., Coco, G., Castelle, B., & Marieu, V. (2015). Storm impact on the seasonal shoreline dynamics of a meso-to macrotidal open sandy beach (Biscarrosse, France). Geomorphology, 228, 448-461.

Shepard, F. P. (1950). Longshore-bars and longshore-troughs.

Shepard, F. P., & Inman, D. L. (1951). Nearshore circulation (pp. 50-59). Scripps Institution of Oceanography.

Sherwood, C. R., Van Dongeren, A., Doyle, J., Hegermiller, C. A., Hsu, T. J., Kalra, T. S., ... & Warner, J. C. (2022). Modeling the morphodynamics of coastal responses to extreme events: What shape are we in?. Annual review of marine science, 14, 457-492.

Short, A. D. (1979). Three-dimensional beach-stage model. The Journal of Geology, 87(5), 553-571.

Short, A. D. (1996). The role of wave height, period, slope, tide range and embaymentisation in beach classifications: a review. Revista chilena de historia natural, 69(4), 589-604.

Short, A. D. (1999). Handbook of beach and shoreface morphodynamics. Great Britain: John Wiley; ISBN 0-471-96570-7.

Short, A. D., & Jackson, D. W. T. (2013). Beach morphodynamics. Treatise on Geomorphology, 106-129.

Short, A. D., & Trembanis, A. C. (2004). Decadal scale patterns in beach oscillation and rotation Narrabeen Beach, Australia—time series, PCA and wavelet analysis. Journal of Coastal Research, 20(2), 523-532.

Short, A. D., & Trenaman, N. L. (1992). Wave climate of the Sydney region, an energetic and highly variable ocean wave regime. Marine and Freshwater Research, 43(4), 765-791.

Siegle, E., & Asp, N. E. (2007). Wave refraction and longshore transport patterns along the southern Santa Catarina coast. Brazilian Journal of Oceanography, 55, 109-120.

Simmons, J. A., & Splinter, K. D. (2022). A multi-model ensemble approach to coastal storm erosion prediction. Environmental Modelling & Software, 150, 105356.

Simmons, J. A., Harley, M. D., Marshall, L. A., Turner, I. L., Splinter, K. D., & Cox, R. J. (2017). Calibrating and assessing uncertainty in coastal numerical models. Coastal Engineering, 125, 28-41.

Small, C., & Nicholls, R. J. (2003). A global analysis of human settlement in coastal zones. Journal of coastal research, 584-599.

Smit, P., Stelling, G., Roelvink, J., Van Thiel de Vries, J., McCall, R., Van Dongeren, A., ... & Jacobs, R. (2010). XBeach: Non-hydrostatic model: Validation, verification, and model description. Delft Univ. Technol, 59.

Sonu, C. J. (1973). Three-dimensional beach changes. The Journal of Geology, 81(1), 42-64.

Soulsby, R. (1997). Dynamics of marine sands.

Spalding, M. D., McIvor, A. L., Beck, M. W., Koch, E. W., Möller, I., Reed, D. J., ... & Woodroffe, C. D. (2014). Coastal ecosystems: a critical element of risk reduction. Conservation Letters, 7(3), 293-301.

Splinter, K. D., & Palmsten, M. L. (2012). Modeling dune response to an East Coast Low. Marine Geology, 329, 46-57.

Splinter, K. D., Carley, J. T., Golshani, A., & Tomlinson, R. (2014). A relationship to describe the cumulative impact of storm clusters on beach erosion. Coastal engineering, 83, 49-55.

Splinter, K. D., Turner, I. L., Davidson, M. A., Barnard, P., Castelle, B., & Oltman-Shay, J. (2014). A generalized equilibrium model for predicting daily to interannual shoreline response. Journal of Geophysical Research: Earth Surface, 119(9), 1936-1958.

Splinter, K. D., Turner, I. L., Reinhardt, M., & Ruessink, G. (2017). Rapid adjustment of shoreline behavior to changing seasonality of storms: Observations and modelling at an open-coast beach. Earth Surface Processes and Landforms, 42(8), 1186-1194.

Steetzel, H. J. (1993). Cross-shore transport during storm surges. Technical University of Delft (Doctoral dissertation, Thesis).

Stephens, S. A., Coco, G., & Bryan, K. R. (2011). Numerical simulations of wave setup over barred beach profiles: implications for predictability. Journal of waterway, port, coastal, and ocean engineering, 137(4), 175-181.

Stive, M. J. (2004). How important is global warming for coastal erosion? Climatic change, 64(1-2), 27.

Stive, M. J., Aarninkhof, S. G., Hamm, L., Hanson, H., Larson, M., Wijnberg, K. M., ... & Capobianco, M. (2002). Variability of shore and shoreline evolution. Coastal engineering, 47(2), 211-235.

Stockdon, H. F., Holman, R. A., Howd, P. A., & Sallenger Jr, A. H. (2006). Empirical parameterization of setup, swash, and runup. Coastal engineering, 53(7), 573-588.

Stockdon, H. F., Sallenger Jr, A. H., List, J. H., & Holman, R. A. (2002). Estimation of shoreline position and change using airborne topographic lidar data. Journal of Coastal Research, 502-513.

Suzuki, T., & Kuriyama, Y. (2007). Medium-term shoreline changes at Hasaki, Japan. In Coastal Engineering 2006: (In 5 Volumes) (pp. 3241-3253).

Suzuki, T., Sakihama, S., & Cox, D. T. (2020). Effect of tidal range on longshore current variation with respect to cross-shore location of a barred beach. Coastal Engineering Journal, 62(2), 217-235.

Svendsen, I. A. (2005). Introduction to nearshore hydrodynamics (Vol. 24). World Scientific Publishing Company.

Takeda, I., & Sunamura, T. (1992). Conditions for beach erosion on a barred beach. Zeitschrift fuer Geomorphologie, 453-464.

Trim, L. K., She, K., & Pope, D. J. (2002). Tidal effects on cross-shore sediment transport on a shingle beach. Journal of Coastal Research, (36), 708-715.

Turner, I. L. (1995). Modelling the time-varying extent of groundwater seepage on tidal beaches. Earth surface processes and landforms, 20(9), 833-843.

Turner, I. L., & Masselink, G. (1998). Swash infiltration-exfiltration and sediment transport. Journal of Geophysical Research: Oceans, 103(C13), 30813-30824.

UN Atlas of the Oceans: Home. (n.d.). http://www.oceansatlas.org

University, O. (1999, January 1). Waves. Elsevier eBooks. https://doi.org/10.1016/b978-008036372-1/50002-7

Ursell, F. (1953, October). The long-wave paradox in the theory of gravity waves. In Mathematical Proceedings of the Cambridge Philosophical Society (Vol. 49, No. 4, pp. 685-694). Cambridge University Press.

Valiela, I. (2009). Global coastal change. John Wiley & Sons.

Van Dongeren, A. R. J. A., Battjes, J., Janssen, T., Van Noorloos, J., Steenhauer, K., Steenbergen, G., & Reniers, A. J. H. M. (2007). Shoaling and shoreline dissipation of low-frequency waves. Journal of Geophysical Research: Oceans, 112(C2).

Van Dongeren, A., Bolle, A., Vousdoukas, M. I., Plomaritis, T., Eftimova, P., Williams, J., ... & Roelvink, D. (2009). MICORE: dune erosion and overwash model validation with data from nine European field sites. In Proceedings of Coastal Dynamics 2009: Impacts of Human Activities on Dynamic Coastal Processes (With CD-ROM) (pp. 1-15).

van Rijn, L. C., Walstra, D. J., Grasmeijer, B., Sutherland, J., Pan, S., & Sierra, J. P. (2003). The predictability of cross-shore bed evolution of sandy beaches at the time scale of storms and seasons using process-based profile models. Coastal Engineering, 47(3), 295-327.

van Rooijen, A., Lowe, R., Ghisalberti, M., McCall, R., & Hansen, J. (2022). Modelling wave attenuation through submerged vegetation canopies using a subgrid canopy flow model. Coastal Engineering, 176, 104153.

Van Thiel de Vries, J. S. M. (2009). Dune erosion during storm surges.

Van Verseveld, H. C. W., Van Dongeren, A. R., Plant, N. G., Jäger, W. S., & Den Heijer, C. (2015). Modelling multi-hazard hurricane damages on an urbanized coast with a Bayesian Network approach. Coastal Engineering, 103, 1-14.

Viles, H., & Spencer, T. (2014). Coastal problems: geomorphology, ecology and society at the coast. Routledge.

Villaret, C., Hervouet, J. M., Kopmann, R., Merkel, U., & Davies, A. G. (2013). Morphodynamic modeling using the Telemac finite-element system. Computers & Geosciences, 53, 105-113.

Vitousek, S., Barnard, P. L., Limber, P., Erikson, L., & Cole, B. (2017). A model integrating longshore and cross-shore processes for predicting long-term shoreline response to climate change. Journal of Geophysical Research: Earth Surface, 122(4), 782-806.

Vos, K., Harley, M. D., Splinter, K. D., Simmons, J. A., & Turner, I. L. (2019). Sub-annual to multi-decadal shoreline variability from publicly available satellite imagery. Coastal Engineering, 150, 160-174.

Voukouvalas, E. (2010). Coastal response during the 1953 and 1976 storm surges in the Netherlands. Field data validation of the XBeach model.

Vousdoukas, M. I., Ferreira, Ó., Almeida, L. P., & Pacheco, A. (2012). Toward reliable storm-hazard forecasts: XBeach calibration and its potential application in an operational early-warning system. Ocean Dynamics, 62, 1001-1015.

Walstra, D. J. R., Van Rijn, L. C., Van Ormondt, M., Brière, C., & Talmon, A. M. (2007). The effects of bed slope and wave skewness on sediment transport and morphology. In Coastal Sediments' 07 (pp. 137-150).

Wang, P., & Davis Jr, R. A. (1998). A beach profile model for a barred coast: Case study from Sand Key, West-Central Florida. Journal of Coastal Research, 981-991.

Wang, P., Ebersole, B. A., & Smith, E. R. (2002). Longshore sand transport-initial results from large-scale sediment transport facility.

Warren, I. R., & Bach, H. (1992). MIKE 21: a modelling system for estuaries, coastal waters and seas. Environmental Software, 7(4), 229-240.

Weir, F. M., Hughes, M. G., & Baldock, T. E. (2006). Beach face and berm morphodynamics fronting a coastal lagoon. Geomorphology, 82(3-4), 331-346.

Wiegel, R. L. (1964). Oceanographical engineering Prentice-Hall. Inc, Englewood Cliffs, NJ.

Wiegel, R. L. (1964). Water wave equivalent of Mach-reflection. In Coastal Engineering 1964 (pp. 82-102).

Williams, J. J., de Alegría-Arzaburu, A. R., McCall, R. T., & Van Dongeren, A. (2012). Modelling gravel barrier profile response to combined waves and tides using XBeach: Laboratory and field results. Coastal Engineering, 63, 62-80.

Williams, J. J., Esteves, L. S., & Rochford, L. A. (2015). Modelling storm responses on a high-energy coastline with XBeach. Modeling Earth Systems and Environment, 1, 1-14.

Wilson, A. M., Huettel, M., & Klein, S. (2008). Grain size and depositional environment as predictors of permeability in coastal marine sands. Estuarine, Coastal and Shelf Science, 80(1), 193-199.

Wolinsky, M. A., & Murray, A. B. (2009). A unifying framework for shoreline migration: 2. Application to wave-dominated coasts. Journal of Geophysical Research: Earth Surface, 114(F1).

Wright, L. D., & Short, A. D. (1984). Morphodynamic variability of surf zones and beaches: a synthesis. Marine geology, 56(1-4), 93-118.

Wright, L. D., & Short, A. D. (2018). Morphodynamics of beaches and surf zones in Australia. In Handbook of coastal processes and erosion (pp. 35-64). CRC press.

Wright, L. D., Chappell, J., Thom, B. G., Bradshaw, M. P., & Cowell, P. (1979). Morphodynamics of reflective and dissipative beach and inshore systems: Southeastern Australia. Marine Geology, 32(1-2), 105-140.

Wright, L. D., Short, A. D., & Green, M. O. (1985). Short-term changes in the morphodynamic states of beaches and surf zones: an empirical predictive model. Marine geology, 62(3-4), 339-364.

Wright, L. D., Short, A. D., & Nielsen, P. (1982). Morphodynamics of high energy beaches and surf zones: a brief synthesis (p. 64). Coastal Studies Unit, Department of Geography, University of Sydney.

Yates, M. L., Guza, R. T., O'Reilly, W. C., Hansen, J. E., & Barnard, P. L. (2011). Equilibrium shoreline response of a high wave energy beach. Journal of Geophysical Research: Oceans, 116(C4).

Zhang, J., & Larson, M. (2021). Decadal-scale subaerial beach and dune evolution at Duck, North Carolina. Marine Geology, 440, 106576.

Zhang, K., Huang, W., Douglas, B. C., & Leatherman, S. (2002). Shoreline position variability and long-term trend analysis. Shore and Beach, 70(2), 31-35.

Appendix

Appendix A

Parameters Used for Simulation

Table A 1 Some selected parameters used for simulation

	Slope	Hs (m)	Tp (s)	Ws (m/s)	$Ws * Tp$	$Hs/Ws * Tp$	Ω
Dissipative	20	0.4	1.0	0.06463	0.06463	6.189057	6.1
Dissipative	20	0.5	1.0	0.06463	0.06463	7.736321	7.7
Dissipative	20	0.6	1.0	0.06463	0.06463	9.283585	9.2
Dissipative	30	0.4	1.0	0.05341	0.05341	7.488069	7.4
Dissipative	50	0.5	2.0	0.03327	0.06655	7.512157	7.5
Dissipative	100	0.5	3.5	0.02188	0.02188	6.527666	6.5
Intermediate	10	0.5	2.0	0.08828	0.176568	2.831769	2.8
Intermediate	20	0.4	3.0	0.06463	0.193891	2.063019	2.0
Intermediate	30	0.2	1.0	0.05341	0.053418	3.744034	3.7
Intermediate	50	0.3	3.0	0.03327	0.099838	3.004863	3.0
Intermediate	100	0.2	3.0	0.02188	0.065655	3.046244	3.0
Reflective	10	0.1	3.5	0.08828	0.308994	0.323631	0.3
Reflective	10	0.1	1.5	0.08828	0.132426	0.755139	0.7
Reflective	10	0.2	3.0	0.08828	0.264852	0.755139	0.7
Reflective	20	0.2	3.5	0.06463	0.226206	0.884151	0.8
Reflective	20	0.1	3.0	0.06463	0.193891	0.515755	0.5
Reflective	30	0.1	3.0	0.05341	0.160255	0.624006	0.6

Appendix B

Beach Profile Changes with Varying Water Levels

B.1 Beach profile changes with varying water levels of 0.15 m

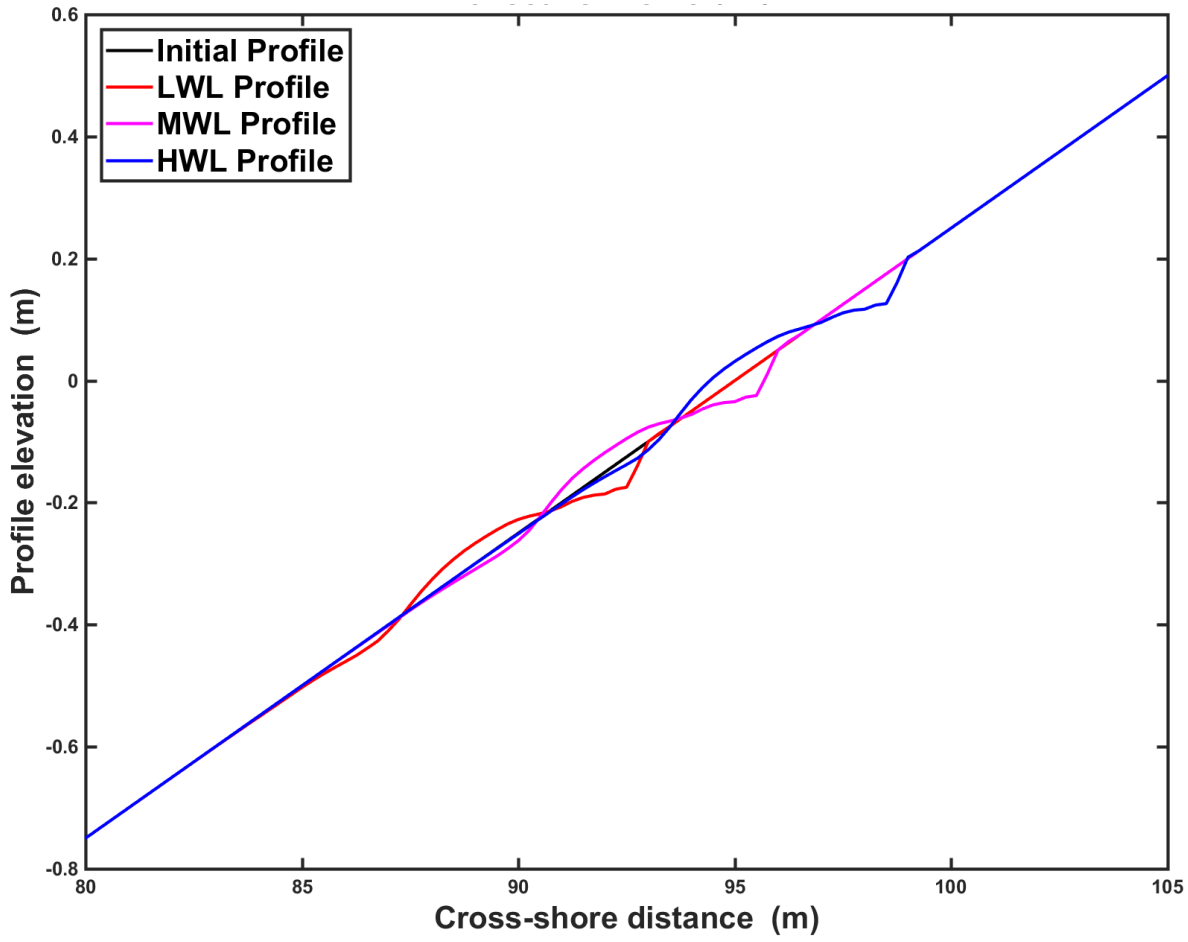

Figure B1.1 Reflective beach profile changes with varying water levels of 0.15 m

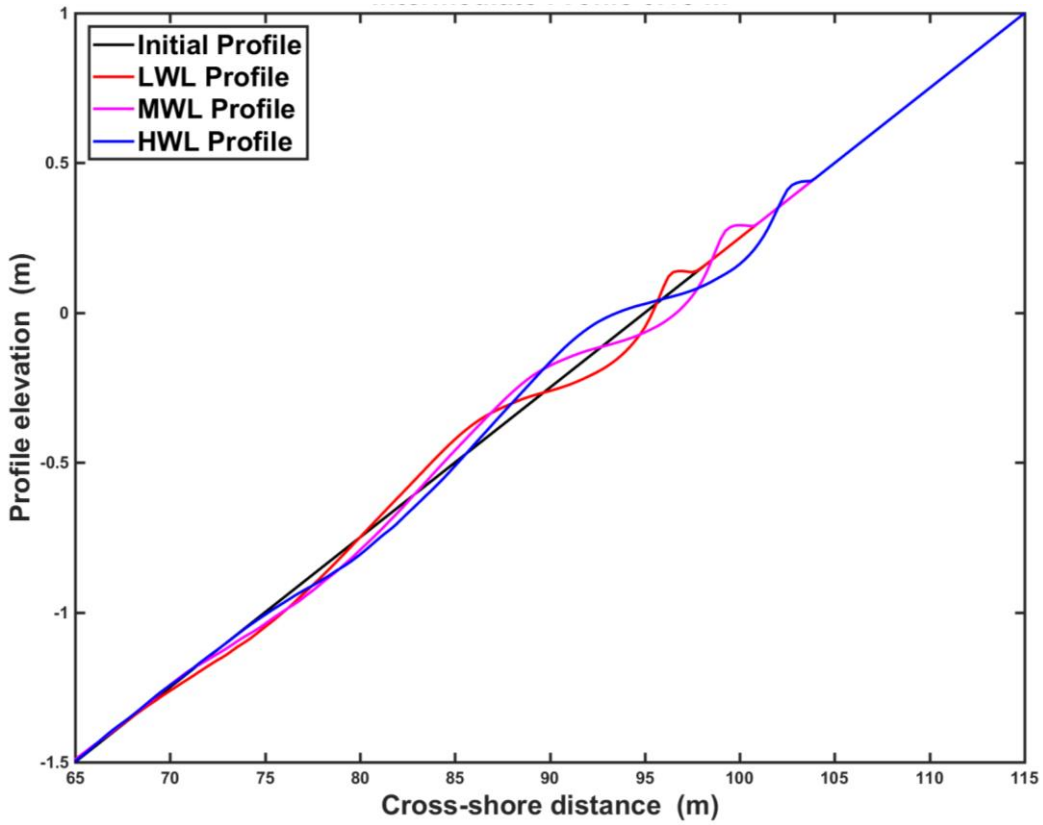

Figure B1.2 Intermediate beach profile changes with varying water levels of 0.15 m

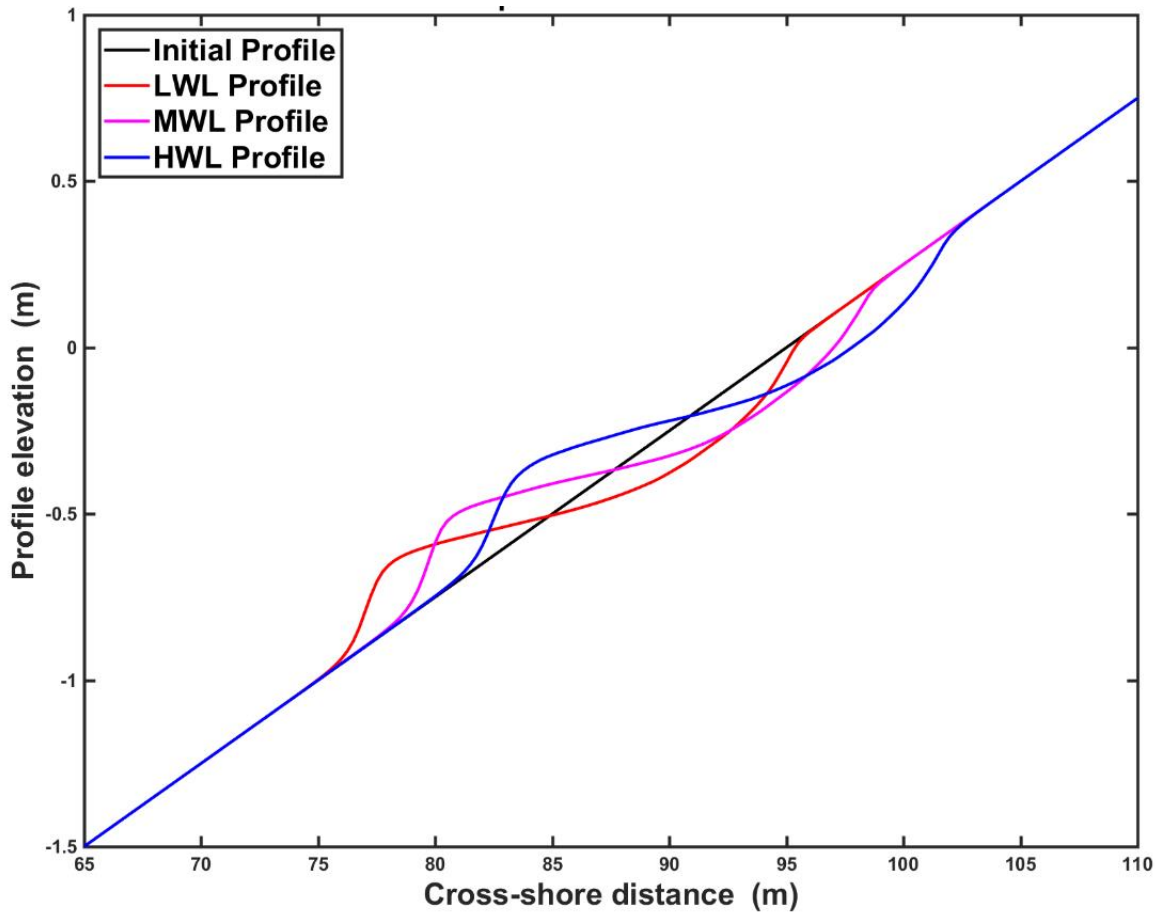

Figure B1.3 Dissipative beach profile changes with varying water levels of 0.15 m

B.2 Beach profile changes with varying water levels of 0.25 m

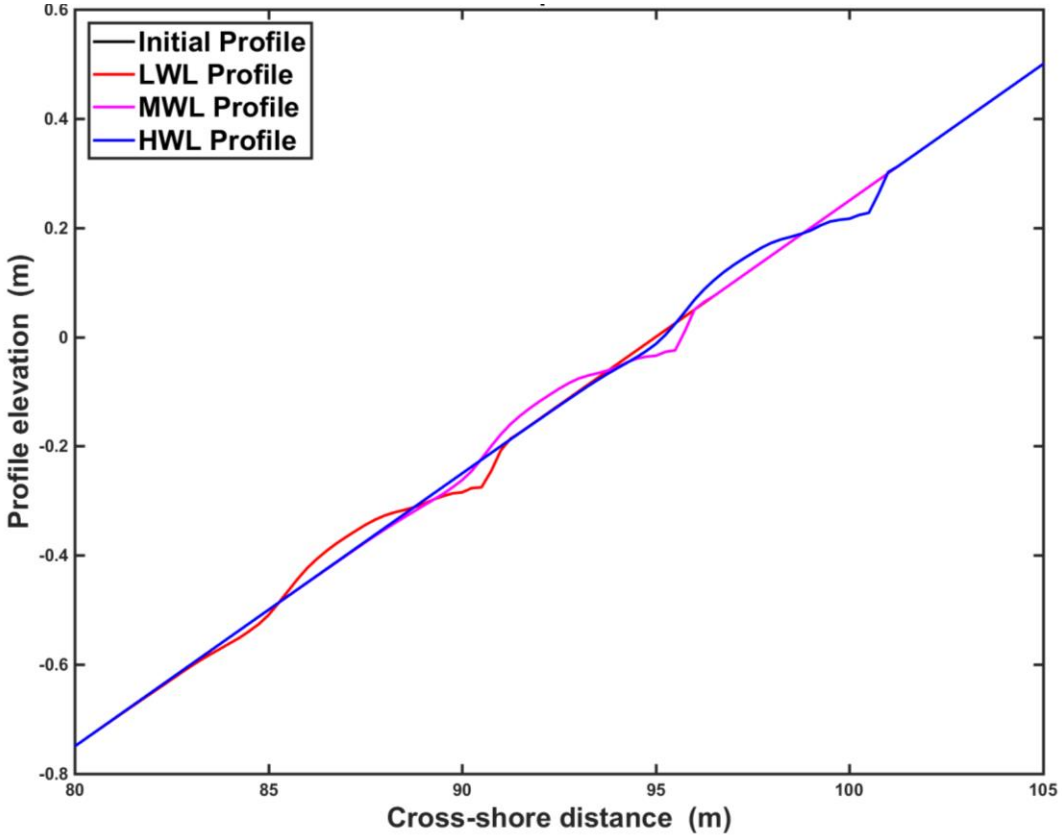

Figure B2.1 Reflective beach profile changes with varying water levels of 0.25 m

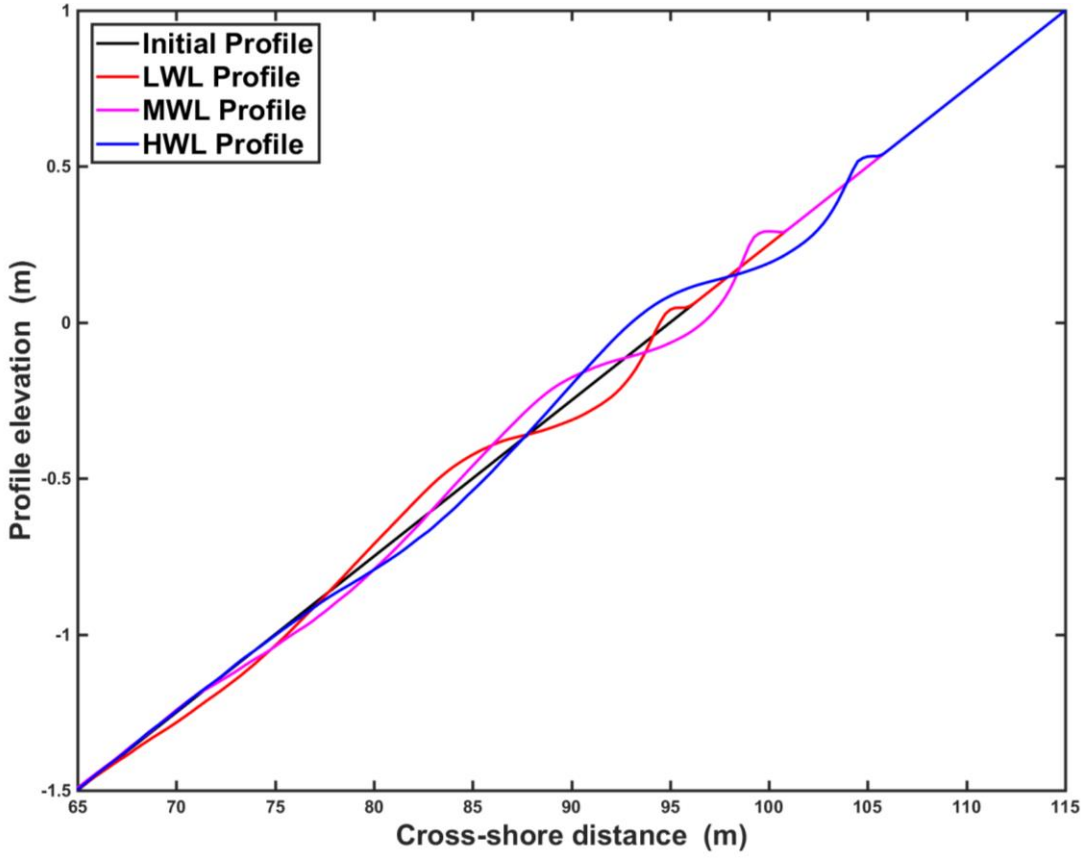

Figure B2.2 Intermediate beach profile changes with varying water levels of 0.25 m

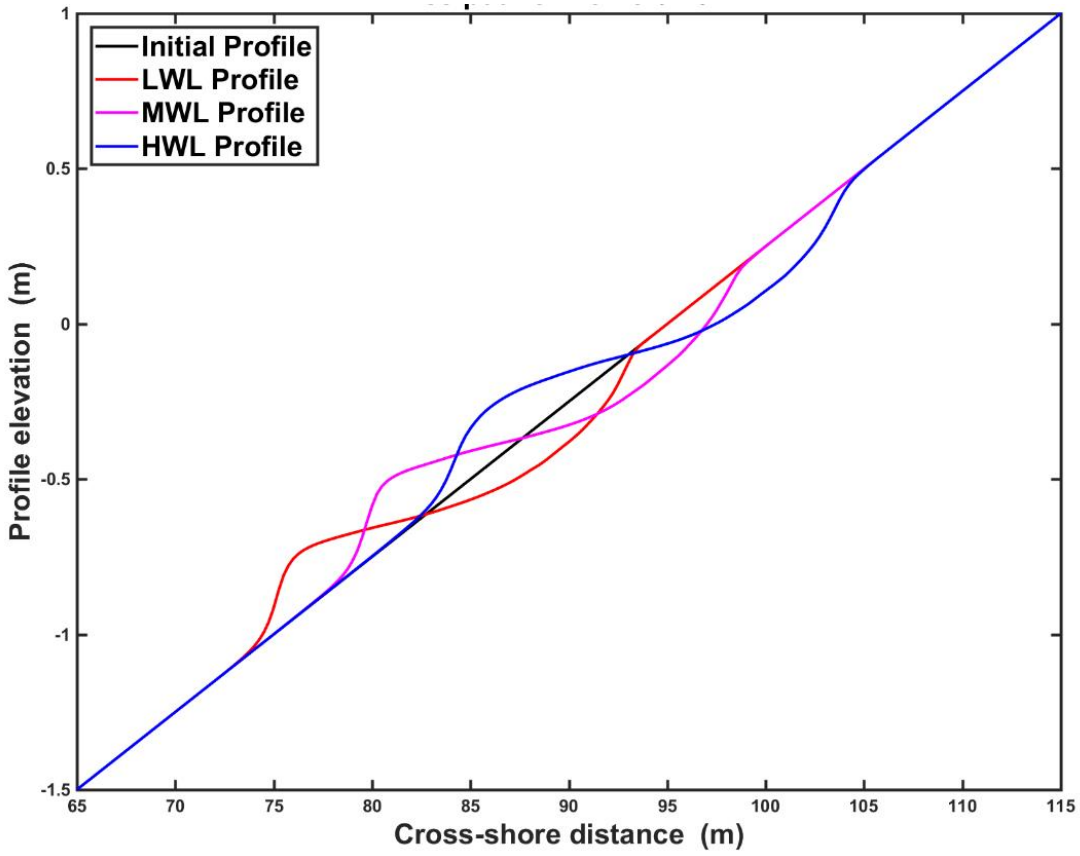

Figure B2.3 Dissipative beach profile changes with varying water levels of 0.25 m

Appendix C

Variability of non-dimensional parameters on different water level against Dean's parameter

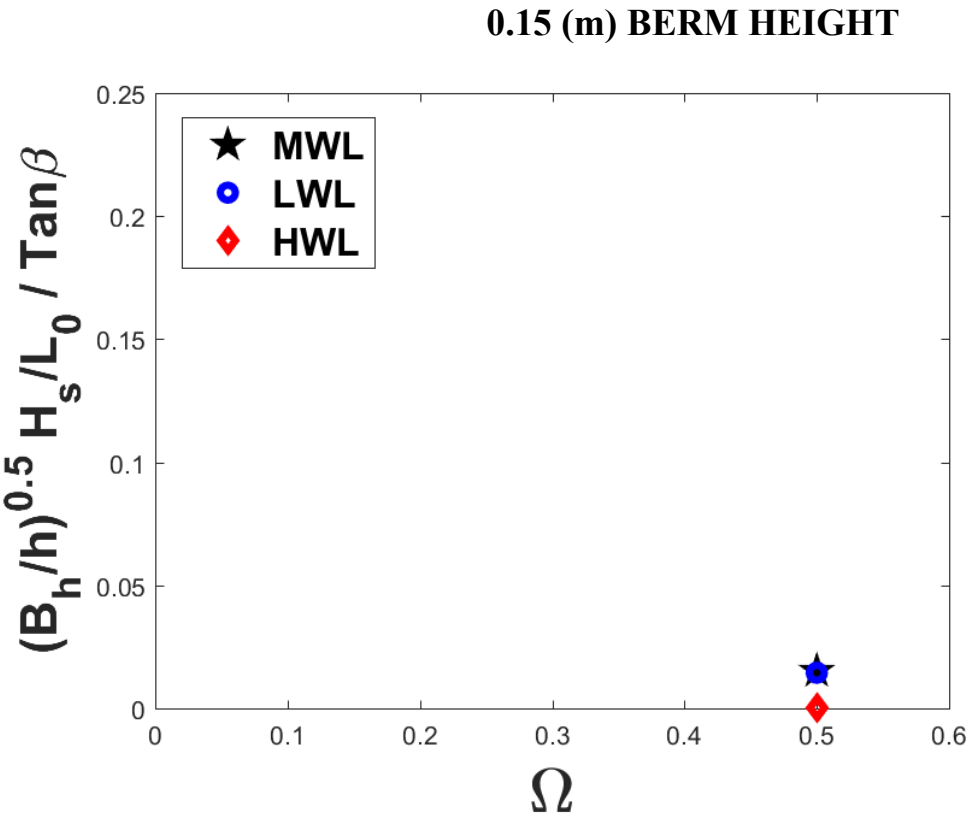

Figure C1.1 Variability of non-dimensional berm height on different water level against Dean's parameter Ω for reflective beach state 0.15 m

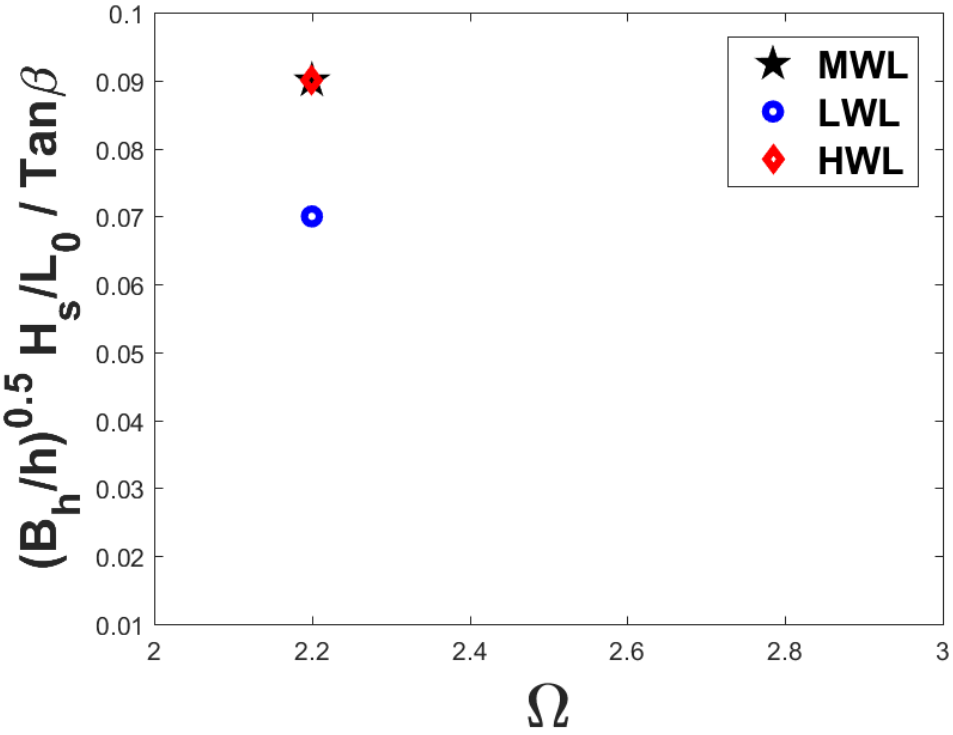

Figure C1.2 Variability of non-dimensional berm height on different water level against Dean's parameter Ω for intermediate beach state 0.15 m

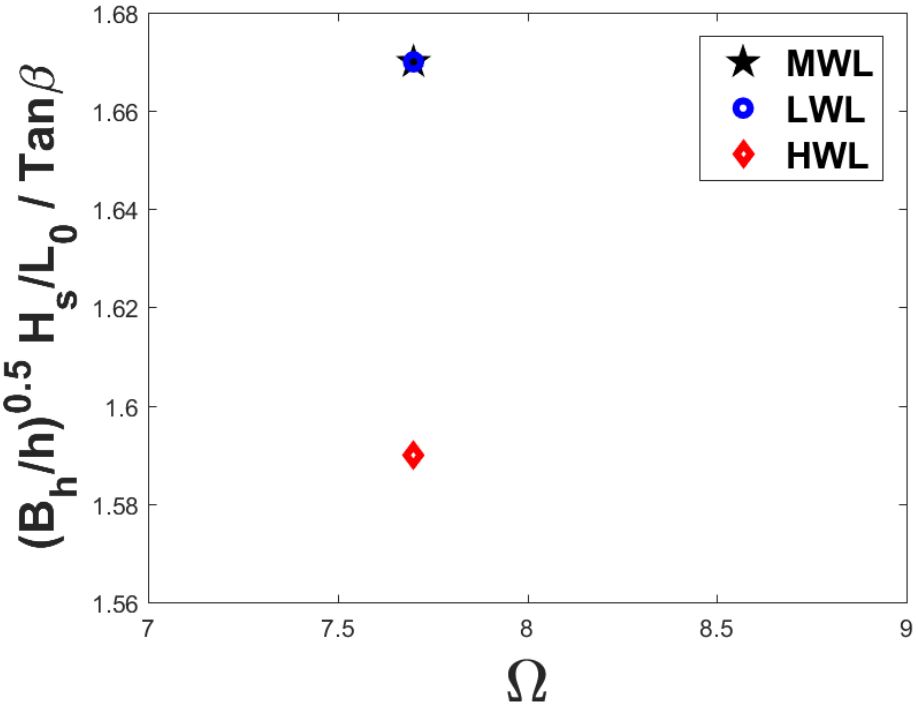

Figure C1.3 Variability of non-dimensional berm height on different water level against Dean's parameter Ω for dissipative beach state 0.15 m

BERM LENGTH

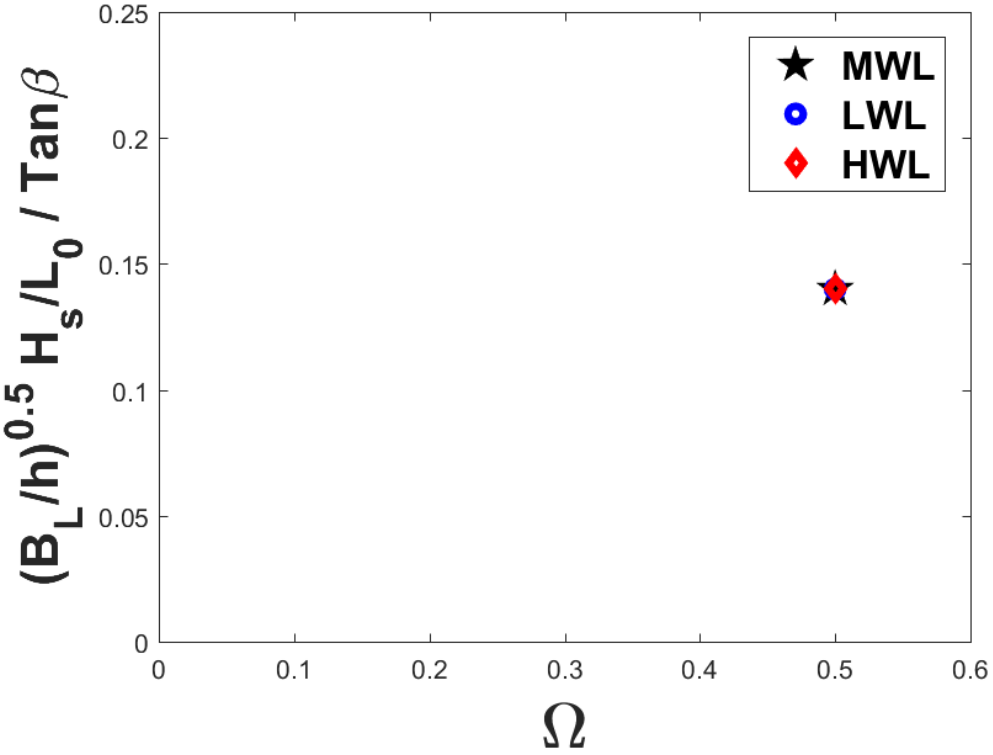

Figure C1.4 Variability of non-dimensional berm length on different water level against Dean's parameter Ω for reflective beach state 0.15 m

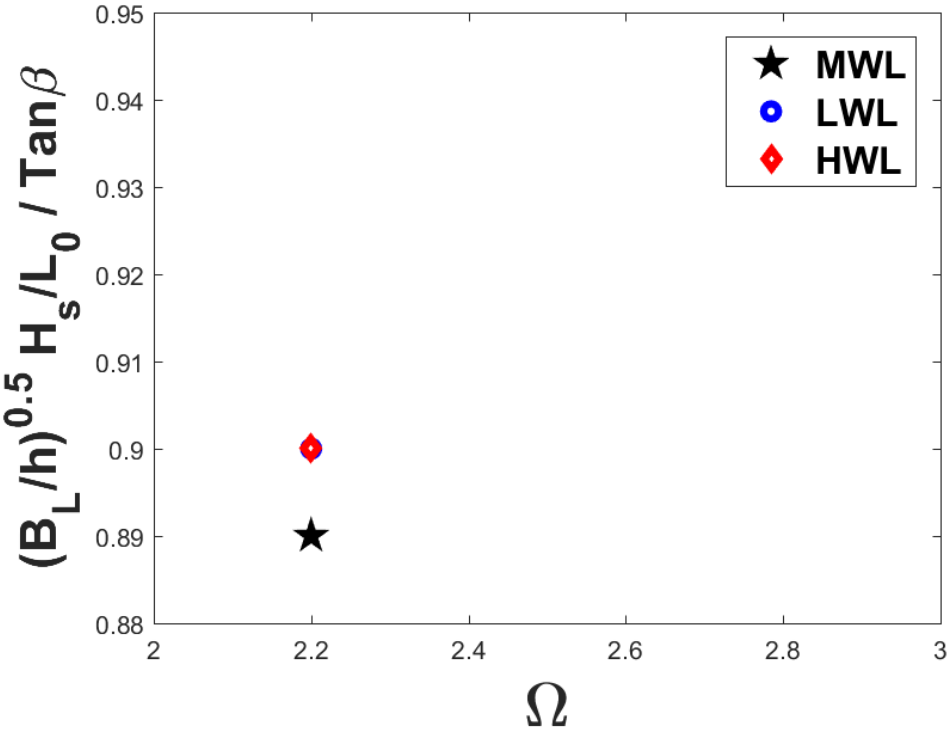

Figure C1.5 Variability of non-dimensional berm length on different water level against Dean's parameter Ω for intermediate beach state 0.15 m

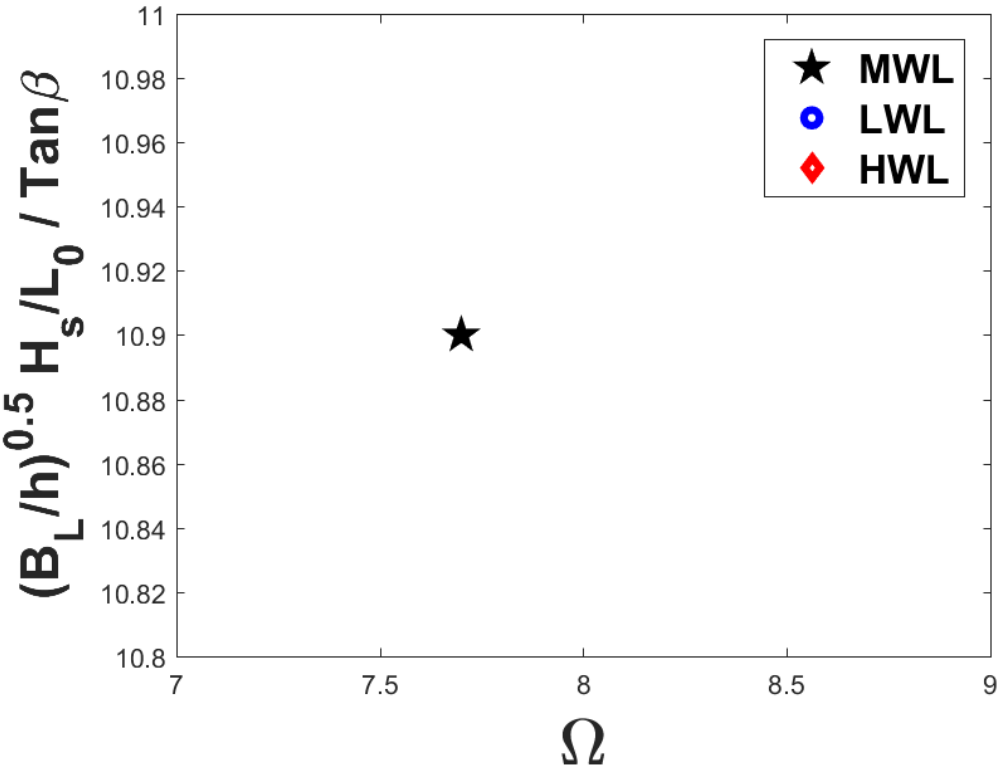

Figure C1.6 Variability of non-dimensional berm length on different water level against Dean's parameter Ω for dissipative beach state 0.15 m

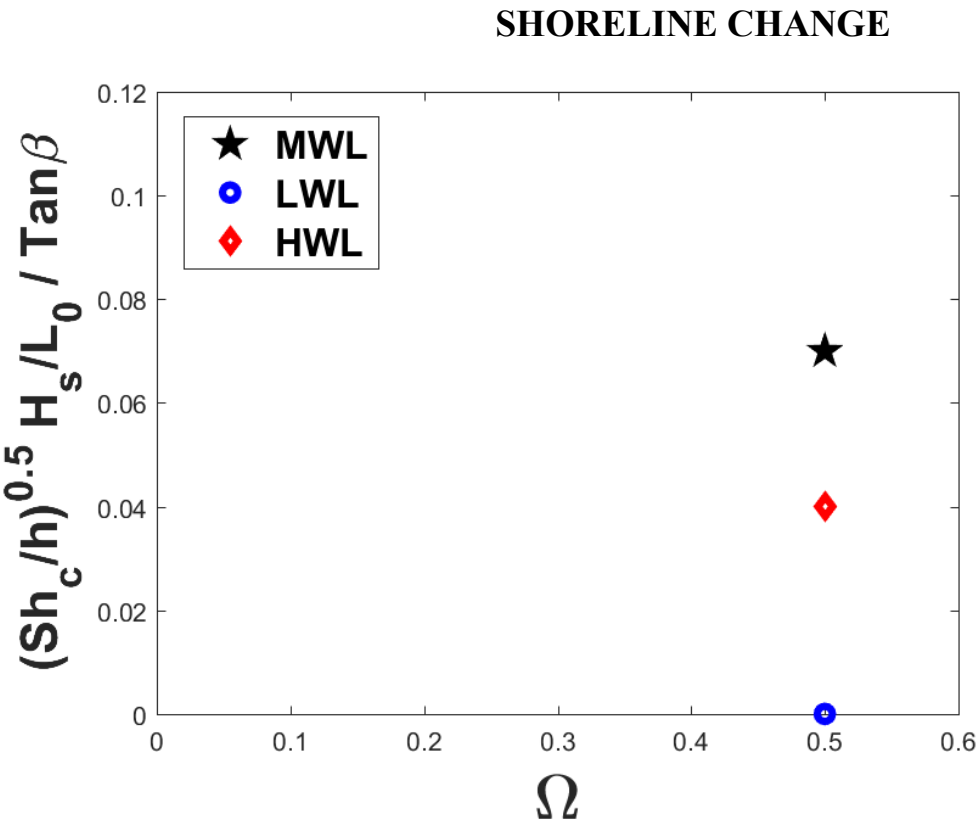

Figure C1.7 Variability of non-dimensional shoreline change on different water level against Dean's parameter Ω for reflective beach state 0.15 m

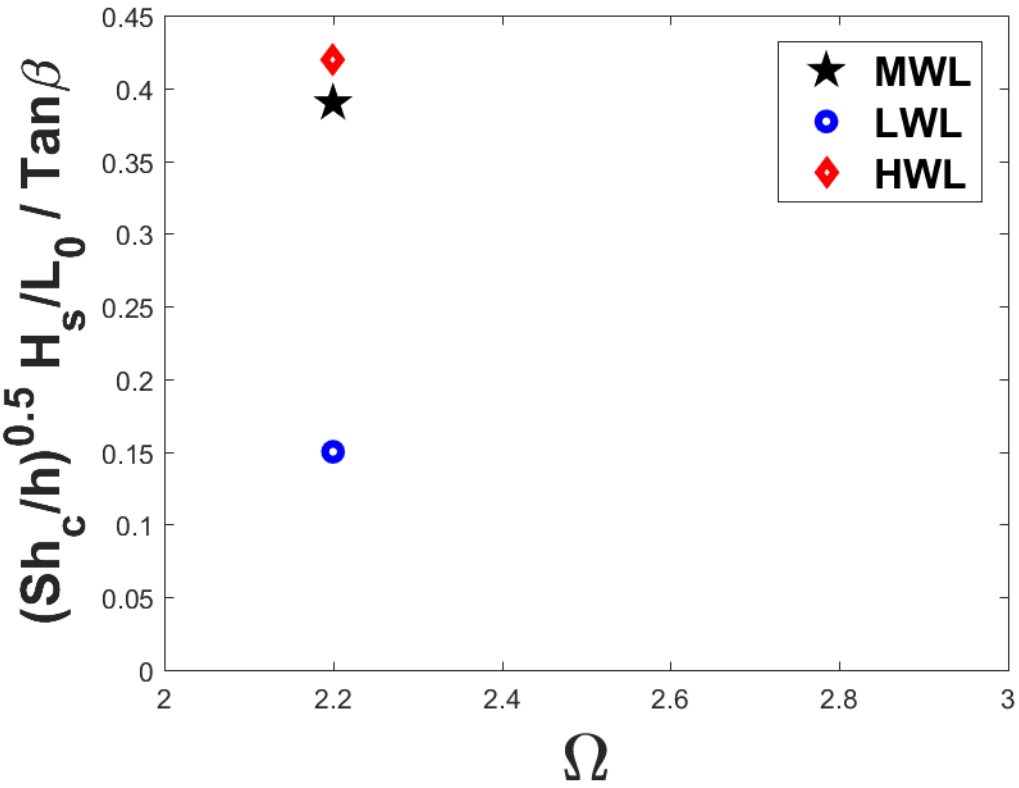

Figure C1.8 Variability of non-dimensional shoreline change on different water level against Dean's parameter Ω for intermediate beach state 0.15 m

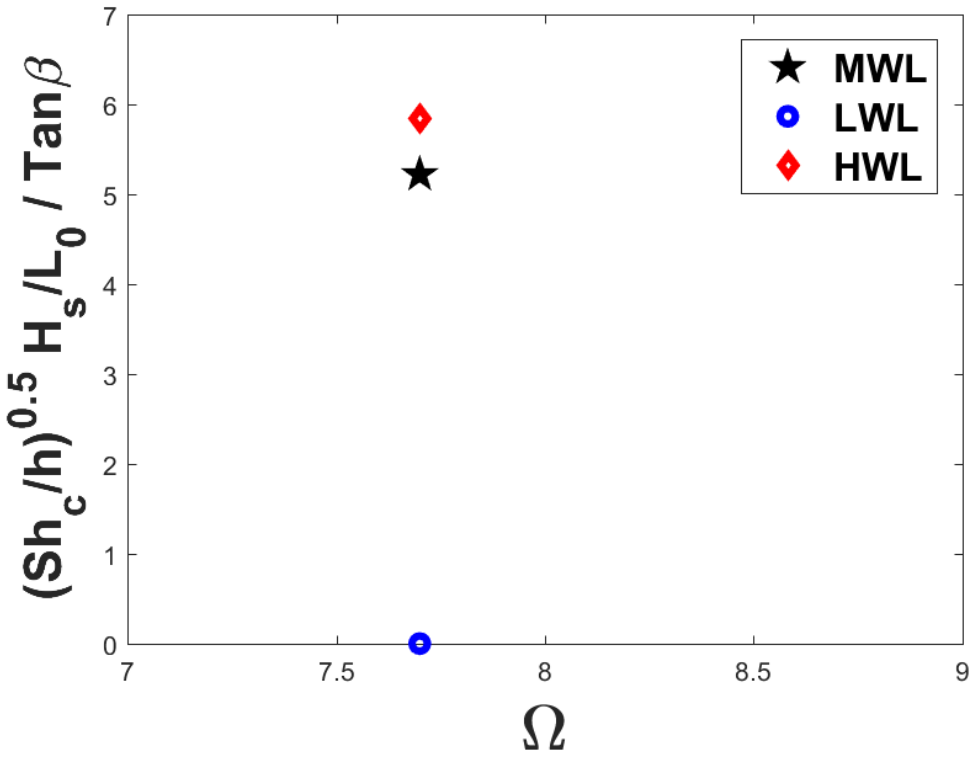

Figure C1.9 Variability of non-dimensional shoreline change on different water level against Dean's parameter Ω for dissipative beach state 0.15 m

0.25 (m) BERM HEIGHT

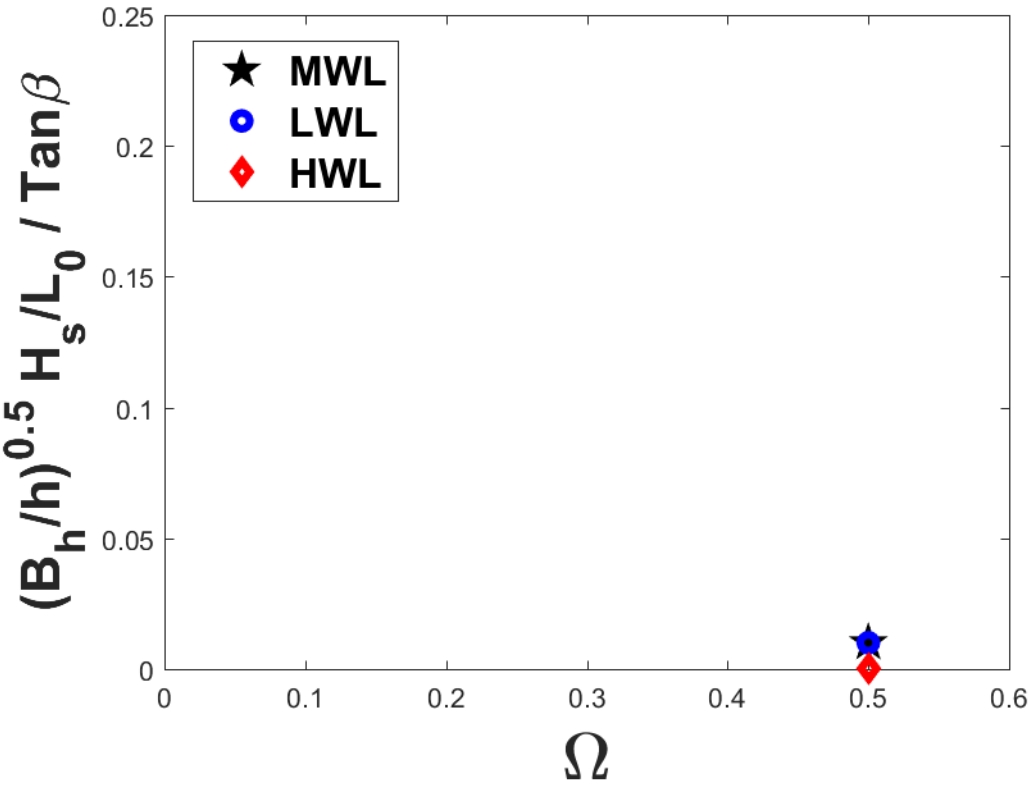

Figure C2.1 Variability of non-dimensional berm height on different water level against Dean's parameter Ω for reflective beach state 0.25 m

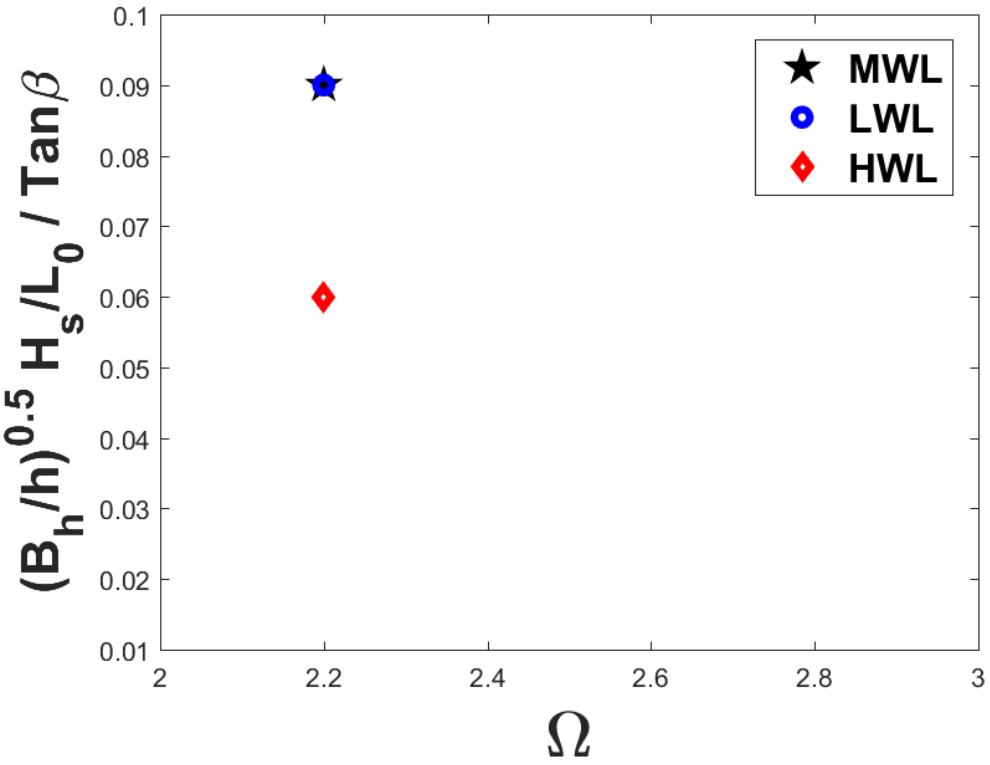

Figure C2.2 Variability of non-dimensional berm height on different water level against Dean's parameter Ω for intermediate beach state 0.25 m

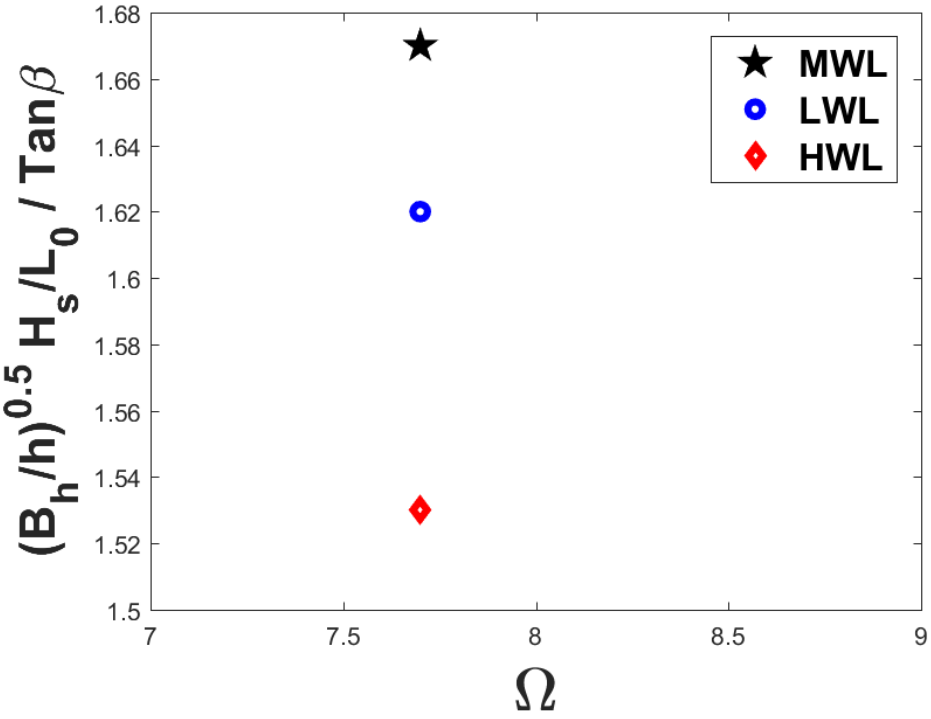

Figure C2.3 Variability of non-dimensional berm height on different water level against Dean's parameter Ω for dissipative beach state 0.25 m

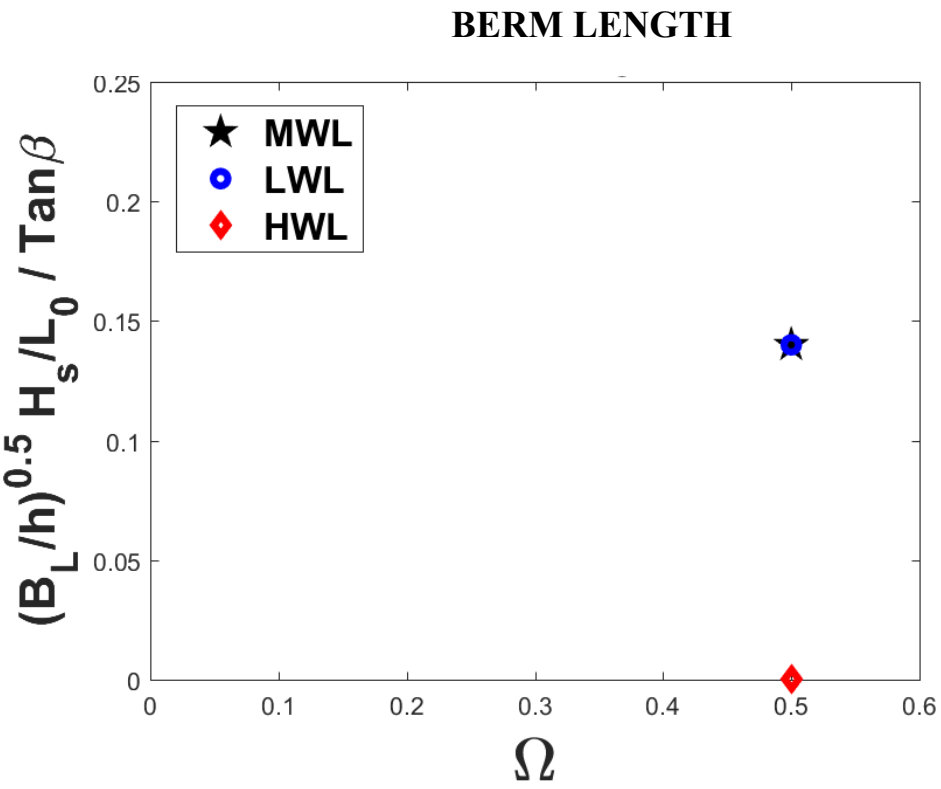

Figure C2.4 Variability of non-dimensional berm length on different water level against Dean's parameter Ω for reflective beach state 0.25 m

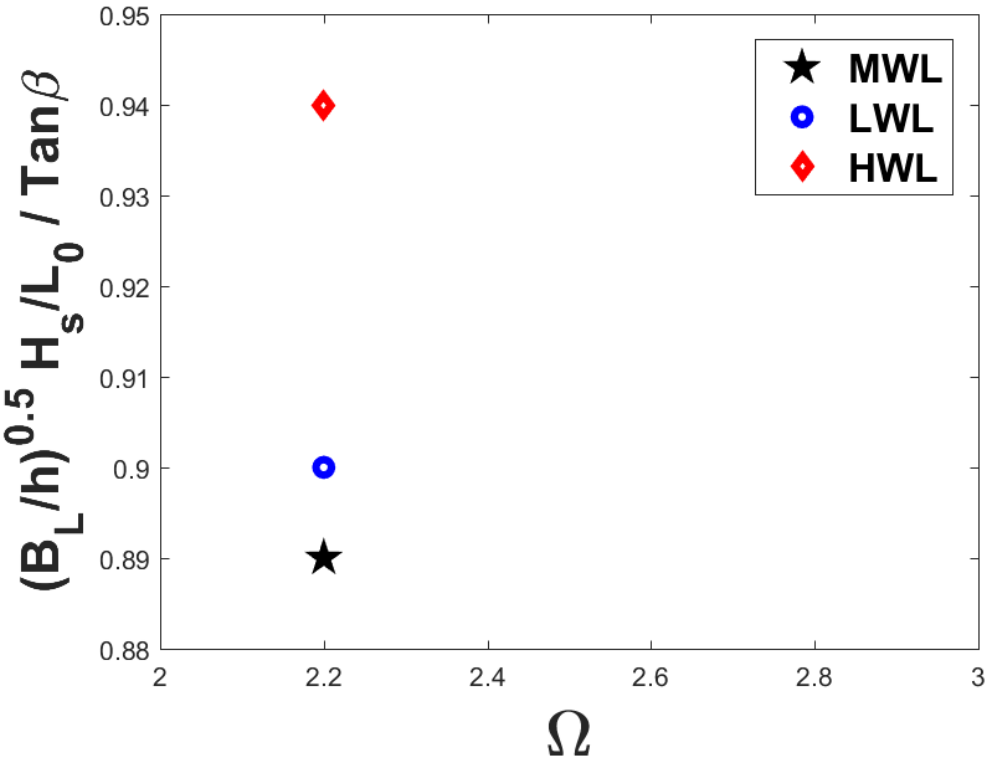

Figure C2.5 Variability of non-dimensional berm length on different water level against Dean's parameter Ω for intermediate beach state 0.25 m

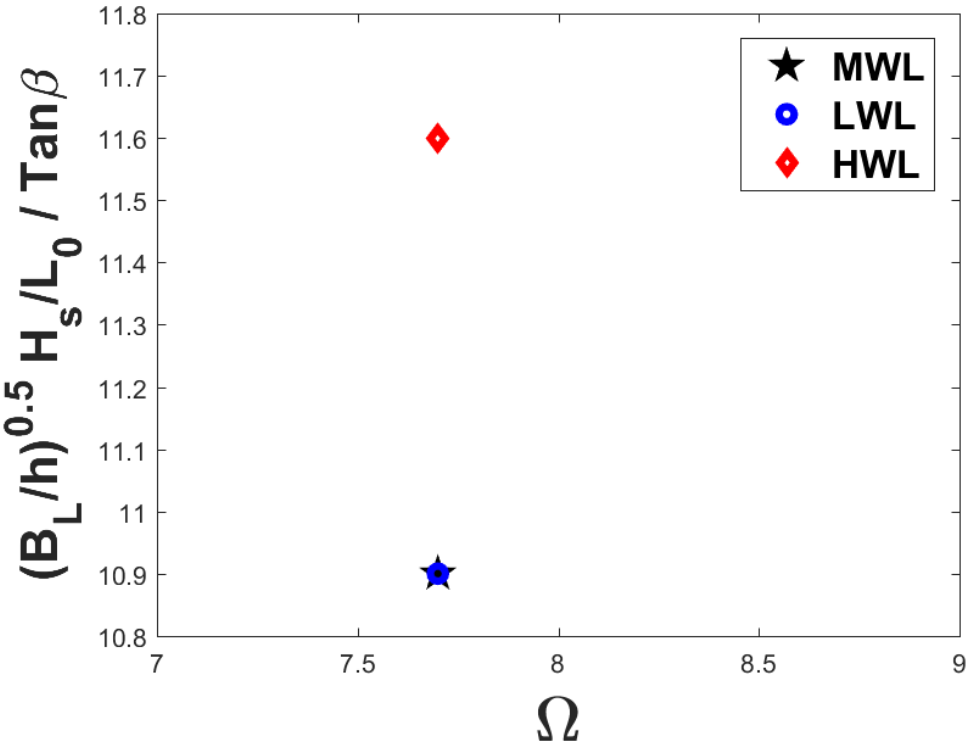

Figure C2.6 Variability of non-dimensional berm length on different water level against Dean's parameter Ω for dissipative beach state 0.25 m

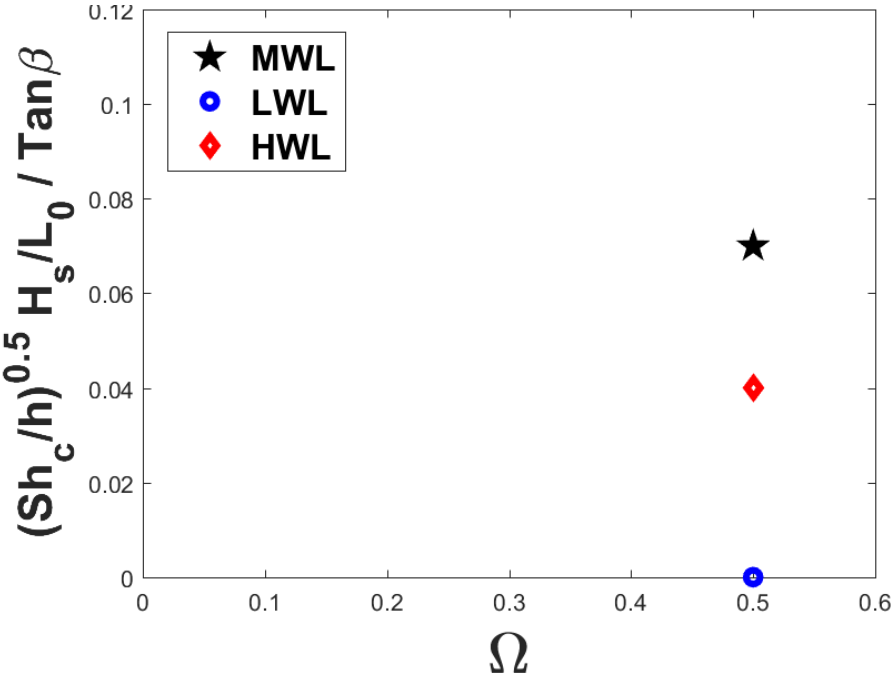

Figure C2.7 Variability of non-dimensional shoreline change on different water level against Dean's parameter Ω for reflective beach state 0.25 m

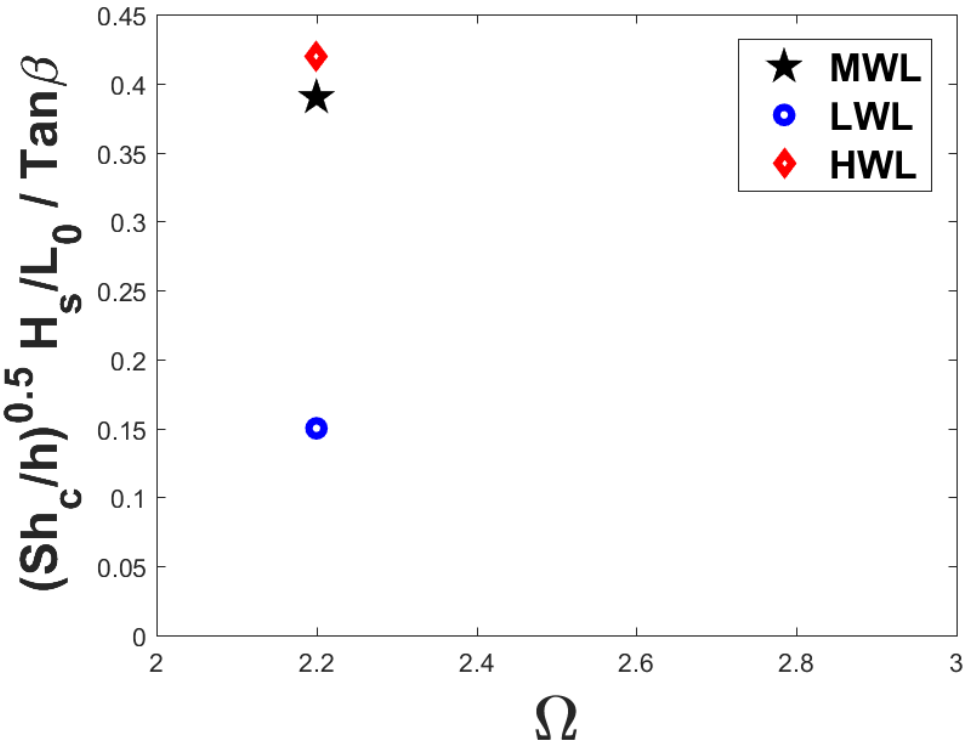

Figure C2.8 Variability of non-dimensional shoreline change on different water level against Dean's parameter Ω for intermediate beach state 0.25 m

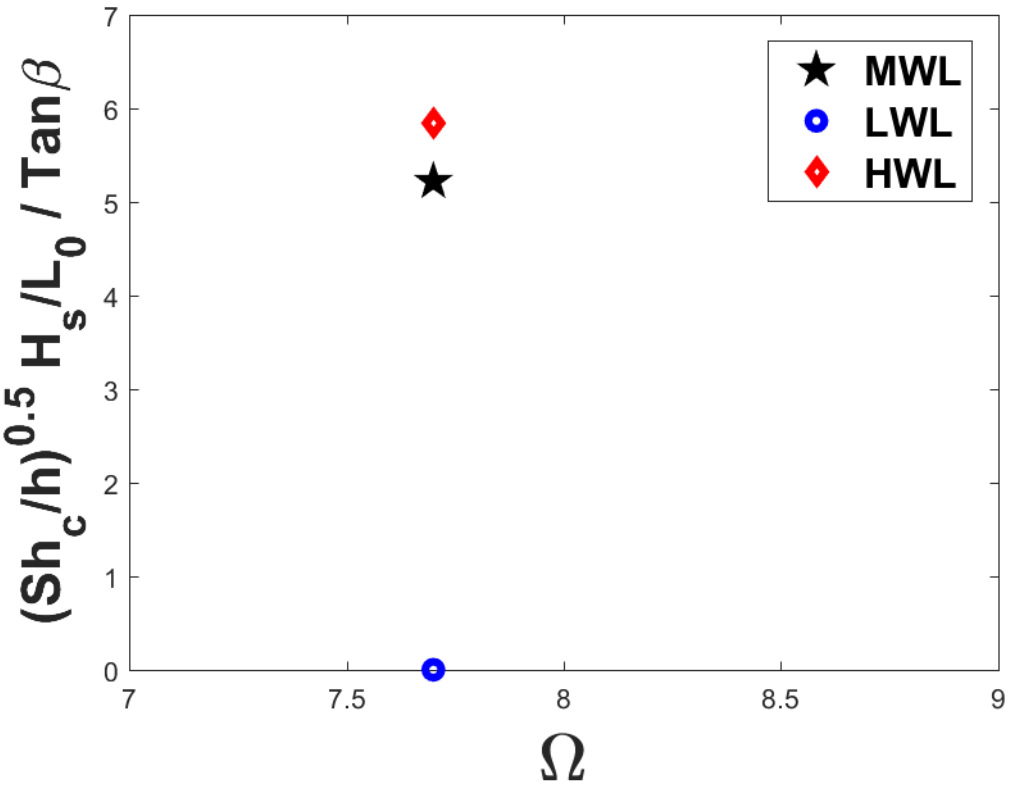

Figure C2.9 Variability of non-dimensional shoreline change on different water level against Dean's parameter Ω for dissipative beach state 0.25 m

Table C 1 Non-dimensional berm height, berm length and shoreline change on 0.15 m water level

Water level (m)	Beach State	Non-dimensional parameter	MWL	LWL	HWL
0.15	Dissipative	$(Bh_h)0.5\ H_s/L_0/\ Tan\beta$	1.67	1.67	1.59
0.15	Intermediate	$(Bh_h)0.5\ H_s/L_0/\ Tan\beta$	0.09	0.07	0.09
0.15	Reflective	$(Bh_h)0.5\ H_s/L_0/\ Tan\beta$	0.01	0.01	0.01
0.15	Dissipative	$(Bl_h)0.5\ H_s/L_0/\ Tan\beta$	10.9	10.7	10.7
0.15	Intermediate	$(Bl_h)0.5\ H_s/L_0/\ Tan\beta$	0.89	0.90	0.90
0.15	Reflective	$(Bl_h)0.5\ H_s/L_0/\ Tan\beta$	0.14	0.14	0.14
0.15	Dissipative	$(shc_h)0.5\ H_s/L_0/\ Tan\beta$	5.22	0	5.84
0.15	Intermediate	$(shc_h)0.5\ H_s/L_0/\ Tan\beta$	0.39	0.15	0.42
0.15	Reflective	$(shc_h)0.5\ H_s/L_0/\ Tan\beta$	0.07	0	0.04

Table C 2 Non-dimensional berm height, berm length and shoreline change on 0.25 m water level

Water level (m)	Beach State	Non-dimensional parameter	MWL	LWL	HWL
0.25	Dissipative	$(Bh_h)0.5\ H_s/L_0/\ Tan\beta$	1.67	1.62	1.53
0.25	Intermediate	$(Bh_h)0.5\ H_s/L_0/\ Tan\beta$	0.09	0.09	0.06
0.25	Reflective	$(Bh_h)0.5\ H_s/L_0/\ Tan\beta$	0.01	0.01	0
0.25	Dissipative	$(Bl_h)0.5\ H_s/L_0/\ Tan\beta$	10.9	10.9	11.6
0.25	Intermediate	$(Bl_h)0.5\ H_s/L_0/\ Tan\beta$	0.89	0.90	0.94
0.25	Reflective	$(Bl_h)0.5\ H_s/L_0/\ Tan\beta$	0.14	0.14	0
0.25	Dissipative	$(shc_h)0.5\ H_s/L_0/\ Tan\beta$	5.22	0	5.84
0.25	Intermediate	$(shc_h)0.5\ H_s/L_0/\ Tan\beta$	0.39	0.15	0.42
0.25	Reflective	$(shc_h)0.5\ H_s/L_0/\ Tan\beta$	0.07	0	0.04